EARLIEST TRIASSIC CLIMATIC, ENVIRONMENTAL AND FLORAL EVOLUTION OF EAST GREENLAND

Dissertation

zur

Erlangung der naturwissenschaftlichen Doktorwürde
(Dr. sc. nat.)

vorgelegt der

Mathematisch-naturwissenschaftlichen Fakultät

der

Universität Zürich

von

Anna Sanson Barrera

aus

Spanien

Promotionskomitee

Prof. Dr. Peter A. Hochuli (Leiter der Dissertation)
Prof. Dr. Hugo Bucher (Vorsitz)
Prof. Dr. Hans Peter Linder
Prof. Dr. Ulrich Heimhofer

Zürich, 2016

Death is only the beginning.
~ *Alan Watts*

Memento mori
(Be mindful of death)

Even in one of the driest places on Earth flowers bloom

"The disruptive weather phenomenon known as El Niño, the cyclical warming of the central Pacific, may be causing droughts and floods in various parts of the world, but in the vast desert of northern Chile it has also caused a vibrant explosion of thousands of species of flowers with an intensity not seen in decades."

Atacama desert - end of October, 2015

www.ticotimes.net

Table of contents

Abstract

Mass extinctions lead to dramatic changes in ecosystem composition and structure. Studying periods of recovery is crucial for understanding the evolutionary diversification and ecosystem evolution. The largest biotic crisis in the history of life is considered to have happened by the end of the Permian. The global environmental perturbations that affected marine and terrestrial ecosystems during the Late Permian also persisted during the Early Triassic. Therefore a good understanding of climate change and ecosystems evolution relies on detailed Early Triassic environmental studies. Two fundamental questions frame the present dissertation, i) how did environmental and carbon cycle disturbances influence terrestrial ecosystems during the latest Permian–earliest Triassic?, and ii) how do high-resolution studies of the earliest Triassic affect our view of regional vs. global paleoclimatic and paleoecological changes?

Earlier studies on Early Triassic communities suggested that no significant recovery took place during the entire stage with an approximate duration of 5 million years. It has been proposed that this delay was caused by persistent environmental stress, which affected ecological and taxonomic recovery. Only recently it has been shown that during the early Smithian some groups (e.g. ammonoids and conodonts) reached high levels of diversity, even higher than in the Permian, and that the recovery of benthic organisms (e.g. gastropods and bivalves) was probably repeatedly reset by multiple minor extinction events during the Early Triassic. The response of land plant ecosystems of this time interval has been controversially dicussed. On one hand, some studies proposed a complete devastation of the Early Triassic terrestrial ecosystems, and a delayed recovery starting only at the onset of the Middle Triassic. On the other hand, another hypothesis postulates a rapid recovery of land plant communities and subsequent floral turnovers during the Early Triassic, coinding with carbon cycle disturbances. Permian–Triassic carbon isotope records are characterized by recurrent positive and negative anomalies, associated also with changes in oxygen and sulfur isotope records. The major carbon isotope shifts occurring in the latest Permian, at the Griesbachian–Dienerian boundary, the early-middle Smithian, and Smithian–Spathian boundaries are used as global correlation markers.

The aim of the present thesis was to reconstruct a detailed picture of the interrelation between climate, environmental disturbances, and land plant ecosystems in northwest Pangea during the latest Permian–earliest Triassic. For this we used organic carbon isotopes, palynofacies, bulk-rock geochemistry, clay mineralogy, and palynological data of selected successions from East Greenland. Comparison with published records from other areas allowed us to distinguish between local and global signals.

The first chapter of this dissertation documents a high-resolution organic carbon isotope record from Kap Stosch (Hold-with-Hope, East Greenland) spanning the latest Permian–earliest Triassic. The Kap Stosch record allowed for the identification of 6 chemostratigraphic intervals, providing the basis for the correlation with other globally distributed C-isotope records. Two global, negative carbon isotopic shifts have been identified - one during the latest Permian, and the other one at the Griesbachian–Dienerian boundary. Other important shifts have been tentatively interpreted as regional features. Their correlation with C-isotope records of the Greenland–Norway Basin allowed the recognition of basin wide transgressive–regressive events, documenting tectonic activity during the opening of the basin. The identification of the main factors influencing the organic carbon isotope signal during the earliest Triassic (Griesbachian to Dienerian) was possible due to the combination of bulk organic carbon isotope, palynofacies and Rock-Eval data.

Active rifting during Late Permian–earliest Triassic times affected the sedimentation of the Permian–Triassic sequences in East Greenland. Correlation between sub-basins is problematic due to poorly defined latest Permian lithostratigraphic units and the scattered ammonoid fossils. The second chapter presents an interbasinal correlation based of two East Greenland sub-basins (Hold-with-Hope and

Scoresby Land) during the latest Permian–earliest Triassic on carbon isotopes. It shows common and different features among sub-basins, and provides a reliable tool for correlating Permian–Triassic sections of diachronous clastic fill, as is the case of East Greenland. Correlation of C-isotope records from East Greenland and Norway provides a revised chemostratigraphic framework for the Greenland–Norway Basin during this time interval.

The third chapter assesses marine and terrestrial environmental conditions during the latest Permian and earliest Triassic at Kap Stosch based on bulk-rock geochemisty and clay minerals. A sedimentation rates model is used to infer bulk accumulation and organic carbon accumulation rates, showing the exceptional high sedimentation rates of Kap Stosch. Due to the high influx of siliciclastics some proxies (e.g. anoxia proxies) appear diluted, providing ambiguous information about marine environmental conditions. The Kap Stosch section is characterized by generally oxic conditions punctuated by three short anoxic intervals during the Griesbachian and early Dienerian. The anoxic intervals coindide with the parts of the section displaying more green-grey siltstone beds. Clay mineralogy, e.g. smectite abundances and smectite/kaolinite ratios, shows a punctual increase in seasonality in the early Dienerian part of the succession. Spore/pollen ratios uringsuggest more humid conditions the Dienerian, suggesting that the increased seasonality affected essentially the precipitation regime.

The fourth chapter shows a fundamental floral turnover associated with the Griesbachian–Dienerian boundary in the Kap Stosch section. This turnover is marked by a change in the dominant floral elements from gymnosperm pollen-dominated associations in the Griesbachian to lycopsid spore-dominated assemblages in the Dienerian. A concomitant organic carbon negative shift shows the close interrelation between the carbon cycle and the land plant assemblages during the earliest Triassic. This floral change can be also interpreted in terms of relative humidity indicating a change from drier conditions in the Griesbachian to more humid conditions in the Dienerian. Correlation with coeval changes documented on the North Indian Margin (Pakistan) indicate that this floral turnover is of global extent.

Keywords: Permian–Triassic boundary, Early Triassic, organic carbon isotopes, particulate organic matter, bulk-rock geochemistry, clay mineralogy, palynology, East Greenland.

Kurzfassung

Massenaussterben in der Erdgeschichte bewirkten dramatische Veränderungen in der Struktur und Zusammensetzung von Ökosystemen. Wissenschaftliche Untersuchungen der nachfolgenden Erholung der Diversität geben Einblick in die Mechanismen der Wiederherstellung komplexer Ökosystemen. Das grösste Massenausterben in der Geschichte des Lebens ereignete sich am Ende des Perm. Die globalen Umweltveränderungen, welche im Späten Perm sowohl marine alsauch terrestrische Ökosysteme beeinflussten, setzten ihre Wirkung in der Frühen Trias fort. Um ein fundiertes Verständnis der klimatischen Veränderungen sowie der Evolution der Ökosysteme in diesem Zeitraum zu erlangen, bedarf es detaillierter Studien der (Paläo-)Umweltbedingungen. Entsprechend bilden die folgenden grundlegenden Fragen den Rahmen der hier vorgelegten Dissertation: i) Wie beeinflussten Umweltveränderungen und Änderungen im Kohlenstoff-Kreislaufs die terrestrischen Ökosysteme vom spätesten Perm bis in die früheste Trias und ii) was tragen hoch-auflösende palynologische Untersuchungen und Messung von stabilen Kohlenstoff-Isotopenbei zum besseren Verständnis regionaler und globaler paläoklimatischer und paläoökologischer Veränderungen in der frühesten Trias.?

Frühere Untersuchungen an marinen Vergesellschaftungen aus der frühen Trias legten nahe, dass während dieser ca. 5 Millionen Jahre keine signifikante Erholung vom Massenausterben an Perm/Triass Grenze stattgefunden hätte. Es wurde vermutet, dass diese Verzögerung der Erholung der Ökosysteme und der Biodiversität durch anhaltenden Umweltstress verursacht wurde. Erst während der letzten Jahre wurde gezeigt, dass während dieser Zeit, namentlich im frühen Smithium, einige Gruppen (z.B. Ammonoideen und Conodonten) durchaus hohe Diversitätsniveau erreichten, welche jene des Perm sogar übertraf. Auch konnte für benthische Organismen (z.B. Gastropoden und Bivalven) gezeigt werden, dass die Erholung nicht generell verzögert, sondern durch mehrfache Rückschläge in Form mehrerer kleinerer Aussterbeereignisse zurückgesetzt wurde. Die Reaktion von Landpflanzen auf die Umweltbedingungen in dieser Zeit wurde kontrovers diskutiert. Auf der einen Seite wurde in manchen Studien vorgeschlagen, dass terrestrische Ökosystemen völlig zerstört wurden und sich ebenfalls nur verzögert in der Mitteltrias erholten. Neuere Studien weisen allerdings darauf hin, dass sich Landpflanzen-Vergesellschaftungen schnell erholten und dass die Änderungen in den Pflanzenassoziationen in der Frühen Trias mit den Kohlenstoff-Kreislauf-Störungen zusammenhängen. Wiederholte positive und negative Anomalien in permotriassischen Kohlenstoff-Isotopen-Verhältnissen sind mit Fluktuationen in Sauerstoff- und Schwefel-Isotopen-Verhältnissen assoziiert. Die wichtigsten Exkursionen in den Kohlenstoff-Isotopen-Verhältnissen fallenins in das späteste Perm, sowie in die Grenzbreiche von Griesbachium–Dienerium, frühes–mittleres Smithium, und Smithium–Spathium datiert und dienen als globale Zeitmarken dar. Ein Ziel der vorliegenden Dissertation war es, für den Zeitraum spätestes Perm bis früheste Trias ein detailliertes Bild des Zusammenspiels von Klima, Umwelt-Veränderungen und Pflanzen-Ökosystemen in Nordwest-Pangäa zu rekonstruieren. Zu diesem Zweck wurden organische Kohlenstoff-Isotopen gemessen, und Analysen von Palynofazies, Palynologie, Geochemie, Tonmineralogie, an ausgewählten Profilen in Ost-Grönland durchgeführt. Der Vergleich dieser Daten mit denen anderer Gebiete ermöglichte die Unterscheidung lokaler und globaler Signale.

Das erste Kapitel dieser Dissertation dokumentiert den Zeitraum vom spätesten Perm bis zur frühesten Trias anhand eines hoch-aufgelösten organischen Kohlenstoff-Isotopen Profils von Kap Stosch (Hold-with-Hope, Ost-Grönland). Diese Daten erlaubten die Unterscheidung von sechs chemostratigraphischen Abschnitten, welche die Grundlage für die weltweite Korrelation mit anderen Kohlenstoff-Isotopen-Profilen bildeten. Im Kap Stosch-Profil konnten zwei globale negative Kohlenstoff-Isotopen-Exkursionen identifiziert werden, eine im spätesten Perm und eine zweite an der Griesbachium–Dienerium Grenze. Weitere markante Isotopen-Exkursionen wurden vorläufig als lokale Signale interpretiert. Die Korrelation der Kohlenstoff-Isotopen Profile Grönlands und Norwegens ermöglichte den Nachweis beckenweiter transgressiver-regressiver Ereignisse, welche tektonische Aktivitäten während der Riftphase im Grönland-

Norwegen Becken dokumentieren. Die Bestimmung der wichtigsten Faktoren, welche die organischen Kohlenstoff-Isotopen-Verhältnisse in der frühesten Trias (Griesbachium bis Dienerium) beeinflussten, wurde ermöglicht durch die Kombination von organischen Kohlenstoff-Isotopen, Palynofazies und Rock-Eval-Daten.

Aktives Rifting während des Späten Perm und der Frühen Trias steuerte die Sedimentation lokaler Abfolgen in Ost-Grönland. Unklare Definitionen der lithostratigraphischen Einheiten und die Seltenheit biostratigraphischer Marker (e.g., Ammonoideen-Reste) erschwert die Korrelation der Abfolgen zwischen kleineren Becken. Das zweite Kapitel widmet sich der Korrelation zweier Becken in Ost-Grönland (Hold-with-Hope und Scoresby Land) basierend auf Kohlenstoff-Isotopen Daten. Gemeinsamkeiten in den Kohlenstoff-Isotopen-Profile dieser Becken liefern ein zuverlässiges Mittel um die diachronen klastischen Sequenzen zu korrelieren. Die Korrelation der Kohlenstoff-Isotopen-Profile Ost-Grönlands und Norwegens liefert eine revidierte chemostratigraphische Abfolge für das Grönland-Norwegen Becken für den untersuchten Zeitraum.

Im dritten Kapitel werden die Umweltbedingungen im Meer und an Land während des spätesten Perm und der frühesten Trias anhand des Kap Stosch Profils beleuchtet, basierend auf geochemischen und tonmineralogischen Analysen der Sedimente. Ein Modell für die Sedimentationsraten- erlaubte die Akkumulationsraten der Sedimente sowie des organischen Kohlenstoffes abzuleiten. Die Ergebnisse für den untersuchten Zeitraum belegen aussergewöhnlich hohe Sedimentationsraten für das Kap Stosch Profil im. Aufgrund des hohen Eintrags an Siliziklastika sind manche Proxies (z.B. für Anoxia) verdünnt; entsprechend sind die Ergebnisse für die Rekonstruktionen der marinen Umweltbedingungen nicht immer eindeutig. Dennoch lassen sich für das untersuchte Profil generell oxische Verhältnisse belegen, diese werden durch drei kurze anoxische Ereignisse während des Griesbachiums und frühen Dieneriums unterbrochen. Die Zusammensetzung der Tonmineral-Assoziationen, wie beispielsweise die Häufigkeit von Smectit und die Smectit/Kaolinit-Verhältnisse, reflektieren eine kurzzeitige Zunahme der Saisonalität im frühen Dienerium. Sporen/Pollen-Verhältnisse weisen auf eher humide Bedingungen während des Dienerium hin und legen nahe, dass die verstärkte Ausprägung der Jahreszeiten im Wesentlichen das Niederschlagsregime betrafen.

Im vierten Kapitel wird ein fundamentaler Florenwechsel an der Griesbachium–Dienerium-Grenze des Kap Stosch-Profiles aufgezeigt, gekennzeichnet von einem Wechsel der dominierenden Floren-Elemente von Gymnospermen-Pollen im Griesbachium hin zu Lycopsiden-Sporen-Vergesellschaftungen im Dienerium. Die begleitende negative Kohlenstoff-Isotopen-Exkursion belegt die enge Verknüpfung zwischen Kohlenstoff-Kreislauf, Klima und der Vergesellschaftung von Landpflanzen. Dieser Florenwechsel reflektiert eine Veränderung in der Verfügbarkeit von Wasser für die Landpflanzen und wird als Wechsel von relativ trockenen Bedingungen im Griesbachium zu feuchteren im Dienerium interpretiert. Die Korrelation mit ähnlichen, gleichzeitigen Veränderungen im Bereich des North Indian Margin (Pakistan) weisen daraufhin, dass dieser Florenwechsel von globalem Ausmass war.

Zusammenfassend kann gezeigt werden, dass der multidisziplinäre Ansatz dieser Dissertation dazu beigetragen hat ein neues chemostratigraphisches Schema für das späteste Perm und die früheste Trias zu entwickeln, das die globalen Änderungen im Kohlenstoffkreislauf wiederspiegelt. Zudem konnten die physischen und chemischen Bedingungen im sedimentären Ablagerungsraum Ost-Grönlands beschrieben werden. Änderungen im Kohlenstoff-Kreislauf an der Griesbachium-Dienerium Grenze verbunden mit Klimawechsel und Änderungen der Pflanzenvergesellschaftung können in einer bisher unerreichten Auflösung erfasst werden. Sie sprechen für Veränderungen im Zeitraum von wenigen tausenden Jahren.

Schlüsselwörter: Perm-Trias-Grenze, Frühe Trias, organische Kohlenstoff-Isotope, Palynofazies, Sediment-Geochemie, Tonminerale, Palynologie, Ost-Grönland.

Introduction

The Permian–Triassic boundary and its aftermath

The Permian and Triassic periods are known for their fundamental environmental disturbances and biotic crises. The largest mass extinction in Earth history is considered to have happened by the end of the Permian (Raup and Sepkoski 1982; Sepkoski 1984) (Fig. 1). About 90% of all animal species on Earth went extinct (Baud et al. 1986). The end Permian mass extinction is associated with a global negative carbon isotope shift that is registered in organic and inorganic carbon isotope records, reflecting profound changes in the carbon cycle (e.g. Baud et al. 1986; Holser et al. 1989). Several negative and positive excursions during the Early Triassic show major changes in the carbon cycle (Payne et al. 2004; Galfetti et al. 2007b; Hermann et al. 2010; Renne et al. 1995). These excursions have been linked to iterative massive flood basalt eruptions and associated CO degassing of the Siberian Traps (Renne et al. 1995; Svensen et al. 2009) or to the metamorphism of organic-rich rock and evaporites during the volcanic intrusions (Retallack and Jahren 2008; Svensen et al. 2009). Other concomitant factors that could cause negative carbon isotope excursions are marine productivity collapse caused by anoxia (Wignall and Twitchett 1996), marine regression and oxidation of organic carbon on the exposed shelfs (Holser et al. 1989), as well as destabilization of methane hydrates (Morante 1996; Krull et al. 2000; Retallack and Krull 2006). On the other hand, only a few mechanisms can explain rapid positive carbon isotope excursions since ^{13}C-rich sources are unknown. One mechanism could be increased organic carbon burial induced by increased primary productivity or increased preservation of organic matter under anoxic oceanic conditions (Kump and Arthur 1999).

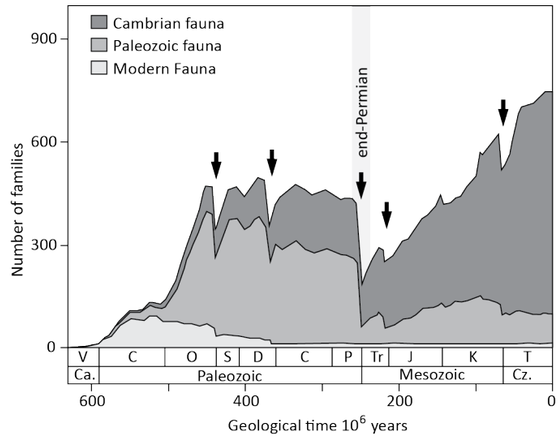

Figure 1. Phanerozoic diversity of marine families (after Sepkoski 1984). E: Ediacaran, Ca: Cambrian, O: Ordovician, S: Silurian, D: Devonian, C: Carboniferous, P: Permian, Tr: Triassic, J: Jurassic, K: Cretaceous, T: Tertiary, Cz: Cenozoic. Black arrows indicate that position of the "big five" mass extinctions.

The recovery from the end Permian mass extinction during the Early Triassic is a complex and controversially discussed topic. The classical view of the recovery phase hypothesizes that the majority of ecosystems did not fully recover until Middle Triassic (e.g. Pruss and Bottjer 2005). It postulates long term anoxic conditions (Isozaki 1997; Wignall and Twitchett 2002; Wignall et al. 2015), intense hot-house climate (Hallam 1991; Dickins 1993) and persistent environmental stress (Visscher et al. 1996; Looy et al. 1999) as main factors for the delayed recovery. However, during the last ten years abundant high-resolution paleontological and geochemical data as well as high-precision radio-isotopic dates, have revealed three key features of the Early Triassic. Firstly, chronological studies affect our understanding of the succession of environmental and biotic events (Ovtcharova et al. 2006; Galfetti et al. 2007a;

Gradstein et al. 2012; Burgess et al. 2014; Ovtcharova et al. 2015) (Fig. 2). This has huge implications for the interpretation of environmental and biotic pace change. Secondly, after the main extinction phase by the end of the Permian, pulses of recovery interrupted by subsequent extinctions of several fossil groups such as ammonoids (Brayard et al. 2009; Galfetti et al. 2007a), conodonts (Orchard 2007; Goudemand et al. 2008), and benthic communities (e.g. bivalves and gastropods, Hofmann et al. 2014) document the existence of several biotic crises during the Early Triassic or merely ecosystem instability. And thirdly, climatic variations within the Early Triassic have been documented by substantial O-isotope excursions and palynological data (Hochuli et al. 2010b; Hermann et al. 2012a; Clarkson et al. 2013; Romano et al. 2013) suggesting important oscillations in the intensity of the prevalent greenhouse climate. Therefore, in contrast to the previously mentioned delayed recovery hypothesis (e.g. Pruss and Bottjer 2005), these new results that during the Early Triassic biodiversity suffered from short term environmental disturbances, resulting in a more complex and heterogeneous ecosystem recovery patterns than previously thought (Krull et al. 2004; de Wit et al. 2002; Payne et al. 2004; Brayard et al. 2006; Galfetti et al. 2007a,b; Hochuli and Vigran 2010; Hochuli et al. 2010b; Retallack et al. 2011; Hermann et al. 2011b; Romano et al. 2013; Clarkson et al. 2013; Hofmann et al. 2014).

The Early Triassic climate change and ecosystems evolution are the main fields of research of the Paleontological Institute and Museum (University of Zurich) under the lead of Professor Hugo Bucher.

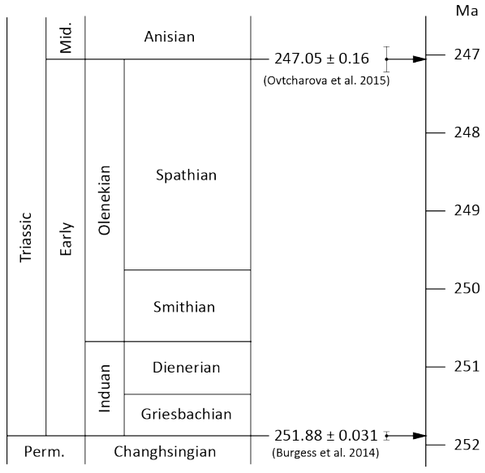

Figure 2. The Early Triassic substages (Gradstein et al. 2012) with calibrations from published radiometric ages (after Burgess et al. 2014; Ovtcharova et al. 2015). Boundaries without an absolute age are approximate.

Completed and ongoing studies investigate the Early Triassic climate, faunal and floral evolution at high precision. This thesis focus on the interrelation between climate change and land plants ecosystems during the earliest Triassic and it is connected to the findings of other projects from the Paleontological Institute. These projects involve the multi-approach analysis of several worldwide key areas such as Oman, Pakistan, Tibet, South China, western USA, Spitsbergen, Greenland and the Italian Alps. The primary insights from these studies are mentioned below:

- As documented in the western USA the fast recovery of benthic ecosystems (e.g. bivalves and gastropods) from the PTB crisis during the Griesbachian, was followed by a decline during the Dienerian and by another recovery during the Smithian (Hofmann et al. 2014). This shows, in contrast to the regularly cited long-term anoxia hypothesis, that intervals with prevailing oxic conditions existed during the Early Triassic. Parallel to the benthic ecosystems study, palynofacies data from Pakistan shows that oxygen deficient conditions were also intermittent throughout the entire Early Triassic. Widespread anoxia was restricted to the middle-late Dienerian and late Smithian time intervals (Hermann et al. 2011b; Schneebeli-Hermann et al. 2012).

- Data on conodonts also provided high biostratigraphic resolution but also new insights concerning recovery patterns. Conodonts underwent an important turnover at the Griesbachian–Dienerian boundary, followed by a huge radiation during the early-middle Smithian, an extinction in the late Smithian, and another radiation during the Spathian (Goudemand et al. 2008). Recently, the index species of the Permian–Triassic boundary, the conodont *Hindeodus parvus*, has been found in several Chinese sections in uppermost Permian beds (Zhang et al. 2014; Brosse et al. 2015; Yuan et al. 2015). This indicates that the first occurrence of *H. parvus* is diachronous, and therefore the Permian–Triassic boundary definition needs revision.

- Based on the Unitary Associations method a new ammonoid biostratigraphic scheme of unprecedented high resolution, has been proposed for the Dienerian of the northern Indian margin resulting in a total of 12 zones. Based on this new zonation, ammonoid biodiversity dynamics for the Dienerian and early Smithian show the following four phases: i) a moderately high diversity in the early Dienerian, ii) a decline followed by a very low diversity throughout the middle Dienerian, iii) a slight increase in diversity in the late Dienerian, and iv) an important radiation in the early Smithian (Ware et al. 2015). The best resolved biostratigraphic schemes for the Smithian was presented by Brühwiler at al. (2010) based on ammonoids from the northern Indian margin showing that ammonoids underwent an important radiation during the early Smithian, constant high diversity and extremely high turnover rates during the middle Smithian and a major extinction in the late Smithian.

- Oxygen isotope data based on apatite of conodonts from the Early Triassic confirm previous interpretations of repetitive climatic changes in the aftermath of the end Permian mass extinction (Romano et al. 2013). Relatively cool climatic conditions are indicated for the interval near the Griesbachian–Dienerian boundary, for the early Smithian, and for the early Spathian, interrupted by episodes of elevated temperatures during the middle-late Dienerian and the middle-late Smithian (Romano et al. 2013). Changes in carbon and oxygen isotope values are paralleled by shifts in the spore-pollen ratio from Norway and Pakistan (Galfetti et al. 2007b; Hermann et al. 2012b). For the Early Triassic, the spore/pollen ratio can be used as proxy for modifications in the net water balance between evaporation and precipitation, and therefore indicating climatic variations between dry and humid conditions.

- Palynological data from Pakistan show a remarkable change in flora associated with the Griesbachian–Dienerian boundary (e.g. Schneebeli-Hermann et al. 2015). The Griesbachian is dominated by gymnosperm pollen, whereas the Dienerian is dominated by spore-bearing plants. This shift in palynomorphs is also interpreted as a climatic change from dry conditions in the Griesbachian to humid conditions in the Dienerian.

Land pants ecosystems during the Permian–Triassic transition

The effect of the end Permian mass extinction on terrestrial ecosystems is still controversially discussed. There is a general agreement that an important floral turnover occured at the Permian–Triassic transition. However, the tempo, biodiversity loss and/or recovery, and climate-flora interactions during the Permian–Triassic transition is still discussed. There is a large difference in the preservation of macro- and microfossil plant record. While plant macrofossils are very rare or absent in most Early Triassic records (Retallack et al. 1995), plant microfossils (i.e. sporomorphs) are common and continuously recorded across the Permian–Triassic transition (e.g. Piasecki 1984; Looy et al. 2001; Lindström and McLoughlin 2007; Hochuli et al. 2010b; Hermann et al. 2011a; Hermann et al. 2012b). Therefore, the palynological record is widely used for Permian–Triassic climatic and ecological studies. The advantage

of using palynology is that palynomorphs are durable and of small size, there is plenty of variety for biostratigraphic studies, they are abundant in space and time, can be used in absence of macrofossils, and wide spread. However, different interpretations of the palynological record led to divergent hypotheses. A distinct spore spike by the end of the Permian appears to be associated with the C-isotope negative shift. On the one hand this spore spike is interpreted as the dieback of woody plants and the onset of the dominance of lycopods lasting up to the Middle Triassic (Looy et al. 1999). On the other hand, it is interpreted as a short-lived environmental deterioration, and followed by the recovery of gymnosperms during the earliest Triassic (Lindström and McLoughlin 2007; Hochuli and Vigran 2010, Hochuli et al. 2010b; Hermann et al. 2012a). The spore spike is an example of how important independent dating is when assessing environmental changes. In this case, the duration of the spore spike is crucial to determine the impact it has on terrestrial ecosystems. Another latest Permian event is commonly cited as the "fungal event", which shows an increase in *Reduviasporonites* in few Permian–Triassic sections (Eshet et al. 1995; Visscher et al. 1996; Sephton et al. 2009; Bercovici et al. 2015; Cui et al. 2015; Tewari et al. 2015). However most of the sections showing the "fungal event" are based on low resolution sampling and/or wrong identification of the organic matter (Hochuli 2016). Additionally, the biological affinity of *Reduviasporonites* is still obscure. Some authors interpreted *Reduviasporonites* as fungal remains, representing hyphae of ascomycetes similar to those of modern Rhizoctonia (Visscher et al. 1996; Visscher et al. 2011). Its abundance has been interpreted to reflect the collapse of terrestrial ecosystems, since saprophytic fungi may have metabolised the dead vegetation formed during the extinction event (Visscher et al. 1996; Steiner et al. 2003; Peng et al. 2006; Sephton et al. 2009; Bercovici et al. 2015; Cui et al. 2015). On the other hand Foster et al. (2002) suggested an algal origin for *Reduviasporonites* based on radio-isotopic studies. The cell wall of *Reduviasporonites* has been shown to be isotopically lighter (in terms of $\delta^{13}C_{org}$) than the plant remains associated to it. Therefore, it is unlikely that the organism related to *Reduviasporonites* has consumed this material, as would be expected from saprophytic fungi (Foster et al. 2002; Spina et al. 2015). Abundance of *Reduviasporonites* has never been reported from extended sections and preservational bias for the abundance peak has been suggested (e.g. Hochuli et al. 2010b; Hochuli 2016). Other studies support a gradual floral transition from the Permian to the Triassic, based on well preserved sporomorphs from extended basal Triassic sequences (Lindström and McLoughlin 2007; Hochuli et al. 2010b; Hermann et al. 2011a; Hermann et al. 2012b). These studies link the gradual floral transition to the environmental and climatic disturbances reflected in the carbon cycle mentioned before (Hochuli et al. 2010b; Schneebeli-Hermann et al. 2012, 2015). Therefore, the observed floral changes would reflect the adaptation of the vegetation to profound and recurrent environmental changes during the Early Triassic without necessarily be associated to a mass extinction. These palynological records show neither a global floral diversity decrease nor a disastrous extinction event (Hochuli et al. 2010b; Hermann et al. 2011a).

East Greenland

The lack of complete, expanded and well-preserved earliest Triassic records represent a shortcoming for Early Triassic ecological studies, and therefore hamper ecological and environmental interpretations. Only a few areas show well-preserved, thick Permian–Triassic successions where a high degree of resolution can be achieved, e.g. northern Indian margin (Hermann et al. 2012a; Clarkson et al. 2013), Pakistan (Hermann et al. 2011a,b), Antarctica (Lindström and McLoughlin 2007). Studies off-shore Norway have showed that Greenland and Norway were conjugated margins of a rift in northwest Pangea (Bugge et al. 2002). Thanks to the expanded nature of the sedimentary successions on the Trøndelag and Finnmark platforms, more detailed shifts in the organic C-isotope records have been revealed (Hermann et al. 2010; Hochuli et al. 2010a,b). During Permian–Triassic times the Greenland–Norway rift was located on the northern margin of Pangea. East Greenland is one of the key areas for Permian–Triassic studies. Wordie (1927) was the first to document rocks of Permian–Triassic age in the Kap Stosch area. Subsequently,

several studies dealt with general Permian–Triassic stratigraphy and paleontology (Koch 1931; Nielsen 1935), with the biostratigraphic subdivision of the Permian–Triassic beds based on ammonoids (Spath 1935; Trümpy 1961; Trümpy 1969), and with palynology (Balme 1979; Piasecki 1984). More detailed lithostratigraphic descriptions of the formations were published by Perch-Nielsen et al. 1974, Surlyk et al. (1986), and Surlyk (1990). Numerous studies focused on the Permian–Triassic boundary (PTB) of East Greenland (Teichert and Kummel 1972; Looy et al. 2001; Stemmerik et al. 2001; Twitchett et al. 2001; Wignall and Twitchett 2002), and on the Greenland–Norway Basin evolution (Surlyk et al. 1984; Surlyk 1990; Stemmerik 1998; Seidler et al. 2004; Hamann et al. 2005; Müller et al. 2005; Oftedal et al. 2005). The Late Permian lithostratigraphic succession of East Greenland comprises the Foldvik Creek Group with the Huledal, Karstryggen, Ravnefjeld, Wegener Halvø, and Schuchert Dal formations. The latest Permian–earliest Triassic succession consists of the Wordie Creek and the Pingo Dal formations (Spath 1935; Surlyk et al. 1986; Surlyk 1990). The Permian Huledal Formation resting unconformably on Carboniferous deposits is composed of alluvial conglomerates including the onset of marine influence in its uppermost part. It is overlain by the marine hypersaline carbonates and evaporites of the Karstryggen Formation. Both the Huledal and the Karstryggen formations are of Capitanian age (Surlyk et al. 1986). In areas representing basin margins and paleo-highs the Karstryggen Formation is overlain by carbonate build-ups of the Wegener Halvø Formation. Black bituminous mudstones deposited in basinal areas have been defined as Ravnefjeld Formation, which contains bivalves (*Posidonia permica*), fishes (Nielsen 1935) and few cephalopods (Spath 1935). Abundant fauna such as brachiopods, crinoids and corals are known from the Wegener Halvø Formation. Both formations are of Wuchiapingian age (Surlyk et al. 1986; Surlyk 1990; Piasecki and Stemmerik 1991). A Changhsingian relative sea-level fall and an increased siliciclastic supply led to the deposition of the grey-black, silty, bioturbated mudstones and sandstones of the Schuchert Dal Formation (Surlyk et al. 1986; Piasecki and Stemmerik 1991). A latest Permian relative sea-level fall and an increase in rifting activity coincide with the deposition of the Wordie Creek Formation (Surlyk 1990). This formation, represented by a thick sequence of siliciclastics influenced by a rapidly fluctuating sea-level rise, was deposited during the latest Changhsingian to Dienerian time interval (Surlyk 1990; Oftedal et al. 2005).

Particularly the Kap Stosch area, on the Hold-with-Hope peninsula, represents one of the most extended Late Permian–earliest Triassic successions worldwide. It consists of low maturity siltstone and fine sandstone beds, essential for the good preservation of organic matter providing great potential for studies based on organic geochemistry and palynology. The lowermost portion of the section comprises the basinal Ravnefjeld Formation, which is unconformably overlain by the deltaic sequence of the Wordie Creek Formation. The latter displays a general shallowing upward trend with coastal deposits near the top of the sequence. Two major sandstone bodies (SB II and SB III) defined and mapped by Nielsen (1935) can be easily followed in the field and allow for regional correlations. Sandstone interfingering with conglomerate foreset beds of a delta constitutes the lower part of SB II and massive sandstone beds characterize its upper part. On the other hand, SB III and other minor sandstone beds show cm- to plurimetric scale channel-like structures that thin laterally towards the Southeast. General trends in grain size, sedimentary structures and thickness of SB II and SB III indicate a WNW–ESE direction of transport of the clastic material.

For the purpose of this thesis, the Kap Stosch area has been chosen as main study area (Fig. 3). Four sections have been logged and sampled during three field work seasons (summers 2010, 2011, and 2012). In stratigraphical order the sections are: Black Ridge, Blåelv, Rævekloft and Nasutdal. These four sections allowed to compile a composite section spanning the Late Permian–earliest Triassic (see Chapter 1). Subsequently, during the field season of summer 2013 two additional sections were sampled in the southern part of Jameson Land – namely Aggersborg and Triaselv (Fig. 3). The development of sub-basins along the western (Greenlandian) margin of the Greenland-Norway Basin provided the space to

develop expanded Permian–Triassic sequences (Bugge et al. 2002; Seidler et al. 2004). However, due to a relative sea-level fall during a Late Permian interval, a hiatus is recorded in these sub-basins (e.g. in Kap Stosch). The field work in the Jameson Land area aimed to log and sample two potentially continuous sections across the Permian–Triassic transition, complementing the Kap Stosch record by filling the sedimentary gap.

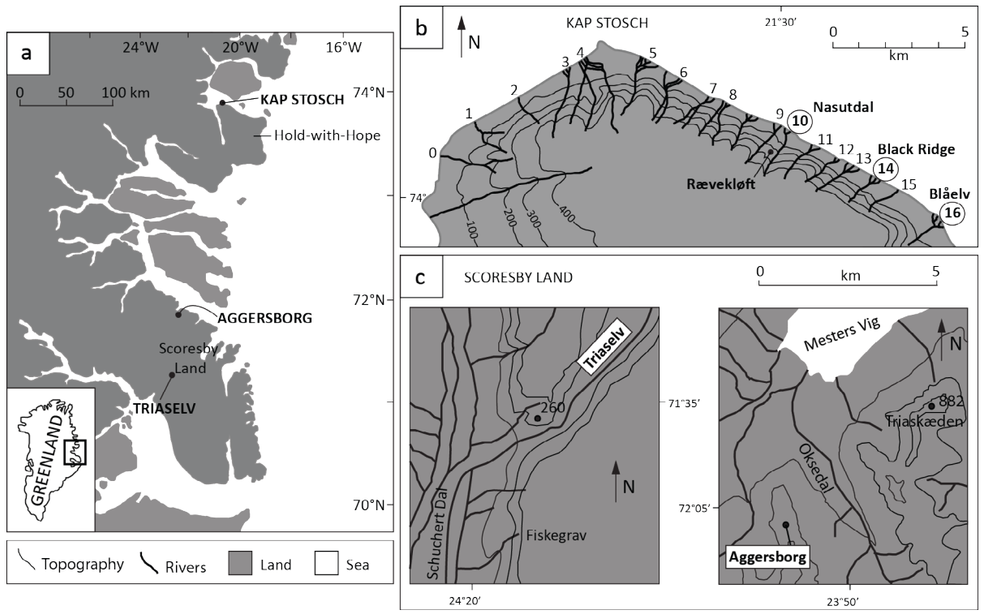

Figure 3. a – Overview of East Greenland and location of the relevant areas and sections for this study; b - Location of the study sections at Kap Stosch (Black Ridge, Blåelv, Rævekloft and Nasutdal), and c – Location of the studied sections at Scoresby Land (Aggersborg and Triaselv). Modified from Bjerager et al. 2006.

Main objectives and general outline

This thesis is a contribution to the Early Triassic research at the Paleontological Institute (UZH). Cornerstones of this study are carbon cycle disturbances, marine and terrestrial environmental changes, and climate and flora evolution in East Greenland during the earliest Triassic (Griesbachian and Dienerian). A multidisciplinary approach including stable carbon isotope, palynofacies, bulk-rock geochemistry, clay mineralogy and palynology has been chosen to i) produce a chemostratigraphic framework for the Permian–Triassic boundary and earliest Triassic, ii) to describe the depositional environments of Kap Stosch and Jameson Land (East Greenland), and iii) to link environmental changes (e.g. disturbances of the carbon cycle) with changes in land plant ecosystems changes during the earliest Triassic. The chapters of this thesis represent published work or manuscripts that are in review or in preparation and are conceived as independent contributions. Because of the common topic, the introductions, the methods, and parts of the discussions may be repeated.

A high-resolution bulk organic carbon isotope record and palynofacies data from Kap Stosch (see Chapter 1) has been published in Global and Planetary Change (Sanson-Barrera et al. 2015). The detailed description of the four sections logged and sampled at Kap Stosch and compiled to a composite section provides the basis for the next three chapters. Particulate organic matter data from this expanded sedimentary sequence reveals three transgressive-regressive cycles that are compared with Triassic

sequence stratigraphy schemes of the Arctic (Embry 1997, Mørk and Smelror 2001). A second-order sequence boundary across the Arctic has been identified as the latest Permian unconformity at Kap Stosch. A third-order sequence boundary associated with the Griesbachian–Dienerian boundary has been identified and correlated with Triassic sequences from southern Spitsbergen and the Barents Sea. The bulk organic carbon isotope record shows the global latest Permian carbon isotope negative shift, and it is used to correlate the Kap Stosch section with worldwide distributed Permian–Triassic records. A second marked negative shift, associated with the Griesbachian–Dienerian boundary, has been correlated with data from the Musandam Peninsula (United Arab Emirates) (Clarkson et al. 2013) (see Chapter 1, Fig. 4). A mid-Griesbachian bulk organic carbon isotope shift is correlated with a C-isotope event data of the Trøndelag Platform, off-shore Norway (Hermann et al. 2010). It is interpreted as a regional signal of the Greenland–Norway Basin showing the influence of regional tectonics on carbon burial on both margins. Particulate organic matter and Rock-Eval data are used to evaluate and discuss the influence of the organic matter origin on the carbon isotope data.

Chapter 2 focuses on an interbasinal correlation between the Kap Stosch and Jameson Land sub-basins based on bulk organic carbon isotope and biostratigraphic (ammonoid) data (Sanson-Barrera et al. in review). Variations in the sedimentary sequences among sub-basins show the different depositional environments present during the upper Permian–lowermost Griesbachian of East Greenland. Poorly defined boundaries between formations hamper correlations based only on lithostratigraphy and the sparse ammonoid record. Organic carbon isotope data proves to be a reliable tool for correlating Permian–Triassic sections and unravelling the diachronous clastic fill of East Greenland sub-basins. Palynofacies data is used to assess the origin of the organic matter. The correlation with coeval sections off-shore Norway - the Trøndelag and Finnmark platforms - provides a broader view of the Greenland–Norway Basin and Boreal Realm basin evolution during the earliest Triassic.

Chapter 3 comprises a study of environmental changes during the latest Permian and earliest Triassic at Kap Stosch based on bulk-rock geochemistry and clay mineralogy (Sanson-Barrera et al. in review). Sedimentation rates were exceptionally high in the Kap Stosch section, with 0.27 m ka^{-1} on average and spanning ca. 1 million years. The dilution effects due to high sedimentation rates affect all the measured proxies e.g., S/TOC and trace element proxies (e.g. Mo, V, and U). However, the combination of the DOP_T, C_{org}:P, and S/TOC proxies show one of the three suboxic-anoxic events in the Griesbachian that have previously been identified by their high relative abundance of marine organic matter (see Chapter 1, Fig. 4). Clay mineralogy shows an important but punctual increase in smectite abundances and smectite/kaolinite ratios near the base of the Dienerian that is interpreted as increase in seasonality. Spore/pollen ratios indicate more humid conditions in the Dienerian, suggesting that the increased seasonality affects especially the precipitation regime.

Hochuli et al. 2016 shows a detailed palynological study of the latest Griesbachian–earliest Dienerian interval from Kap Stosch (Hochuli et al. 2016). The palynological record shows a fundamental floral turnover, postdating the Permian–Triassic boundary and associated with the Griesbachian–Dienerian boundary (see Chapter 4, Fig. 1). This change reflects a rapid shift from the gymnosperm-dominated flora of the Griesbachian to lycopod-dominated flora in the Dienerian. This floral change can be also interpreted in terms of relative humidity, indicating a change from drier conditions in the Griesbachian to more humid conditions in the Dienerian. A concomitant negative shift of organic carbon isotopes shows the close interrelation between the carbon cycle and the land plant assemblages during the earliest Triassic. Similar and coeval changes documented from a North Indian Margin (Pakistan) succession indicate that this floral turnover is of global extent.

References

Balme, B.E., 1979. Palynology of Permian–Triassic Boundary beds at Kap Stosch, East Greenland. Meddelelser om Grønland 200.

Baud, A., Atudorei, V., Sharp, Z., 1986. Late Permian and Early Triassic evolution of the Northern Indian margin: carbon isotope and sequence stratigraphy. Geodininamica Acta 9, 57-77.

Benton, M.J., and Twitchett, R.J., 2003. How to kill (almost) all life: the end-Permian extinction event. Trends in Ecology and Evolution 18, 358-365.

Bercovici, A., Cui, Y., Rorel, M-B., Yu, J., Vajda, V., 2015. Terrestrial paleoenvironment characterization across the Permian–Triassic boundary in South China. Journal of Asian Earth Sciences 98, 225-246, doi:10.1016/j.jseaes.2014.11.016.

Birkenmajer, K., 1977. Erosional unconformity at the base of marine Lower Triassic at Wegner Ø, Central East Greenland. Bulletin of the Geological Society of Denmark, 25, 107-116.

Bjerager, M., Seidler, L., Stemmerik, L., Surlyk, F., 2006. Ammonoid stratigraphy and sedimentary evolution across the Permian–Triassic boundary in East Greenland. Geological Magazine 143, 635-656, doi: 10.1017/S0016756806002020.

Brayard, A., Bucher, H., Escarguel, G., Fluteau, F., Bourquin, S., Galfetti, T., 2006. The Early Triassic ammonoid recovery: paleoclimatic significance of diversity gradients. Palaeogeography, Palaeoclimatology, Palaeoecology 239, 374–395, doi:10.1016/j.palaeo.2006.02.003.

Brayard, A., Escarguel, G., Bucher, H., Monnet, C., Brühwiler, T., Goudemand, N., Galfetti, T., Guex, J., 2009. Good genes and good luck: Ammonoid diversity and the end-Permian mass extinction. Science 325, 1118-1121.

Brosse, M., Bucher, H., Bagherpour, B., Baud, A., Frisk, A.M., Goudun, K., Goudemand, N., 2015. Conodonts from the Early Triassic microbialite of Guangxi (South China): Implications for the definition of the base of the Triassic system. Palaeontology 58, 563-584, doi:10.1111/pala.12162.

Brühwiler, T., Bucher, H., Brayard, A. & Goudemand, N., 2010. High-resolution biochronology and diversity dynamics of the Early Triassic ammonoid recovery: The Smithian faunas of the Northern Indian Margin. Palaeogeography, Palaeoclimatology, Palaeoecology 297, 491-501.

Bugge, T., Ringas, J.E., Leith, D.A., Mangerud, G., Weiss, H.M., Leith, T.L., 2002. Upper Permian as new play model on the mid-Norwegian continental shelf: investigated by shallow stratigraphic drilling. The American Association of Petroleum Geologists 86, 107-127.

Burgess, S.D., Bowring, S., Shen, S., 2014. High-precision timeline for Earth's most severe extinction. Proceedings of the Natural Academy of Science 111, 3316-3321, doi:10.1073/pnas.1317692111.

Clarkson, M.O., Richoz, S., Wood, R.A., Maurer, F., Krystyn, L., McGurty, D.J., Astratti, D., 2013. A new high-resolution $\delta^{13}C$ record for the Early Triassic: insights from the Arabian Platform. Gondwana Research 24, 233-242, doi:10.1016/j.gr.2012.10.002.

Cui, Y., Bercovici, A., Yu, J., Kump, L.R., Freeman, K.H., Su, S., Vajda, V., 2015. Carbon cycle perturbation expressed in terrestrial Permian–Triassic boundary sections in South China. Global and Planetary Change (in press), doi:10.1016/j.gloplacha.2015.10.018.

de Wit, M.J., Ghosh, J.G., de Villiers, S., Rakotosolofo, N., Alexander, J., Tripathi, A., Looy, C., 2002. Multiple organic carbon isotope reversals across the Permo–Triassic boundary of terrestrial Gondwana sequences: clues to extinction patterns and delayed ecosystem recovery. The Journal of Geology 110, 227-240, doi:10.1086/338411.

Dickins, J.M., 1993. Climate of the Late Devonian to Triassic. Palaeogeography, Palaeoclimatology, Palaeoecology 100, 89-94.

Embry, A.F., 1997. Global sequence boundaries of the Triassic and their identification in the western Canada sedimentary basin. Bulletin of Canadian Petroleum Geology 45, 415-433.

Eschet, Y., Rampino, M.R., Visscher, H., 1995. Fungal event and palynological record of ecological crisis recovery across the Permian – Triassic boundary. Geology 23, 967-970.

Foster, C.B., Stephenson, M. H., Marshall, C., Logan, G. A., Greenwood, P. F., 2002. A revision of Reduviasporonites Wilson 1962: Description, illustration, comparison and biological affinities. Palynology 26, 35-58.

Galfetti, T., Bucher, H., Ovtcharova, M., Schaltegger, U., Brayard, A., Brühwiler, T., Goudemand, N., Weissert, H., Hochuli, P.A., Cordey, F., and Goudun, K., 2007a. Timing of the Early Triassic carbon cycle perturbations inferred from new U-Pb ages and ammonoid biochronozones. Earth and Planetary Science Letters 258, 593-604.

Galfetti, T., Hochuli, P.A., Brayard, A., Bucher, H., Weissert, H., Vigran, J.O., 2007b. Smithian/Spathian boundary event: Evidence for global climatic change in the wake of the end-Permian biotic crisis. Geology 35, 291-294.

Gradstein, F.M., Ogg, J.G., Schmitz, M.D., and Ogg, G.M., 2012. The Geologic Time Scale 2012. Published by Elsevier Amsterdam BV. Press.

Goudemand, N., Orchard, M., Bucher, H., Brayard, A., Brühwiler, T., Galfetti, T., Hochuli, P.A., Hermann, E. & Ware, D., 2008. Smithian-Spathian boundary: The biggest crisis in Triassic conodont history. Geological Society of America 40, 505.

Hallam, A., 1991. Why was there a delayed radiation after the end-Permian mass extinction? Historical Biology 5, 257-262.

Hamann, N.E.,Whittaker, R.C., Stemmerik, L., 2005. Geological development of the Northeast Greenland Shelf. In: Doré, A.G., Vining, B.A. (Eds.), PetroleumGeology: North-West Europe and Global Perspectives. Proceedings of the 6th Petroleum Geology Conference, Geological Society, London, 887-902.

Hermann, E., Hochuli, P.A., Bucher, H., Vigran, J.O., Weissert, H., Bernasconi, S.M., 2010. A close-up view of the Permian–Triassic boundary based on expanded organic carbon isotope records from Norway (Trøndelag and Finnmark Platform). Global and Planetary Change 74, 156–167, doi: 10.1016/j.gloplacha.2010.10.007

Hermann, E., Hochuli, P.A., Bucher, H., Brühwiler, T., Hautmann, M., Ware, D. & Roohi, G., 2011a. Terrestrial ecosystems on North Gondwana following the end-Permian mass extinction. Gondwana Research 20, 630-637.

Hermann, E., Hochuli, P.A., Méhay, S., Bucher, H., Brühwiler, T., Ware, D., Hautmann, M., Roohi, G., ur-Rehman, K. and Yaseen, A., 2011b. Organic matter and palaeoenvironmental signals during the Early Triassic biotic recovery: The Salt Range and Surghar Range records. Sedimentary Geology 234, 19-41.

Hermann, E., Hochuli, P.A., Bucher, H., Brühwiler, T., Hautmann, M., Ware, D., Weissert, H., Roohi, G., Yaseen, A. & ur-Rehman, K., 2012a. Climatic oscillations at the onset of the Mesozoic inferred from palynological records from the North Indian Margin. Journal of the Geological Society, London 169, 227-237.

Hermann, E., Hochuli, P.A., Bucher, H. & Roohi, G., 2012b. Uppermost Permian to Middle Triassic palynology of the Salt Range and Surghar Range, Pakistan. Review of Palaeobotany and Palynology 169, 61-95.

Hochuli, P.A., and Vigran, J.O., 2010. Climate variations in the Boreal Triassic - Inferred from palynological records from the Barents Sea. Palaeogeography, Palaeoclimatology, Palaeoecology 290, 20-42.

Hochuli, P.A., Vigran, J.O., Hermann, E., Bucher, H., 2010a. Multiple climatic changes around the Permian–Triassic boundary event revealed by an expanded palynological record from mid-Norway. Geological Society of America Bulletin 122, 884-896, doi:10.1130/B26551.1.

Hochuli, P.A., Hermann, E., Vigran, J.O., Bucher, H.,Weissert, H., 2010b. Rapid demise and recovery of plant ecosystems across the end-Permian extinction event. Global and Planetary Change 74, 144-155, doi:10.1016/j.gloplacha.2010.10.004.

Hochuli, P.A., Sanson-Barrera, A., Schneebeli-Hermann, E., Bucher, H., (2016). Severest crisis overlooked—Worst disruption of terrestrial environments postdates the Permian–Triassic mass extinction. Nature Scientific Reports 6, 28372, doi: 10.1038/srep28372.

Hochuli, P.A., (2016). Comments on the assumed "fungal spike" in: "Carbon cycle perturbation expressed in terrestrial Permian–Triassic boundary sections in South China." Global and Planetary Change.

Hofmann, R., Hautmann, M., Brayard, A., Nützel, A., Bylund, K.G., Jenks, J., Vennin, E., Olivier, N., Bucher, H., 2014. Recovery of benthic marine communities from the end-Permian mass extinction at the low-latitudes of Eastern Panthalassa. Palaeontology 57, 547-589.

Holser, W.T., Schönlaub, H.-P., Attrep, M., Boekelmann, K., Klein, P., Magaritz, M., Orth, C.J., Fenninger, A., Jenny, C., Kralik, M., Mauritsch, H., Pak, E., Schramm, J.-M., Stattegger, K., and Schmöller, R., 1989. A unique geochemical record at the Permian/Triassic boundary. Nature 337, 39-44.

Isozaki, Y., 1997. Permo-Triassic boundary superanoxia and stratified superocean: Records from lost deep sea. Science 276, 235-238.

Lindström, S., and McLoughlin, S., 2007. Synchronous palynofloristic extinction and recovery after the end-Permian event in the Prince Charles Mountains, Antarctica: Implications for palynofloristic turnover across Gondwana. Review of Palaeobotany and Palynology 145, 89-122.

Looy, C.V., Brugman, W.A., Dilcher, D.L., and Visscher, H., 1999. The delayed resurgence of equatorial forests after the Permian-Triassic ecologic crisis. Proceedings of the National Academy of Sciences 96, 13857-13862.

Looy, C.V., Twitchett, R.J., Dilcher, D.L., Van Konijnenburg-VanCittert, J.H.A., and Visscher, H., 2001. Life in the end-Permian dead zone. Proceedings of the National Academy of Sciences 98, 7879-7883.

Koch, L., 1931. Carboniferous and Triassic stratigraphy of East Greenland. Meddelelser om Grønland 83.

Krull, E.S., Retallack, G.J., Campbell, H.J., Lyon, G.L., 2000. δ13Corg chemostratigraphy of the Permian–Triassic boundary in the Maitai Group, New Zealand: evidence for high latitudinal methane release. New Zealand Journal of Geology and Geophysics 43, 21-32.

Krull, E.S., Lehrmann, D.J., Druke, D., Kessel, B., Yu, Y., Li, R., 2004. Stable carbon isotope stratigraphy across the Permian–Triassic boundary in shallow marine carbonate platforms, Nanpanjiang Basin, south China.

Palaeogeography, Palaeoclimatolology, Palaeoecology 204, 297-315, doi:10.1016/S0031-0182(03)00732-6
Kump, L.R., and Arthur, M.A., 1999. Interpreting carbon–isotope excursions: carbonates and organic matter. Chemical Geology 161, 181-198, doi:10.1016/S0009-2541(99)00086-8
Morante, R., 1996. Permian and Early Triassic isotopic records of carbon and strontium in Australia and a scenario of events about the Permian–Triassic boundary. Historical Biology 11, 289-310.
Mørk, A., and Smelror, M., 2001. Correlation and non-Correlation of high order circum-Arctic Mesozoic sequences. Polarforschung 69, 65-72.
Müller, R., Nystuen, J.P., Eide, F., Lie, H., Mqiler, R., 2005. Late Permian to Triassic basin infill history and palaeogeography of the mid-Norwegian–East Greenland region. In: Wandas, B., et al. (Eds.), Onshore–Offshore Relationships on the North Atlantic Margin NPF Special Publication 12. Elsevier B.V., Amsterdam, 165-189.
Nielsen, E., 1935. The Permian and Eotriassic vertebrate-bearing beds at Godthaab Gulf (East Greenland). Meddelelser om Grønland, 98.
Oberhänsli, H., Hsü, K.J., Piasecki, S., Weissert, H., 1989. Permian–Triassic carbon-isotope anomaly in Greenland and in the Southern Alps. Historical Biology 2, 37-49.
Oftedal, B.T., Andresen, A., Müller, R., 2005. Early Triassic syn-rift sedimentation at Hold with Hope, Northeast Greenland. In: Wandas, B., et al. (Eds.), Onshore–Offshore Relationships on the North Atlantic MarginNPF Special Publication 12. Elsevier B.V., Amsterdam, 191-206.
Orchard, M.J., 2007. Conodont diversity and evolution through the latest Permian and Early Triassic upheavals. Palaeogeography, Palaeoclimatology, Palaeoecology 252, 93-117.
Ovtcharova, M., Bucher H., Schaltegger, U., Galfetti, T., Brayard, A., and Guex J., 2006. New Early to Middle Triassic U–Pb ages from South China: Calibration with ammonoid biochronozones and implications for the timing of the Triassic biotic recovery. Earth and Planetary Science Letters 243, 463-475, doi:10.1016/j.epsl.2006.01.042
Ovtcharova, M., Goudemand, N., Hammer, Ø., Guodun,K., Cordey. F., Galfetti, T., Schaltegger, U., and Bucher, H. 2015. Developing a strategy for accurate definition of a geological boundary through radio-isotopic and biochronological dating: The Early-Middle Triassic boundary (South China). Earth Science Reviews 146, 65-76, doi:10.1016/j.earscirev.2015.03.006
Payne, J.L., Lehrmann, D.J., Wei, J., Orchard, M.J., Schrag, D.P., Knoll, A.H., 2004. Large perturbations of the carbon cycle during recovery from the end-Permian extinction. Science 305, 506-509, doi:10.1126/science.1097023
Payne, J.L., Kump, L.R., 2007. Evidence for recurrent Early Triassic massive volcanism from quantitative interpretation of carbon isotope fluctuations. Earth and Planetary Science Letters 256, 264-277, doi:10.1016/j.epsl.2007.01.034
Perch-Nielsen, K., Birkenmajer, K., Birkelund, T., Aellen, M., 1974. Revision of Triassic stratigraphy of the Scoresby Land and Jameson Land region, East Greenland. Meddelelser om Grønland, 193.
Peng, Y., Yu, J., Gao, Y., and Yang, F., 2006. Palynological assemblages of non-marine rocks at the Permian–Triassic boundary, western Guizhou and eastern Yunnan, South China. Journal of Asian Earth Sciences 28, 291-305, doi:10.1016/j.jseaes.2005.10.007
Piasecki, S., 1984. Preliminary palynostratigraphy of the Permian–Lower Triassic sediments in Jameson Land and Scoresby Land, East Greenland. Bulletin of the Geological Society of Denmark 32, 139-144.
Piasecki, S., and Stemmerik, L., 1991. Late Permian anoxia in central East Greenland. In: Tyson, R.V., Pearson, T.H. (Eds.), Modern and Ancient Continental Shelf Anoxia. Geological Society Special Publications, 275-290.
Pruss, S.B., and Bottjer, D.J., 2005, The reorganization of reef communities following the end-Permian mass extinction. Comptes Rendus Palevol 4, 553-568.
Raup, D.M., and Sepkoski, J.J., 1982. Mass extinction in the marine fossil record. Science 215, 1501-1503.
Renne, P.R., Zhang, Z., Richards, M.A., Black, M.T., Basu, A.R., 1995. Synchrony and causal relations between Permian-Triassic Boundary Crisis and Siberian Flood Volcanism. Science 269, 1413-1416.
Retallack, G.J., 1995. Permian-Triassic life crisis on land. Science 267, 77-80.
Retallack, G.J., and Krull, E.S., 2006. Carbon isotopic evidence for terminal-Permian methane outbursts and their role in extinctions of animals, plants, coral reefs, and peat swamps. Geological Society of America Special Paper 399, 249-268.
Retallack, G.J., and Jahren, A.H., 2008. Methane release from igneous intrusion of coal during Late Permian extinction events. The Journal of Geology 116, 1-20.
Retallack, G.J., Sheldon, N.D., Carr, P.F., Fanning, M., Thompson, C.A.,Williams, M.L., Jones, B.G., Hutton, A., 2011. Multiple Early Triassic greenhouse crises impeded recovery from Late Permian mass extinction. Palaeogeography, Palaeoclimatology, Palaeoecology 308, 233-251, doi:10.1016/j.palaeo.2010.09.022
Romano, C., Goudemand, N., Vennemann, T.W., Ware, D., Schneebeli-Hermann, E., Hochuli, P.A., Brühwiler, T., Brinkmann, W., Bucher, H., 2013. Climatic and biotic upheavals following the end-Permian mass extinction. Nature Geoscience 6, 57-60, doi: 10.1038/ngeo1667
Sanson-Barrera, A., Hochuli, P.A., Bucher, H., Schneebeli-Hermann, E., Weissert, H., Adatte, T., Bernasconi S.M, 2015. Late Permian–earliest Triassic high-resolution organic carbon isotope and palynofacies records from Kap Stosch (East Greenland). Global and Planetary Change 133, 149-166, doi: 10.1016/j.gloplacha.2015.08.006
Sanson-Barrera, A., Bucher, H., Schneebeli-Hermann, Hochuli, P.A., E., Weissert, H., Bernasconi S.M. Late Permian –earliest Triassic organic carbon isotope: Correlations across East Greenland basins. Swiss Journal of Geosciences (in review).
Geochemistry
Schneebeli-Hermann, E., Kürschner, W.M., Hochuli, P.A., Bucher, H., Ware, D., Goudemand, N. & Roohi, G., 2012. Palynofacies analysis of the Permian–Triassic transition in the Amb section (Salt Range, Pakistan): Implications for the anoxia on the South Tethyan Margin. Journal of Asian Earth Sciences 60, 225-234.
Schneebeli-Hermann, E. and Bucher, H., 2015. Palynostratigraphy at the Permian-Triassic boundary of the Amb section, Salt Range, Pakistan. Palynology 39, 1-18, doi: 10.1080/01916122.2014.921648.
Seidler, L., Steel, R., Stemmerik, L., Surlyk, F., 2004. North Atlantic marine rifting in the Early Triassic: new evidence from East Greenland. Journal of the Geological Society 161, 583-592, doi: 10.1144/0016-764903-063
Sephton, M.A., Visscher, H., Looy, C.V., Verchovsky, A.B., Watson, J.S., 2009. Chemical constitution of a Permian-Triassic disaster species . Geology 37, 875-878.
Sepkoski, J.J., 1984. A kinetic model of Phanerozoic taxonomic diversity. III. Post-Palaeozoic families and mass extinctions. Paleobiology 10, 246-267.
Spina, A., Cirilli, S., Utting, J., Jansonius, J, 2015. Palynology of the Permian and Triassic of the Tesero and Bulla sections (Western Dolomites, Italy) and consideration about the enigmatic species Reduviasporonites chalastus. Review of Palaeobotany and Palynology 218, 3-14.
Steiner, M.B., Eshet, Y., Rampino, M.R., and Schwindt, D.M., 2003. Fungal abundance spike and the Permian-Triassic boundary in the Karoo Supergroup (South Africa). Palaeogeography. Palaeoclimatology. Palaeoecology 194, 405-414, doi:10.1016/S0031-0182(03)00230-X
Stemmerik, L., 1998. Diagenesis of Upper Carboniferous shallowmarine carbonates, North Greenland. American Association of Petroleum Geologists 1998 Annual Meeting. American Association of Petroleum Geologists and Society of Economic Paleontologists and Mineralogists.
Stemmerik, L., Bendix-Almgreen, S.E., Piasecki, S. 2001. The Permian–Triassic boundary in central East Greenland: past and present views. Bulletin of the Geological Society of Denmark 48, 159-167.
Spath, L.F., 1935. Additions to the Eotriassic invertebrate faunas of East Greenland. Meddelelser om Grønland 98.
Surlyk, F., 1990. Timing, style and sedimentary evolution of Late Palaeozoic–Mesozoic extensional basins of East Greenland. In: Hardman, R.F.P., Brooks, J. (Eds.), Tectonic Events Responsible for Britain's Oil and Gas Reserves, 107-125.
Surlyk, F., Piasecki, S., Rolle, F., Stemmerik, L., Thomsen, E., Wrang, P., 1984. The Permian Basin of East Greenland. In Petroleum geology of the North European Margin, 303-315. Norwegian Petroleum Society.
Surlyk, F., Piasecki, S., Rolle, F., Scholle, P.A., Stemmerik, L., Thomsen, E., 1986. The Permian of the western margin of the Greenland Sea — a future exploration target. In: Halbouty,M.T. (Ed.), Future Petroleum Provinces of theWorld. American Association of Petroleum Geologists, 629-659.
Svensen, H., Planke, S., Polozov, A.G., Schmidbauer, N., Corfu, F., Podladchikov, Y., Jamtveit, B., 2009. Siberian gas venting and the end-Permian environmental crisis. Earth and Planetary Science Letters 277, 490-500.
Teichert, C., and Kummel, B., 1972. Permian–Triassic Boundary in the Kap Stosch Area, East Greenland. Bulletin of Canadian Petroleum Geology 20, 659-675.
Tewari, R., Awatar, R., Pandita, S.K., McLoughlin, S., Agnihotri, D., Pillai, S.S.K., Singh, V., Kumar, K., Bhat, G.D., 2015. The Permian-Triassic palynological transition in the Guryul Ravine section, Kashmir, India: implications for Tethyan-Gondwana correlations. Earth Science Reviews 149, 53-66.
Trümpy, R., 1961. Triassic of East Greenland. Geology of the Arctic. University of Toronto Press, Toronto, 248-254.
Twitchett, R.J., Looy, C.V., Morante, R., Vissher, H.,Wignall, P.B., 2001. Rapid and synchronous collapse of marine and terrestrial ecosystems during the end-Permian biotic crisis. Geological Society of America 29, 351-354.
Visscher, H., Brinkhuis, H., Dilcher, D.L., Elsik, W.C., Eshet, Y., Looy, C.V., Rampino, M.R., Traverse, A., 1996. The terminal Paleozoic fungal event: Evidence of terrestrial ecosystem destabilization and collapse. Proceedings of the National Academy of Sciences 93, 2155-2158.
Visscher, H., Sephton, M.A., Looy, C.V., 2011. Fungal virulence at the time of the end-Permian biosphere crisis?. Geology 39, 883-886.
Ware, D., Bucher, H., Brayard, A., Schneebeli-Hermann, E., Brühwiler, T., 2015. High-resolution biochronology and

diversity dynamics of the Early Triassic ammonoid recovery: The Dienerian faunas of the Northern Indian Margin. Palaeogeography, Palaeoclimatology, Palaeoecology 440, 363-373, doi:10.1016/j.palaeo.2015.09.013.
Wignall, P.B., and Twitchett, R.J., 1996. Oceanic anoxia and the end Permian mass extinction. Science 272, 1155-1158.
Wignall, P.B., and Twitchett, R.J., 2002. Extent, duration, and nature of the Permian-Triassic superanoxic event. Geological Society of America Special Paper 356, 395-413.
Wignall, P.B., Bond, D.P.G., Sun, Y., Grasby, S.E., Beauchamp, B., Joachimsky, M.M., Blomeier, D.P.G., 2015. Ultra-shallow-marine anoxia in an Early Triassic shallow-marine clastic ramp (Spitsbergen) and the suppression of benthic radiation. Geological Magazine 1-16, doi:10.1017/S0016756815000588.
Wordie, J.M., 1927. The Cambridge expedition to East Greenland in 1926. Geological Journal 75, 225-265.
Yuan, D.X., Chen, J., Zhang, Y.C., Zheng, Q.F., Shen, S.Z., 2015. Changhsingian conodont succession and the end-Permian mass extinction event at the Daijiagou section in Chongqing, Southwest China. Journal of Asian Earth Sciences 105, 234-251, doi:10.1016/j.jseaes.2015.04.002.
Zhang, Y., Zhang, K.X., Shi, G.R., He, W.H., Yuan, D.X., Yue, M.L., Yang, Ting-Lu., 2014. Restudy of conodont biostratigraphy of the Permian–Triassic boundary section in Zhongzhai, southwestern Guizhou, South China. Journal of Asian Earth Sciences 80, 75-83, doi:10.1016/j.jseaes.2013.10.032.

Chapter 1

Late Permian–earliest Triassic high-resolution organic carbon isotope and palynofacies records from Kap Stosch (East Greenland)

Anna Sanson-Barrera, Peter A. Hochuli, Hugo Bucher, Elke Schneebeli-Hermann, Helmut Weissert, Thierry Adatte, Stefano M. Bernasconi

published in Global and Planetary Change
http://dx.doi.org/10.1016/j.gloplacha.2015.08.006

Global and Planetary Change 133 (2015) 149–166

Contents lists available at ScienceDirect

Global and Planetary Change

journal homepage: www.elsevier.com/locate/gloplacha

Late Permian–earliest Triassic high-resolution organic carbon isotope and palynofacies records from Kap Stosch (East Greenland)

Anna Sanson-Barrera [a,*], Peter A. Hochuli [a], Hugo Bucher [a,b], Elke Schneebeli-Hermann [a], Helmut Weissert [b], Thierry Adatte [c], Stefano M. Bernasconi [b]

[a] Paleontological Institute and Museum, University of Zurich, Zurich, Switzerland
[b] Department of Earth Sciences, ETH Zurich, Zurich, Switzerland
[c] Institute of Earth Sciences, University of Lausanne, Lausanne, Switzerland

ARTICLE INFO

Article history:
Received 15 December 2014
Received in revised form 28 July 2015
Accepted 5 August 2015
Available online 7 August 2015

Keywords:
East Greenland
Latest Permian
Earliest Triassic
$\delta^{13}C_{org}$ record
Particulate organic matter
Carbon cycle

ABSTRACT

During and after the end Permian mass extinction terrestrial and marine biota underwent major changes and reorganizations. The latest Permian and earliest Triassic is also characterized by major negative carbon isotope shifts reflecting fundamental changes in the carbon cycle. The present study documents a high-resolution bulk organic carbon isotope record and palynofacies analysis spanning the latest Permian–earliest Triassic of East Greenland. An almost 700 meter thick composite section from Kap Stosch allowed discriminating 6 chemostratigraphic intervals that provide the basis for the correlation with other coeval records across the world, and for the recognition of basin wide transgressive–regressive events documenting tectonic activity during the opening of the Greenland–Norway Basin. The identification of the main factors that influenced the organic carbon isotope signal during the earliest Triassic (Griesbachian to Dienerian) was possible due to the combination of bulk organic carbon isotope, palynofacies and Rock-Eval data. Two negative carbon isotopic shifts in the Kap Stosch record can be correlated with negative shifts recorded in coeval sections across the globe. A first negative shift precedes the base of the Triassic as defined by the first occurrence of the conodont *Hindeodus parvus* in the Meishan reference section, and the second one coincides with the suggested Griesbachian–Dienerian boundary. This new organic carbon isotope record from the extended Kap Stosch section from the Boreal Realm documents regional and global carbon cycle signals of the interval between the latest Palaeozoic and the onset of the Mesozoic.

1. Introduction

The Permian–Triassic boundary interval is characterized by a synchronous negative excursion in organic and inorganic carbon records on a world-wide scale (e.g., Magaritz et al., 1988; Holser et al., 1989; Oberhänsli et al., 1989; Payne et al., 2004; Hermann et al., 2011). High-magnitude disturbances in the carbon cycle are known to continue throughout the entire Early Triassic. Based on organic and inorganic carbon isotopes, as well as on palynological and faunal evidence, several authors demonstrate the occurrence of severe environmental perturbations during the Early Triassic (Krull et al., 2000; de Wit et al., 2002; Payne et al., 2004; Brayard et al., 2006, 2009; Galfetti et al., 2007a,b; Hochuli et al., 2010a,b; Retallack et al., 2011; Hermann et al., 2011, 2012; Romano et al., 2012). However, expanded and well-preserved Early Triassic records are rare and are essential for the reconstruction of a comprehensive picture of environmental changes, both at global and regional scales. The most recent radio-isotopic ages show that the Early Triassic represents a time interval of about 5 million years (Ovtcharova et al., 2006; Galfetti et al., 2007a; Burgess et al., 2014; Baresel et al., 2015). Therefore the drastic environmental disturbances reflected in the carbon isotope and paleontological records took place during a relatively short time. Even more dramatic are changes within the lower part of this interval represented by the first two substages of the Early Triassic (Griesbachian and Dienerian) representing less than 1 million years (Ovtcharova et al., 2006; Galfetti et al., 2007a; Burgess et al., 2014; Baresel et al., 2015). High-resolution records of the carbon cycle are essential to fully assess the timing and potential causes and effects of the environmental conditions in the aftermath of the end-Permian extinction event.

The biogeochemical cycle of carbon is a complex interaction between the organic and inorganic carbon pools. Some geochemical signatures stored in the sea water and/or atmosphere, such as the CO_2 isotopic composition, can be recorded as biogeochemical proxies in

* Corresponding author at: Paleontological Institute and Museum, University of Zurich, Karl Schmid-Strasse 4, CH-8006 Zurich, Switzerland.
E-mail addresses: anna.sanson@pim.uzh.ch (A. Sanson-Barrera), peter.hochuli@pim.uzh.ch (P.A. Hochuli), hugo.fr.bucher@pim.uzh.ch (H. Bucher), elke.schneebeli@pim.uzh.ch (E. Schneebeli-Hermann), helmut.weissert@erdw.ethz.ch (H. Weissert), Thierry.Adatte@unil.ch (T. Adatte), stefano.bernasconi@erdw.ethz.ch (S.M. Bernasconi).

http://dx.doi.org/10.1016/j.gloplacha.2015.08.006
0921-8181/

the sediments and can be used as accurate stratigraphic markers. Carbon isotope stratigraphy is based on changes in the isotopic composition of carbonate and organic matter. After sorting out regional effects and artefacts from the record, the shifts reflecting the global carbon cycle represent a powerful stratigraphic tool (Weissert et al., 2008) for precise correlations of records from different areas and different depositional settings.

Understanding of the Early Triassic environmental instability has been traditionally based on moderate resolution records mainly from low latitude carbonate platforms in the Tethyan Realm (e.g., Clemmensen et al., 1984; Holser et al., 1989; Oberhänsli et al., 1989; Baud et al., 1996; Morante, 1996). Nevertheless in the last decade an increasing number of high-resolution studies were published, leading to a more widespread representation of Early Triassic records, attempting to shed light onto this critical time period (e.g., Payne et al., 2004; Galfetti et al., 2007a,b; Grasby and Beauchamp, 2008; Hermann et al., 2010, 2011; Algeo et al., 2012; Grasby et al., 2012; Clarkson et al., 2013).

The present study of material from Kap Stosch (Hold-with-Hope, East Greenland) provides a detailed bulk organic carbon isotope ($\delta^{13}C_{org}$) record combined with palynofacies and Rock-Eval analyses. The two latter are used to establish the respective contributions of terrestrial and marine origin to the bulk organic matter, allowing to differentiate between regional and global carbon signals expressed in the bulk isotopic data. The essentially siliciclastic succession of Griesbachian and Dienerian age from Kap Stosch provides so far the most expanded $\delta^{13}C_{org}$ and palynofacies records documented world-wide for this time interval with two horizons with marine fauna providing biostratigraphic tie points. This high-resolution record of an almost 700 m thick section has been correlated with other records from East Greenland (Stemmerik et al., 2001; Twitchett et al., 2001), as well as from the Norwegian Trøndelag and Finnmark platforms (Hermann et al., 2010), from Arctic Canada (Grasby and Beauchamp, 2008; Grasby et al., 2012), South China (Cao et al., 2002), and the United Arab Emirates (Clarkson et al., 2013).

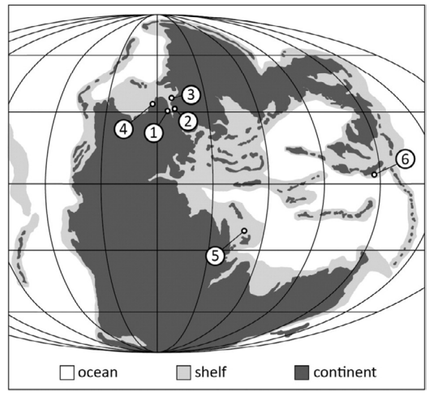

Fig. 1. Global paleogeographic reconstruction for the Early Triassic after Blakey (2012) and location of the study area and other areas used for correlation: (1) East Greenland, (2) Trøndelag Platform, (3) Finnmark Platform, (4) Arctic Canada, (5) Musandam Peninsula, and (6) South China.

2. Geological setting

2.1. Overview of the Permian–Triassic paleogeography and lithostratigraphy of East Greenland

During Permian and Triassic times East Greenland was located in Northwest Pangea, on the western margin of a rift basin separating Greenland from Norway (Fig. 1). During the Late Permian and Early Triassic the N–S oriented Greenland–Norway Basin was about 400 km wide (Doré, 1991). The reactivation of Late Carboniferous–Early Permian basin margin faults during the latest Permian–earliest Triassic, and the associated crustal extension created several sub-basins on both margins, which led to the deposition of thick siliciclastic sedimentary sequences (Surlyk, 1990; Peacock et al., 2000; Bugge et al., 2002; Seidler et al., 2004; Hamann et al., 2005; Oftedal et al., 2005).

Sedimentary rocks exposed along the East Greenland coast represent an ideal area for studying Upper Permian–Lower Triassic sequences (Fig. 2A). Wordie (1927) was the first to document rocks of Permian–Triassic age in the Kap Stosch area. Subsequently, several studies dealt with general Permian–Triassic stratigraphy and paleontology (Koch, 1931; Nielsen, 1935), with the biostratigraphic subdivision of the Permian–Triassic beds based on ammonoids (Spath, 1935; Trümpy, 1961; Bjerager et al., 2006), and with palynology (Balme, 1979; Piasecki, 1984). More detailed lithostratigraphic descriptions of the formations were published by Perch-Nielsen et al. (1974), Surlyk et al. (1986), and Surlyk (1990). Numerous studies focused on the Permian–Triassic boundary (PTB) of East Greenland (Teichert and Kummel, 1972; Looy et al., 2001; Stemmerik et al., 2001; Twitchett et al., 2001; Wignall and Twitchett, 2002), and on the Greenland–Norway Basin evolution (Surlyk et al., 1984; Surlyk, 1990; Stemmerik, 1998; Seidler et al., 2004; Hamann et al., 2005; Müller et al., 2005; Oftedal et al., 2005).

The Late Permian lithostratigraphic succession of East Greenland comprises the Foldvik Creek Group with the Huledal, Karstryggen, Ravnefjeld, Wegener Halvø, and Schuchert Dal formations. The latest Permian–earliest Triassic succession consists of the Wordie Creek and the Pingo Dal formations (Fig. 3) (Perch-Nielsen et al., 1974; Surlyk et al., 1986; Surlyk, 1990). The Permian Huledal Formation resting unconformably on Carboniferous deposits is composed of alluvial conglomerates including the onset of marine influence in its uppermost part. It is overlain by the marine hypersaline carbonates and evaporites of the Karstryggen Formation. Both the Huledal and the Karstryggen formations are of Capitanian age (Surlyk et al., 1986). In areas representing basin margins and paleo-highs the Karstryggen Formation is overlain by carbonate build-ups of the Wegener Halvø Formation. Black bituminous mudstones deposited in basinal areas have been defined as Ravnefjeld Formation, which contains bivalves (*Posidonia permica*), fishes (Nielsen, 1935) and few cephalopods (Perch-Nielsen et al., 1974). Abundant fauna such as brachiopods, crinoids and corals are known from the Wegener Halvø Formation.

Both formations are of Wuchiapingian age (Surlyk et al., 1986; Surlyk, 1990; Piasecki and Stemmerik, 1991). A Changhsingian relative sea-level fall and an increased siliciclastic supply led to the deposition of the grey-black, silty, bioturbated mudstones and sandstones of the Schuchert Dal Formation (Surlyk et al., 1986; Piasecki and Stemmerik, 1991). A latest Permian relative sea-level fall and an increase in rifting activity coincide with the deposition of the Wordie Creek Formation (Surlyk, 1990). This formation, represented by a thick sequence of siliciclastics influenced by a rapidly fluctuating sea-level rise, was deposited during the latest Changhsingian to Dienerian time interval (Surlyk, 1990; Oftedal et al., 2005). Basin geometry, facies, and thickness of the Wordie Creek Formation vary from one sub-basin to another, reflecting the strong tectonic control on deposition (Seidler et al., 2004). In northern sub-basins (e.g., Hold-with-Hope; Fig. 2A) the high sedimentation rates, and the marked lateral thickness variations of the main sandstone bodies of the deltaic deposits indicate steep basin margins during the latest Permian–earliest Triassic (Oftedal et al., 2005). The deposition of the Wordie Creek Formation has been interpreted to represent the rift climax stage of the Greenland–Norway Basin (Clemmensen, 1980; Seidler et al., 2004; Oftedal et al., 2005). In some

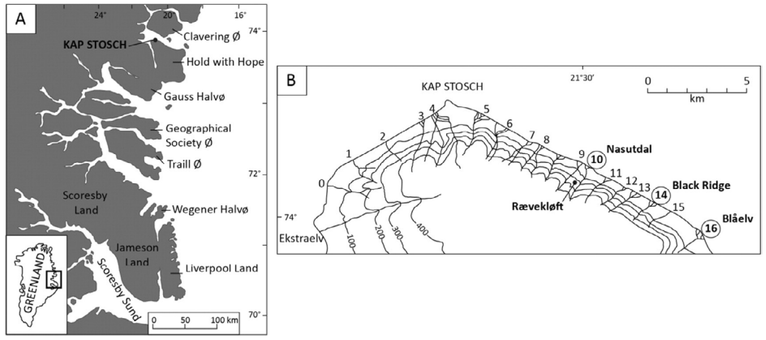

Fig. 2. A — East Greenland coast between latitudes 70°N to 74°30′N, location of the study area and other important sites (modified from Seidler et al., 2004). B — Kap Stosch area and the sampled sections: Black Ridge (river 14), Blåelv (river 16), Nasutdal (river 10), and Rævekløft (between river 9 and 10). Numbers of rivers according to Koch (1931) (modified from Teichert and Kummel, 1972).

areas the base of the Wordie Creek Formation is marked by transgressive plurimetric conglomerate beds (Surlyk et al., 1984; Wignall and Twitchett, 2002; Seidler et al., 2004; Oftedal et al., 2005), and continues with the deposition of marine shales and mudstones with some intercalated sandstones and thin conglomerate beds. In the northern sub-basins this formation consists essentially of marine mudstones and shoreface sandstones, changing in its uppermost part to tidally influenced shallow marine siltstones and sandstones. In the southern sub-basins (e.g., Jameson Land; Fig. 2A) it is dominated by marine silts with increasing turbiditic input up section (Surlyk et al., 1984). The Pingo Dal Formation represents the top of the earliest Triassic basin infill. In the northern sub-basins its lower and its upper part are dominated by dark red, usually cross-bedded sandstones, while its middle part consists of red, pink and yellowish to white or variegated arkoses and arkosic conglomerates and breccias. In many localities were both, the Wordie Creek and the Pingo Dal formations are exposed, there is a gradual transition between the two formations (Perch-Nielsen et al., 1974).

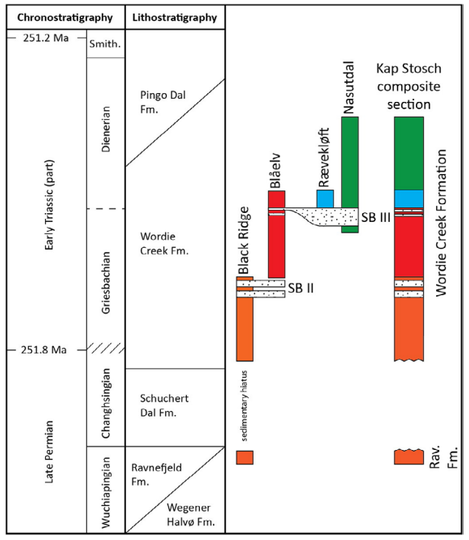

Fig. 3. Chrono- and lithostratigraphy of the Late Permian–earliest Triassic of Kap Stosch, based on Perch-Nielsen et al. (1974) and Bjerager et al. (2006). Vertical scale is arbitrary. Sampled sections – Black Ridge (orange), Blåelv (red), Nasutdal (green), and Rævekløft (blue) – and their relative stratigraphic position in the composite section. The two regional sandstone bodies SB II and SB III defined by Nielsen (1935) were used for the correlation of the sections during field work. The Permian–Triassic boundary interval is marked by a diagonal lines area, and the Griesbachian–Dienerian boundary is marked with a dashed line. The ages are inferred from U/Pb dating of zircons, 251.8 million years for the Permian–Triassic boundary (Burgess et al., 2014) and 251.2 million years for the Early Smithian (Galfetti et al., 2007a). (For interpretation of the references to colour in this figure legend, the reader is referred to the web version of this article.)

2.2. Lithostratigraphy of the Hold-with-Hope sub-basin

At Kap Stosch, on the Hold-with-Hope peninsula, Upper Permian–lowermost Triassic sequences are exposed between 73°60′N–21°12′W and 74°04′N–21°43′W. Several creeks numbered by Koch (1931) cut through the succession (Fig. 2B). Subsequently, Koch's numbering was used by Nielsen (1935) and Teichert and Kummel (1972).

This paper presents a composite section comprising about 700 m of sediments of Late Permian to earliest Triassic age from Kap Stosch (Fig. 3). The lowermost portion of the section comprises the basinal Ravnefjeld Formation, which is unconformably overlain by the deltaic sequence of the Wordie Creek Formation. The latter displays a general shallowing upward trend with coastal deposits near the top of the sequence. Two major sandstone bodies (SB II and SB III) defined and mapped by Nielsen (1935) can be easily followed in the field and allow for regional correlations. Sandstone interfingering with conglomerate foreset beds of a delta constitutes the lower part of SB II and massive sandstone beds characterize its upper part. On the other hand, SB III and other minor sandstone beds show cm- to plurimetric-scale channel-like structures that thin laterally towards the Southeast. General trends in grain size, sedimentary structures and thickness of SB II and SB III indicate a WNW–ESE direction of transport of the clastic material. In order to optimally cover the complete Late Permian to earliest Triassic interval, four sections (Black Ridge, Blåelv, Rævekløft, and Nasutdal) have been sampled at high-resolution (Fig. 3 and Supplementary data 1, 2, and 3).

The Black Ridge section (River 14) comprises 110 m of Upper Permian and lowermost Triassic sediments. The first 7 m of the section correspond to the Ravnefjeld Formation of Wuchiapingian (Late Permian) age. Dark and thin bedded siltstones and shales intercalated with

some limestone beds are the dominant lithologies. The unconformably overlying Wordie Creek Formation consists of dark grey and greenish siltstones intercalated with cm- to dm-scale sandstone beds. At some places small lenses of ~20-cm thick conglomerate underlie the base of the Wordie Creek Formation. In the uppermost part of the Black Ridge section, two sandstone bodies of about 20 and 10 m respectively, which are separated by six meters of siltstones with intercalated cm-scale sandstone beds, correspond to SB II. Above SB II this section ends with seven meters of siltstones, and is covered above. So far no age-diagnostic macrofossils have been observed within this section (Supplementary data 1).

The Blåelv section (River 16) comprises about 400 m of sediments of the Wordie Creek Formation. The accessible part of the section starts about five meters above SB II. Pods of gypsum have been locally observed immediately above SB II. The section is mainly composed of dark grey and greenish siltstones with intercalations of cm- to plurimetric-scale sandstone beds. About 60 m above the base, there is a 20-meter thick interval of reddish siltstone beds ending with a sharp change to grey coloured beds. Towards the top of the section another increase in reddish over grey siltstone beds has been observed. Near the base of the section ammonoids belonging to the *Ophiceras commune* zone (Bjerager et al., 2006) are abundant, providing a first robust ammonoid age control (Supplementary data 1). Two horizons with extraformational, rounded pebbles are found at around 180 and 430 m. They are interpreted as spill-overs of coarse material transported through distributary channels that were embedded in the fine grained and laminated sediments of the bottom lobes of the delta. Thin sandstone beds around 230 m above the base of the Blåelv section correspond to SB III. Near the top of the section, at around 370 m, there are two beds containing the bivalve *Claraia* sp. (Supplementary data 1).

The Rævekløft section is located between the rivers 9 and 10 starting immediately above SB III. It comprises about 50 m of dark grey-green siltstones and mudstones intercalated with cm-thick sandstone beds. It represents the most completely exposed interval above SB III, thus complementing the Nasutdal (see below) and Blåelv sections. It includes beds with the ammonoid *Bukkenites rosenkrantzi*, the common bivalve *Claraia* sp., and the gastropod *Naticopsis* sp. (Brayard et al., 2015) (Supplementary data 2). The ammonoids are characteristic of the *B. rosenkrantzi* zone and provide a second robust ammonoid age control (Bjerager et al., 2006).

The Nasutdal section (River 10 and adjacent western ridge) comprises an approximately 400-meter thick sequence representing the upper part of the composite section. The base of this section has been logged in River 10, and it consists of 38 m of siltstones with intercalated sandstone beds. At this location the overlying SB III is about 60 meter thick. The section above SB III was sampled on the western ridge adjacent to river 10. This section consists of dark grey-green siltstones intercalated with cm- to plurimetric-scale sandstone beds. Ammonoids (*B. rosenkrantzi*), the bivalve *Claraia* sp. and the gastropod *Naticopsis* sp. (Brayard et al., 2015) were found about 30 m above SB III. From the middle part towards the top of the section there is a gradual increase of reddish siltstones and sandstones. In the middle part of the section, a ca. 50-cm thick bed contains abundant, poorly-preserved plant remains. Two beds in the upper part of the section contain bivalves. The upper one contains fragments of *Promyalina* sp. and other unidentified bivalves, while in the lower one none of the bivalves could be identified. Between these two beds a few isolated metric-scale build-ups of microbial limestone have been observed. The plant remains, the bivalve beds, and the microbial limestone build-ups occur within the two *Anodontophora* zones (Bjerager et al., 2006). The topmost part of the Nasutdal section with predominance of red sandstones and siltstones probably reflects the transition between the marine Wordie Creek and the terrestrial Pingo Dal formations. However, the presence of acritarchs in the uppermost samples suggests a marine depositional environment up to the top of the section (Supplementary data 3).

2.3. The Permian–Triassic boundary in East Greenland

In East Greenland the PTB has traditionally been placed at the lithostratigraphical boundary between the Schuchert Dal and the Wordie Creek formations based on ammonoid zones (Tozer, 1994; Trümpy, 1961). In areas were the Schuchert Dal Formation is missing, the PTB has been interpreted to fall within a significant subaerial erosional hiatus (Birkenmajer, 1977; Seidler, 2000; Stemmerik et al., 2001). Thus, at Kap Stosch the PTB was described as an unconformable boundary between the Ravnefjeld and the Wordie Creek formations (Nielsen, 1935; Teichert and Kummel, 1972).

Paleontological data from conformable but rather poorly exposed PTB sections from Jameson Land describe the end-Permian extinction horizon in the top most part of the Schuchert Dal Formation (Oberhänsli et al., 1989; Stemmerik et al., 2001; Twitchett et al., 2001), and locate the PTB, based on the first occurrence (FO) of the conodont *Hindeodus parvus*, about 20 m above the base of the Wordie Creek Formation (Twitchett et al., 2001). They correlated their geochemical $\delta^{13}C_{org}$ and $\delta^{13}C_{carb}$ data from this area with the PTB Global Stratotype Section and Point (GSSP) at Meishan in China (Jin et al., 2000; Yin et al., 2001). In Jameson Land the $\delta^{13}C_{org}$ and $\delta^{13}C_{carb}$ negative excursion is located above the extinction event, but below the FO of *H. parvus*. Therefore, according to the $\delta^{13}C$ records and paleontological data from Jameson Land, the onset of the Wordie Creek Formation deposition begins during the late Changhsingian (Stemmerik et al., 2001; Twitchett et al., 2001).

3. Materials and methods

From the Kap Stosch sections a total of 605 samples were collected. In order to ensure sufficient amounts of organic matter for the analyses of bulk organic carbon isotope, palynofacies and Rock-Eval, sampling focused on grey-green siltstones to fine sandstone beds. A comparatively small number of samples from reddish siltstones were collected for comparison.

To analyse the bulk organic carbon isotope composition, all samples were finely ground and treated with 3 N HCl for at least 24 h to remove all carbonates. The residue was homogenized and analysed with a ThermoFisher Flash-EA 1112 elemental analyser coupled with a Conflo IV interface to a ThermoFisher Delta V isotope ratio mass spectrometer (IRMS). Isotope ratios are reported in the conventional δ-notation with respect to V-PDB (Vienna Pee Dee Belemnite) standard. The system was calibrated with NBS22 ($\delta^{13}C = -30.03$) and IAEA CH-6 ($\delta^{13}C = -10.46$). Reproducibility of the measurements is better than ±0.15‰. The organic carbon isotope data of the four sampled sections have been used to recognize tie points and overlaps, to ensure an accurate correlation and produce a robust composite section.

Palynofacies analysis has been performed on 162 samples to cover the entire record at a medium resolution. The samples have been crushed to mm-size pieces and treated with 3 N HCl and 70% HF to remove all carbonate and silicate particles (Traverse, 2007). The residues were sieved with an 11 μm mesh screen and mounted on slides for the analysis of the particulate organic matter (POM). For each sample a minimum of 250 particles were counted using a transmitted light microscope. The organic particles have been classified into 10 categories: amorphous organic matter (AOM), marine palynomorphs (Prasinophyceae and acritarchs), membranes, degraded terrestrial organic matter (DTOM), terrestrial palynomorphs (pollen grains and spores), cuticles, translucent woody particles, fungal remains, opaque woody particles, and inertinite. In order to calculate the marine/terrestrial ratio, two categories account for the marine fraction (AOM and marine palynomorphs), whereas seven categories account for the terrestrial fraction (DTOM, terrestrial palynomorphs, cuticles, translucent and opaque woody particles, fungal remains, and inertinite). The POM classified as membranes includes flat, structured or unstructured, thin-walled particles of unclear origin, i.e., algal and land plant

tissues. In the present study membranes are excluded from the marine/terrestrial ratio. In contrast to membranes, cuticles show distinct structures of land plant leaves. POM classified as DTOM includes degraded organic matter with residual structures revealing its terrestrial origin. These structures also differentiate DTOM from AOM, which is structureless under the transmitted light microscope (Tyson, 1995).

Rock-Eval analysis has been performed on 120 samples. About 100 mg of ground and homogenized sample was subject to pyrolysis followed by the complete oxidation of the residual sample. A flame ionization detector measured the hydrocarbon released during pyrolysis, while CO_2 and CO were detected by infrared absorbance during both steps. In the applied standard cycle for the whole rock analysis (IFP, 2001), pyrolysis started isothermally at 300 °C for 3 min, after that the sample was heated to 650 °C. The oxidation step started isothermally at 400 °C (3 min) and then heated up to 850 °C. Organic carbon decomposition resulted in four main peaks: peak S1 (hydrocarbons released during the isothermal phase), peak S2 (hydrocarbons produced between 300 and 650 °C), peak S3 (CO_2 from pyrolysis of organic matter up to 400 °C), peak S4 (CO_2 released from residual organic matter below ca. 550 °C during the oxidation step), and peak S5 (CO_2 released above ca. 550 °C during the oxidation step). These peaks were used to calculate the amount of total organic carbon (TOC, 0.082 (S1 + S2) + S4/10), the hydrogen index (HI, S2/TOC), and the oxygen index (OI, S3/TOC). The HI and OI data are proportional to the H/C and O/C ratios of the organic matter, respectively, and can be used for the classification of the organic matter in Van–Krevelen diagrams (Espitalié et al., 1985,1986). The relative errors associated with HI and OI of source rock samples do not exceed 1.5 and 10.5 of the measured values, respectively (Behar et al., 2001). Moreover, minerals such as calcium carbonate and clay minerals may artificially decrease HI values of Type II kerogen (Espitalié et al., 1984; Spiro, 1991). Despite these limitations, the use of HI and OI values are valuable since it allows the characterization of the same bulk organic material as that analysed for $\delta^{13}C_{org}$, by contrast to palynomorph assemblages (Sluijs and Dickens, 2012), which generally represent only a small fraction of the bulk organic carbon. The organic carbon isotope, HI, and marine/terrestrial ratio data have been correlated using the ordinary least squares method with the Past3 program.

4. Results

4.1. Organic carbon isotope ($^{13}C_{org}$) and palynofacies data

The composite section has been subdivided into 6 chemostratigraphic intervals based on marked shifts and trends observed in the $\delta^{13}C_{org}$ record. The relative abundances of the marine and terrestrial POM reflected in the palynofacies analysis are described for each interval (Fig. 4). Together the Black Ridge and Blåelv sections comprise the intervals 1–5 and the base of interval 6 (Supplementary data 1). The Rævekløft section comprises interval 5 (Supplementary data 2). The Nasutdal section includes part of interval 4, and intervals 5 and 6 (Supplementary data 3).

4.1.1. Interval 1

Interval 1 comprises the seven topmost meters of the Ravnefjeld Formation. It is characterized by $\delta^{13}C_{org}$ values around −23.7‰ ± 0.7‰. The boundary between interval 1 and 2 is marked by a negative shift of about 4‰ that correlates with the unconformity between the Ravnefjeld and the Wordie Creek formations. This unconformity corresponds to a change in lithology from dark mudstones with intercalated limestones to grey siltstones. A distinct purplish colour indicating subaerial weathering of the Ravnefjeld Formation beds marks the top of the unit. The marine POM is dominated by AOM around 50% and punctually up to 70%. The terrestrial fraction is represented by abundant opaque woody particles up to 70% and translucent woody particles up to 20%. The percentage of DTOM increases towards the top of the interval reaching values of around 30%. Within this interval terrestrial palynomorphs and acritarchs are regularly observed (Fig. 4 and Supplementary data 1).

4.1.2. Interval 2

The basal part of the Wordie Creek Formation is characterized by a negative trend observed over ca. 80 m of section with $\delta^{13}C_{org}$ values changing from −27‰ to −33‰ with an amplitude ranging from 2 to 4‰. This negative trend shows two $\delta^{13}C_{org}$ peaks, one at around 40 m (−32‰), and another at around 90 m (−33‰) above the base. The latter marks the top of the interval (Fig. 4 and Supplementary data 1). In comparison with the underlying Ravnefjeld Formation, POM assemblages of interval 2 show a distinct change. DTOM ranges from 20% to 60% within the interval 2, except at the very top were DTOM abundances are <10%. Terrestrial palynomorphs abundances reach values up to 20%, and membranes reach up to 10%. Marine palynomorphs are regularly observed. Opaque woody particles abundances are reduced to ca. 10%, and translucent woody particles are observed in relative quantities of less than 10%. AOM abundances vary from 10 to 60%. Changes in AOM and DTOM abundances are reflected in variable marine/terrestrial ratio values, with an overall increasing trend and values around 70% at the top of interval 2 (Fig. 4 and Supplementary data 1). Interval 2 ends within the siltstone beds intercalated in the SB II.

4.1.3. Interval 3

The base of interval 3 observed within the upper beds of SB II is represented by a rapid, positive shift from $\delta^{13}C_{org}$ values around −33‰ to −26‰ (Fig. 4 and Supplementary data 1). Subsequently, $\delta^{13}C_{org}$ values continue in a positive trend from −27‰ to −24‰ before they abruptly drop again to values around −32‰ within the last 7 m of the interval. At the base of the interval, beds containing ammonoids belonging to the *O. commune* zone have been found (Bjerager et al., 2006) (Fig. 4 and Supplementary data 1). POM assemblages are characterized by a dominance of terrestrial OM with high abundances of DTOM and common occurrence of opaque woody particles and terrestrial palynomorphs. At the base of the interval DTOM shows a distinct increase from ca. 20% to 40–50%, and an overall decrease of AOM from ca. 50% to 20%. At the top of the interval AOM abundances rise up to 90%, whereas DTOM abundances drop to <10%. Terrestrial palynomorph abundances show values between 10–20% and translucent woody particles ca. 10%. Opaque woody particles abundances increase from values around 10% to 40%. Terrestrial palynomorphs, translucent and opaque woody particles abundances drop close to 0% at the top of the interval. At the base of interval 3 the marine/terrestrial ratio decreases from 60% to 10%. The values remain around 10–20% in the middle part of the interval. Coinciding with the sharp $\delta^{13}C_{org}$ negative shift near the top of the interval there is a significant increase in the marine/terrestrial ratio reaching up to 80–90%.

4.1.4. Interval 4

Interval 4 corresponds to increasing $\delta^{13}C_{org}$ values from around −32‰ to −25‰ over almost 200 m of section, with high amplitude fluctuations up to 4‰. Interval 4 ends on top of SB III (Fig. 4 and Supplementary data 1 and 3). POM assemblages are dominated by AOM near the base, followed by AOM fluctuating values in the middle and terrestrial dominance towards the top. POM assemblages of the first 50 m show clear dominance of AOM up to 90–95% and DTOM values are mostly <10%, only occasionally reaching 20%. This results in a clear increase in the marine/terrestrial ratio up to values around 80–90%. Percentages of membranes, terrestrial palynomorphs, and opaque woody particles are close to 5%. In the middle part of the interval (from 200 to 280 m in Fig. 4) AOM decreases to values around 10–30% and then displays fluctuating values between 5–60%, while DTOM percentages increase up to ~40%, and shows also fluctuating values between 10% and 50%. Membranes and terrestrial palynomorphs percentages are around 10–15%, whereas translucent woody particles increase up to 10% and opaque woody particles up to 50%. In this part of the section

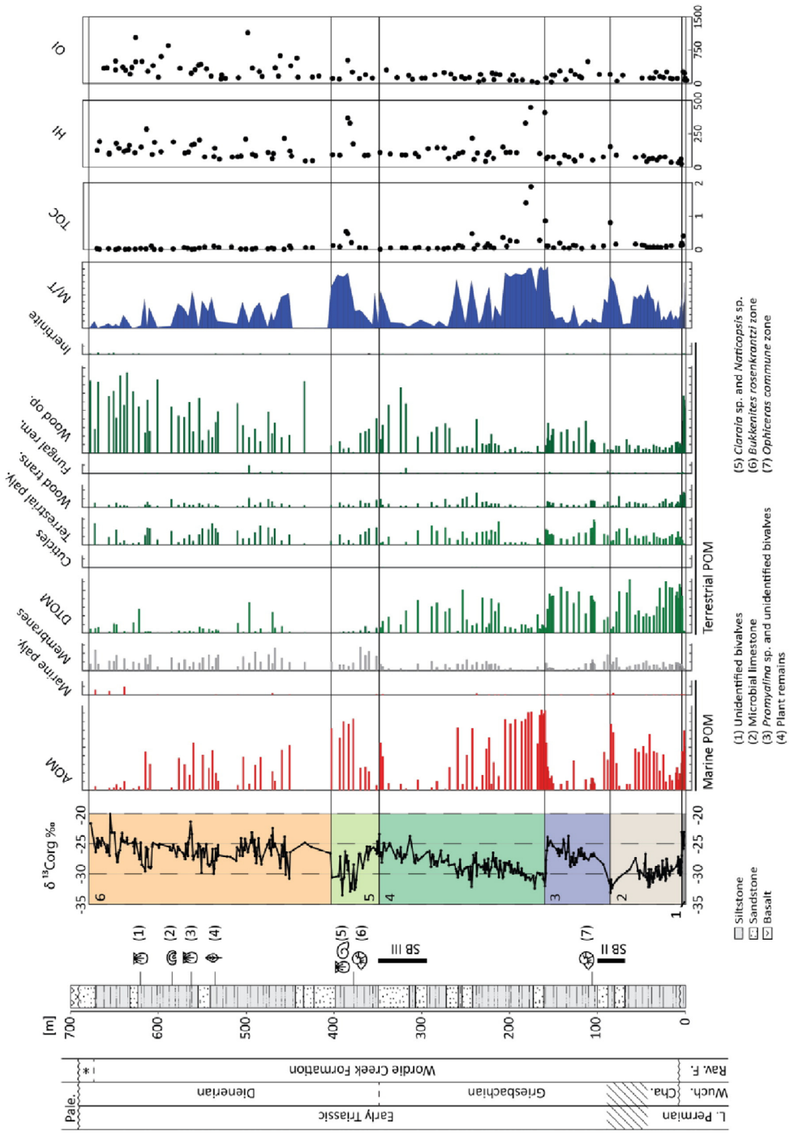

Fig. 4. Bulk organic carbon isotope, palynofacies, total organic carbon, hydrogen index, and oxygen index data of the Kap Stosch composite section. From left to right: chronostratigraphy, the Permian–Triassic boundary interval is marked by a diagonal lines area, and the Griesbachian–Dienerian boundary is marked with a dashed line, asterisk (*) refers to the Pingo Dal Formation, and Pale. refers to Paleogene; simplified lithology of the composite section; macrofossil content; bulk organic carbon isotope data ($\delta^{13}C_{org}$) with isotopic intervals (1 — black, 2 — beige, 3 — violet, 4 — dark green, 5 — light green, and 6 — orange); particulate organic matter expressed in %, each bar represents 10%, AOM — amorphous organic matter, marine palynomorphs, DTOM — degraded terrestrial organic matter, membranes, terrestrial palynomorphs, cuticles, translucent woody particles, fungal remains, opaque woody particles, inertinite (marine categories are in red, membranes in grey, and terrestrial categories in green); the marine/terrestrial ratio in dark blue; TOC — total organic carbon; HI — hydrogen index; and OI — oxygen index. (For interpretation of the references to colour in this figure legend, the reader is referred to the web version of this article.)

the marine/terrestrial ratio is alternating between low and high values reflecting the changing abundances of AOM and DTOM (Fig. 4). In the upper part of interval 4 (from 280 to 350 m in Fig. 4) POM assemblages show AOM abundances around 10%, increasing up to 50% in the uppermost portion of the interval. DTOM shows steady decreasing abundances from ca. 50% to <10%. Membranes and terrestrial palynomorphs abundances are <10%. Opaque woody particles show a significant increase from ~10% to 80%, followed by a decrease to ~20% in the topmost part of the interval. The marine/terrestrial ratios in this upper part of interval 4 are characterized by low values (between 10–20%), increasing up to 50–60% in the uppermost part of this interval (Fig. 4 and Supplementary data 1).

4.1.5. Interval 5

This interval is most completely exposed in the Rævekløft section. There is an overlap with the Blåelv and Nasutdal sections. $\delta^{13}C_{org}$ has been measured in all three sections (Fig. 3 and 4, and Supplementary data 1, 2 and 3). In the Rævekløft section interval 5 starts directly on top of SB III. $\delta^{13}C_{org}$ values show a negative trend changing from ca. −25‰ to −34‰, with increasing amplitude from 2‰ to 5‰. The most negative values coincide with the fossiliferous beds containing the ammonoid *B. rosenkrantzi*, the bivalve *Claraia* sp. and the gastropod *Naticopsis* sp. (Brayard et al., 2015). These beds consist of finely bedded dark green-grey siltstones alternating with mudstones. POM assemblages of this interval show an increase in AOM from 10% to 90%, resulting in a significant increase in the marine/terrestrial ratio. DTOM values fluctuate around 10%, and decrease to values around 1% at the top of the interval. Terrestrial palynomorphs and membranes percentages decrease from ca. 15–20% to 5%, and opaque woody particles from 40% to 10% (Fig. 4).

4.1.6. Interval 6

Interval 6 shows a positive trend of $\delta^{13}C_{org}$ values over the last 270 m of section, increasing from around −31‰ to −24‰. The base of this interval corresponds to a 40-meter thick sandy interval with relatively positive $\delta^{13}C_{org}$ values around −25‰. Due to the rare occurrence of siltstone layers, palynofacies data from only one sample is available (at around 430 m in Fig. 4). This POM assemblage is dominated by opaque woody particles (ca. 80%). Above this level POM assemblages show variable abundances of AOM between 60% to <10%, with an overall decreasing trend in the AOM abundance. At some levels in the upper part of the interval marine palynomorphs show values up to 10%. DTOM abundances vary between 30% to <10% and terrestrial palynomorphs between 25% to <10%. Translucent woody particles are usually represented in numbers below 10%, while opaque woody particles display an increasing trend from ca. 20% to almost 90% of the assemblage. The overall marine/terrestrial ratio fluctuates between 60% and <10%, with a decreasing trend to <10% at the top of the section. In the middle part of the interval, with $\delta^{13}C_{org}$ values fluctuating between −30‰ and −25‰, a ca. 50-cm thick sandy bed containing plant remains can be found (Fig. 4 and Supplementary data 3). At about 560 and 620 m there are two beds containing bivalves. The lower one contains the bivalve *Promyalina* sp. and other unidentified bivalves, and the upper one only unidentified bivalves (Fig. 4 and Supplementary data 3). The lower bivalve-bearing bed shows $\delta^{13}C_{org}$ values around −24‰, whereas the upper ones show values around −27‰. Between the two bivalve-bearing beds a few isolated patches of microbial limestone have been observed.

4.2. Rock-Eval pyrolysis data

The combination of organic carbon isotope and palynofacies data provides a good control of the origin of the POM. However, the finer fraction (<11 μm) of the total organic matter present in a sample is lost during the POM preparation (see Materials and Methods). Figs. 4 and 5 includes TOC, HI, and OI data from the Kap Stosch composite section. TOC values are generally very low, below 0.1%. Exceptionally, a few samples reach TOC values between 1% and 2%, at the boundary between interval 2 and 3 (ca. 90 m) and at the base of interval 4 (ca. 180 m). The HI follows a slight positive trend throughout the whole section from values ~50 to ~240 and punctually increasing up to ca. 450 at about 180 m above the base of the section (base of interval 4). The HI data show higher variability in the upper part of the section. The OI values scatter around 200 in the lower 400 m of the section, showing a small peak of ~500 at around 120 m above the base (interval 3). In the upper part of the section, from 400 to 680 m (interval 6), OI values show higher variation, between ca. 200 and 1000 (Fig. 4). The cross-plot between HI and OI displayed in Fig. 5a shows that the majority of the samples fall between OI values up to 600 and HI values up to 200. Just few samples show OI values above 600 and HI values above 200. The OI-TOC cross-plot (Fig. 5e) shows a negative logarithmic relationship. The highest TOC values yield the lowest OI values. On the other hand, the HI-TOC cross-plot shows a linear positive trend (Fig. 5f) with the highest TOC values corresponding to the highest HI data. The relation between $\delta^{13}C_{org}$ values and TOC and HI (Fig. 5c) shows a correspondence between the most negative $\delta^{13}C_{org}$ values and the highest HI and TOC values. Fig. 5d displays a linear relationship between the S2 and TOC, with S2 values ranging from 0 to 8. Samples with the highest TOC values (ca. 2%) show S2 values around 8. Finally, Fig. 5g represents the relation between the marine/terrestrial ratio and the HI. High HI values correspond to high marine/terrestrial ratios.

5. Interpretation and discussion

5.1. Controlling factors of the $\delta^{13}C_{org}$ record and significance of depositional environments

For the interpretation of a bulk organic carbon isotope record it is essential to understand which factors may influence the $\delta^{13}C_{org}$ values. In our record we identified the following.

5.1.1. Sampling and lithology

The sampling focused on grey-green siltstone and fine sandstone beds in order to ensure a sufficient amount of organic matter per sample. Few reddish siltstone beds have been sampled to avoid major gaps in the section and to assess the degree of preservation bias of the organic matter from deposits exposed to oxidation. In the studied section palynofacies of sandstone dominated intervals usually show a strong terrestrial signal reflected by high abundance of opaque woody particles, indicating increased oxidation and/or reworking of the organic matter (see Fig. 4). The most labile marine organic matter components (e.g., AOM) are prone to a faster degradation when exposed to oxic conditions; therefore refractory terrestrial organic matter particles are enriched in reddish beds. Conversely, palynofacies from siltstone dominated intervals commonly show assemblages of well-preserved mixed marine and terrestrial POM. The increase in red over grey siltstone and sandstone beds in the upper part of the section indicating well oxygenated marine conditions is also reflected in higher OI values.

5.1.2. Organic carbon pools

Marine and terrestrial organic matter has different ranges of carbon isotopic values, therefore the origin of the organic matter must be considered when interpreting bulk $\delta^{13}C_{org}$ records. Furthermore, the isotopic composition of the atmosphere and the isotopic composition of the dissolved carbon in the ocean have a direct influence on the isotopic composition of the organic matter accumulated in the sediments. Changes in the atmospheric and ocean carbon pools cause synchronous changes of different magnitude in the $\delta^{13}C_{org}$ values of the marine and terrestrial end-members (Weissert et al., 2008). In the studied material the marine/terrestrial ratio tends to follow the main trends and shifts of the $\delta^{13}C_{org}$ record (Fig. 4). In the observed pattern the most negative $\delta^{13}C_{org}$ values coincide with the highest marine/terrestrial ratios, and

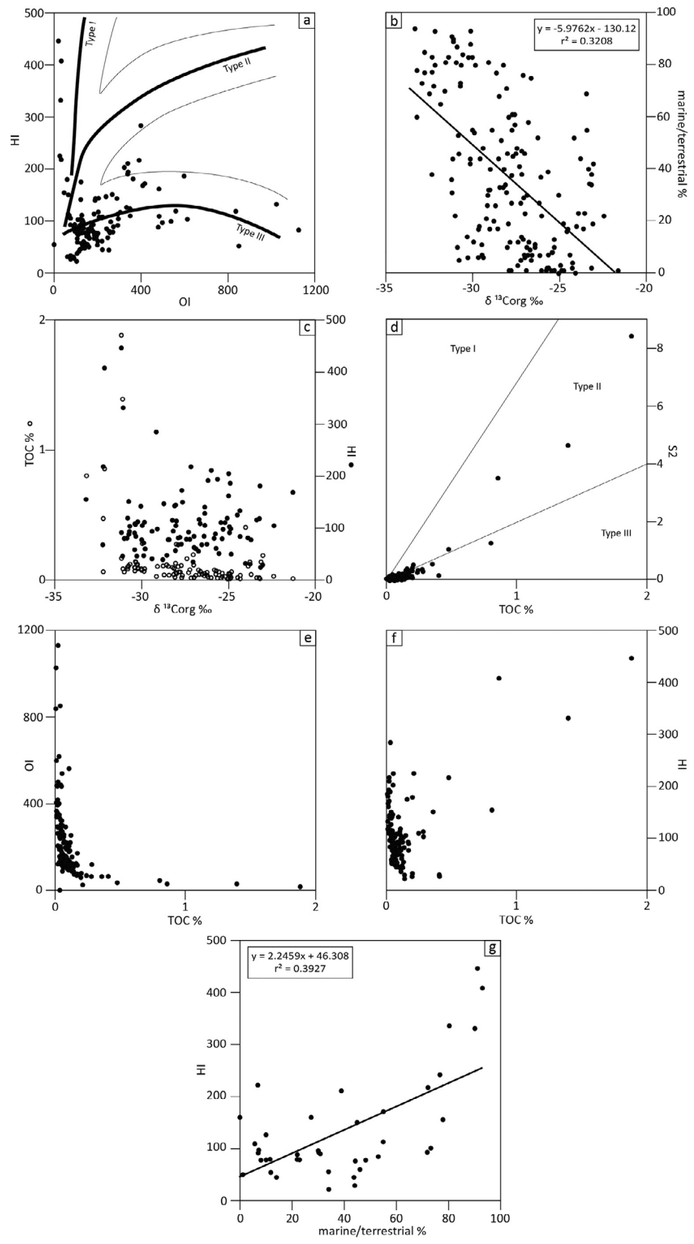

vice versa. For instance, in a cross-plot between the marine/terrestrial ratio and the $\delta^{13}C_{org}$ values with an r^2 value of ca. 1 would imply a total influence of the POM on the $\delta^{13}C_{org}$ values. Fig. 5b shows the cross-plot between the $\delta^{13}C_{org}$ values and the marine/terrestrial ratio of the Kap Stosch record. The samples scatter between $\delta^{13}C_{org}$ values of −21‰ and −33‰ and marine/terrestrial ratios between 0 and 95%. The regression line has an r^2 value of about 0.3, indicating that the origin of the POM influences the $\delta^{13}C_{org}$ signal partly. Additional vital effects in fractionation may explain the scatter of the data. However, considering the complexity of the studied system, an r^2 value of about 0.3 can be considered significant. Factors of global extent, such as the isotopic composition of the CO_2 and/or changes of the CO_2 concentrations in the atmosphere, are also affecting the carbon isotopic composition of marine and terrestrial organic matter. Another relevant correlation concerning the influence of the POM on the bulk organic carbon isotope values is shown in the cross-plot between the HI and the marine/terrestrial ratio (Fig. 5g). The regression line has an r^2 value of about 0.4, indicating some degree of correlation between high HI values and high marine/terrestrial ratio. Therefore, some bias in the organic carbon isotope values might be due to the origin of the POM. If changes in $\delta^{13}C_{org}$ values are measured without knowledge of concomitant POM data it will remain unclear whether variations are related to biotic or environmental changes. Although some authors question the validity of $\delta^{13}C_{org}$ curve for global correlations, several studies (e.g., Menegatti et al., 1998; Gröcke et al., 1999; Heimhofer et al., 2003; Weissert et al., 2008; Schneebeli-Hermann et al., 2013) show that $\delta^{13}C_{org}$ curves can be used for reliable chemostratigraphic correlations.

Most of the samples with TOC values below 0.15% show a strong terrestrial origin of the OM (kerogen type III) as seen in the HI/OI (Fig. 5a) and in the S2/TOC plots (Fig. 5d). The few samples showing TOC values between 0.15% and 2% fall within the kerogen type II field (Fig. 5d), indicating mixed marine-terrestrial derived origin of the OM (Tyson, 1995). The highest TOC values coincide with the highest marine/terrestrial ratios and the most negative $\delta^{13}C_{org}$ values (Fig. 5c). Samples with the most negative $\delta^{13}C_{org}$ and highest TOC and HI values (Fig. 5c) belong to kerogen type I and indicate marine origin of the OM (Fig. 5b). Therefore the strongest marine influence is documented at the base of interval 4 and on top of interval 5. However OI data from samples with low TOC values (<2%) are not reliable enough according to Cooper (1990) because low TOC values can yield a wide range of OI values (Fig. 5e). In the Kap Stosch record only samples with TOC values above 0.15% show low variability in the OI values. Due to the general low TOC values in the Kap Stosch record, only TOC data showing >0.15% values is considered to yield reliable information.

5.1.3. Relative sea-level and transgressive–regressive cycles

In the present study the combination of the marine/terrestrial ratio inferred from the POM assemblages and sedimentological observations are used to identify transgressive and regressive episodes. Decreasing or low marine/terrestrial ratios define regressive episodes, and conversely, increasing or high marine/terrestrial ratios reflect transgressive episodes. Applying this relationship, three transgressive–regressive (T–R) cycles in the Wordie Creek Formation are shown in Fig. 6. Interval 2 shows an overall increasing trend in the marine/terrestrial ratio and a parallel trend towards more negative $\delta^{13}C_{org}$ values. This interval is dominated by grey siltstones and includes the lower part of SB II. Interval 2 can be considered as a first transgressive episode (T1) in the studied section modulated by a short regressive phase (Fig. 6). A maximum flooding surface is interpreted at around 90 m. Almost the entire interval 3 is considered a regressive episode (R1 in Fig. 6). It shows a decreasing trend in the marine/terrestrial ratio and less negative $\delta^{13}C_{org}$ values. R1 includes the top part of SB II and the short interval above comprises lithologies with increasing reddish over grey sediment colour. Beds containing ammonoids belonging to the *O. commune* zone (Bjerager et al., 2006) are located within the lower part of this regressive episode. The top of interval 3 is characterized by a sharp shift in the marine/terrestrial ratio and in the $\delta^{13}C_{org}$ values (ca. −8‰). It is interpreted as a second transgressive episode (T2 in Fig. 6). A drastic change in the colour from reddish to grey siltstones occurs within T2 coinciding with a peak in TOC values up to ca. 2%. Interval 4 shows first high marine/terrestrial ratios, followed by variable ratios in the middle, and ending with low marine/terrestrial ratios coinciding with an overall decreasing trend of $\delta^{13}C_{org}$ values from ca. −32‰ to ca. −24‰. It has been interpreted as second regressive episode (R2 in Fig. 6). Grey coloured siltstones dominate at the onset of this regressive episode, while in the upper part there is an increase in reddish beds. The top of R2 is reached at the top of SB III at around 350 m. The third transgressive episode starts above SB III and includes interval 5 (T3 in Fig. 6). It is characterized by dark green-grey siltstones and mudstones intercalated with thin sandstone beds. This interval shows an increase in the marine/terrestrial ratio and a $\delta^{13}C_{org}$ negative trend decreasing from values of ca. −24‰ to ca. -34‰. This strong marine influence is also documented by the occurrence of the ammonoid *B. rosenkrantzi*, the bivalve *Claraia* sp., and the gastropod *Naticopsis* sp. (Brayard et al., 2015). Interval 6 starts with the deposition of a massive sandstone body, followed towards the top by grey and reddish siltstones with increasing predominance of reddish over grey coloured sediments. Oscillating marine/terrestrial ratios show a general decreasing trend and $\delta^{13}C_{org}$ values become more positive towards the top of the section. Thus interval 6 has been interpreted as a third regression episode (R3), which is modulated by short transgressive episodes.

The identification of three T–R cycles within the Wordie Creek Formation allows the interpretation of the Kap Stosch section in terms of depositional environments and basin evolution. The sedimentary sequence at Kap Stosch is characterized by shallow marine deltaic settings influenced by relative sea-level changes due to increased rifting activity (Teichert and Kummel, 1972; Surlyk, 1990; Oftedal et al., 2005). The deposition of the Wordie Creek Formation occurred partly during the synrift phase (Griesbachian) of the opening of the Greenland–Norway Basin (Surlyk et al., 1986; Seidler et al., 2004; Oftedal et al., 2005) and changes in the sedimentary sequence and depositional environment are reflected in the marine/terrestrial ratio (Fig. 6). In the present study, distal depositional environments are interpreted as transgressive episodes, while proximal depositional environments are interpreted as regressive episodes (Fig. 6).

The three above described T–R cycles of the Wordie Creek Formation are compared with studies of Triassic sequence stratigraphy in the Arctic (Fig. 7). For the Triassic six second-order sequence boundaries have been defined in the Sverdrup Basin (Embry, 1997). Correlation with other globally distributed Triassic sections allowed Embry to consider the second-order boundaries observed in the Sverdrup Basin as global sequence boundaries. Applying this scheme the sedimentary hiatus between the Ravnefjeld and the Wordie Creek formations, traditionally known as the PTB, can be related to the second-order sequence boundary located close to the PTB in the Sverdrup Basin (Embry, 1997) as shown in Fig. 7. According to this author the next sequence boundary was interpreted to be a third-order of latest Dienerian age. This excludes a correlation of the upper T–R cycles observed at Kap Stosch with any subsequent sequence defined by Embry (1997).

On the other hand, Skjold et al. (1998) defined five second-order sequence boundaries for the Triassic of the Southwest Barents Shelf.

Fig. 5. a — Oxygen index (OI) and hydrogen index (HI) cross-plot, and the kerogen types (I, II, and III) fields as defined in Tyson (1995); b — Marine/terrestrial ratio and organic carbon isotope values ($\delta^{13}C_{org}$) cross-plot inferred from the particulate organic matter counting from Kap Stosch; c — Total organic carbon (TOC, black dots), hydrogen index (HI, white dots), and organic carbon isotope values ($\delta^{13}C_{org}$) cross-plot; d — S2 and total organic carbon (TOC) cross-plot, and the kerogen types (I, II, and III) fields as defined in Tyson (1995); e — Oxygen index (OI) and total organic carbon (TOC) cross-plot; f — Hydrogen index (HI) and total organic carbon (TOC) cross-plot; g — Hydrogen index (HI) and marine/terrestrial record cross-plot.

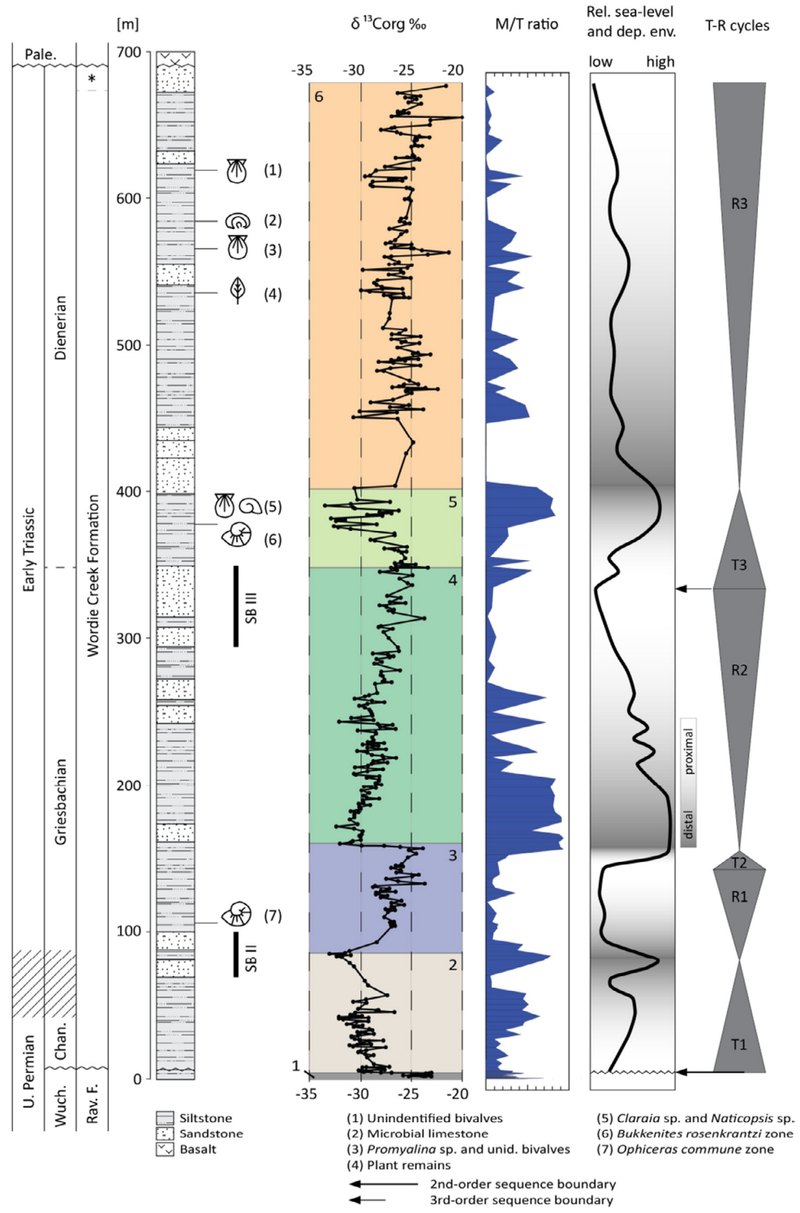

Their first second-order sequence boundary can also be correlated with the sedimentary hiatus between the Ravnefjeld and the Wordie Creek formations. Within this first second-order sequence (latest Permian to Spathian–Anisian in Fig. 7), Skjold et al. (1998) described five third-order sequences, of which the first two comprise the Griesbachian and the Dienerian, respectively (Fig. 7; T1-1 and T1-2 in Skjold et al., 1998). Thus, the first and the second T–R cycles from Kap Stosch fall within the range of the first third-order sequence of Griesbachian age (T1-1). The pronounced transgressive event T2 suggests a correlation with the maximum flooding surface of T1-1, and T3 might be correlated with the maximum flooding surface of the second third-order sequence of Dienerian age (T1-2 of Skjold et al., 1998) (Fig. 7).

Mørk et al. (1989) and Mørk and Smelror (2001) applied the sequence stratigraphic scheme of Embry and Podruski (1988), Embry (1997) to the Svalbard–Barents Shelf and to the Eastern Siberian successions. These authors recognized 10 transgressive episodes along the northern margin of Pangea during the Triassic. All of them are also recognizable in the Sverdrup Basin (Embry and Podruski, 1988; Mørk et al., 1989). Four of these episodes are well dated as earliest Griesbachian, earliest Smithian, earliest Anisian, and earliest Carnian, respectively and can be followed from the Arctic Canada (British Columbia and Sverdrup Basin) to Svalbard–Barents Shelf and to Eastern Siberia (Mørk, 1994). The earliest Griesbachian transgression can be correlated with the transgression in the basal part of the Wordie Creek Formation (T1, Fig. 7). A Dienerian transgression has been observed on Bjørnøya (Mørk et al., 1990) and on southernmost Spitsbergen (Worsley and Mørk, 1978; Nakrem and Mørk, 1991). This transgressive event seems to be coeval with T3 in the Kap Stosch section (Fig. 7) suggesting that T3 corresponds to an at least regional and probably eustatically controlled event (Mørk, 1994).

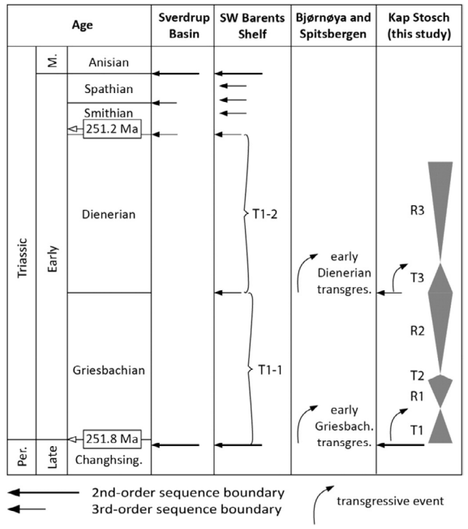

Fig. 7. Sequence stratigraphy scheme. Correlation of the Kap Stosch transgressive–regressive episodes of the Wordie Creek Formation with sequence stratigraphy studies of the Sverdrup Basin (Embry, 1997), the Barents Shelf (Skjold et al., 1998), Bjørnøya (Mørk et al., 1990) and southernmost Spitsbergen (Worsley and Mørk, 1978; Nakrem and Mørk, 1991). Vertical scale is arbitrary.

5.2. Comparison of the $\delta^{13}C_{org}$ record from Kap Stosch and $\delta^{13}C$ records from Jameson Land (East Greenland)

Correlations of $\delta^{13}C$ isotope records from various areas enable us to differentiate between regional (basin-wide) and global signals. Fig. 8 shows the correlation between two PTB sections in Jameson Land–East Greenland (Stemmerik et al., 2001; Twitchett et al., 2001) and the Kap Stosch section.

Two $\delta^{13}C_{org}$ records from stratigraphically complete sections from Fiskegrav (Jameson Land) cover the uppermost Permian Schuchert Dal Formation and the transition to the overlying Wordie Creek Formation (Stemmerik et al., 2001; Twitchett et al., 2001) (Fig. 8). The depositional environment at Fiskegrav has been described as bioturbated, grey offshore marine siltstones (Stemmerik et al., 2001). Biostratigraphic control of the latest Permian interval is provided by the spore peak marking the palynological PTB of Stemmerik et al. (2001), as well as faunal evidence including agglutinating foraminifera, brachiopods, and ammonoids (Stemmerik et al., 2001; Twitchett et al., 2001). Both $\delta^{13}C_{org}$ records from Jameson Land start with stable values around −24‰ in the Schuchert Dal Formation corresponding to values found in interval 1 in the Ravnefjeld Formation at Kap Stosch (Fig. 8). Due to the sedimentary gap, interval 1 ends in the unconformity at Kap Stosch. However, as recorded in Fiskegrav, stable $\delta^{13}C_{org}$ values around −24‰ continue in the overlying Schuchert Dal Formation (Stemmerik et al., 2001; Twitchett et al., 2001). The record of Stemmerik et al. (2001) shows an essentially continuous decrease from $\delta^{13}C_{org}$ values around −24‰ to around −29‰ in the upper part of the Schuchert Dal Formation. The end of this first decrease in the $\delta^{13}C_{org}$ values has been correlated with the base of interval 2 at Kap Stosch. A second drop to $\delta^{13}C_{org}$ values around −32‰ above the boundary between the Schuchert Dal and the Wordie Creek formations occurs within interval 2. The $\delta^{13}C_{org}$ record of Twitchett et al. (2001) also shows values of around −24‰ in the upper part of the Schuchert Dal Formation. Near the base of the Wordie Creek Formation the values drop to about −33‰ similarly to the two-step negative shift shown by Stemmerik et al. (2001). The base of interval 2 is correlated with the part with $\delta^{13}C_{org}$ values between −25‰ and −30‰. The $\delta^{13}C_{carb}$ record of Twitchett et al. (2001) follows the general trend of their $\delta^{13}C_{org}$ record and drops from about −4‰ to about −10‰ near the formational boundary. Compared to the $\delta^{13}C_{org}$ curve, the $\delta^{13}C_{carb}$ record includes slightly younger sediments showing a minor positive excursion to around −6‰ towards the top of the Fiskegrav section (Twitchett et al., 2001). The isolated occurrence of *H. parvus* reported by Twitchett et al. (2001) indicates a Griesbachian age for the upper part of interval 2 (Fig. 8) (Zhang et al., 2014; Brosse et al., 2015; Yuan et al., 2015). Both curves from Fiskegrav have been correlated with the GSSP PTB from Meishan (China) (Yin et al., 2001) and the end of the two-step negative shift has been interpreted as a global signal of the carbon cycle.

5.3. Comparison of the $\delta^{13}C_{org}$ record from Kap Stosch with other Early Triassic $\delta^{13}C$ records from the Boreal and Tethyan realms

Fig. 9 shows the correlation of five globally distributed $\delta^{13}C$ records, three from the Boreal Realm: Norway (Hermann et al., 2010; Hochuli et al., 2010b), and Arctic Canada (Grasby and Beauchamp, 2008; Grasby et al., 2012), as well as two Tethyan records, one from South China (Cao et al., 2002) and a $\delta^{13}C_{carb}$ record from United Arab Emirates (Clarkson et al., 2013).

Fig. 6. Transgressive–regressive cycles of Kap Stosch inferred from the particulate organic matter and interpretation of the depositional environments. From left to right: chronostratigraphy, the Permian–Triassic boundary interval is marked by a diagonal lines area, and the Griesbachian–Dienerian boundary is marked with a dashed line, asterisk (*) refers to the Pingo Dal Formation, and Pale. refers to Paleogene; simplified lithology of the composite section; macrofossil content; bulk organic carbon isotope data ($\delta^{13}C_{org}$) and isotopic intervals (as in Fig. 4); marine/terrestrial ratio in dark blue; relative sea-level variations (solid line) and interpreted depositional environment in grey-scale; transgressive (T) and regressive (R) episodes and sequence boundaries within the Wordie Creek Formation.

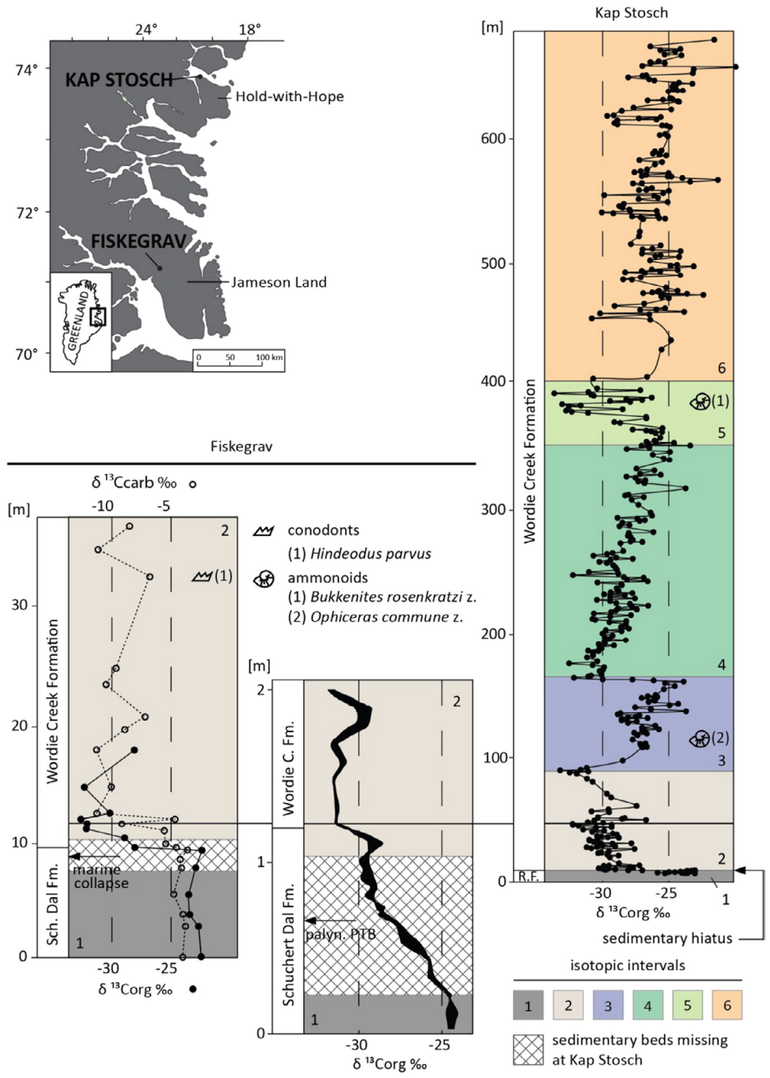

Fig. 8. Correlation of the $\delta^{13}C_{org}$ record from Kap Stosch with $\delta^{13}C$ records from Fiskegrav–Jameson Land (East Greenland), $\delta^{13}C_{org}$ and $\delta^{13}C_{carb}$ records on the left (Twitchett et al., 2001), and $\delta^{13}C_{org}$ record in the middle (Stemmerik et al., 2001). The end-Permian C-isotope negative shift is used as baseline.

5.3.1. Norway

A record covering the latest Permian to earliest Triassic interval has been published from shallow cores from the Finnmark Platform (Hermann et al., 2010; Hochuli et al., 2010b). The Permian part of this

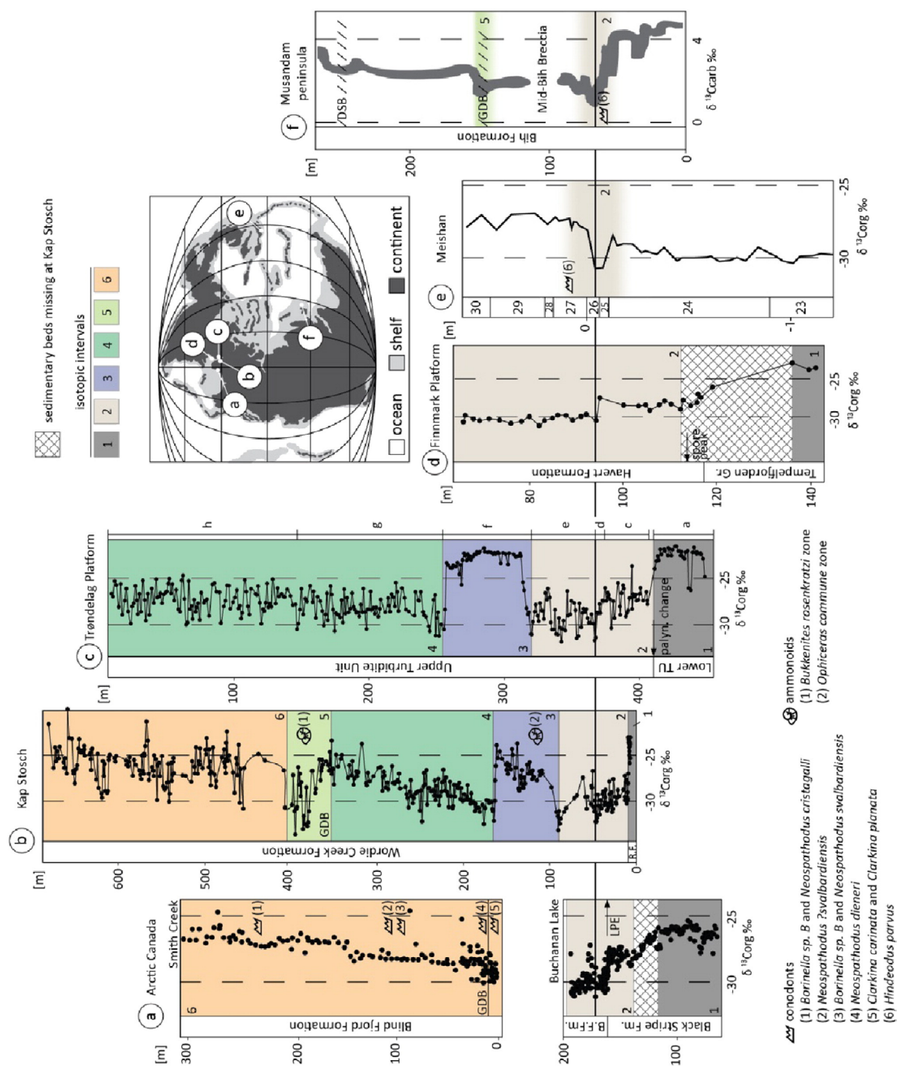

Fig. 9. Correlation of the $\delta^{13}C_{org}$ record from Kap Stosch with $\delta^{13}C$ records from other areas. Boreal Realm: Trøndelag and Finnmark platforms (Hermann et al., 2010), Arctic Canada (Grasby and Beauchamp, 2008; Grasby et al., 2012); Tethyan Realm: South China (Cao et al., 2002), and the Musandam Peninsula (Clarkson et al., 2013). LPE: Late Permian events, GDB: Griesbachian–Dienerian boundary, DSB: Dienerian–Smithian boundary. The end-Permian C-isotope negative shift is used as baseline.

record has been described as carbonates and siltstones deposited in shallow to outer shelf environment, while the Triassic part is interpreted as shallow, storm-influenced shelf deposits with alternating silty sandstones and sandstones (Bugge et al., 1995). From base to top it shows a two-step decrease of $\delta^{13}C_{org}$ values from about −24‰ to about −30‰. The base of the section with values of about −24‰ can be correlated with interval 1 from Kap Stosch. The interval of continuous decrease of the $\delta^{13}C_{org}$ values (from ca. −24‰ to ca. −29‰) observed over about 30 m in the Finnmark record is missing at Kap Stosch due to the sedimentary gap. The decrease in the $\delta^{13}C_{org}$ values below −30‰ characterizing the base of the Wordie Creek Formation (interval 2) at Kap Stosch can be observed in the Finnmark Platform (Fig. 9). This

pattern can also be recognized in the Trøndelag Platform (Hermann et al., 2010, see below), in Jameson Land (Stemmerik et al., 2001; Twitchett et al., 2001), and in Spitsbergen (Wignall et al., 1998). The spore peak observed in Jameson Land (Stemmerik et al., 2001) and on the Finnmark Platform (Hochuli et al., 2010b) falls between intervals 1 and 2. The Kap Stosch interval 2 correlates with the Finnmark section where the record shows $\delta^{13}C_{org}$ values around −29‰ and the second drop to values around −30‰ near the top of the section. So far the Finnmark Platform record represents the most complete and best resolved $\delta^{13}C_{org}$ dataset covering the PTB.

An expanded succession of Upper Permian–Lower Triassic has been recovered from the mid-Norwegian shelf (Trøndelag Platform). The sedimentary sequence has been interpreted to be a fully marine succession of sandstones, coarse-grained turbidites, shales and reworked sabkha (Bugge et al., 2002). It represents a thick sedimentary sequence similar to the one exposed at Kap Stosch according to Bugge et al. (2002). The Lower Turbidite Unit seems to be equivalent to the Ravnefjeld and Schuchert Dal formation in East Greenland, while the Upper Turbidite Unit corresponds to the Wordie Creek Formation (Fig. 9). A sedimentary gap has also been described between the two units (Bugge et al., 2002). Hermann et al. (2010) subdivided the $\delta^{13}C_{org}$ record of this section into eight intervals ("a" to "h"). Their curve is closely comparable with the one from Kap Stosch (Fig. 9). In both records the Late Permian section shows $\delta^{13}C_{org}$ values around −24‰ (Fig. 9; interval 1 from Kap Stosch and interval "a" in Hermann et al., 2010). These values are followed by a sharp drop in the $\delta^{13}C_{org}$ values, corresponding to the sedimentary hiatus. The Kap Stosch interval 2 corresponds to the interval between the sedimentary hiatus up to the base of the sharp positive $\delta^{13}C_{org}$ shift around 320 m corresponding to the intervals "c", "d", and "e" in the Trøndelag record (Hermann et al., 2010). The interval immediately above the sedimentary hiatus is characterized by $\delta^{13}C_{org}$ values around −27‰ followed by a decrease towards a minimum of ca. −32‰ at about 40 m above the hiatus (intervals "c" and "d" in Hermann et al., 2010). The top of interval "d" is correlated with the first $\delta^{13}C_{org}$ minimum within interval 2 at Kap Stosch, and interpreted to represent the global end-Permian negative shift. The upper part of interval 2 of the Kap Stosch record shows a decreasing trend while in the Trøndelag $\delta^{13}C_{org}$ record the values remain stable around −29‰ (interval "e" in Hermann et al., 2010). In the Kap Stosch section, the upper part of interval 2 is dominated by the sandstone beds of SB II, whereas in the Trøndelag Platform succession siltstones are the dominant lithology. Differences in the structure of the Greenland–Norway Basin may have led to different evolution of the depositional settings at the two margins, leading to different contributions of the marine and terrestrial POM fractions, as suggested by the $\delta^{13}C_{org}$ values and palynofacies records (Hermann et al., 2010). In the Kap Stosch section, interval 3 can be correlated with the Trøndelag interval "f" (Hermann et al., 2010). This interval is marked by the onset of a sharp $\delta^{13}C_{org}$ positive shift in both records, followed by a slight positive $\delta^{13}C_{org}$ trend at Kap Stosch and stable values in the Trøndelag record ending in both sections with a sharp negative $\delta^{13}C_{org}$ shift. In contrast to the hypothesis of Hermann et al. (2010), that the sharp shift in interval "f" might be due to a sedimentary gap, there are no sedimentological evidences for a hiatus, neither in the descriptions of the Trøndelag Platform well (Bugge et al., 2002) nor in the Kap Stosch section (Oftedal et al., 2005). The stable $\delta^{13}C_{org}$ values observed in the upper part of the Trøndelag section (intervals "g" and "h" in Hermann et al., 2010) can be correlated with interval 4 from Kap Stosch. However, interval 4 shows a positive $\delta^{13}C_{org}$ trend at Kap Stosch, whereas the Trøndelag $\delta^{13}C_{org}$ values are rather stable. Similar to interval 2, the data from interval 4 suggest some differences in the carbon burial dynamics between the two margins of the Greenland–Norway Basin.

5.3.2. Arctic Canada

Two sections from the Sverdrup Basin in the Arctic Canada spanning the latest Permian to the Early Triassic are compared with the Kap Stosch record (Grasby and Beauchamp, 2008; Grasby et al., 2012). The depositional setting in the Sverdrup Basin has been interpreted to represent a deep basin surrounded by shallow shelves dominated by carbonate and chert prior to the Late Permian events (LPE) (Grasby et al., 2012), and by clastic sediments in the lowermost Triassic (Grasby and Beauchamp, 2008). Intervals 1 and 2 can be correlated with the older section from Arctic Canada (Buchanan Lake) and the overall positive trend described as interval 6 at Kap Stosch is similar to the younger part of the Canadian section (Smith Creek) (Fig. 9). Parts of the Griesbachian, corresponding to the intervals 3–5, are missing in the Canadian record (Grasby et al., 2012). The Buchanan Lake record starts with $\delta^{13}C_{org}$ values around −26‰, which are slightly more negative than the Kap Stosch interval 1 values. Despite the generally lower values at Buchanan Lake the pattern of the $\delta^{13}C_{org}$ curves are very similar. Following interval 1 the Canadian record displays a decreasing $\delta^{13}C_{org}$ values from about −26‰ to −29‰. In the Kap Stosch record this negative trend is missing, falling within the sedimentary hiatus between the Ravnefjeld and the Wordie Creek formations. However, it can be observed in the more complete sections from Jameson Land (East Greenland) (Stemmerik et al., 2001; Twitchett et al., 2001), and from the Finnmark Platform (Hermann et al., 2010). In the Buchanan Lake record stable $\delta^{13}C_{org}$ values around −27‰ correspond to the onset of interval 2, followed by a pronounced decrease to $\delta^{13}C_{org}$ values to around −30‰. This minimum has been correlated with the global end-Permian carbon negative shift (Grasby and Beauchamp, 2008) and it corresponds to the first $\delta^{13}C_{org}$ minimum within interval 2 in the Kap Stosch record (Fig. 9).

For the younger Canadian record (Smith Creek) adequate age control could be obtained thanks to the common occurrence of conodonts and ammonoids. The fossil content of this section has been described by Tozer (1967), Baud et al. (2008), and Grasby and Beauchamp (2008). The Smith Creek record ranges from the latest Griesbachian to the late Smithian. For the purpose of correlation with Kap Stosch only part of this record has been reproduced in Fig. 9. At Kap Stosch the presence of the ammonoid *B. rosenkrantzi* near the top of interval 5 indicates an early Dienerian age (Fig. 8). For the basal part of the succession at Smith Creek the conodonts *Clarkina planata* and *Clarkina carinata* indicate a latest Griesbachian age, whereas *Neospathodus dieneri* and *Neospathodus svalbardensis* provide an earliest Dienerian age (Orchard, 2007). Thus based on conodont assemblages Grasby and Beauchamp (2008) placed the Griesbachian–Dienerian boundary (GBD) a few meters above the base of the Smith Creek section (Fig. 9). At Kap Stosch the occurrence of the Dienerian ammonoid *B. rosenkrantzi* within interval 5 suggests placing the GDB below these beds. Therefore the GDB has been tentatively placed at the boundary between interval 4 and 5 at Kap Stosch, coinciding with a pronounced turn in the $\delta^{13}C_{org}$ trend. Based only on the $\delta^{13}C_{org}$ data we correlate the Smith Creek record with the Kap Stosch interval 6. The protracted character of the Smith Creek record, and the gap between the latter and the Buchanan Lake record do not allow for precise correlations with Kap Stosch.

5.3.3. China

An attempt is made to correlate the record from Kap Stosch with the $\delta^{13}C_{org}$ record of the PTB GSSP at Meishan in China (Cao et al., 2002). The extremely condensed character of the Chinese section allows only the identification of the negative spike with $\delta^{13}C_{org}$ values around −31‰, and it is correlated with the first minimum $\delta^{13}C_{org}$ values in interval 2 (Fig. 9). Consequently, the FO of the conodont *H. parvus* used as marker for the PTB would fall within interval 2 in Kap Stosch, after the end-Permian $\delta^{13}C$ negative shift in Meishan.

5.3.4. United Arab Emirates

A $\delta^{13}C_{carb}$ curve from the Tethyan Realm representing a shallow marine carbonate record from the Musandam Peninsula spans the Late Permian–Early Triassic interval (Clarkson et al., 2013). Compared to the Kap Stosch record this data set comprises a comparable degree of

resolution of the carbon isotope data, including also conodont age control. The Musandam Peninsula record starts with an interval of relatively positive $\delta^{13}C_{carb}$ values around 4‰. This is followed by a sharp negative shift that reaches the lowest values (ca. 1‰) in the entire record. These negative values are correlated with the first minimum in the $\delta^{13}C_{org}$ values of the Kap Stosch record (interval 2). However, in the Musandam Peninsula record *H. parvus* – the marker of the PTB – appears shortly before the minimum values, suggesting that the FO of *H. parvus* is diachronous, as suggested in other studies (Korte et al., 2010; Zhang et al., 2014; Brosse et al., 2015; Yuan et al., 2015). Relying on the chemostratigraphic evidence and using the FO of *H. parvus* as official marker of the PTB, this boundary falls probably within interval 2 or might even be represented by the sedimentary gap at Kap Stosch. After the negative shift the $\delta^{13}C_{carb}$ values of the Musandam Peninsula record recover to ca. 2‰. A second negative shift is observed near the GDB (Clarkson et al., 2013). In the Kap Stosch section this event most likely coincides with the negative values of interval 5 interpreted as the GDB (Fig. 9).

5.4. Regional and global carbon cycle signals at Kap Stosch

The correlation with globally distributed carbon isotope records from the Late Permian–earliest Triassic allows differentiating regional and global carbon isotope signals in the $\delta^{13}C_{org}$ record at Kap Stosch. The most distinct features of the Kap Stosch and the Trøndelag Platform $\delta^{13}C_{org}$ records, representing the two margins of the Greenland–Norway Basin, such as the marked positive excursion and the subsequent fast decline (interval 3) have so far no equivalent in any other basin. Short-lived isotope excursions can be easily missed in coeval, low resolution records. Thus interval 3 is considered to reflect a distinct feature of the Greenland–Norway Basin. It is interpreted as a first abrupt regression, followed by a period of relative low sea-level and finally ending with an abrupt transgression. A Griesbachian synrift phase of the opening of the basin has been postulated by Seidler et al. (2004) and Oftedal et al. (2005). The correlation between the HI and the marine/terrestrial ratio in the Kap Stosch section (Fig. 5g) indicates that some degree of amplification in the most marine influenced parts of the $\delta^{13}C_{org}$ record has to be taken into account (e.g., the transgression on top of interval 3 or interval 5) (Suan et al., accepted for publication). Although interval 3 is interpreted as a regional carbon isotope signal, contribution of global carbon isotope variations cannot be completely dismissed. As summarized by Hermann et al. (2010) positive shifts close to the PTB have also been recorded in the $\delta^{13}C_{carb}$ records of Austria (Gartnerkofel, Holser et al., 1989) and China (Meishan, Xie et al., 2007). However, compared to the records in the Greenland–Norway Basin, the magnitude of the positive shifts is less pronounced in these sections, and the insufficient biostratigraphic control hampers the correlation of these isotopic events.

Two other features observed at Kap Stosch can be followed in different areas and are interpreted to represent variations of the global carbon cycle. The first is the negative shift in the carbonate and organic carbon values near the PTB. According to the chemostratigraphic correlations of the Kap Stosch section with sections with biostratigraphic control (Jameson Land, Musandam Peninsula and GSSP of Meishan), the base of the Triassic falls within the lowermost part of the Wordie Creek Formation (Fig. 4). Thus, the first negative shift within interval 2 can be considered as a global carbon cycle signal. A second negative shift (interval 5) interrupting the general positive trend observed in the upper part of the section (intervals 4–6) is located just below the beds containing the ammonoid *B. rosenkrantzi* of Dienerian age. This suggests a correlation with the negative shift in the $\delta^{13}C_{carb}$ record of the Musandam Peninsula at the base of the Dienerian (Clarkson et al., 2013). The following overall positive trend observed in the Dienerian of the latter record and in the record of the Canadian Arctic (Grasby et al., 2012) is similar to the one of interval 6 at Kap Stosch. The carbonate isotope record from South China (Payne et al., 2004) and the non-marine $\delta^{13}C_{org}$ record from Australia (Retallack et al., 2011) show a similar negative trend near the inferred base of the Dienerian. This leads to the conclusion that the shift of interval 5 represents a global negative isotope event close to the GDB.

5.5. Possible causes for the changing $\delta^{13}C_{org}$ patterns in the Kap Stosch record

The world-wide end-Permian negative carbon isotope excursion can be considered to be the first of several large perturbations of the Early Triassic carbon cycle (Payne et al., 2004; Galfetti et al., 2007a,b; Hermann et al., 2011, 2012; Retallack et al., 2005, 2011; Clarkson et al., 2013). Tethyan marine sections in South China, the North Indian Margin, and the Arabian Peninsula show major positive excursions across the Dienerian–Smithian, Smithian–Spathian, and Spathian–Anisian boundaries (Payne et al., 2004; Galfetti et al., 2007a; Hermann et al., 2012; Clarkson et al., 2013). A Gondwanan non-marine section from Australia (Retallack et al., 2011) also reported marked Early Triassic carbon cycle perturbations comparable to the marine records. Boreal sections from Spitsbergen (Galfetti et al., 2007b) and Arctic Canada (Grasby et al., 2012) show a positive excursion at the Smithian–Spathian boundary indicating that the Early Triassic carbon isotope variations are not restricted to the Tethyan realm. The magnitude of all carbonate and organic carbon isotope excursions is in the range of 4–8‰ during the latest Permian and Early Triassic.

The origin of the disturbances of the carbon cycle during the Early Triassic has been widely debated. A combination of several factors may explain the observed positive and negative excursions in the carbon records, rather than a single linear explanation (Payne and Kump, 2007). The Siberian large igneous province has been proposed to affect the stability of the carbon cycle during the Late Permian and Early Triassic (Renne et al., 1995; Berner, 2002; Reichow et al., 2009; Svensen et al., 2009). However, volcanic emissions alone would generate relatively small negative excursions in the carbon isotope record. Carbon isotope data of land plant cuticles show a negative shift illustrating a change in atmospheric carbon isotope composition across the PTB (Schneebeli-Hermann et al., 2013). Hence other sources of isotopically light carbon must have played an important role (Payne and Kump, 2007; Svensen et al., 2009). A hypothesis for the release of large amounts of ^{13}C-depleted carbon associated with the emplacement of the Siberian Trap is the metamorphism of organic-rich rock during volcanic intrusions (Svensen et al., 2009). Other concomitant factors that could cause negative carbon isotope excursions are marine productivity collapse caused by anoxia (Wignall and Twitchett, 1996), marine regression and oxidation of organic carbon on the exposed shelf (Holser et al., 1989), as well as destabilization of methane hydrates (Morante, 1996; Krull et al., 2004; Retallack and Krull, 2006). Sobolev et al. (2011) suggested that the Siberian Trap eruption alone could trigger the end-Permian mass extinction due to the massive degassing of CO_2 from recycled crust in the plume head. On the other hand, just a few mechanisms can explain rapid positive carbon isotope excursions since ^{13}C-rich sources are unknown. One mechanism could be an increase in organic carbon burial by increased primary productivity or increased preservation of organic matter under anoxic oceanic conditions (Kump and Arthur, 1999).

In the Kap Stosch record two global carbon isotope signals have been recognized. The negative shift within interval 2 has been correlated with the world-wide negative shift pre-dating the base of the Triassic (Figs. 8 and 9). This negative shift is recorded in carbonate and organic carbon isotope records world-wide with nearly the same magnitude. Simultaneous rapid negative excursions in inorganic and organic carbon must have been triggered by an event affecting both the marine and terrestrial carbon pools. The most recent dating indicates that the main stage of the Siberian Trap emplacement partially pre-dates and partially is synchronous with the end-Permian events; late volcanic eruptive stages occur later in the Early Triassic. Therefore, it could have triggered

the negative shift within interval 2 in the Kap Stosch record. The second global signal is the negative shift associated to the GDB (interval 5) (Fig. 9). The most negative values of the Kap Stosch record (ca. −33‰) are documented at the end of interval 5. Corresponding shifts have been recorded in other sections, such as in South China (Payne et al., 2004), Australia (Retallack et al., 2011), and in the Musandam Peninsula (Clarkson et al., 2013 in Fig. 9) documenting the global extent of this event. It can be explained by a renewed input of light carbon, probably from a further eruptive pulse of the Siberian Trap and/or the effect of positive feedbacks (e.g., destabilization of methane hydrates) due to previous eruptive pulses. The base of interval 3 of the Kap Stosch record and the base of interval "f" of the Trøndelag Platform record (Hermann et al., 2010) represent a very fast positive excursion (from ca. −32‰ to −26‰). A possible explanation is that the carbon isotope positive shift is regionally magnified by the tectonic activity of the Greenland–Norway Basin. Likewise the negative shift occurring at the top of interval 3 may reflect a combination of regional and global causes.

6. Conclusions

The high-resolution Late Permian–earliest Triassic bulk organic carbon isotope ($\delta^{13}C_{org}$) record from East Greenland combined with palynofacies and Rock-Eval data are correlated with other world-wide distributed sections. These correlations allow differentiating regional and global carbon isotope signals. The palynofacies and Rock-Eval analyses were performed for two purposes. Firstly, they were used to identify probable causes for the observed $\delta^{13}C_{org}$ variations, and secondly, they represent the basis for defining transgressive–regressive cycles. Key points in this study are:

1. The alternation of distal/proximal settings as indicated by palynofacies assemblages allowed the identification of three transgressive–regressive cycles within the Wordie Creek Formation at Kap Stosch. The transgressive–regressive cycles have been compared with the sequence stratigraphic scheme developed for the Sverdrup Basin in Arctic Canada and for the Norwegian Barents Shelf. The latest Permian sedimentary hiatus in the Kap Stosch section, formerly recognized as PTB, comprises the second-order sequence boundary defined close to the PTB in both areas, the Sverdrup Basin and Barents Shelf. The third-order sequence boundary, placed at the Griesbachian–Dienerian boundary in the Barents Shelf, correspond to the boundary between the second and third T–R cycle defined at Kap Stosch.
   - The subdivision of the $\delta^{13}C_{org}$ record from Kap Stosch into 6 chemostratigraphic intervals allowed the correlation with world-wide distributed carbon isotope records from the Boreal and Tethyan realms and the distinction between regional and global signals. Despite the fact that the marine/terrestrial ratio follows the general $\delta^{13}C_{org}$ trends, the origin of the organic matter is not the main driver of the $\delta^{13}C_{org}$ variations. The trends observed within the studied sections are summarized as follows:
   - Interval 1 shows positive and rather stable $\delta^{13}C_{org}$ values as documented from other PTB sections.
   - Interval 2 contains the world-wide synchronous $\delta^{13}C$ negative shift that is immediately followed by the FO of *H. parvus* in the Meishan GSSP section. Therefore, using the carbon isotope signal as a correlation tool between the GSSP reference section and East Greenland we suggest that the PTB should be placed ca. 50 m above the unconformity between the Ravnefjeld and the Wordie Creek formations implying a latest Permian (Changhsingian) age for the base of the Wordie Creek Formation. However, according to the FO of *H. parvus* documented by Clarkson et al. (2013) in the Musandam Peninsula section, the PTB falls below the world-wide $\delta^{13}C$ synchronous negative shift, suggesting diachronism of the FO of this marker with respect to global isotopic changes of the carbon cycle.
   - Interval 3 displays a positive and negative excursion by ca. 7‰ that can be correlated with the $\delta^{13}C_{org}$ record from the Trøndelag Platform. This feature shows that the opening of the Greenland–Norway Basin during the Griesbachian affected carbon burial of both margins similarly, resulting in a distinct regional component of the carbon isotope signal. However, a contribution of the global carbon cycle on these events cannot be completely excluded. Interval 4 shows a positive trend from $\delta^{13}C_{org}$ values ca. −32‰ to −25‰. So far the only comparable record for these two intervals comes from the Trøndelag Platform (Hermann et al., 2010).
   - The negative $\delta^{13}C_{org}$ shift defined as interval 5 is associated with the occurrence of the ammonoid *B. rosenkrantzi*. Based on the correlation of the Kap Stosch record with the $\delta^{13}C_{org}$ record of Arctic Canada and the $\delta^{13}C_{carb}$ record of the Musandam Peninsula, the Griesbachian–Dienerian boundary is tentatively placed at the boundary between the intervals 4 and 5.
   - Interval 6 showing an overall positive trend of $\delta^{13}C_{org}$ values from ca. −34‰ to −24‰ is correlative with the biostratigraphically calibrated Dienerian section from the Arctic Canada (Smith Creek), confirming a Dienerian age for the upper part of the Kap Stosch record.

Supplementary data to this article can be found online at http://dx.doi.org/10.1016/j.gloplacha.2015.08.006.

Conflict of interest statement

The authors declare that the research was conducted in the absence of any commercial or financial relationship that could be constructed as a potential conflict of interest.

Acknowledgements

The authors are very thankful to Madalina Jäggi-Berechet, Stewart Bishop, and Maria Coray from the Stable Isotope Laboratory of the Geology Department of the ETH Zurich for the bulk $\delta^{13}C_{org}$ analysis. Maximiliano Meier is thanked for his assistance during field work. We are also thankful to Richard Hofmann for his help with the bivalve identification, and to Steven D. Andrews and Audrey Decou for their comments and useful insights about East Greenland. Gunn Mangerud, Sofie Lindström, and an anonymous reviewer are thanked for the constructive reviews and improvements of the manuscript. We are in debt to Morten Bjerager and Stefan Piasecki for their help in the preparation of the project. The project was supported by the Swiss NSF project 20021-135446/1 to H. Bucher.

References

Algeo, T.J., Henderson, C.M., Ellwood, B., Rowe, H., Elswick, E., Bates, S., Lyons, T., Hower, J.C., Smith, C., Maynard, B., Hays, L.E., Summons, R.E., Fulton, J., Freeman, K.H., et al., 2012. Evidence for a diachronous Late Permian marine crisis from the Canadian Arctic region. Geol. Soc. Am. Bull. 124, 1424–1448. http://dx.doi.org/10.1130/B30505.1.

Balme, B.E., 1979. Palynology of Permian–Triassic Boundary beds at Kap Stosch, East Greenland. Medd. Grønland 200.

Baresel, B., Bucher, H., Brosse, M., Bagherpour, B., Schaltegger, U., 2015. High precision time calibration of the Permian–Triassic boundary mass extinction event in a deep marine context. EGU General Assembly, Vienna 12–17 April, Abstract Number EGU2015-10130. Geophysical Research Abstracts 17.

Baud, A., Atudorei, V., Sharp, Z., 1996. Late Permian and Early Triassic evolution of the Northern Indian margin: carbon isotope and sequence stratigraphy. Geodin. Acta 9, 57–77.

Baud, A., Nakrem, H.A., Beauchamp, B., Beatty, T.W., Embry, A.F., Henderson, C.M., 2008. Lower Triassic bryozoan beds from Ellesmere Island, High Arctic, Canada. Polar Res. 27, 428–440. http://dx.doi.org/10.1111/j.1751-8369.2008.00071.x.

Behar, F., Beaumont, V., De, B., Penteado, H.L., 2001. Technologie Rock-Eval 6: performances et développements. Oil Gas Sci. Technol. Rev. IFP 56 (2), 111–134.

Berner, R.A., 2002. Examination of hypotheses for the Permo-Triassic boundary extinction by carbon cycle modeling. Proc. Natl. Acad. Sci. U. S. A. 99, 4172–4177. http://dx.doi.org/10.1073/pnas.032095199.

Birkenmajer, K., 1977. Erosional unconformity at the base of marine Lower Triassic at Wegner Ø, Central East Greenland. Bull. Geol. Soc. Den. 25, 107–116.

Bjerager, M., Seidler, L., Stemmerik, L., Surlyk, F., 2006. Ammonoid stratigraphy and sedimentary evolution across the Permian–Triassic boundary in East Greenland. Geol. Mag. 143, 635–656. http://dx.doi.org/10.1017/S0016756806002020.

Blakey, R., 2012. Global Paleogeography. http://www2.nau.edu/rcb7/globaltext2.html (accessed March 2015).

Brayard, A., Bucher, H., Escarguel, G., Fluteau, F., Bourquin, S., Galfetti, T., 2006. The Early Triassic ammonoid recovery: paleoclimatic significance of diversity gradients. Palaeogeogr. Palaeoclimatol. Palaeoecol. 239, 374–395. http://dx.doi.org/10.1016/j.palaeo.2006.02.003.

Brayard, A., Escarguel, G., Bucher, H., Monnet, C., Brühwiler, T., Goudemand, N., Galfetti, T., Guex, J., 2009. Good genes and good luck: ammonoid diversity and the end-Permian mass extinction. Science 325, 1118–1121. http://dx.doi.org/10.1126/science.1174638.

Brayard, A., Meier, M., Escarguel, G., Fara, E., Nützel, A., Olivier, N., Bylund, K.G., Jenks, J.F., Stephen, D.A., Hautmann, M., Vennin, E., Bucher, H., 2015. Early Triassic Gulliver gastropods: spatio-temporal distribution and significance for biotic recovery after the end-Permian mass extinction. Earth Sci. Rev. 146, 31–64. http://dx.doi.org/10.1016/j.earscirev.2015.03.005.

Brosse, M., Bucher, H., Bagherpour, B., Baud, A., Frisk, A.M., Goudun, K., Goudemand, N., 2015. Conodonts from the Early Triassic microbialite of Guangxi (South China): implications for the definition of the base of the Triassic system. Palaeontology 58, 563–584. http://dx.doi.org/10.1111/pala.12162.

Bugge, T., Mangerud, G., Mørk, A., Nilsson, I., Elvebakk, G., Fanavoll, S., Vigran, J.O., 1995. The upper Paleozoic succession of the Finnmark Platform, Barents Sea. Nor. Geol. Tidsskr. 75, 3–30.

Bugge, T., Ringas, J.E., Leith, D.A., Mangerud, G., Weiss, H.M., Leith, T.L., 2002. Upper Permian as new play model on the mid-Norwegian continental shelf: investigated by shallow stratigraphic drilling. Am. Assoc. Pet. Geol. 86, 107–127.

Burgess, S.D., Bowring, S., Shen, S., 2014. High-precision timeline for Earth's most severe extinction. Proc. Nat. Acad. Sci. 111, 3316–3321. http://dx.doi.org/10.1073/pnas.1317692111.

Cao, C., Wang, W., Jin, Y., 2002. Carbon isotope excursions across the Permian–Triassic boundary in the Meishan section, Zhejiang Province, China. Chin. Sci. Bull. 47, 1125–1129.

Clarkson, M.O., Richoz, S., Wood, R.A., Maurer, F., Krystyn, L., McGurty, D.J., Astratti, D., 2013. A new high-resolution $\delta^{13}C$ record for the Early Triassic: insights from the Arabian Platform. Gondwana Res. 24, 233–242. http://dx.doi.org/10.1016/j.gr.2012.10.002.

Clemmensen, L.B., 1980. Triassic rift sedimentation and paleogeography of central East Greenland. Bull. Grønl. Geol. Unders. 139, 1–56.

Clemmensen, L.B., Holser, W.T., Winter, D., 1984. Stable isotope study through the Permian–Triassic boundary in East Greenland. Bull. Geol. Soc. Den. 33, 253–260.

Cooper, B.S., 1990. Practical Petroleum Geochemistry. Robertson Scientific, London.

de Wit, M.J., Ghosh, J.G., de Villiers, S., Rakotosolofo, N., Alexander, J., Tripathi, A., Looy, C., 2002. Multiple organic carbon isotope reversals across the Permo–Triassic boundary of terrestrial Gondwana sequences: clues to extinction patterns and delayed ecosystem recovery. J. Geol. 110, 227–240. http://dx.doi.org/10.1086/338411.

Doré, A.G., 1991. The structural foundation and evolution of Mesozoic seaways between Europe and the Arctic. Palaeogeogr. Palaeoclimatol. Palaeoecol. 87, 441–492. http://dx.doi.org/10.1016/0031-0182(91)90144-G.

Embry, A.F., 1997. Global sequence boundaries of the Triassic and their identification in the western Canada sedimentary basin. Bull. Can. Petrol. Geol. 45, 415–433.

Embry, A.F., Podruski, J.A., 1988. Third-order depositional sequences of the Mesozoic succession of Sverdrup Basin. In: James, D.A., Leckie, D.P. (Eds.), Sequences, Stratigraphy, Sedimentology: Surface and Subsurface. Canadian Society Petroleum Geologists Memoir 15, pp. 73–84.

Espitalié, J., Senga Makadi, K., Trichet, J., 1984. Role of the mineral matrix during kerogen pyrolysis. Org. Geochem. 6, 365–382.

Espitalié, J., Deroo, G., Marquis, F., 1985,1986. La pyrolyse Rock-Eval et ses applications. *Revue de l'Institut Français du Pétrole* 40 and 41.

Galfetti, T., Bucher, H., Ovtcharova, M., Schaltegger, U., Brayard, A., Brühwiler, T., Goudemand, N., Weissert, H., Hochuli, P.A., Cordey, F., Guodun, K., 2007a. Timing of the Early Triassic carbon cycle perturbations inferred from new U–Pb ages and ammonoid biochronozones. Earth Planet. Sci. Lett. 258, 593–604. http://dx.doi.org/10.1016/j.epsl.2007.04.023.

Galfetti, T., Hochuli, P.A., Brayard, A., Bucher, H., Weissert, H., Vigran, J.O., 2007b. Smithian–Spathian boundary event: evidence for global climatic change in the wake of the end-Permian biotic crisis. Geology 35, 291–294. http://dx.doi.org/10.1130/G23117A.1.

Grasby, S.E., Beauchamp, B., 2008. Intrabasin variability of the carbon–isotope record across the Permian–Triassic transition, Sverdrup Basin, Arctic Canada. Chem. Geol. 253, 141–150. http://dx.doi.org/10.1016/j.chemgeo.2008.05.005.

Grasby, S.E., Beauchamp, B., Embry, A., Sanei, H., 2012. Recurrent Early Triassic ocean anoxia. Geology 41, 175–178. http://dx.doi.org/10.1130/G33599.1.

Gröcke, D.R., Hesselbo, S.P., Jenkyns, H.C., 1999. Carbon–isotope composition of Lower Cretaceous fossil wood: ocean–atmosphere chemistry and relation to sea-level change. Geology 27, 155–158.

Hamann, N.E., Whittaker, R.C., Stemmerik, L., 2005. Geological development of the Northeast Greenland Shelf. In: Doré, A.G., Vining, B.A. (Eds.), *Petroleum Geology: North-West Europe and Global* Perspectives. Proceedings of the 6th Petroleum Geology Conference, Geological Society, London, pp. 887–902.

Heimhofer, U., Hochuli, P.A., Burla, S., Andersen, N., Weissert, H., 2003. Terrestrial carbon–isotope records from coastal deposits (Algarve, Portugal): a tool for chemostratigraphic correlation on an intrabasinal and global scale. Terra Nova 15, 8–13.

Hermann, E., Hochuli, P.A., Bucher, H., Vigran, J.O., Weissert, H., Bernasconi, S.M., 2010. A close-up view of the Permian–Triassic boundary based on expanded organic carbon isotope records from Norway (Trøndelag and Finnmark Platform). Glob. Planet. Chang. 74, 156–167. http://dx.doi.org/10.1016/j.gloplacha.2010.10.007.

Hermann, E., Hochuli, P.A., Méhay, S., Bucher, H., Brühwiler, T., Ware, D., Hautmann, M., Roohi, G., Ur-Rehman, K., Yaseen, A., 2011. Organic matter and palaeoenvironmental signals during the Early Triassic biotic recovery: the Salt Range and Surghar Range records. Sediment. Geol. 234, 19–41. http://dx.doi.org/10.1016/j.sedgeo.2010.11.003.

Hermann, E., Hochuli, P.A., Bucher, H., Ware, D., Weissert, H., Roohi, G., Yaseen, A., Brühwiler, T., Hautmann, M., 2012. Climatic oscillations at the onset of the Mesozoic inferred from palynological records from the North Indian Margin. J. Geol. Soc. 169, 227–237. http://dx.doi.org/10.1144/0016-76492010-130.

Hochuli, P.A., Vigran, J.O., Hermann, E., Bucher, H., 2010a. Multiple climatic changes around the Permian–Triassic boundary event revealed by an expanded palynological record from mid-Norway. Geol. Soc. Am. Bull. 122, 884–896. http://dx.doi.org/10.1130/B26551.1.

Hochuli, P.A., Hermann, E., Vigran, J.O., Bucher, H., Weissert, H., 2010b. Rapid demise and recovery of plant ecosystems across the end-Permian extinction event. Glob. Planet. Chang. 74, 144–155. http://dx.doi.org/10.1016/j.gloplacha.2010.10.004.

Holser, W.T., Schönlaub, H.P., Attrep Jr., M., Boeckelmann, K., Klein, P., Magaritz, M., Orth, C.J., Fenninger, A., Jenny, C., Kralik, M., Mauritsch, H., Pak, E., Schramm, J.M., Stattegger, K., et al., 1989. A unique geochemical record at the Permian/Triassic boundary. Nature 337, 39–44.

IFP, 2001. Rock-Eval 6 User's Guide. Institut Français de Pétrole, Rueil-Malmaison, France.

Jin, Y.G., Wang, Y., Wang, W., Shang, Q.H., Cao, C.Q., Erwin, D.H., 2000. Pattern of marine mass extinction near the Permian–Triassic boundary in South China. Science 289, 432–436.

Koch, L., 1931. Carboniferous and Triassic stratigraphy of East Greenland. Medd. Grønland 83.

Korte, C., Pande, P., Kalia, P., Kozur, H.W., Joachimski, M.M., Oberhänsli, H., 2010. Massive volcanism at the Permian–Triassic boundary and its impact on the isotopic composition of the ocean and atmosphere. J. Asian Earth Sci. 37, 293–311. http://dx.doi.org/10.1016/j.jseaes.2009.08.012.

Krull, E.S., Retallack, G.J., Campbell, H.J., Lyon, G.L., 2000. $\delta^{13}C_{org}$ chemostratigraphy of the Permian–Triassic boundary in the Maitai Group, New Zealand: evidence for high-latitudinal methane release. N. Z. J. Geol. Geophys. 43, 21–32.

Krull, E.S., Lehrmann, D.J., Druke, D., Kessel, B., Yu, Y., Li, R., 2004. Stable carbon isotope stratigraphy across the Permian–Triassic boundary in shallow marine carbonate platforms, Nanpanjiang Basin, south China. Palaeogeogr. Palaeoclimatol. Palaeoecol. 204, 297–315. http://dx.doi.org/10.1016/S0031-0182(03)00732-6.

Kump, L.R., Arthur, M.A., 1999. Interpreting carbon–isotope excursions: carbonates and organic matter. Chem. Geol. 161, 181–198. http://dx.doi.org/10.1016/S0009-2541(99)00086-8.

Looy, C.V., Twitchett, R.J., Dilcher, D.L., Van Konijnenburg-Van Cittert, J.H., Visscher, H., 2001. Life in the end-Permian dead zone. Proc. Natl. Acad. Sci. 98, 7879–7883. http://dx.doi.org/10.1073/pnas.131218098.

Magaritz, M., Bär, R., Baud, A., Holser, W.T., 1988. The carbon isotope shift at the Permian/Triassic boundary in the southern Alps is gradual. Nature 331, 337–339.

Menegatti, A.P., Weissert, H., Brown, R.S., Tyson, R.V., Farrimond, P., Strasser, A., Caron, M., 1998. High-resolution δ13C stratigraphy through the Early Aptian "Livello selli" of the Alpine Tethys. Paleoceanography 13 (5), 530–545.

Morante, R., 1996. Permian and Early Triassic isotopic records of carbon and strontium in Australia and a scenario of events about the Permian–Triassic boundary. Hist. Biol. 11, 289–310.

Mørk, A., 1994. Triassic transgressive–regressive cycles of Svalbard and other Arctic areas: a mirror of stage subdivision. In: Guex, J., Baud, A. (Eds.), Recent Developments on Triassic Stratigraphy. Mémories de Géologie 22, pp. 69–82.

Mørk, A., Smelror, M., 2001. Correlation and non-Correlation of high order circum-Arctic Mesozoic sequences. Polarforschung 69, 65–72.

Mørk, A., Embry, A.F., Weitschat, W., 1989. Triassic transgressive–regressive cycles in the Sverdrup Basin, Svalbard and the Barents Shelf. In: Collinson, J.D. (Ed.), Correlation in Hydrocarbon Exploration. Norwegian Petroleum Society, Graham and Trotman, pp. 113–130.

Mørk, A., Vigran, J.O., Hochuli, P.A., 1990. Geology and palynology of the Triassic succession of Bjørnøya. Polar Res. 8, 141–163.

Müller, R., Nystuen, J.P., Eide, F., Lie, H., Mqiler, R., 2005. Late Permian to Triassic basin infill history and palaeogeography of the mid-Norwegian–East Greenland region. In: Wandas, B., et al. (Eds.), Onshore–Offshore Relationships on the North Atlantic MarginNPF Special Publication 12. Elsevier B.V., Amsterdam, pp. 165–189.

Nakrem, H.A., Mørk, A., 1991. New Early Triassic bryozoa (Trepostomata) from Spitsbergen, with some remarks on the stratigraphy of the investigated horizons. Geol. Mag. 128, 129–140.

Nielsen, E., 1935. The Permian and Eotriassic vertebrate-bearing beds at Godthaab Gulf (East Greenland). Medd. Grønland 98.

Oberhänsli, H., Hsü, K.J., Piasecki, S., Weissert, H., 1989. Permian–Triassic carbon–isotope anomaly in Greenland and in the Southern Alps. Hist. Biol. 2, 37–49.

Oftedal, B.T., Andresen, A., Müller, R., 2005. Early Triassic syn-rift sedimentation at Hold with Hope, Northeast Greenland. In: Wandas, B., et al. (Eds.), Onshore–Offshore Relationships on the North Atlantic MarginNPF Special Publication 12. Elsevier B.V., Amsterdam, pp. 191–206.

Orchard, M.J., 2007. Conodont diversity and evolution through the latest Permian and Early Triassic upheavals. Palaeogeogr. Palaeoclimatol. Palaeoecol. 252, 93–117. http://dx.doi.org/10.1016/j.palaeo.2006.11.037.

Ovtcharova, M., Bucher, H., Schaltegger, U., Galfetti, T., Brayard, A., Guex, J., 2006. New Early to Middle Triassic U–Pb ages from South China: calibration with ammonoid biochronozones and implications for the timing of the Triassic biotic recovery. Earth Planet. Sci. Lett. 243, 463–475.

Payne, J.L., Kump, L.R., 2007. Evidence for recurrent Early Triassic massive volcanism from quantitative interpretation of carbon isotope fluctuations. Earth Planet. Sci. Lett. 256, 264–277. http://dx.doi.org/10.1016/j.epsl.2007.01.034.

Payne, J.L., Lehrmann, D.J., Wei, J., Orchard, M.J., Schrag, D.P., Knoll, A.H., 2004. Large perturbations of the carbon cycle during recovery from the end-Permian extinction. Science 305, 506–509. http://dx.doi.org/10.1126/science.1097023.

Peacock, D.C.P., Price, S.P., Whitham, A.G., Pickles, C.S., 2000. The world's biggest relay ramp: hold with hope, NE Greenland. J. Struct. Geol. 22, 843–850. http://dx.doi.org/10.1016/S0191-8141(00)00012-2.

Perch-Nielsen, K., Birkenmajer, K., Birkelund, T., Aellen, M., 1974. Revision of Triassic stratigraphy of the Scoresby Land and Jameson Land region, East Greenland. Medd. Grønland 193.

Piasecki, S., 1984. Preliminary palynostratigraphy of the Permian–Lower Triassic sediments in Jameson Land and Scoresby Land, East Greenland. Bull. Geol. Soc. Den. 32, 139–144.

Piasecki, S., Stemmerik, L., 1991. Late Permian anoxia in central East Greenland. In: Tyson, R.V., Pearson, T.H. (Eds.), Modern and Ancient Continental Shelf Anoxia. Geological Society Special Publications, pp. 275–290.

Reichow, M.K., Pringle, M.S., Al'Mukhamedov, A.I., Allen, M.B., Andreichev, V.L., Buslov, M.M., Davies, C.E., et al., 2009. The timing and extent of the eruption of the Siberian Traps large igneous province: implications for the end-Permian environmental crisis. Earth Planet. Sci. Lett. 277, 9–20. http://dx.doi.org/10.1016/j.epsl.2008.09.030.

Renne, P.R., Zichao, Z., Richards, M.A., Black, M.T., Basu, A.R., 1995. Synchrony and causal relations between Permian–Triassic boundary crisis and Siberian flood volcanism. Science 269, 1413–1416.

Retallack, G.J., Krull, E.S., 2006. Carbon isotopic evidence for terminal-Permian methane outbursts and their role in extinctions of animals, plants, coral reefs, and peat swamps. Geol. Soc. Am. Spec. Pap. 399, 249–268.

Retallack, G.J., Jahren, A.H., Sheldon, N.D., Chakrabarti, R., Metzger, C.A., Smith, R.M.H., 2005. The Permian–Triassic boundary in Antarctica. Antarct. Sci. 17, 241–258. http://dx.doi.org/10.1017/S0954102005002658.

Retallack, G.J., Sheldon, N.D., Carr, P.F., Fanning, M., Thompson, C.A., Williams, M.L., Jones, B.G., Hutton, A., 2011. Multiple Early Triassic greenhouse crises impeded recovery from Late Permian mass extinction. Palaeogeogr. Palaeoclimatol. Palaeoecol. 308, 233–251. http://dx.doi.org/10.1016/j.palaeo.2010.09.022.

Romano, C., Goudemand, N., Vennemann, T.W., Ware, D., Schneebeli-Hermann, E., Hochuli, P.A., Brühwiler, T., Brinkmann, W., Bucher, H., 2012. Climatic and biotic upheavals following the end-Permian mass extinction. Nat. Geosci. 6, 57–60. http://dx.doi.org/10.1038/ngeo1667.

Schneebeli-Hermann, E., Kurschner, W.M., Hochuli, P.A., Ware, D., Weissert, H., Bernasconi, S.M., Roohi, G., Ur-Rehman, K., Goudemand, N., Bucher, H., 2013. Evidence for atmospheric carbon injection during the end-Permian extinction. Geology 41, 579–582. http://dx.doi.org/10.1130/G34047.1.

Seidler, L., 2000. Incised submarine canyons governing new evidence of Early Triassic rifting in East Greenland. Palaeogeogr. Palaeoclimatol. Palaeoecol. 161, 267–293.

Seidler, L., Steel, R., Stemmerik, L., Surlyk, F., 2004. North Atlantic marine rifting in the Early Triassic: new evidence from East Greenland. J. Geol. Soc. 161, 583–592. http://dx.doi.org/10.1144/0016-764903-063.

Skjold, L.J., Van Veen, P.M., Kristensen, S.E., Rasmussen, A.R., 1998. Triassic sequence stratigraphy of the southwestern Barents Sea. In: de Graciansky, P.C., Hardenbol, J., Jacquin, T., Vail, P.R. (Eds.), Mesozoic and Cenozoic Sequence Stratigraphy of Europena Basins. Society for Sedimentary Geology, Special Publication no 60, pp. 651–666.

Sluijs, A., Dickens, G.R., 2012. Assessing offsets between the δ13C of sedimentary components and the global exogenic carbon pool across early Paleogene carbon cycle perturbations. Glob. Biogeochem. Cycles 26 (4), GB4005.

Sobolev, S.V., Sobolev, A.V., Kuzmin, D.V., Krivolutskaya, N.A., Petrunin, A.G., Arndt, N.T., Radko, V.A., Vasiliev, Y.R., 2011. Linking mantle plumes, large igneous provinces and environmental catastrophes. Nature 477, 312–316. http://dx.doi.org/10.1038/nature10385.

Spath, L.F., 1935. Additions to the Eotriassic invertebrate faunas of East Greenland. Medd. Grønland 98.

Spiro, B., 1991. Effects of minerals on Rock Eval pyrolysis of kerogen. J. Therm. Anal. 37 (7), 1513–1522.

Stemmerik, L., 1998. Diagenesis of Upper Carboniferous shallow marine carbonates, North Greenland. American Association of Petroleum Geologists 1998 Annual Meeting. American Association of Petroleum Geologists and Society of Economic Paleontologists and Mineralogists.

Stemmerik, L., Bendix-Almgreen, S.E., Piasecki, S., 2001. The Permian–Triassic boundary in central East Greenland: past and present views. Bull. Geol. Soc. Den. 48, 159–167.

Suan, G., van de Schootbrugge, B., Adatte, T., Fiebig, J., Oschmann, W., 2015. Calibrating the magnitude of the Toarcian carbon cycle perturbation. Paleoceanography http://dx.doi.org/10.1002/2014PA002758 (accepted for publication).

Surlyk, F., 1990. Timing, style and sedimentary evolution of Late Palaeozoic–Mesozoic extensional basins of East Greenland. In: Hardman, R.F.P., Brooks, J. (Eds.), Tectonic Events Responsible for Britain's Oil and Gas Reserves, pp. 107–125.

Surlyk, F., Piasecki, S., Rolle, F., Stemmerik, L., Thomsen, E., Wrang, P., 1984. The Permian Base of East Greenland. Petroleum Geology of the North European Margin. Norwegian Petroleum Society, pp. 303–315.

Surlyk, F., Piasecki, S., Rolle, F., Scholle, P.A., Stemmerik, L., Thomsen, E., 1986. The Permian of the western margin of the Greenland Sea — a future exploration target. In: Halbouty, M.T. (Ed.), Future Petroleum Provinces of the World. American Association of Petroleum Geologists, pp. 629–659.

Svensen, H., Planke, S., Polozov, A.G., Schmidbauer, N., Corfu, F., Podladchikov, Y.Y., Jamtveit, B., 2009. Siberian gas venting and the end-Permian environmental crisis. Earth Planet. Sci. Lett. 277, 490–500. http://dx.doi.org/10.1016/j.epsl.2008.11.015.

Teichert, C., Kummel, B., 1972. Permian–Triassic Boundary in the Kap Stosch Area, East Greenland. Bull. Can. Petrol. Geol. 20, 659–675.

Tozer, E.T., 1967. A standard Triassic time. Bull. Geol. Surv. Can. 156.

Tozer, E.T., 1994. Canadian Triassic ammonoid faunas. Bull. Geol. Surv. Can. 467.

Traverse, A., 2007. Paleopalynology. Topics in Geobiology 28. Springer.

Trümpy, R., 1961. Triassic of East Greenland. Geology of the Arctic. University of Toronto Press, Toronto, pp. 248–254.

Twitchett, R.J., Looy, C.V., Morante, R., Vissher, H., Wignall, P.B., 2001. Rapid and synchronous collapse of marine and terrestrial ecosystems during the end-Permian biotic crisis. Geol. Soc. Am. 29, 351–354.

Tyson, R.V., 1995. Sedimentary Organic Matter — Organic Facies and Palynofacies. Chapman & Hall.

Weissert, H., Joachimski, M., Sarnthein, M., 2008. Chemostratigraphy. Newsl. Stratigr. 42, 145–179.

Wignall, P.B., Twitchett, R.J., 1996. Oceanic anoxia and the end-Permian mass extinction. Science 272, 1155–1158.

Wignall, P.B., Twitchett, R.J., 2002. Permian–Triassic sedimentology of Jameson Land, East Greenland: incised submarine channels in an anoxic basin. J. Geol. Soc. 159, 691–703. http://dx.doi.org/10.1144/0016-764900-120.

Wignall, P.B., Morante, R., Newton, R., 1998. The Permo–Triassic transition in Spitsbergen: $\delta^{13}C_{org}$ chemostratigraphy, Fe and S geochemistry, facies, fauna and trace fossils. Geol. Mag. 135, 47–62.

Wordie, J.M., 1927. The Cambridge expedition to East Greenland in 1926. Geol. J. 75, 225–265.

Worsley, D., Mørk, A., 1978. The Triassic stratigraphy of southern Spitsbergen. Nor. Polarinst. Aarb. 43–60.

Xie, S., Pancost, R.D., Huang, J., Wignall, P.B., Yu, J., Tang, X., Chen, L., Huang, X., Lai, X., 2007. Changes in the global carbon cycle occurred as two episodes during the Permian Triassic crisis. Geology 35, 1083–1086.

Yin, H., Zhang, K., Tong, J., Yang, Z., Wu, S., 2001. The Global Stratotype and Point (GSSP) of the Permian–Triassic Boundary. Episodes 24, 102–114.

Yuan, D.X., Chen, J., Zhang, Y.C., Zheng, Q.F., Shen, S.Z., 2015. Changhsingian conodont succession and the end-Permian mass extinction event at the Daijiagou section in Chongqing, Southwest China. J. Asian Earth Sci. 105, 234–251. http://dx.doi.org/10.1016/j.jseaes.2015.04.002.

Zhang, Y., Zhang, K.X., Shi, G.R., He, W.H., Yuan, D.X., Yue, M.L., Yang, Ting-Lu., 2014. Restudy of conodont biostratigraphy of the Permian–Triassic boundary section in Zhongzhai, southwestern Guizhou, South China. J. Asian Earth Sci. 80, 75–83. http://dx.doi.org/10.1016/j.jseaes.2013.10.032.

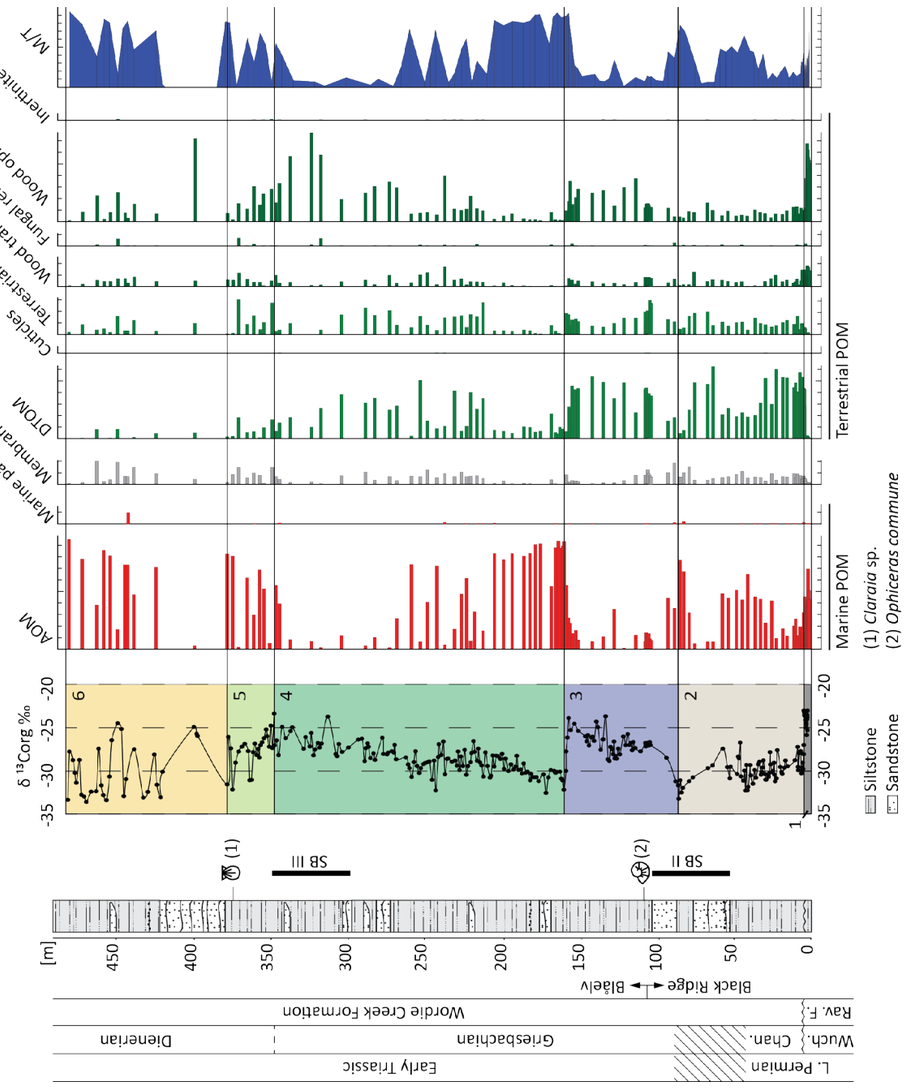

Supplementary data 1. Bulk organic carbon isotope and palynofacies data of the Black Ridge and Blåelv sections. From left to right, chronostratigraphy, the Permian–Triassic boundary interval is marked by a diagonal lines area, and the Griesbachian–Dienerian boundary is marked with a dashed line, asterisk (*) refers to the Pingo Dal Formation, and Pale. refers to Paleogene; simplified lithology of the section; macrofossil content; bulk organic carbon isotope data and isotopic intervals, and particulate organic matter categories (as in Figure 4).

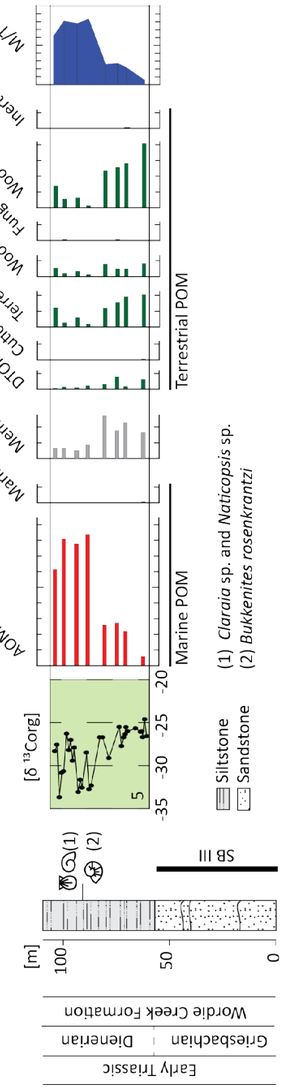

Supplementary data 2. Bulk organic carbon isotope and palynofacies data of the Rævekløft section. See legend Supplementary data 1.

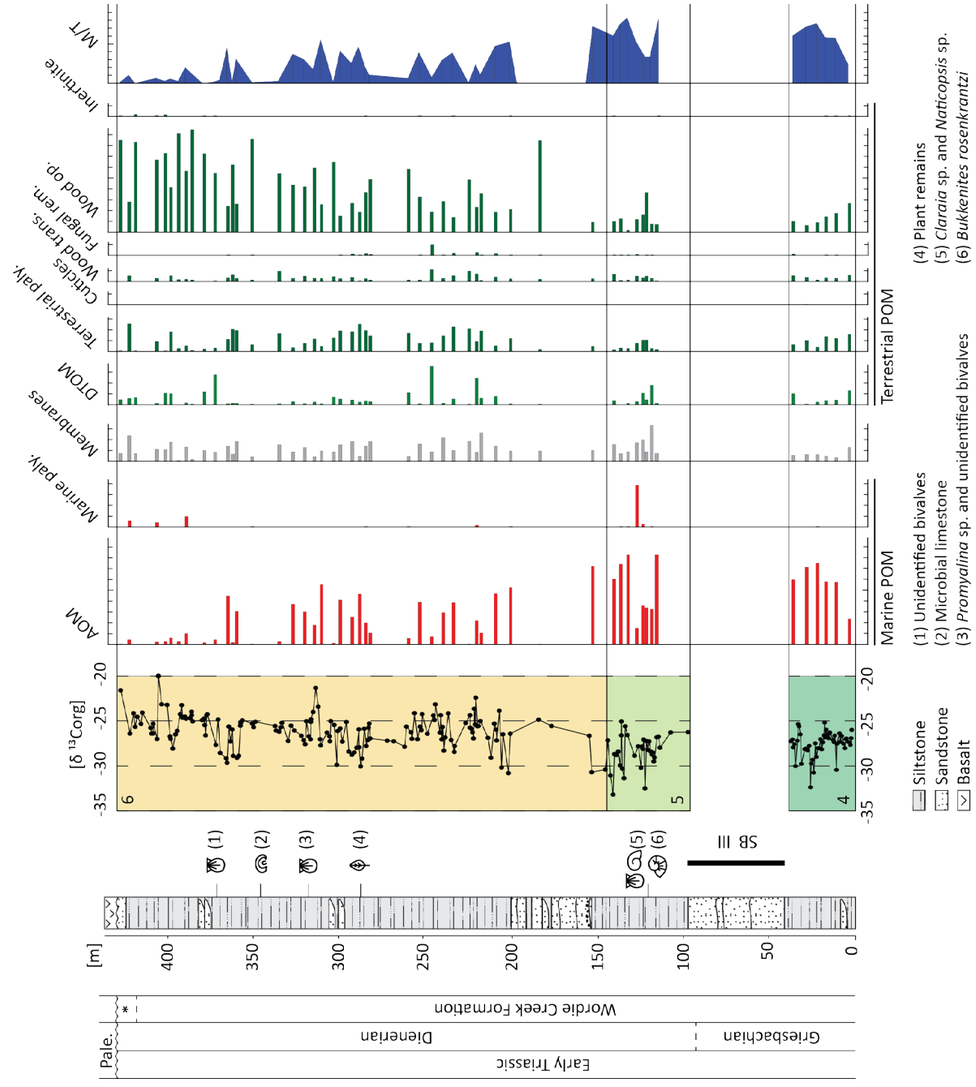

Supplementary data 3. Bulk organic carbon isotope and palynofacies data of the Nasutdal section. See legend Supplementary data 1.

Supplementary data 4. Please check online in http://dx.doi.org/10.1016/j.gloplacha.2015.08.006.

Chapter 2

Late Permian –earliest Triassic organic carbon isotope: Correlations across East Greenland basins

Anna Sanson-Barrera, Hugo Bucher, Elke Schneebeli-Hermann,
Peter A. Hochuli, Helmut Weissert, Stefano M. Bernasconi

in review in the Swiss Journal of Geosciences

Abstract

Bulk organic carbon isotope, palynofacies and ammonoid data based on an Upper Permian–lowermost Triassic succession (Aggersborg and Triaselv, Scoresby Land, East Greenland) are presented and correlated with coeval records from East Greenland. By the end of the Paleozoic and during the early Mesozoic increased rifting activity in the Greenland–Norway Basin largely influenced the sedimentation in sub-basins, hindering interbasinal correlations based on lithostratigraphy and the sparse ammonoid age control. The Aggersborg and Triaselv sections record the global latest Permian carbon isotope negative shift. Together with an early Griesbachian positive excursion, this end-Permian negative shift allows for a correlation with records from Kap Stosch, in East Greenland, and with the Trøndelag Platform, off-shore Norway. The ammonoids *Hypophiceras triviale*, *Otoceras boreale* and *Ophiceras commune* provide biostratigraphic constraints for the isotopic correlations. The presented interbasinal correlation between Scoresby Land and Kap Stosch (Hold-with-Hope) questions the distinction between the Schuchert Dal and the Wordie Creek formations and illustrates the more general problem of how to correlate a vast majority of sections showing a substantial gap straddling the Permian–Triassic boundary. The correlation between East Greenland and Norway provides a revised isotope stratigraphy framework for the Greenland–Norway Basin for the interval between the uppermost Permian and the lowermost Triassic. It also documents common features and different levels of completeness of Boreal Late Permian–Early Triassic sedimentary records.

Key words: particulate organic matter, ammonoids, Schuchert Dal Formation, Wordie Creek Formation, Greenland–Norway Basin

1. Introduction

The end of the Palaeozoic encompasses a severe biodiversity crisis and the onset of several carbon cycle disturbances during the following Early Triassic (e.g., Payne et al. 2004; Galfetti et al. 2007; Hermann et al. 2011; Clarkson et al. 2013; Korte and Kozur 2010). Globally distributed organic and carbonate carbon isotope records show a common decreasing trend in the carbon isotope values during the latest Permian (Morante 1996; Krull et al. 2004; Payne et al. 2004; Hermann et al. 2010). This trend is considered to represent a synchronous global carbon cycle signal and is used to correlate Permian–Triassic successions from different depositional settings worldwide (e.g., Hermann et al. 2010).

East Greenland is a classic area for the study of the Permian–Triassic interval (Nielsen 1935; Teichert and Kummel 1972; Spath 1935; Surlyk et al. 1986; Stemmerik et al. 2001; Trümpy 1969). Coeval successions off-shore Norway indicate that a wide marine rift complex extended between Greenland and Norway (Bugge et al. 2002; Seidler et al. 2004). In East Greenland rifting during the Permian and Triassic led to the formation of a series of smaller sub-basins (Surlyk et al. 1986; Seidler et al. 2004; Müller et al. 2005). Generally, the Permian–Triassic successions were predominantly deposited in terrestrial settings; however, the Upper Permian–lowermost Triassic sediments were deposited in marine environments (Surlyk 1990). This marine succession represents one of the most extended Upper Permian–lowermost Triassic successions world-wide. However, a relative sea-level fall during the latest Permian caused a significant hiatus leading to discontinuous Permian–Triassic records in some sub-basins (e.g., Hold-with-Hope, Fig. 1) (Birkenmajer 1977; Surlyk et al. 1986; Surlyk 1990; Seidler et al. 2004).

Carbon isotope and palaeontological data have been previously published from Scoresby Land sections interpreted as being continuous across the Permian–Triassic transition (Oberhänsli et al. 1989; Stemmerik et al. 2001; Twitchett et al. 2001). Recent high-resolution organic carbon isotope and palynofacies data from Kap Stosch (Hold-with-Hope) show the exceptional, expanded nature of the Permian–Triassic successions of East Greenland, even though they failed to record the latest Permian due to an erosional hiatus in the Kap Stosch area (Sanson-Barrera et al. 2015). Correlation between the sub-basins including the sedimentary gap (e.g., Hold-with-Hope) with those that registered continuous sedimentation (e.g., Scoresby Land) are not straightforward because of rapid lateral facies changes, and present a double challenge. On the one hand, the Upper Permian and Lower Triassic ammonoid record in East Greenland (Spath 1930; Trümpy 1969; Trümpy 1969) is laterally too discontinuous for biostratigraphic correlations between these sub-basins. On the other hand, the poorly defined uppermost Permian–lowermost Triassic formations (i.e., Schuchert Dal and Wordie Creek formations) lead to an interchangeable usage of the lithostratigraphic terms in previous works (e.g., Surlyk et al. 1986; Stemmerik et al. 1997; Stemmerik et al. 2001).

The present study proposes a correlation of two Upper Permian–lowermost Triassic bulk organic carbon isotope records from Scoresby Land (Aggersborg and Triaselv) with the high-resolution record from Kap Stosch (Hold-with-Hope). The aim is to present an interbasinal isotope stratigraphy framework based on organic carbon isotope data for East Greenland combined with palynofacies and ammonoid data providing biostratigraphic constraints. Previously published successions from off-shore Norway, the Barents Sea, and from Buchanan Lake area in Arctic Canada (Hermann et al. 2010; Grasby and Beauchamp 2008) allows for the construction of an uppermost Permian–lowermost Triassic chemostratigraphic framework for the Boreal Realm in general, and the Greenland–Norway Basin in particular.

2. Geological Setting

The Upper Permian–lowermost Triassic marine successions of East Greenland were deposited in a N-S trending rift basin in northwest Pangea, with its western margin corresponding to the post-Devonian major fault system (Surlyk et al. 1986) (Fig. 1a). These successions are dominated by siliciclastic deltaic to shallow marine sediments (Surlyk et al. 1986) and are exposed along the coast between Jameson Land and Wollaston Forland. In East Greenland the uppermost Permian–lowermost Triassic is represented by the Wegener Halvø, Ravnefjeld, Schuchert Dal, and Wordie Creek formations (Spath 1935; Surlyk et al. 1986) (Fig. 2). The Wegener Halvø Formation

records a major transgressive sequence expressed as marine limestones surrounded and overlain by the Ravnefjeld Formation (Surlyk et al. 1986). The Ravnefjeld Formation represents basinal and inter-reef mudstones (Surlyk et al. 1986; Piasecki and Stemmerik 1991). Both, the Wegener Halvø and the Ravnefjeld formations are of Wuchiapingian age (Bjerager et al. 2006; Piasecki and Stemmerik 1991). The overlaying Schuchert Dal Formation documents a relative sea-level fall and it is subdivided in stratigraphic order into two members – the Oksedal Member and Bredehorn Member. Grey-black silty bioturbated mudstones characterise the Oksedal Member. The overlying fine- to medium-grained sandstones and conglomerates have been described as the Bredehorn Member (Surlyk et al. 1986).

The Ravnefjeld and Schuchert Dal formations were originally described from the same exposure along the Schuchert Dal area (Scoresby Land) (Surlyk et al. 1986). However, no type sections have been defined so far, and the use of the Schuchert Dal Formation in particular remains unclear. While describing the Ravnefjeld shales and overlaying grey bioturbated shales of the Oksedal Member Piasecki and Stemmerik (1991) presented not a lithological, but an environmental distinction between the upper Ravnefjeld Formation and the Oksedal Member. Stemmerik et al. (1997) mentioned that "field observations indicate that earlier concepts of the stratigraphic relationships between the Ravnefjeld and Schuchert Dal formations require revision", and proposed that the basal part of the Schuchert Dal Formation is more coarse-grained in comparison to the Ravnefjeld Formation. Another study described the Bredehorn Member – the upper member of the Schuchert Dal Formation – as intermediate unit between the upper Ravnefjeld Formation and the lower part of the Schuchert Dal Formation (Kreiner-Müller and Stemmerik 2001). However, in this publication the Oksedal Member is not mentioned. Despite this variable use of the Schuchert Dal Formation, Stemmerik et al. (2001) defined the "Permian-Triassic boundary interval" within the uppermost meters of the Schuchert Dal Formation and the lowermost meters of the Wordie Creek Formation in the Fiskegrav section (Fig. 1b). The same year, Twitchett et al. (2001) published organic and inorganic carbon isotope records from the same locality (Fiskegrav), and described the lithology of both, the upper Schuchert Dal and the basal Wordie Creek formations, as micaceous muddy siltstone. In the latest ammonoid zonation of East Greenland (Surlyk et al. 1986) the Schuchert Dal Formation is included the late Permian Paramexicoceras/Changhsingoceras Zone (Fig. 2). In most areas a latest Permian relative sea-level fall led to the interruption of the sedimentation and in some cases to substantial erosion and/or non-deposition of what is thought to be the Schuchert

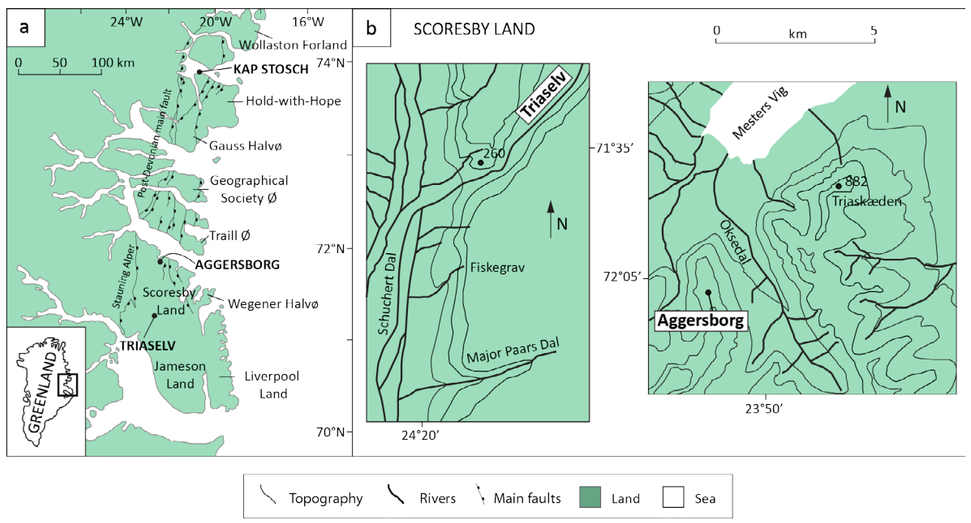

Figure 1. a – Geographic overview of East Greenland with the names of the main areas and the location of the study sections; b – Detailed location of the sections (Aggersborg and Triaselv in Scoresby Land). Modified from Bjerager et al. 2006.

Dal Formation and the underlying Permian sediments (Surlyk et al. 1986; Seidler et al. 2004). The latest Permian unconformity is best developed in the sub-basin margins and in uplifted intrabasinal areas. In the deeper, down-thrown parts of the Scoresby Land sub-basin (Fig. 1a) there is no apparent sedimentary gap between the Schuchert Dal and the Wordie Creek formations (Spath 1935; Oberhänsli et al. 1989; Surlyk et al. 1986; Stemmerik et al. 2001; Twitchett et al. 2001). North of Scoresby Land the unconformity becomes clearer and the Schuchert Dal Formation is missing at Kap Stosch (Hold-with-Hope) (Spath 1935; Surlyk et al. 1986; Stemmerik et al. 2001; Sanson-Barrera et al. 2015). The uppermost Permian–lowermost Triassic basin fill, represented by the Wordie Creek Formation, reflects increased rifting activity and rapid and fluctuating sea-level changes (Surlyk et al. 1986; Seidler et al. 2004; Sanson-Barrera et al. 2015). The initial transgression was followed by rapid progradation of deltaic deposits (Surlyk et al. 1986). The Wordie Creek Formation has been defined at Blåelv, Kap Stosch (Hold-with-Hope) (Spath 1935). Marine, grey shales with ammonoids and fish-bearing concretions and subordinate grey or green glauconitic or arkosic sandstones dominate the lower part of the formation at Kap Stosch (Spath 1935). In the Schuchert Dal area, the Wordie Creek Formation is characterised by thick bodies of conglomerate and coarse pebbly sandstones of fan-delta origin along the sub-basin margins with gypsum and/or conglomeratic layers occurring locally at its base, whereas in shelf areas the deposition is dominated by fine-grained sandstones and siltstones (Surlyk et al. 1986). Depending on the area the boundary between the Schuchert Dal and Wordie Creek formations is also equivocal (Spath 1935). In the Schuchert Dal region "the lower boundary of the Wordie Creek Formation usually coincides with the appearance of a thicker zone of grey shale above fossiliferous Permian siltstones; concretions with ammonites and fishes appear a short distance above the base of that shale" (Spath 1935, p. 20). Progradation and basin infill continued up to the top of the Wordie Creek Formation, representing the end of the Early Triassic marine deposition (Surlyk et al. 1986). In East Greenland the occurrence of macrofossils (ammonoids and bivalves) led to a biostratigraphic subdivision of the Permian–Triassic succession into eight ammonoid and two bivalve zones (Spath 1935; Trümpy 1969; Bjerager et al. 2006) (Fig. 2) and enabled correlation with other areas of the Boreal Realm, such as the Canadian Arctic (Bjerager et al. 2006) and Svalbard (Weitschat and Dagys 1989).

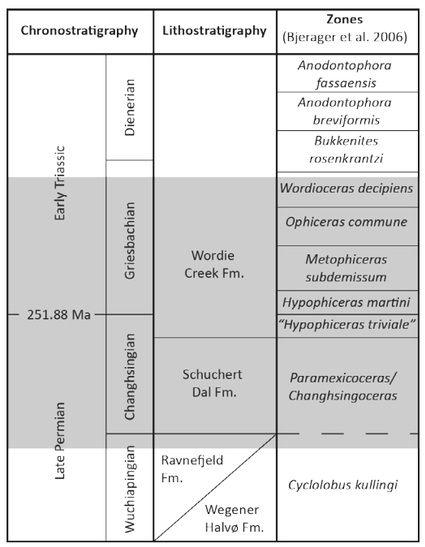

Figure 2. Upper Permian–lowermost Triassic chrono- and lithostratigraphy, and ammonoid zones of East Greenland, modified from Perch-Nielsen et al. (1974) and Bjerager et al. 2006. The age of the Permian–Triassic boundary (251.88 million years) is based on U/Pb dating of zircons (Burgess et al. 2014). Vertical scale arbitrary.

2.1. Scoresby Land sub-basin

In NW Scoresby Land the oldest sedimentary rocks (Upper Palaeozoic) are exposed along the northern coast and the western basin margin. The youngest (Cretaceous) rocks occur along the southernmost Scoresby Land margin. In order to study the Upper Permian and lowermost Triassic interval two sections have been sampled: Aggersborg in the north and Triaselv in the central part (Fig. 1b).

2.1.1. Aggersborg section

The Aggersborg section is exposed on the western ridge of Oksedal (Fig. 1b) (GPS coordinates: 72°4.4'N–23°52'W) and comprises about 90 m of uppermost Permian and lowermost Triassic sediments. This section consists of alternating light and dark grey siltstone with fine-grained sandstone beds crossed by several meter-thick basaltic dykes. The beds are dipping about 30°N and striking E-W. The study section begins above a yellowish fossil-rich productid limestone corresponding to a bioherm or an accumulation of debris of the Wegener Halvø Formation (Fig. 2). Observed macrofossils include corals, crinoids, and brachiopods (Supplementary data 1, a-c). The basal 5 m of the section consist of cross-bedded, dark grey, fine-grained sandstone beds (Fig. 3), overlain by irregularly bedded dark grey siltstone alternating with consolidated cm-thick sandstone beds, ranging from 5 to about 30 m of the section. The bivalve *Claraia* sp. and a few unidentified plant remains were found at 36 m. Four metres above this level a few beds yielded specimens of the ammonoid *Hypophiceras triviale*. Above this horizon, the sandstone beds are up to one-metre thick and consist of coarsening up successions including small conglomerate lenses at their base. The section is topped by two conglomeratic sandstone beds each about 7 m thick, separated by 3 m of siltstones (Fig. 3 and Supplementary data 1). Ammonoids identified as *Otoceras boreale* were found in the upper conglomeratic sandstone beds. About 5 m above these beds, specimens of *Ophiceras commune* were found in floating early diagenetic limestone nodules (Fig. 3 and Supplementary data 1). The gradual lithological changes, the presence of basaltic dykes cutting across the section, and the ambiguous boundaries between formations made it difficult to locate the formational boundaries in this section. For the studied section the definition of the base of the Wordie Creek Formation (type section in Kap Stosch after Perch-Nielsen et al. 1974) does not help in placing the boundary between the Schuchert Dal and Wordie Creek formations. However, Surlyk et al. (1984) and Surlyk (1990) described the base of the Wordie Creek Formation as a major sequence boundary, reflecting a marked regression, followed by a transgression and rapid progradation dominated by shale and fine sandstone deposition. Therefore, based on Surlyk et al.'s interpretation, the formational boundary between the Schuchert Dal and Wordie Creek formations has been placed at 36 m, at the base of the first coarsening upward sandstone bed.

2.1.2.Triaselv section

The ca. 120 meters thick Triaselv section was sampled along Triaselv (GPS coordinates: 71°40'N–24°14.34'W) (Fig. 1b). The section comprises 3 m of the Ravnefjeld Formation, consisting of an alternation of organic-rich mudstone and limestone beds. The Ravnefjeld Formation is unconformably overlain by a ca. 65 m thick succession of coarse pebbly sandstone and conglomerate beds that have been described as channel-like structures and interpreted as the basal part of the Wordie Creek Formation (Surlyk et al. 1986; Wignall and Twitchett 2002) (Figs. 8 and Fig. 4). Above this coarse-grained succession the section consists of alternating grey siltstone and sandstone beds. At around 18 m, the bivalve *Claraia* sp., poorly preserved plant remains, and a few unidentified ammonoids imprints were observed in siltstone and sandstone beds. 20 m above the base the succession is interrupted by a 10 m thick basaltic dyke. At around 55 m, float ammonoid specimens assigned to the *Ophiceras commune* and *Wordioceras decipiens* were found (Fig. 4 and Supplementary data 2).

3. Materials and Methods

A total of 38 and 35 samples were collected from the Aggersborg and Triaselv sections, respectively. To analyse the bulk organic carbon isotope composition ($\delta^{13}C_{org}$), all samples were finely ground and treated with 3 N HCl for at least 24 hours to remove all carbonates. The residue was homogenized and analysed with a ThermoFisher Flash-EA 1112 elemental analyser coupled with a Conflo IV interface to a ThermoFisher Delta V isotope ratio mass spectrometer (IRMS). Isotope ratios are reported in the conventional δ-notation with respect to V-PDB (Vienna Pee Dee Belemnite) standard. The system was calibrated with NBS22 ($\delta^{13}C$ = -30.03) and IAEA CH-6 ($\delta^{13}C$ = -10.46). Reproducibility of the measurements is better than ±0.15‰.

Palynofacies analysis has been performed on 25 samples from the Aggersborg section and 17 samples from the Triaselv section. The samples were crushed to mm-size particles and then treated with 3 N HCl and 70% HF to remove all carbonate and siliciclastic particles (Traverse 2007). The residues were sieved through an 11µm mesh screen and mounted on slides for the analysis of the particulate organic matter (POM). For each sample a minimum of 250 particles were counted. The organic particles have been classified into 10 categories: amorphous organic matter (AOM), marine palynomorphs (acritarchs and foraminifer linings), degraded terrestrial organic matter

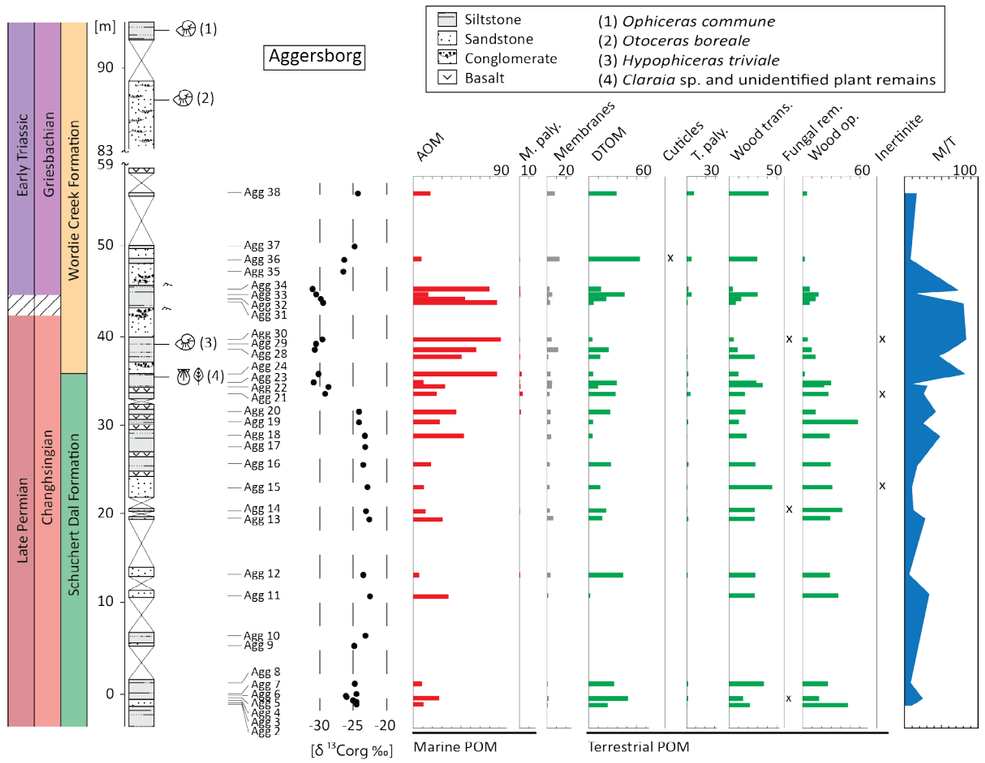

Figure 3. Bulk organic carbon isotope and palynofacies data of the Aggersborg section. From left to right: chronostratigraphy - the Permian-Triassic transition is marked with a dashed area; simplified lithology of the section (for graphical reasons, only part of the upper conglomeratic sandstone bed is represented); macrofossil content; bulk organic carbon isotope data ($\delta^{13}C_{org}$); particulate organic matter expressed in %, each bar represents 10%, with AOM (amorphous organic matter, marine palynomorphs), DTOM (degraded terrestrial organic matter), membranes, terrestrial palynomorphs, cuticles, translucent woody particles, fungal remains, opaque woody particles, inertinite (cuticles, fungal remains, and inertinite are very rare throughout the record, their presence is marked with (x). Particulate organic matter (POM) of marine origin are in red, membranes in grey, terrestrial POM in green and the marine/terrestrial ratio in blue.

(DTOM), membranes, terrestrial palynomorphs (pollen grains and spores), cuticles, translucent and opaque woody particles, fungal remains, and inertinite. In order to calculate the marine/terrestrial ratio, two categories account for the marine fraction (AOM and marine palynomorphs), whereas seven categories account for the terrestrial fraction (DTOM, terrestrial palynomorphs, cuticles, translucent and opaque woody particles, fungal remains, and inertinite). Membranes can be of marine and terrestrial origin and are therefore left out of the marine/terrestrial ratio.

4. Results

4.1. Organic carbon isotopes and palynofacies of the Aggersborg section

The Aggersborg section shows $\delta^{13}C_{org}$ values scattered between -23‰ and -26‰ from 0 to 32 m) (Fig. 3). Between 32 and 35 m, there is a distinct $\delta^{13}C_{org}$ negative shift from values around -24‰ to -30‰. Above this shift and up to 45 m the $\delta^{13}C_{org}$ values scatter around -30‰. The isotopic record ends below the thick conglomeratic sandstone beds with a positive $\delta^{13}C_{org}$ shift from about -30‰ to -25‰ (Fig. 3).

Palynofacies data show an increasing trend in the AOM relative abundances from ca. 20% to ca. 90% from the base up to 45 m and a subsequent decrease to ca. 10-20% from 45 to 55 m. The highest AOM relative abundances coincide with the most negative $\delta^{13}C_{org}$ values in the section (Fig. 3). Marine palynomorphs are generally rare, they show relative abundances of up to 5% between 30 and 35 m. DTOM relative abundances are between <10% to ca. 50% throughout the entire record, showing a slight increase from 45 to 55 m. Terrestrial palynomorphs are rare in the lower part of the section and increase in relative abundance to about 10% between 45 and 55 m. Translucent woody particles show relative abundances between <10% and 40% throughout the section. Relative abundances of opaque woody particles vary between 30 and 50% in the lower half of the section and tend to decrease to <20% in its upper part. The marine/terrestrial ratio essentially determined by the amount of AOM begins with values around 30% at the base of the section, increasing to 90% between 27 to 40 m, and dropping to 10-20% at around 50 m.

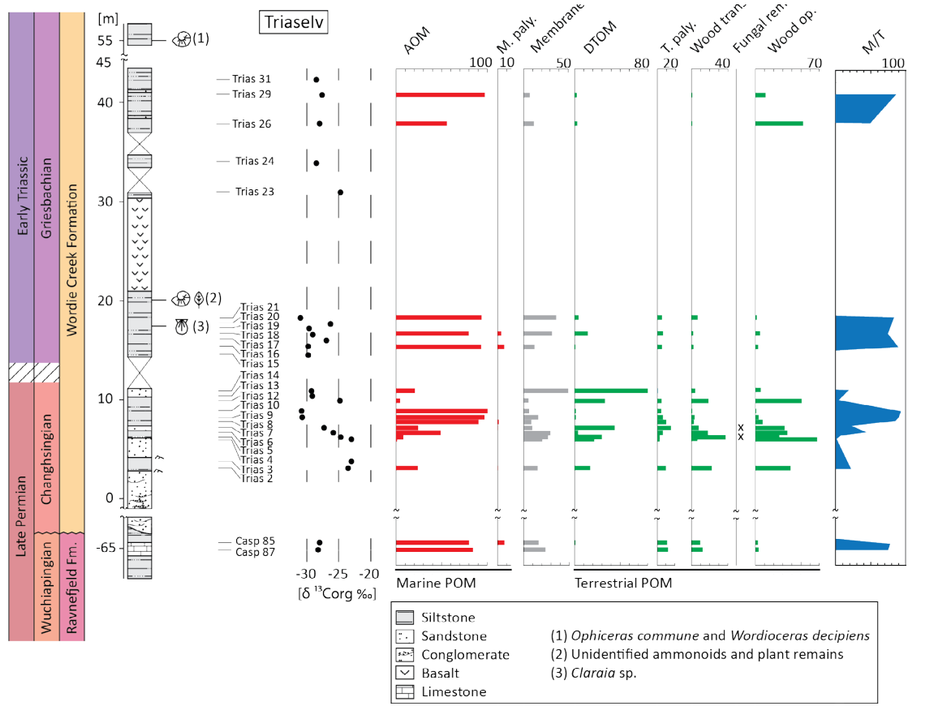

Figure 4. Bulk organic carbon isotope and palynofacies of the Triaselv section. For captions see Figure 3.

4.2. Organic carbon isotopes and palynofacies of the Triaselv section

In the Triaselv record two $\delta^{13}C_{org}$ values of around -28‰ have been measured in the Ravnefjeld Formation (samples CASP 87 and CASP 85). Above the coarse pebbly sandstone and conglomerate beds, the samples Trias 2 and Trias 3 show $\delta^{13}C_{org}$ values around -23‰, followed by a negative shift from -23‰ to -30‰ in the interval 5 to 9 m in the Wordie Creek Formation (Fig. 4). From 9 m up to the top of the section the $\delta^{13}C_{org}$ values scatter between -25‰ and -30‰.

In the Ravnefjeld Formation palynofacies show AOM dominance up to 85%. In the interval from 3 to 5 m of the Wordie Creek Formation the relative abundance of AOM is reduced to 5-25%. It shows an increasing trend to values around 90% coinciding with the $\delta^{13}C_{org}$ negative shift between 5 to 9 m. It decreases around 10 m to values around 20% and increases again to 50-80% from this level up to the top of the section. Marine palynomorphs contribute only low numbers to the POM assemblages. However, there are two exceptions, at -65 m, in the Ravnefjeld Formation, and at 15 m, in the Wordie Creek Formation; in both samples the relative abundance of marine palynomorphs reaches 7% (Fig. 4). Membrane abundances vary between 10-50% within the whole record. DTOM is rare in the Ravnefjeld Formation and shows abundances between 5-40% in the Wordie Creek Formation, peaking to 80% at around 10 m. Terrestrial palynomorphs are regularly

represented in the Ravnefjeld Formation and in the lower part of the Wordie Creek Formation (from 3 to 18 m) with abundances of up to 20%. Translucent woody particles show abundances between <10% and 40% in the lower part of the section and abundances of opaque woody particles vary between <10% and 70% (Fig. 4). The marine/terrestrial ratio displays a strong marine influence in the Ravnefjeld Formation with values up to 80%. Pronounced terrestrial influence is restricted to the interval between 3 and 5 m (samples Trias 2 and 3), and around 9 m (Trias 12) of the Wordie Creek Formation, whereas marine influence dominates the rest of the formation (Fig. 4).

5. Discussion

5.1. Correlation of the Aggersborg and Triaselv sections with coeval $\delta^{13}C$ records

Figure 5 is showing the correlation of the $\delta^{13}C_{org}$ records of the Aggersborg and the Triaselv sections with published coeval records from Scoresby Land: one $\delta^{13}C_{carb}$ record from Fiskegrav (referred to as north of Major Paars Dal in Oberhänsli et al. 1989), and two $\delta^{13}C_{org}$ records as well as one $\delta^{13}C_{carb}$ record also from Fiskegrav (Stemmerik et al. 2001; Twitchett et al. 2001). The Fiskegrav section consists mainly of well bedded marly siltstones, occasionally intercalated with cm-scale clay and pyritic beds as described by Oberhänsli et al. 1989. In the Schuchert Dal Formation it shows $\delta^{13}C_{carb}$ values between -3‰ and -5‰, followed by a drop to values around -22‰ in the basal meters of the Wordie Creek Formation. Above, the $\delta^{13}C_{carb}$ values recover to around -5‰, and from 29.5 m to the top of the section they display a decreasing trend from ca. -5‰ to -9‰ (Fig. 5a). Coinciding with the negative $\delta^{13}C_{carb}$ shift at around 28 m, there is a distinct change in the POM, changing from opaque woody particles to AOM dominance (Fig. 5a). This change coincides with a significant increase in trilete, cavate spores that has been interpreted as the palynological Permian–Triassic boundary by Oberhänsli et al. (1989) and Oberhänsli et al. (1989) (Fig. 5a).

Organic and inorganic carbon isotope values were measured at Fiskegrav by Twitchett et al. (2001) (Fig. 5d). These authors describe the section as bioturbated green and grey, micaceous muddy siltstones, attributed to the upper part of the Oksedal Member of the Schuchert Dal Formation, and overlain by dark grey, micaceous and pyritic muddy siltstones assigned to the basal part of the Wordie Creek Formation (Twitchett et al. 2001). The record shows $\delta^{13}C_{carb}$ values around -4‰ in the Schuchert Dal Formation followed by a drop to ca. -11‰ in the basal meters of the Wordie Creek Formation. Above, the $\delta^{13}C_{carb}$ values scatter around -10‰ up to the top of the section. The $\delta^{13}C_{org}$ record shows values around -23‰ in the Schuchert Dal Formation dropping to -32‰ in the basal metres of the Wordie Creek Formation. The top of the $\delta^{13}C_{org}$ record, about 8 m above the base of the Wordie Creek Formation, shows values of ca. -28‰, (Twitchett et al. 2001) (Fig. 5d). Coinciding with the formational boundary and with the isotopic negative shift, a spore peak (mostly non-cavate *Uvaesporites*) has also been observed in this section (Looy et al. 2001) (Fig. 5d).

A third $\delta^{13}C_{org}$ record from Fiskegrav focused on the 2 m of section including the $\delta^{13}C_{org}$ negative shift (Stemmerik et al. 2001) (Fig. 5e). The $\delta^{13}C_{org}$ values show a two-step decrease from ca. -25‰ to -31‰. In the interpretation of Stemmerik et al. (2001) the formational boundary between the Schuchert Dal and the Wordie Creek formations is close to the top of the $\delta^{13}C_{org}$ negative shift, i.e. the $\delta^{13}C_{org}$ negative shift would lie within the topmost meters of the Schuchert Dal Formation (Stemmerik et al. 2001). The spore peak, described as the "palynological PTB" by Piasecki (1984), has been observed within the $\delta^{13}C_{org}$ negative shift, about 50 cm below its end.

The $\delta^{13}C_{org}$ negative shift recorded in the Aggersborg and the Triaselv sections can be correlated with the negative $\delta^{13}C$ shift observed in the above mentioned records from Major Paars Dal (Oberhänsli et al. 1989) and from Fiskegrav (Stemmerik et al. 2001; Twitchett et al. 2001) (Fig. 5). The correlation is supported by the similar trends in all these sections, and by similar absolute $\delta^{13}C_{org}$ values recorded in Aggersborg, Triaselv, and Fiskegrav.

The correlation obtained by using the latest Permian $\delta^{13}C$ isotopic negative shift as an isotope stratigraphic marker conflicts with established lithological correlations. In the Aggersborg section the $\delta^{13}C_{org}$ negative shift occurs in the topmost metres of the Schuchert Dal Formation, whereas in Triaselv it occurs, according to our lithological interpretation, about 70 m above the base of the Wordie Creek Formation. Similar to the Aggersborg

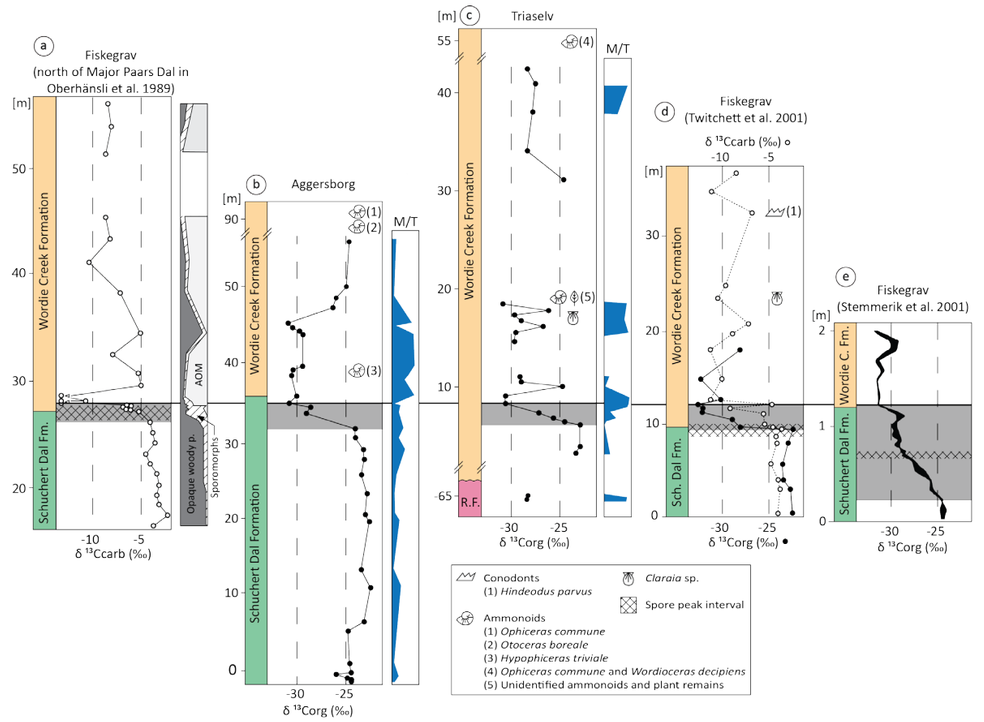

Figure 5. Correlation of the carbon records from Scoresby Land (East Greenland), (a) $\delta^{13}C_{carb}$ record from Fiskegrav (referred as north of Major Paars Dal in Oberhänsli et al. 1989), (b) $\delta^{13}C_{carb}$ record from Aggersborg and (c) $\delta^{13}C_{carb}$ record from Triaselv (this study), (d) $\delta^{13}C_{org}$ and $\delta^{13}C_{carb}$ records from Fiskegrav (Twitchett et al. 2001), and (e) $\delta^{13}C_{org}$ record from Fiskegrav (Stemmerik et al. 2001) from Fiskegrav. The end-Permian C-isotope negative shift is used as baseline.

section the negative $\delta^{13}C$ shift in the Fiskegrav records has been interpreted by Stemmerik et al. (2001) to occur within the topmost metres of the Schuchert Dal Formation, whereas according to the interpretation of Oberhänsli et al. (1989) and Twitchett et al. (2001) it would fall within the basal meters of the Wordie Creek Formation. The lack of a distinct lithological change between the Schuchert Dal and the Wordie Creek formations probably led to the two different interpretations of the formational boundary (Stemmerik et al. 2001; Twitchett et al. 2001). Assuming that the $\delta^{13}C$ signal recorded in the various sections has a chronological significance, it can be used as a reliable time marker to correlate the abovementioned boundary sections and Permian–Triassic sections in general.

5.2. Interbasinal correlation between NW Scoresby Land and Hold-with-Hope

The $\delta^{13}C_{org}$ record of the Aggersborg and Triaselv sections have been correlated with the Upper Permian–lowermost Triassic record from Kap Stosch in the Hold-with-Hope sub-basin (Sanson-Barrera et al. 2015) (Fig. 6). The Kap Stosch section comprises the topmost 7 m of the basinal Ravnefjeld Formation, which are unconformably overlain by ~650 m of the deltaic shallowing-up succession of the Wordie Creek Formation. For the present correlation with the Aggersborg and the Triaselv sections only the lowest 180 m of section are shown in Figure 6. Between 50 and 100 m above the base of the Kap Stosch section, two sandstone bodies 20 and 10 m thick respectively, separated by 6 m of siltstones correspond to SB II, a regional sandstone body used for correlation in the Kap Stosch area (Nielsen 1935; Bjerager et al. 2006; Sanson-Barrera et al. 2015). Above SB II specimens of the ammonoids *Ophiceras commune* zone have been found, indicating a mid-Griesbachian age (Fig. 2).

At Hold-with-Hope the samples of the Ravnefjeld Formation show $\delta^{13}C_{org}$ values around -23‰ to -25‰ (Fig. 6). Above the unconformity between the Ravnefjeld and the Wordie Creek formations,

within the basal 85 m of the latter, $\delta^{13}C_{org}$ values decrease from ca. -27‰ to -33‰ (interval 2 in Sanson-Barrera et al. 2015), showing two minimum $\delta^{13}C_{org}$ values at around 40 and 85 m, respectively. The drop to the first minimum $\delta^{13}C_{org}$ value of -32‰ has been correlated with the global end-Permian negative shift (Sanson-Barrera et al. 2015), and it is correlated with the $\delta^{13}C_{org}$ minima in the Aggersborg and Triaselv sections. In the Aggersborg, Triaselv, and Kap Stosch sections this shift correlates with an increase in the marine/terrestrial ratio, which is interpreted to reflect a latest Permian sea-level rise. This minimum is succeeded by a slight recovery of $\delta^{13}C_{org}$ values in the Aggersborg and Kap Stosch sections, which is followed by a second drop to a minimum $\delta^{13}C_{org}$value of -33‰, positioned at 85 m in the Kap Stosch section and at 45 m in the Aggersborg section. The following positive shift from -33‰ to -27‰ at Kap Stosch (lower part of interval 3 of Sanson-Barrera et al. (2015) has its chemostratigraphic equivalent in the upper part of the Aggersborg section, providing a second correlation marker between the two areas (Fig. 6). In the Aggersborg section the marine/terrestrial ratio decreases between 45 and 55 m, which correlates with a similar decrease in the lower part of interval 3 at Kap Stosch (Fig. 6). This feature is interpreted as a widespread regressive event in the Greenland–Norway Basin (Sanson-Barrera et al. 2015).

In the Aggersborg section (Figs. 3 and 5) specimens of *Hypophiceras triviale* occur within the interval characterized by the most negative $\delta^{13}C_{org}$ values. However, the age assignment of the *H. triviale* Zone is unclear with respect to the Permian–Triassic boundary. Traditionally it has been assigned to the basal Lower Triassic (Spath 1930, 1935; Trümpy 1969) and more recently to the uppermost Permian (Bjerager et al. 2006). However, xenodiscids, of which *Hypophyceras* is a representative, are known to bridge the Permian–Triassic interval (Tozer 1981). Hence, presently no firm age assignment can be based on the sole occurrence of *H. triviale*. At Kap Stosch, we documented the oldest unambiguous Triassic ammonoid (*Ophiceras* sp.) in strata assigned to the basal Griesbachian *H. martini* Zone by Bjerager et al. (2006). In the Aggersborg section the occurrences of *Otoceras boreale* and *Ophiceras commune* within and above the conglomeratic sandstone beds (Fig. 3) yield a Griesbachian age. At Kap Stosch *O. commune* has been found above SB II (Sanson-Barrera et al. 2015) and *O. boreale* and *O. commune*, belonging to the *Metophiceras subdemisum* Zone, have been reported from above SB II by Bjerager et al. (2006). Finally, about 10 m above the top of the Triaselv section, a few float specimens identified as *O. commune* and *Wordioceras decipiens* have been observed, thus providing a mid- and late-Griesbachian age for this interval (Trümpy 1969; Bjerager et al. 2006).

The correlation between Scoresby Land and Hold-with-Hope also shows that the boundary between the Schuchert Dal and the Wordie Creek formations is poorly defined and ambiguous. At Hold-with-Hope and Triaselv the Upper Permian regression probably caused emergence and erosion of the youngest beds of the Ravnefjeld Formation and/or non-deposition of the Schuchert Dal Formation, while sedimentation was apparently more continuous at Aggersborg. Subsequently, deposition started earlier at Triaselv than at Hold-with-Hope with the thick and coarse pebbly sandstone and channelled conglomerate bodies of the Wordie Creek Formation. Thus, the Triaselv section recorded the complete $\delta^{13}C_{org}$ negative shift, whereas according to the isotopic stratigraphy correlation discussed above, sedimentation in the Kap Stosch area started again during the latest Permian $\delta^{13}C_{org}$ negative shift, therefore later than at Triaselv (Fig. 6).

5.3. The Greenland–Norway Basin during the Late Permian–earliest Triassic

The $\delta^{13}C_{org}$ records from the Trøndelag and Finnmark platform (Hermann et al. 2010) were used to correlate the Aggersborg, Triaselv and Kap Stosch sections within the context of the evolution of the Greenland–Norway Basin (Fig. 7). Additionally, the Permian–Triassic section from the Buchanan Lake in Arctic Canada (Grasby and Beauchamp 2008) was used to extend this correlation beyond this basin. The composite organic carbon isotope records from the Trøndelag and Finnmark platforms produced one of the most expanded, essentially continuous latest Permian–earliest Triassic isotope curve (Hermann et al. 2010). According to the correlation of Sanson-Barrera et al. (2015) the Trøndelag Platform and Hold-with-Hope curves show a similar latest Permian sedimentary gap and a distinct change

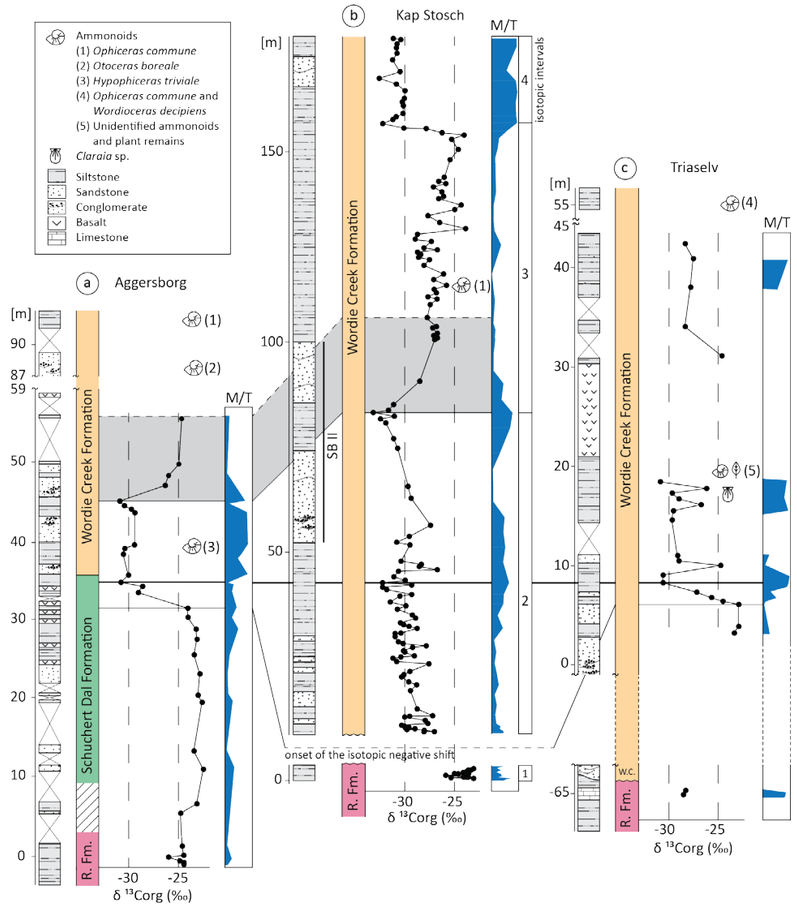

Figure 6. Correlation of the $\delta^{13}C_{org}$ records from Scoresby Land (a) Aggersborg and (c) Triaselv with the $\delta^{13}C_{org}$ record from Kap Stosch (Hold-with-Hope) (Sanson-Barrera et al. 2015).

in palynofacies coinciding with the unconformity (Hermann et al. 2010; Sanson-Barrera et al. 2015), whereas the Finnmark Platform recorded a continuous succession across the Permian–Triassic transition. In all sections the end-Permian $\delta^{13}C_{org}$ negative shift is completely or partly recorded and is used as correlation baseline in Figure 7. The positive shift in the upper part of the Aggersborg section correlates with the base of the isotopic interval 3 at Kap Stosch (Sanson-Barrera et al. 2015) and with the base of interval "f" in the Trøndelag Platform record (Hermann et al. 2010). The ammonoid data from Aggersborg and Kap Stosch provide a mid-Griesbachian age for this positive shift. The *Ophiceras commune* and *Wordioceras decipiens* specimens found in the Triaselv section also indicate a mid- and late-Griesbachian age. However, the lack of more detailed isotopic and paleontological age control for the upper part this section does not allow further correlations (Fig. 7). Sequence stratigraphy studies of the Arctic Triassic successions from Svalbard, the Barents Shelf, and Sverdrup Basin (Embry and Podruski 1988; Mørk et al. 1989; Skjold et al. 1998; Mørk and Smelror 2001) defined a second-order sequence boundary of latest Permian age across the Boreal Realm. Thus, the end-Permian major sea-level fall in East Greenland, corresponds to the latest Permian second-order sequence boundary of the Arctic (Surlyk 1990; Sanson-Barrera et al. 2015), and to a major global regression noticeable in most of the marine Permian–Triassic sections

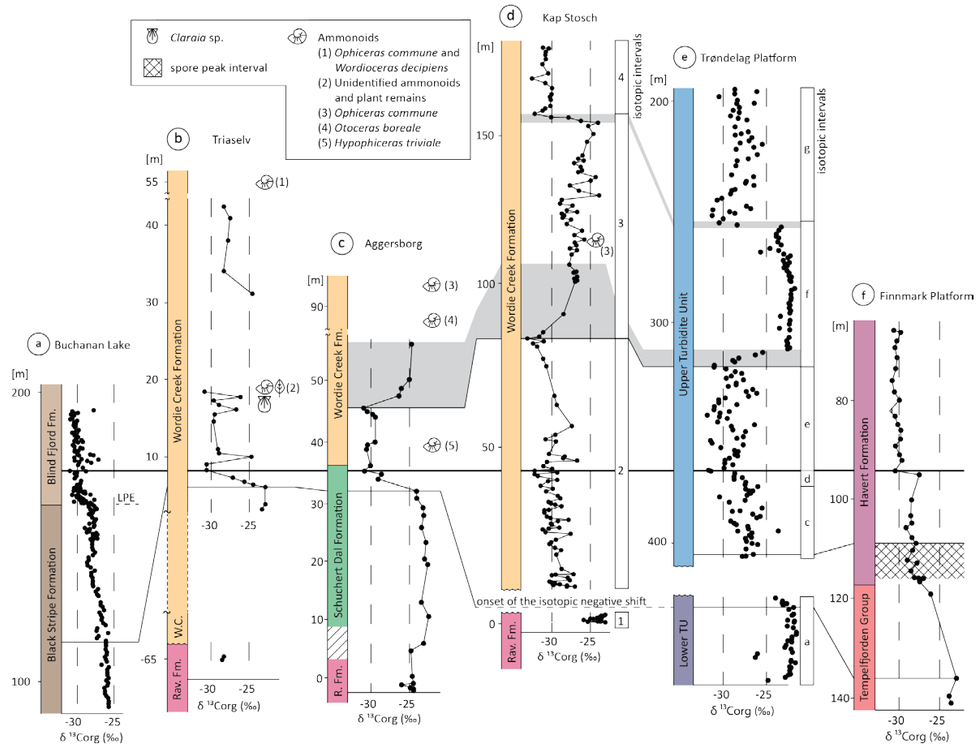

Figure 7. Correlation of the $\delta^{13}C_{org}$ records from (c) Aggersborg, (b) Triaselv, (d) Kap Stosch from East Greenland with records from the (e, f) Trøndelag and Finnmark platforms, off-shore Norway (Hermann et al. 2010; Hochuli et al. 2010), and from (a) Buchanan Lake (Arctic Canada) (Grasby and Beauchamp 2008).

(Holser and Magaritz 1987; Holser et al. 1989). This marked sea-level fall led to the erosion of the Schuchert Dal Formation and part of the Ravnefjeld Formation as recorded in the Triaselv and Kap Stosch sections, and part of the Lower Turbidite Unit on the Trøndelag Platform off-shore Norway (Bugge et al. 2002). On the other hand, more basinal depositional settings as Aggersborg or the Finnmark Platform recorded continuous sedimentation. Many records from the Sverdrup Basin (Arctic Canada) also include a latest Permian sedimentary gap corresponding to the second-order sequence boundary (Embry 1997; Grasby and Beauchamp 2008). However, the Buchanan Lake record (Fig. 7) (Grasby and Beauchamp 2008) also suggests a continuous sedimentation across the Permian–Triassic transition probably due to its more basinal location and/or a higher subsidence rate.

6. Conclusions

In order to provide an interbasinal correlation of organic carbon isotope records for East Greenland, stable organic carbon isotope ($\delta^{13}C_{org}$), palynofacies and ammonoid data of two sections from the Scoresby Land sub-basin (Aggersborg and Triaselv) are presented. These sections can be correlated with three coeval records from the same sub-basin (Fiskegrav, Scoresby Land) and with the Kap Stosch section from the northern Hold-with-Hope sub-basin. One common feature of the above mentioned sections is the latest Permian $\delta^{13}C_{org}$ negative shift, reflecting a major carbon cycle signature of global extent. The latest Permian carbon isotope negative shift proved to be a reliable tool for to correlating these Permian–Triassic sections and unravelling the diachronous clastic fill of a contrasted rift palaeotopography.

The correlation between the East Greenland records (Scoresby Land and Hold-with-Hope) provides a regional chemostratigraphic framework across the Permian–Triassic transition. Aggersborg and Triaselv (Scoresby Land), and Kap Stosch (Hold-with-Hope) have the latest Permian negative $\delta^{13}C_{org}$ shift in common. A prominent early Griesbachian $\delta^{13}C_{org}$ positive shift provides a second correlation tie between the upper part of the Aggersborg section and the Kap Stosch record. The presence of the ammonoids *O. boreale* and *O. commune* in the upper part of the Aggersborg section, and of *O. commune* above the SB II at Kap Stosch indicates a mid-Griesbachian age for this interval.

The $\delta^{13}C_{org}$ records of East Greenland and Norway provide a chemostratigraphic framework for the Greenland–Norway Basin for the interval between the Late Permian and the earliest Triassic. This framework provides the base for reconstructing the sedimentary history of various Permian–Triassic sedimentary records of the Boreal Realm. The latest Permian second-order sequence boundary recorded across the Arctic is expressed in the Triaselv, Kap Stosch, and Trøndelag Platform reflects a sedimentary gap, whereas sedimentation in the Aggersborg, Fiskegrav, Finnmark Platform and Buchanan Lake sections appears to be continuous across the Permian–Triassic transition.

Acknowledgements

The authors are very thankful to Madalina Jäggi-Berechet and Stewart Bishop from the Stable Isotope Laboratory of the Geology Department of the ETH Zurich for the bulk $\delta^{13}C_{org}$ analysis of the samples. Maximiliano Meier is thanked for his support during field work. We are also thankful to the CASP Greenland team who provided very useful discussion of the East Greenland sedimentology and two samples from Triaselv. This work was supported by the Swiss NSF project 200021_135446 to H. Bucher.

References

Birkenmajer, K. (1977). Erosional unconformity at the base of marine Lower Triassic at Wegener Ø, Central East Greenland. Bulletin of the Geological Society of Denmark, 25, 107-116.

Bjerager, M., Seidler, L., Stemmerik, L., Surlyk, F. (2006). Ammonoid stratigraphy and sedimentary evolution across the Permian–Triassic boundary in East Greenland. Geological Magazine, 143, 635-656, doi: 10.1017/S0016756806002020.

Bugge, T., Ringas, J.E., Leith, D.A., Mangerud, G., Weiss, H.M., Leith, T.L. (2002). Upper Permian as new play model on the mid-Norwegian continental shelf: investigated by shallow stratigraphic drilling. The American Association of Petroleum Geologists, 86, 107-127.

Burgess, S.D., Bowring, S., Shen, S. (2014). High-precision timeline for Earth's most severe extinction. Proceedings of the Natural Academy of Sciences, 111, 3316-3321, doi: 10.1073/pnas.1317692111.

Clarkson, M.O., Richoz, S., Wood, R.A., Maurer, F., Krystyn, L., McGurty, D.J., Astratti, D. (2013). A new high-resolution $\delta^{13}C$ record for the Early Triassic: insights from the Arabian Platform. Gondwana Research, 24, 233-242, doi: 10.1016/j.gr.2012.10.002.

Embry, A.F. & Podruski, J.A. (1988). Third-order depositional sequences of the Mesozoic succession of Sverdrup Basin. In James D.A., and Leckie, D.P. (Eds.), Sequences, Stratigraphy, Sedimentology: surface and subsurface (pp. 73-84). Canadian Society Petroleum Geologists Memoir 15.

Embry, A.F. (1997). Global sequence boundaries of the Triassic and their identification in the western Canada sedimentary basin. Bulletin of Canadian Petroleum Geology, 45, 415-433.

Galfetti, T., Hochuli, P.A., Brayard, A., Bucher, H., Weissert, H., Vigran, J.O. (2007). Smithian–Spathian boundary event: evidence for global climatic change in the wake of the end-Permian biotic crisis. Geology, 35, 291-294, doi: 10.1130/G23117A.1.

Grasby, S.E. & Beauchamp, B. (2008). Intrabasin variability of the carbon-isotope record across the Permian–Triassic transition, Sverdrup Basin, Arctic Canada. Chemical Geology, 253, 141-150, doi: 10.1016/j.chemgeo.2008.05.005.

Hermann, E., Hochuli, P.A., Bucher, H., Vigran, J.O., Weissert, H., Bernasconi, S.M. (2010). A close-up view of the Permian–Triassic boundary based on expanded organic carbon isotope records from Norway (Trøndelag and Finnmark Platform). Global and Planetary Change, 74, 156–167, doi: 10.1016/j.gloplacha.2010.10.007.

Hermann, E., Hochuli, P.A., Méhay, S., Bucher, H., Brühwiler, T., Ware, D., Hautmann, M., Roohi, G., Ur-Rehman, K., Yaseen A. (2011). Organic matter and palaeoenvironmental signals during the Early Triassic biotic recovery: the Salt Range and Surghar Range records. Sedimentary Geology, 234, 19–41, doi:10.1016/j.sedgeo.2010.11.003.

Hochuli, P.A., Hermann, E., Vigran, J.O., Bucher, H., Weissert, H. (2010). Rapid demise and recovery of plant ecosystems across the end-Permian extinction event. Global and Planetary Change, 74, 144–155, doi:10.1016/j.gloplacha.2010.10.004.

Holser, W.T. & Magaritz, M. (1987). Events Near the Permian-Triassic Boundary. Modern Geology 11, 155-180.

Holser, W.T., Schönlaub, H.P., Attrep Jr, M., Boeckelmann, K., Klein, P., Magaritz, M., Orth, C.J., Fenninger, A., Jenny, C., Kralik, M., Mauritsch, H.,

Pak, E., Schramm, J.M., Stattegger, K., et al. (1989). A unique geochemical record at the Permian/Triassic boundary. Nature 337, 39-44.

Korte C. & Kozur H.W. (2010). Carbon-isotope stratigraphy across the Permian–Triassic boundary: a review. Journal of Asian Earth Sciences 39, 215-235, doi:10.1016/j.jseaes.2010.01.005.

Kreiner-Møller, M., & Stemmerik, L. 2001. Upper Permian lowstand fans of the Bredehorn Member, Schuchert Dal Formation, East Greenland. In O.J. Martinsen and T. Dreyer (Eds.), Sedimentary Environments Offshore Norway - Palaeozoic to Recent (pp. 51-65). Norwegian Petroleum Society (NPF) Special Publication 10, Elsevier Science B.V. (Amsterdam).

Krull, E.S., Lehrmann, D.J., Druke, D., Kessel, B., Yu, Y., Li, R. (2004). Stable carbon isotope stratigraphy across the Permian–Triassic boundary in shallow marine carbonate platforms, Nanpanjiang Basin, south China. Palaeogeography, Palaeoclimatology, Palaeoecology, 204, 297-315, doi: 10.1016/S0031-0182(03)00732-6.

Looy, C.V., Twitchett, R.J., Dilcher, D.L., Van Konijnenburg-Van Cittert, J.H.A., Visscher, H. (2001). Life in the end-Permian dead zone. Proceedings of the National Academy of Science, 98, 7879-7883, doi: 10.1073/pnas.131218098.

Morante, R. (1996). Permian and Early Triassic isotopic records of carbon and strontium in Australia and a scenario of events about the Permian–Triassic boundary. Historical Biology 11, 289–310.

Mørk, A., Embry, A.F., Weitschat W. (1989). Triassic transgressive–regressive cycles in the Sverdrup Basin, Svalbard and the Barents Shelf. In Collinson, J.D. (Ed.), Correlation in Hydrocarbon Exploration (pp. 113-130). Norwegian Petroleum Society.

Mørk, A., & Smelror, M. (2001). Correlation and non-Correlation of high order circum-Arctic Mesozoic sequences, Polarforschung, 69, 65-72.

Müller, R., Nystuen, J.P., Eide, F., Lie, H., Mqiler, R. (2005). Late Permian to Triassic basin infill history and palaeogeography of the mid-Norwegian – East Greenland region. In Wandås, B. et al. (Eds.), Onshore–Offshore relationships on the North Atlantic Margin (pp. 165-189). Norwegian Petroleum Society (NPF) Special Publication 12, Elsevier B.V.

Nielsen, E. (1935). The Permian and Eotriassic vertebrate-bearing beds at Godthaab Gulf (East Greenland). Meddelelser om Grønland, 98.

Oberhänsli, H., Hsü, K.J., Piasecki, S., Weissert, H. (1989). Permian–Triassic carbon-isotope anomaly in Greenland and in the Southern Alps. Historical Biology, 2, 37-49.

Payne, J.L., Lehrmann, D.J., Wei, J., Orchard, M.J., Schrag, D.P., Knoll, A.H. (2004). Large perturbations of the carbon cycle during recovery from the end-Permian extinction. Science, 305, 506-509, doi: 10.1126/science.1097023.

Perch-Nielsen, K., Birkenmajer, K., Birkelund, T., Aellen, M. (1974). Revision of Triassic stratigraphy of the Scoresby Land and Jameson Land region, East Greenland. Meddelelser om Grønland, 193.

Piasecki, S. (1984). Preliminary palynostratigraphy of the Permian–Lower Triassic sediments in Jameson Land and Scoresby Land, East Greenland. Bulletin of the Geological Society of Denmark, 32, 139-144.

Piasecki, S., & Stemmerik, L. (1991). Late Permian anoxia in central East Greenland. In Tyson, R. V. & Pearson T.H. (Eds.), Modern and Ancient Continental Shelf Anoxia (pp. 275–290). Geological Society Special Publications.

Sanson-Barrera, A., Hochuli, P.A., Bucher, H., Schneebeli-Hermann, E., Weissert, H., Adatte, T., Bernasconi S.M (2015). Late Permian–earliest Triassic high-resolution organic carbon isotope and palynofacies records from Kap Stosch (East Greenland). Global and Planetary Changes, 133, 149-166, doi: 10.1016/j.gloplacha.2015.08.006.

Seidler, L., Steel, R., Stemmerik, L., Surlyk, F. (2004). North Atlantic marine rifting in the Early Triassic: new evidence from East Greenland. Journal of the Geological Society, 161, 583-592, doi: 10.1144/0016-764903-063.

Skjold, L.J., Van Veen, P.M., Kristensen, S.E., Rasmussen, A.R. (1998). Triassic sequence stratigraphy of the southwestern Barents Sea. In de Graciansky, P.C., Hardenbol, J., Jacquin, T., Vail, P.R (Eds.), Mesozoic and Cenozoic Sequence Stratigraphy of European Basins (pp. 651-666). Society for Sedimentary Geology, Special Publication no.60.

Spath, L.F. (1930). The Eotriassic invertebrate fauna of East Greenland. Meddelelser om Grønland, 83.

Spath, L.F. (1935). Additions to the Eotriassic invertebrate faunas of East Greenland. Meddelelser om Grønland, 98.

Stemmerik, L., Clausen, O.R., Korstgård, J., Larsen, M., Piasecki, S., Seidler, L., Surlyk, F., Therkelsen, J. (1997). Petroleum geological investigations in East Greenland: project 'Resources of the sedimentary basins of North and East Greenland'. Geology of Greenland Survey Bulletin, 176, 29-38.

Stemmerik, L., Bendix-Almgreen, S.E., Piasecki, S. (2001). The Permian–Triassic boundary in central East Greenland: past and present views. Bulletin of the Geological Society of Denmark, 48, 159–167.

Surlyk, F., Piasecki, S., Rolle, F., Stemmerik, L., Thomsen, E., Wrang, P. (1984). The Permian Basin of East Greenland. In Petroleum geology of the North European Margin (pp. 303-315). Norwegian Petroleum Society.

Surlyk, F., Piasecki, S., Rolle, F., Scholle, P.A., Stemmerik, L., Thomsen, E. (1986). The Permian of the western margin of the Greenland Sea - A future exploration target. In Halbouty, M.T. (Ed.), Future Petroleum Provinces of the World (pp. 629–659). American Association of Petroleum Geologists.

Surlyk, F. (1990). Timing, style and sedimentary evolution of Late Palaeozoic–Mesozoic extensional basins of East Greenland. In Hardman, R.F.P. & Brooks, J. (Eds.), Tectonic Events Responsible for Britain's Oil and Gas Reserves (pp. 107-125).

Teichert, C., & Kummel, B. (1972). Permian–Triassic Boundary in the Kap Stosch Area, East Greenland. Bulletin of Canadian Petroleum Geology, 20, 659-675.

Tozer, E.T. (1981). Triassic ammonoidea: classification, evolution and relationship with Permian and Jurassic forms. In M.R. House and J.R. Senior (Eds.), The Ammonoidea: the classification, mode of life and geological usefulness of a major fossil group (pp. 66-100). Systematics Association special volume 18.

Tozer, E.T. (1994). Canadian Triassic ammonoid faunas. Geological Survey of Canada Bulletin, 467.

Traverse, A. (2007). Paleopalynology. Topics in Geobiology, 28, Springer.

Trümpy, R. (1969). Lower Triassic ammonites from Jameson Land (East Greenland). Meddelelser om Grønland, 168(2), 77-116.

Twitchett, R.J., Looy, C.V., Morante, R., Visscher, H., Wignall, P.B. (2001). Rapid and synchronous collapse of marine and terrestrial ecosystems during the end-Permian biotic crisis. Geological Society of America, 29, 351–354.

Weitschat, W. & Dagys, A. (1989). Triassic biostratigraphy of Svalbard and comparison with NE-Siberia. Mitteilungen aus dem Geologisch-Paläontologischen Institut der Universität Hamburg, 68, 179-213.

Wignall, P.B., & Twitchett, R.J. (2002). Permian–Triassic sedimentology of Jameson Land, East Greenland: incised submarine channels in an anoxic basin. Journal of the Geological Society, 159, 691-703, doi: 10.1144/0016-764900-120.

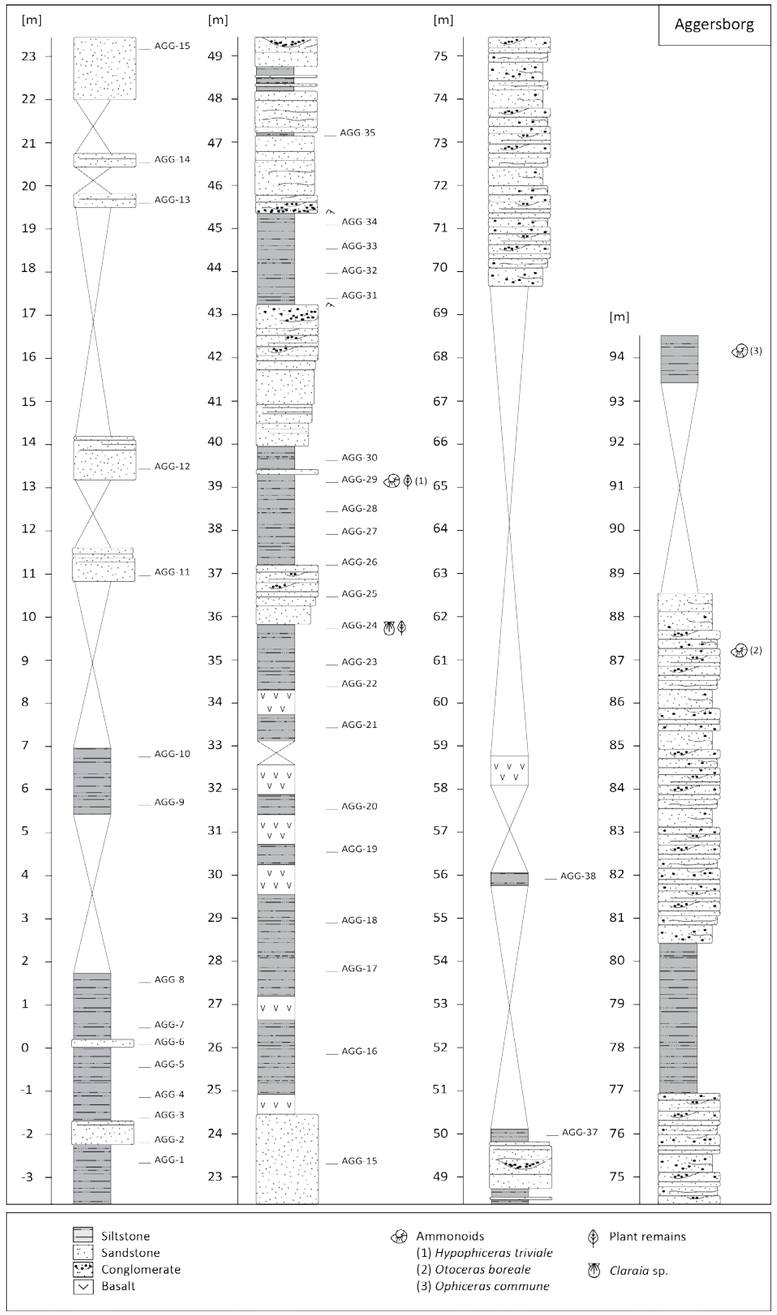

Supplementary data 1. Lithostratigraphy of the Aggersborg section, and photographs (a) base of the Aggersborg section (Wegener Halvø Formation), (b) and (c) macrofossil content of the Wegener Halvø Formation: brachiopods, corals, and bivalves; (d) overview of the Aggersborg section from sample location Agg 2; and (e) Aggersborg section from around sample location Agg 6.

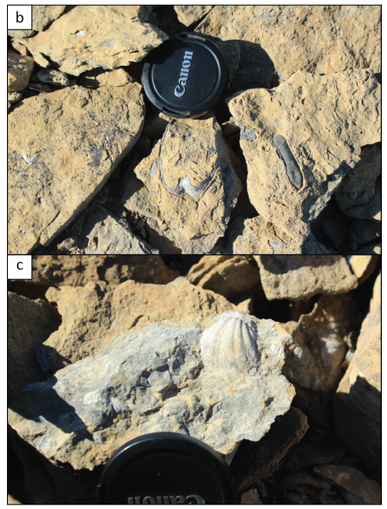

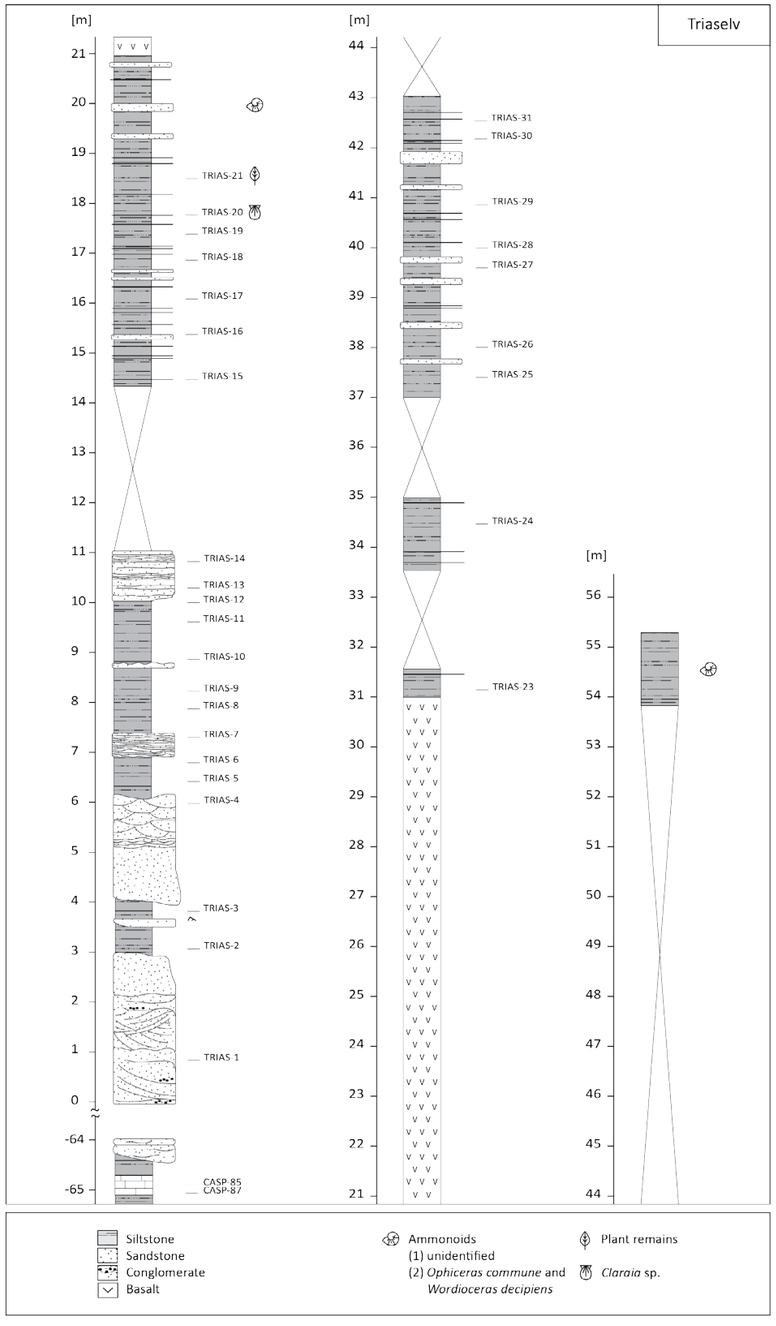

Supplementary data 2. Lithostratigraphy of the Triaselv section, and photographs, (a) overview of the Triaselv from the top of the section; (b and c) base of the Triaselv section at sample location Trias 2, looking upstream (b), and downstream (c); (d) Triaselv section around sample location Trias 4; (e) the Triaselv section around sample location Trias 20; (f) the Triaselv section around sample location Trias 21; and (g) plant remains from sample location Trias 21.

Chapter 3

Sediment geochemistry and clay mineralogy of an expanded earliest Triassic marine succession (Kap Stosch, East Greenland): environmental implications

Anna Sanson-Barrera, Thomas J. Algeo, Alex Reis,
Allison Young, Thierry Adatte, Hugo Bucher

in review in Palaeogeography, Palaeoclimatology, Palaeoecology

Abstract

Various scenarios for marine environmental conditions in the aftermath of the end-Permian mass extinction have been proposed, including long-lasting anoxia to rapidly fluctuating redox conditions. Here, we present marine and terrestrial environmental changes of the latest Permian to Dienerian succession at Kap Stosch, East Greenland utilizing bulk-rock geochemistry and clay mineralogy. The study section, which has an average sedimentation rate of 0.68 m kyr^{-1} spanning an interval of ~1 Myr, offers exceptional stratigraphic resolution of earliest Triassic environmental changes. Several proxies such as S/TOC and trace element proxies (e.g., Mo, V, and U) were affected by strong siliciclastic dilution. However, DOP_T, C_{org}:P, and S/TOC reflect one of the three suboxic-anoxic events in the Griesbachian that have previously been identified by their high relative abundance of marine organic matter. Clay mineralogy shows slightly increased smectite abundances and smectite/kaolinite ratios in the Dienerian part of the succession, combined with an increase in red sediment colour, reflecting an increase in climate seasonality. Spore/pollen ratios indicate more humid climates in the Dienerian, suggesting that the increase in seasonality strongly affected the precipitation regime.

Keywords: organic carbon; major elements; trace elements; redox; clay minerals; paleoclimate

1. Introduction

The environmental disturbances that led to the Permian–Triassic mass extinction, the largest biotic crisis of the Phanerozoic, persisted into the Early Triassic (e.g., Payne et al. 2004; Retallack et al. 2011; Wei et al. 2015), influencing the pattern and tempo of the post-extinction biotic recovery. Carbon-isotope records of the Early Triassic document high amplitude fluctuations of the global carbon cycle from the latest Changhsingian (end-Permian) up to the onset of the Spathian substage, an interval of <2 Myr (Payne et al. 2004; Brayard et al. 2006; Galfetti et al. 2007; Tong et al. 2007; Hermann et al. 2012; Romano et al. 2013). Correlative fluctuations in the $\delta^{34}S$ of seawater sulfate indicate that both the C- and S-isotopic fluctuations were probably linked to variation in rates of organic carbon and pyrite burial (Luo et al. 2010; Song et al. 2014). These large isotopic perturbations occurred at timescales of ~100-500 thousand years (kyr) (Song et al. 2014), although there is evidence for shorter-term (<20-kyr) perturbations as well (e.g., Algeo et al. 2007, 2008a).

The causes for these environmental fluctuations may have been complex (e.g., Berner 2002; Yin et al. 2007; Algeo et al. 2011a), although two factors stand out. First, the Early Triassic was a predominantly warm interval (Sun et al. 2012; Romano et al. 2013), and pulses of climatic warming may have occurred in response to episodic emissions of greenhouse gases (Ovtcharova et al. 2006; Retallack et al. 2011). Second, at least in the Tethys Ocean, persistence of an intermediate-depth reservoir of sulfidic ocean waters (Feng and Algeo 2014) is likely to have set the stage for short-term incursions of hydrogen sulfide into the ocean-surface layer (Kump et al. 2005; Algeo et al. 2007, 2008a). Such incursions may have been linked to warming events that resulted in increased oceanic stratification (Song et al. 2014) and oxygen-minimum zone expansion (Algeo et al. 2010, 2011b; Winguth and Winguth 2012). This is in agreement with recent studies that documented short-term environmental perturbations rather than long-lasting stress as a major control on Early Triassic biodiversity (Krystyn et al. 2003; Brayard et al. 2009; Hermann et al. 2012; Hofmann et al. 2011, 2013).

So far research focussing on environmental instability in Late Permian and Early Triassic marine systems was mainly based on sections in the Paleotethyan and Neotethyan regions (e.g., Wignall and Twitchett 1996; Newton et al. 2004; Algeo et al. 2007, 2008a; Riccardi et al. 2006; Wei et al. 2015). Comparatively fewer studies have examined marine redox and paleoenvironmental variation in the Boreal Realm. Euxinic depositional conditions have been inferred for the Upper Permian of East Greenland (Piasecki and Stemmerik 1991; Nielsen and Shen 2004; Fenton et al. 2007; Nielsen et al. 2010; Hays et al. 2012), the Upper Permian–Lower Triassic of the Trøndelag Platform off the Norway continental shelf (Bugge et al. 2002), the Lower Triassic Vardebukta Formation in western Spitsbergen (Wignall et al. 1998; Wignall et al. 2015), and for the Sverdrup Basin of Arctic Canada (Grasby et al. 2012).

Here, we present high-resolution bulk-rock geochemistry data including records of total organic carbon (TOC), total sulfur (S), degree of pyritization (DOP_T), major and trace element concentrations, organic and inorganic fluxes, and clay mineralogy from Kap Stosch in the Hold-with-Hope region of East Greenland (Fig. 1). These data are combined with particulate organic matter and bulk organic carbon isotope analyses of Sanson-Barrera et al. (2015). The proxies are used to infer environmental conditions such as marine redox conditions, paleoproductivity, relative sea-level changes, terrestrial weathering, and climatic conditions during the latest Permian and specially during the earliest Triassic recovery interval. The aim is to assess not only marine and terrestrial environmental changes but also to evaluate the impact of high sedimentation rates on geochemical proxies and their environmental interpretation.

2. Geological setting

2.1. Basin architecture and stratigraphy of East Greenland

East Greenland is a reference area for studying the Permian–Triassic succession of the Boreal Realm owing to thick and well-exposed successions of marine sediments along its coast. Geological research in this area has been carried out since the early twentieth century. James Wordie (1927) was the first to describe Permian and Triassic rocks along the East Greenland coast. Later these units were studied in greater detail and with different objectives. Studies include lithostratigraphic and biostratigraphic works examining the fish content

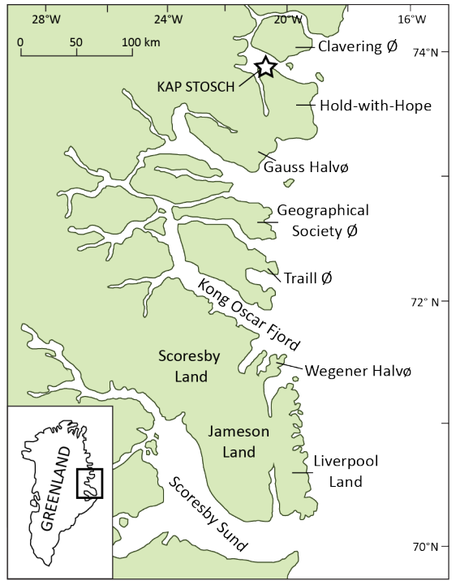

Figure 1. General map of East Greenland and the location of the study section - Kap Stosch (after Seidler et al. 2004).

(Koch 1931; Nielsen 1935), ammonoids (Spath 1935; Trümpy 1969; Teichert and Kummel 1972; Bjerager et al. 2006), and palynology (Balme 1979; Piasecki 1984; Looy et al. 2001), and works on basin evolution and hydrocarbon potential (Stemmerik et al. 1998, 2001; Twitchett et al. 2001; Seidler et al. 2004; Surlyk et al. 1984; Surlyk 1990). The present lithostratigraphic division of the Upper Permian–Lower Triassic is based on the work of Perch-Nielsen et al. (1974) and Surlyk (1990). More recently, the study area has been the subject of biostratigraphic and chemostratigraphic studies of the latest Permian–earliest Triassic interval (Stemmerik et al. 2001; Looy et al. 2001; Twitchett et al. 2001; Wignall and Twitchett 2002; Nielsen and Shen 2004; Fenton et al. 2007; Nielsen et al. 2010; Hays et al. 2012; Sanson-Barrera et al. 2015). During Permian–Triassic times East Greenland was located on the northern margin of Pangea. This margin was embayed by a large rift located between Greenland and Norway. The East Greenland basin represents the western margin of this Greenland–Norway rift basin where reactivation of Late Carboniferous–Early Permian basin-margin faults led to the deposition of thick sedimentary successions during the Late Permian and Early Triassic (Surlyk 1990; Stemmerik 2000). The Late Permian–earliest Triassic interval coincided with the most active phase of rifting and deepening of the Greenland–Norway Basin, and the Griesbachian strata deposited there are considered to be synrift (Surlyk 1990; Hamann et al. 2005; Oftedal et al. 2005). Besides the main basin boundary faults, both the western (East Greenland) and eastern (Norwegian) margins of the basin developed a series of smaller internal faults, resulting in the subdivision of each margin into several sub-basins (Seidler et al. 2004; Oftedal et al. 2005; Hamann et al. 2005). The East Greenland sub-basins are characterized by thick sedimentary successions ranging from delta fan to basinal depositional environments, influenced by relative sea-level rises and falls during the Late Permian and Early Triassic (Surlyk 1990). In the Kap Stosch area, up to ~750 m of sediments were deposited between the Late Permian (Wuchiapingian) and the earliest Triassic (Dienerian) (Oftedal et al. 2005; Sanson-Barrera et al. 2015), generating the framework for high-resolution chemostratigraphic studies.

The Middle–Upper Permian lithostratigraphy is defined by the Foldvik Creek Group (Perch-Nielsen et al. 1974; Surlyk 1990). The base of this group consists of alluvial conglomerates of the Huledal Formation. Due to a relative sea-level rise, the uppermost Huledal conglomerates exhibit marine influence, followed by a shift to marine, hypersaline carbonates and evaporites of the Karstryggen Formation. Both the Huledal and Karstryggen formations are of Capitanian age (Surlyk et al. 1986; Surlyk 1990). During the Wuchiapingian, the Karstryggen Formation was overlain by carbonate build-ups of the Wegener Halvø Formation in basin-margin areas and on paleo-highs, whereas black bituminous mudstones of the Ravnefjeld Formation were deposited laterally (Surlyk et al. 1986; Surlyk 1990; Piasecki and Stemmerik 1991). A relative sea-level fall during the latest Permian is represented by the grey-black bioturbated siltstones and turbiditic sandstones of the Schuchert Dal Formation (Fig. 2).

The end-Permian relative sea-level drop recorded in the Schuchert Dal Formation terminated deposition in the northern sub-basins of East Greenland (Teichert and Kummel 1972; Birkenmajer 1977; Surlyk 1990). In the Hold-with-Hope sub-basin (i.e., our study area), this event correspond to an erosional unconformity, and consequently the Wordie Creek Formation rests

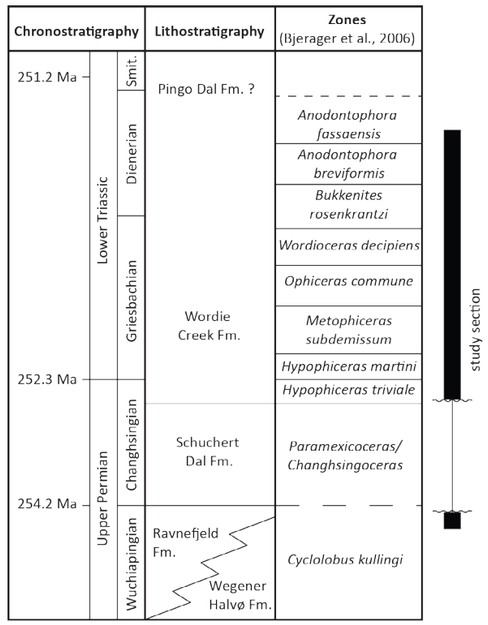

Figure 2. Chrono- and lithostratigraphy, and biozonation of the Upper Permian–Lower Triassic strata of East Greenland (after Bjerager et al. 2006). See Figure 3 for age sources.

unconformably on the Ravnefjeld Formation. This unconformity is located 7 m above the base of the study section. The sediments of the Wordie Creek Formation reflect several relative sea-level rises and falls coinciding with increased tectonic rift activity (Surlyk et al. 1986; Surlyk 1990; Seidler et al. 2004).

2.2. Kap Stosch section (Hold-with-Hope)

The study interval represents a composite section that includes 7 m of the Wuchiapingian Ravnefjeld Formation at its base, and 680 m of the Wordie Creek Formation spanning the latest Changhsingian into the Dienerian. Kap Stosch represents a shallowing-up deltaic succession of alternating siltstone and sandstone beds. A detailed description of the sections and correlation procedure can be found in Sanson-Barrera et al. (2015).

In East Greenland the Permian–Triassic mass extinction is documented in the upper Schuchert Dal Formation, where marine fauna diversity decreases, and the terrestrial microflora shows a marked shift in relative abundances of individual plant groups (Stemmerik et al. 2001; Looy et al. 2001; Twitchett et al. 2001). In East Greenland, the boundary between the Schuchert Dal and the Wordie Creek formations has been traditionally considered to represent the Permian–Triassic boundary (PTB). However, the PTB is currently defined by the first occurrence of the conodont *Hindeodus parvus* in Meishan (China) (Yin et al. 2001). *H. parvus* was documented in the apparently continuous section across the PTB at Fiskegrav (Jameson Land, East Greenland), 23.5 m above the Schuchert Dal and Wordie Creek formational boundary (Twitchett et al. 2001), postdating the Permian–Triassic mass extinction and the global negative carbon isotope excursion. However, the first occurrence of *H. parvus* has been shown to be globally diachronous (e.g., Zhang et al. 2014; Brosse et al. 2015; Brosse et al. 2016). The new reliable biochronology of the PTB in South China using Unitary Associations Zones demonstrates that the biotic crisis straddles the Permian–Triassic boundary (Brosse et al. 2016). The negative carbonate carbon isotope spike at Meishan would be of latest Permian age (Brosse et al. 2016). So far conodonts have not been reported from the Kap Stosch section, therefore the exact positioning of the paleontological PTB is not exactly known. However, bulk organic carbon isotope data show a distinct negative shift in the lowermost part of the study section within a first minimum at ca. 42 m. In comparison with the Meishan record and the biochronological data there (e.g., Brosse et al. 2016) these lowermost 42 m including the negative carbon isotope shift would be of latest Permian age. The Griesbachian ammonoid *Ophiceras commune* was documented at about 110 m of the composite section (Sanson-Barrera et al. 2015). The oldest occurrence of *Ophiceras* sp. Indet. was identified ca. 40 m above the formational boundary (i.e., ca. 44m above the base of the section, personal communication Bucher). Therefore, the PTB lies in the interval between 42 m (negative bulk organic carbon isotope spike) and 44 m of the composite section.

3. Materials and methods

The study samples were collected during three field seasons (the summers of 2011–2013). The sampling focused mainly on grey-green, siltstone to fine sandstone beds in order to ensure sufficient organic matter for the analyses of bulk organic carbon isotopes, particulate organic matter data, major and trace element geochemistry, and clay mineralogy. A total of 605 samples weighing between 50 and 100 g each were collected. For a detailed description for bulk organic carbon isotope measurements and preparation of particulate organic matter samples, see Sanson-Barrera et al. (2015).

3.1. Major and trace element analysis

Elemental geochemical analyses were performed on 450 samples in the Department of Geology of the University of Cincinnati. Major- and trace-element concentrations of whole-rock samples were determined using a wavelength-dispersive Rigaku 3040 XRF spectrometer. Results were calibrated using both USGS and internal laboratory standards. Analytical precision based on replicate analyses was better than ±2% for major and minor elements and ±5% for trace elements. Detection limits were ~5 ppm for most trace elements.

Carbon and sulfur elemental concentrations were measured in the Department of Geology of the University of Cincinnati using an Eltra 2000 C-S analyser. Data quality was monitored via multiple analyses of the USGS standard SDO-1 (TC = 9.68 wt%; TS = 5.35 wt%) and an internal lab standard DBS-1 (TC = 3.50 wt%; TS = 1.97 wt%), yielding an analytical precision (2σ) of ±2.5% of reported values for carbon and ±5% for sulfur. An aliquot of each sample was digested in 2N HCl at 50°C for 12 hours to dissolve carbonate minerals, and the residue was analysed for total organic carbon (TOC) and non-acid-volatile sulfur (NAVS); total inorganic carbon (TIC) and acid-volatile sulfur (AVS) were obtained by difference.

Excess barium (Ba_{xs}) is used as a paleoproductivity proxy and determined by estimating a detrital Ba/Al ratio from the barium (Ba) versus aluminum (Al) crossplot, and then subtracting the detrital Ba fraction (Ba_{detr}) from the total Ba concentration of each sample:

$$[Ba_{xs}]_{sample} = [Ba]_{sample} - [Al]_{sample} \times (Ba/Al)_{detr} \quad (1)$$

We assume that all Ba_{xs} is of biogenic origin, although it is possible that small amounts were present as Ba adsorbed onto carbonates and ferromanganese oxyhydroxides (e.g., Eagle et al. 2003).

The chemical index of alteration (CIA) (Nesbitt and Young 1982) is calculated as:

$$CIA\text{-}K = Al_2O_3 / (Al_2O_3 + Na_2O + CaO^*) \times 100 \quad (2)$$

This index does not include potassium (K) because diagenetic processes can yield elevated concentrations of K (Sheldon et al. 2002; Adams et al. 2011). The calculation is based on molar proportions, where the CaO* represents the CaO in silicate minerals (Nesbitt and Young 1982). In this study, a CaO* correction is needed due to the presence of carbonates (e.g., McLennan 1993). In the case of a remaining amount of CaO* after the correction higher than Na_2O content, it is assumed that the CaO* is equivalent to the Na_2O content (McLennan 1993).

The degree of pyritization (DOP) is the proportion of highly reactive iron (Fe_{HR}) that has been converted to pyrite (Fe_{py}), i.e., $Fe_{py} / (Fe_{py} + Fe_{HR})$. In our calculations, total Fe (Fe_T) is used as a proxy for Fe_{HR}, a procedure that enlarges the denominator of the ratio and reduces DOP estimates (which are denoted DOP_T) relative to true DOP.

The mineralogic composition of the study section is dominated by clay minerals, quartz, and calcite. Geochemical concentration data can be used to estimate the relative proportions of the major mineralogical fractions in each sample as follows (cf. Algeo and Twitchett 2010):

$$\text{Clay minerals (\%)} = Al_{sample} \times 100 / \kappa 1 \quad (3)$$

$$\text{Quartz (\%)} = SiO_{2(sample)} - (Al_{sample} / 27.0 \times \kappa 2 \times 60.1) \quad (4)$$

$$\text{Calcite (\%)} = TIC_{sample} \times 100.1 / 12.0 \quad (5)$$

Equations 3 and 4 calculate model amounts of clay minerals and quartz (or chert) in a sample based on measured aluminum (Al) and silica (SiO_2) concentrations. The constants 12.0, 27.0, and 60.1, represent the molar weights in grams of C, Al, and SiO_2. The coefficients κ1 (11.11) and κ2 (1.29×10^{-4}) were empirically determined so that a mean sum of 100.0% for all components in each sample was generated. Equation 5 calculates the amount of calcium carbonate in a sample from the TIC. Where deviating from unity, the three-component sum for each sample was normalized to 100% for display purposes.

3.2. Biostratigraphic control, age model, and flux calculations

The Late Permian–Early Triassic biostratigraphy of East Greenland is based on 6 ammonoid and 2 bivalve zones (Bjerager et al. 2006) (Fig. 2). The Kap Stosch study section yielded only sparse ammonoid fossil finds that did not allow for the full identification of these zones (Sanson-Barrera et al. 2015). However, two age-diagnostic ammonoids were found in the Wordie Creek Formation, *Ophiceras commune* and *Bukkenites rosenkrantzi*, which are characteristic of the mid-Griesbachian and early Dienerian, respectively (Sanson-Barrera et al. 2015).

Good age control is required for sedimentation rate and flux calculations. Permian–Triassic radiometric ages are based mainly on ID-TIMS dating of zircons in volcanic ashes from South China (Shen et al. 2011; Ovtcharova et al. 2006, 2015; Galfetti et al. 2007; Fig. 3). Recent improvements in decay constants and calibration techniques have led to revisions of the ages for the PTB (251.88 ± 0.031 Ma; Burgess et al. 2014) and Early-Middle Triassic boundary (247.05 ± 0.16 Ma; Ovtcharova et al. 2015). These new age estimates are younger relative to the previously accepted ages of the PTB (252.17 ± 0.06 Ma; Shen et al. 2011) and Early-Middle Triassic boundary (247.2 Ma; Lehrmann et al. 2006; Ovtcharova et al. 2006), suggesting that the new procedure will ultimately result in revision of all ID-TIMS ages to younger values. However, the duration of substages within the Early Triassic are unlikely to change appreciably. In the absence of intermediate ages based on the new technique, the age model we used to calculate sedimentation rates for the study units is based on a PTB age of 252.17 ± 0.06 Ma (Shen et al. 2011) and an early Smithian age of 251.22 ± 0.2 Ma (Galfetti et al. 2007) (Fig. 3). These ages are comparable because they are based on the same ID-TIMS dating method (Shen et al. 2011; Galfetti et al. 2007). Based on these studies, we infer a duration for the Griesbachian–Dienerian interval of ~1.0 ± 0.2 Myr.

The sedimentation rates calculations of the study section include the sediments of the Wordie Creek Formation from the late Changhsingian to Dienerian. Although we cannot delineate (i) the duration of the Changhsingian part of the section and (ii) the duration of the missing topmost part of the Dienerian, we regard a total duration of ~1.0 ± 0.2 Myr for the entire section as reasonable upper value approximation. Our sedimentation rate model is based on the following premises: (i) field observations allowed us to assume continuous sedimentation through the entire Wordie Creek Formation; (ii) time was allocated within the section based on facies-specific relative sedimentation rates, with rates for pure sandstone beds (100% SiO_2) being 5× that of pure shale (100% clays), (iii) the average bulk accumulation rate for pure shale was empirically adjusted to yield the chosen cumulative duration of the 680-m-thick study section (i.e., ~1.0 Myr). Sampling in the field was focused on fine-grained lithologies for studying palynology and bulk organic carbon isotopes and sandstone intervals have not been sampled. To achieve a higher sample density and more equal sample distances for the calculation of the sedimentation rate, virtual sandstone samples have been inserted where field observations documented sandstone intervals that were not sampled. A total of 162 of these samples have been inserted and are marked by numbers with the format (XXX-S-000). The algorithm for this calculation is:

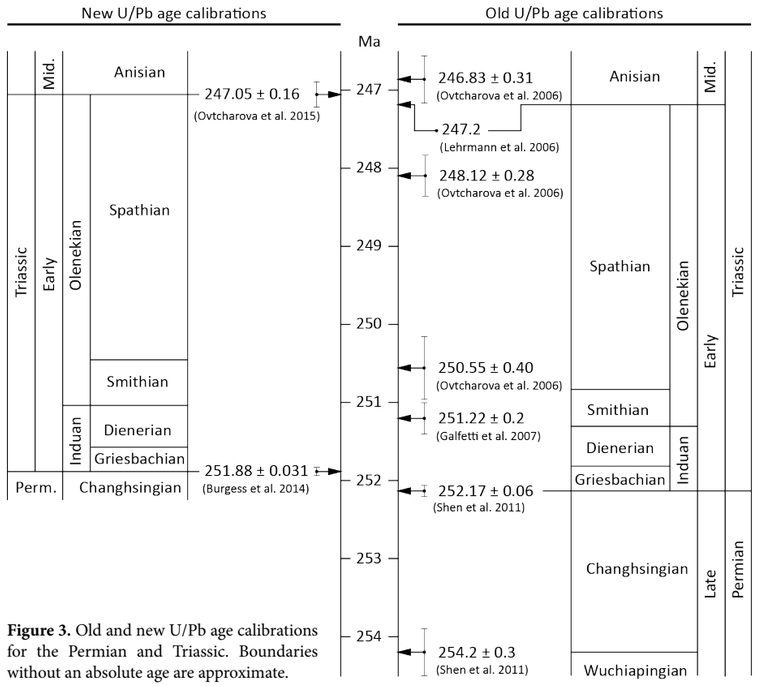

Figure 3. Old and new U/Pb age calibrations for the Permian and Triassic. Boundaries without an absolute age are approximate.

$$t_{(0\text{-}680)} = \sum_{i=0}^{680} I_i^{i+1} / [\theta \times (f_{sh} + 5 \times f_{ss})_i] \quad (6)$$

where I_i^{i+1} is the stratigraphic interval of sample i, f_{sh} and f_{ss} are the fractional amounts of clays and SiO_2 in sample i (note that $f_{sh} + f_{ss} = 1.0$), and θ is the average bulk accumulation rate for pure shale. The ratio of depositional rates between coarse- and fine-grained siliciclastics (i.e., sandstone and shale) surely varies in different settings, but gamma analyses in studies of various formations yielded ratios between ~5:1 and 10:1 (e.g., table 1 of Kominz and Bond 1990; table 2 of Kominz and Bond 1992; Kominz, 1996; table 1 of Yang and Kominz 1999), so our adopted ratio is reasonable. This procedure yielded the sedimentation rate (SR; in units of m kyr^{-1}) for each sample, from which the fluxes of individual sedimentary components (in units of g cm^{-2} kyr^{-1}) were calculated:

$$Flux_i = \rho \times SR \times C_i \quad (7)$$

where $Flux_i$ and C_i are the flux and concentration (in percent) of component i in a given sample and ρ is the average dry bulk density (assumed equal to 2.5 g cm^{-3}). Equation 7 was also used to calculate organic carbon accumulation rates (OCAR) and bulk accumulation rates (BAR), with the term 'C_i' deleted from Equation 7 for calculation of the latter. BAR and OCAR are presented in g m^{-2} yr^{-1} for the purpose of comparison with published data reported in the same units (Fig. 10).

3.3. Clay-mineral analysis

Clay-mineral analysis was performed on 64 samples in the Department of Earth Sciences of the University of Lausanne. Clay mineralogy composition was analysed using a Thermo Scientific ARL X-TRA diffractometer using a semi-quantitative method following the procedures described by Klug and Alexander (1974), Kübler (1983), and Adatte et al. (1996). Clay mineral analyses were performed on powdered and decarbonated samples. Ultrasonic disaggregation was accomplished during 3 min intervals. The target fraction (<2 μm) was separated and pressed into a powder holder. The intensities of selected peaks characterizing each clay mineral present in the <2 μm size fraction (chlorite, mica, kaolinite, illite/smectite mixed-layers and smectite) were measured for a semi-quantitative estimate of the proportion of clay minerals present in the size-fractions <2 μm. Clay mineral proportions are given in relative percentage abundance. Smectite/kaolinite and smectite/mica+chlorite+kaolinite are expressed in CPS (counts per second).

4. Results

4.1. Major element proxies

Aluminum (Al), silicon (SiO_2) and total inorganic carbon (TIC) have been used to infer the dominant mineral fractions using Equations 3-5. There is a clear dominance of phyllosilicates (clay minerals, mica and chlorite) throughout the section with values ranging from ~23 % up to ~96 % (~74 % on average) (Fig. 4 and Supplementary data). Minima in clay-mineral content coincide with sandstone-dominated intervals. The $CaCO_3$ values (Fig. 4) change at the unconformity between the Ravnefjeld and the Wordie Creek formations from values of ~21 % to ~1%. Between 100 and 160 m $CaCO_3$ values scatter around 18%. Above 160 m they decrease to an average of ~ 5%. From 400 m upsection the average $CaCO_3$ concentration is ~13 % and shows higher variability. SiO from quartz siltstones (Q-silt) (Fig. 4) ranges between 3 % and 34 % in the sampled siltstones. Significant amounts of quartz can be expected in the sandstone-dominated intervals that are underrepresented in

the sample record.

Aluminum (Al_2O_3) concentrations range around ~9-14 % in the Ravnefjeld Formation. These concentrations scatter around 18 % in the lowermost part of the Wordie Creek Formation and drop to values around 14% at ca. 150 m of the composite section. These values are followed by a distinct peak of 21 % at ca. 165 m. Between 165 and 340 m Al_2O_3 concentrations are rather stable (~16 %) and drop to average values of ~14% between 340 and 400 m. In the uppermost part of the section (ca. 400 m – 680 m) Al_2O_3 concentrations show a higher variability compared to the lower part of the section. Potassium (K_2O) (range: 1.3-4.7 %, average: 3.1 %), sodium (Na_2O) (range: 0.38-1.74 %, average: 0.89 %), magnesium (MgO) (range: 1.4-8.2 %, average: 4.3 %), and calcium (CaO) (range: 1.3-4.7 %, average: 3.1 %) are not shown in Figure 4 (see Supplementary data). Iron (Fe_2O_3) varies between 1.4 to 12.7 % (average: 5.8 %) (Fig. 4). Titanium (TiO_2) concentrations scatter between 0.22 % and 1.13 % (average 0.93 %) (not shown, see Supplementary data). The Ti/Al ratios vary mainly between 0.03 and 0.1 (average 0.06) through the whole record (Fig. 4). Iron, potassium, titanium, and Ti/Al ratios show variations throughout the section that are similar to the variation in the aluminum data. These include low values at ca. 150 m of the section, rather stable values in its middle part and values with higher variability from 400 m upsection.

Manganese (MnO_2) values range between 0.04 and 0.32 % (average: 0.08 %). At the boundary between the Ravnefjeld and Wordie Creek formations, the MnO_2 concentrations drop from ~0.2 % to ~0.05 %. In the interval between 150 m and 200 m and in the uppermost part of the section, manganese concentrations are around ~0.1 and show a higher variability (Fig. 4). Phosphorus (P_2O_5) concentrations (range: 0.05-0.18 %, average: 0.10 %) show a slight increase from average values of ~0.08 % in the lower 160 m, average values of 0.11 % between 160 and 400 m, and average values of ~0.12 % from 400 m upsection (see Supplementary data).

The Fe/Al ratios do not change significantly and range around an average value of ~0.54 (Fig. 4). A slight decrease in values (by ~0.07 on average) is documented at about 150 and from 400 m upsection. The chemical index of alteration (CIA-K) values range between 68.5 % and 91.3 % with an average value of ~83.6 %. Highest values are documented from ~8 m and ~166 m of the composite section, whereas lower values with a higher variability are characteristic for the uppermost 200 m of the section (Fig. 4).

In the study section, most DOP_T values are close to 0. Between ca. 75 and 90 m of the section values are slightly increased to 0.21 on average, and between 150 and 210 m to average values of 0.28. In the latter interval, five values are higher than 0.45 with the highest value of 0.62 (Figs. 5 and 6).

4.2. Trace element proxies

Excess barium (Ba_{xs}) was calculated using Eq. 1. The detrital Ba/Al ratio was estimated from the barium (Ba) versus aluminum (Al) crossplot (Fig. 6). Around 95% of the samples show a Ba/Al ratio indicating a detrital origin. The detrital Ba fraction (Ba_{detr}) accounts for 495 ppm. Therefore, in the present study samples with barium contents higher than 495 ppm are considered to show an excess of barium. Niobium (Nb) (range: 2.7-25.7 ppm, average: 16.9 ppm), nickel (Ni) (range: 12.2-62.6 ppm, average: 43.0 ppm), rubidium (Rb) (range: 31-176 ppm, average: 121 ppm), vanadium (V) (range: 40-175 ppm, average: 115 ppm), yttrium (Y) (range: 22-74 ppm, average: 60 ppm), and zinc (Zn) (range: 16-91 ppm, average: 57 ppm) show similar trends throughout the section with decreased values in an interval between 100 and 150 m, rather stable values from 150 to 400 m and higher variability from 400 m upwards (Table 1and Supplementary data). Strontium (Sr) (range: 70-576 ppm, average: 194 ppm) on the contrary shows higher values in the interval between 100 and 150 m (Table 1 and Supplementary data). Molybdenum (Mo) values scatter around 2.9 ppm on average throughout the section with slightly lower values between 100 and 150 m and slightly higher values between 150 and 200 m of section. Uranium (U) values scatter around 2.9 ppm on average with slightly higher values close to the top of the section (Table 1 and Supplementary data).

4.3. Organic carbon and sulfur

Figure 4. Major elements and mineral fractions. Lithostratigraphic column, particulate organic matter data (M/T ratios), and transgressive-regressive cycles after Sanson-Barrera et al. (2015). In light grey dashed-lines, upper crust average shale values for Al_2O_3, Fe_2O_3, MnO_2, Ti/Al, and Fe/Al (Table 1).

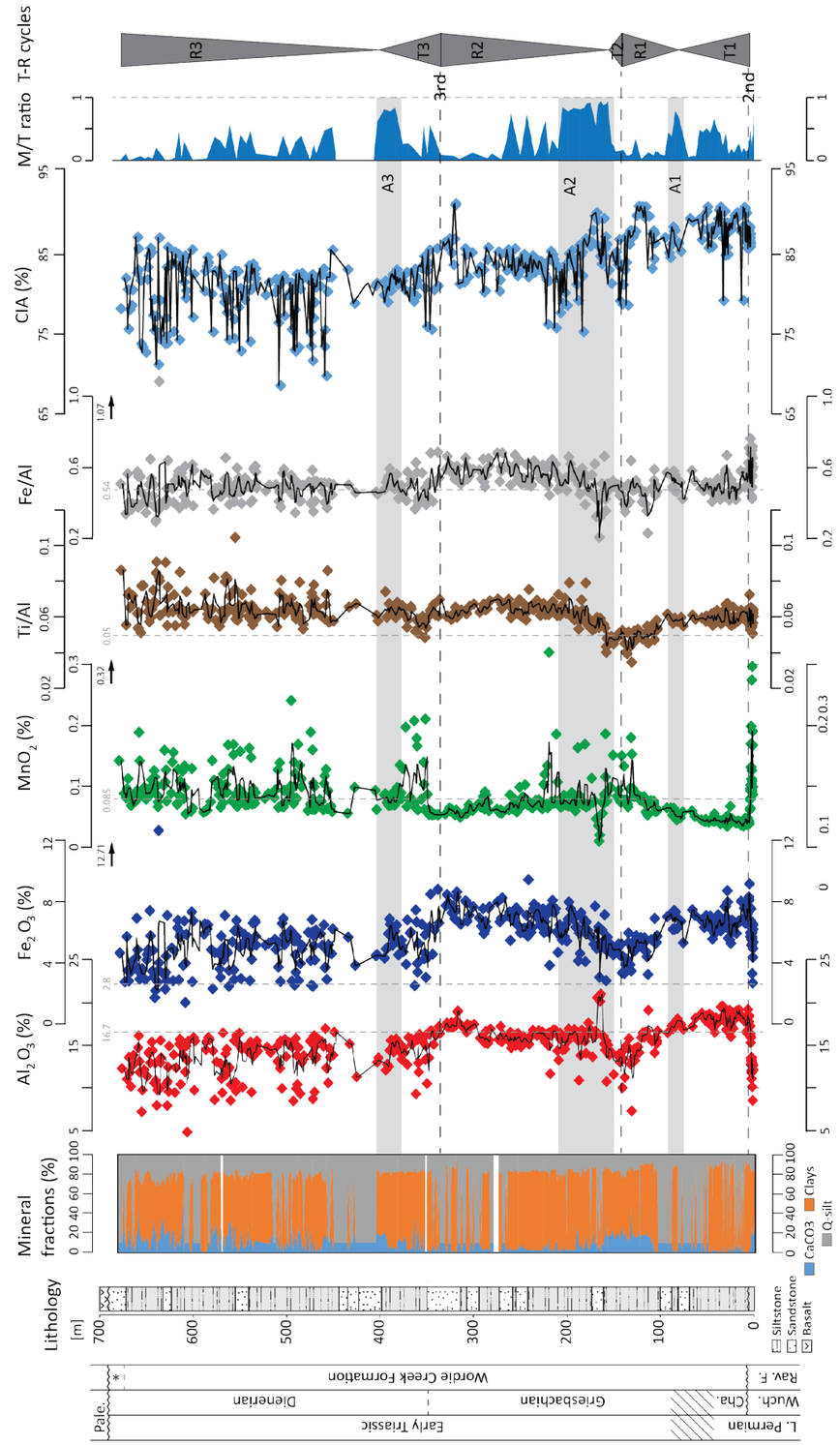

		Below A1	A1	Between A1 and A2	A2	Between A2 and A3	A3	above A3	average shale (Wedepohl 1971, 1991)
		1.50-75.00 m	76.05-93.10 m	94.00-145.90 m	150.50-210.50 m	212.10-374.35 m	375.35-403.45 m	416.50-676.25 m	
SiO_2	%	52.64	56.15	51.24	54.80	56.22	53.46	53.51	58.9
TiO_2	%	0.86	0.89	0.63	0.82	0.89	0.80	0.76	0.78
Al_2O_3	%	16.40	17.34	14.48	15.70	15.87	14.31	13.18	16.7
Fe_2O_3	%	6.50	6.71	5.00	5.85	6.71	5.43	4.83	2.8
MgO	%	4.70	4.74	4.14	4.01	4.59	4.45	3.90	2.6
CaO	%	3.46	1.27	7.56	3.87	3.01	5.91	8.15	2.2
Na_2O	%	0.71	0.84	0.67	0.91	0.98	0.99	0.98	1.6
K_2O	%	3.58	3.46	2.95	3.05	3.33	2.90	2.77	3.6
P_2O_5	%	0.08	0.09	0.08	0.10	0.11	0.11	0.12	0.16
TS [%]	%	0.5	1.15	0.19	1.32	0.19	0.19	0.03	0.24
TOC [%]	%	0.2	0.19	0.18	0.59	0.14	0.20	0.11	
S/TOC		3.00	6.53	1.03	3.68	1.35	0.83	0.25	
TIC	%	0.76	0.16	2.16	1.02	0.50	1.25	1.53	0.35
Ba	ppm	359	387	412	417	439	734	391	580
Co	ppm	20	23	13	18	18	18	14	19
Cr	ppm	99	91	80	83	91	105	104	90
Cu	ppm	30	31	21	25	25	26	19	45
Mn	ppm	436	348	556	526	504	520	608	850
Mo	ppm	2.7	3.4	2.2	3.5	2.5	3.3	3.2	1.3
Nb	ppm	17	18	12	17	17	19	16	18
Ni	ppm	50	51	34	42	41	47	40	68
Pb	ppm	22	20	15	19	15	14	14	22
Rb	ppm	140	139	109	119	130	110	105	140
Sr	ppm	207	187	313	195	158	199	177	300
Th	ppm	12	11	9.8	10	11	10	9.3	12
U	ppm	2.2	3.5	2.2	2.7	2.6	3.5	3.6	3.7
V	ppm	145	138	98	115	116	115	97	130
Y	ppm	62	62	53	59	63	59	57	41
Zn	ppm	65	60	45	51	60	61	52	95
Zr	ppm	186	203	192	204	208	239	240	160
Fe/Al		0.53	0.51	0.46	0.49	0.55	0.50	0.47	0.54
Ti/Al		0.05	0.05	0.04	0.05	0.06	0.06	0.06	0.05
Zr/Al	$*10^{-2}$	0.215	0.222	0.250	0.247	0.251	0.318	0.361	0.181

Table 1. Comparison of average element contents and element/Al ratios of Kap Stosch sediments and upper continental crust "average shale" (Wedepohl 1971, 1991).

Total organic carbon (TOC) shows low values around 0.19% throughout the section (Fig. 5). Nevertheless, the TOC values of the Ravnefjeld Formation are higher than the average values of the Wordie Creek Formation. Within the Wordie Creek Formation a TOC maximum (2.34%) can be observed in the samples at 171.45 m, and a slight TOC increase between 350 and 400 m. C_{org}:P ratios scatter around 23 in the Ravnefjeld Formation, whereas the values scatter around 12 throughout the Wordie Creek Formation. Exceptional values of >50:1 are reached in an interval between 160 to 180 m (Figs. 5 and 6). Sulphur (S) concentrations vary mainly between 0 and 1% (Fig. 5). However, around 100 m and between 160 and 240 m, S values range up to 2% occasionally exceeding 3%.

The S/TOC crossplot (Fig. 6) shows a correlation between high TOC values (between 0.5 and 2.3 %) and high S values (between 1 and 3%). The S/TOC ratio shows a distinct positive trend in the basal 100 m of the section from values~0.3 up to ~10, followed by a drop to values around ~1. In the interval between 160 and 240 m S/TOC values are again increased with values ranging up to ~10 (Fig. 5 and Supplementary data).

4.4. Sedimentation rates and fluxes

Based on a duration of ~1 Myr and a thickness of 680 m, we developed a sedimentation rate model using Equation 6 (Fig. 7). This model allowed use to calculate bulk accumulation rates (BAR) and the fluxes of individual sediment components using Equations 3-5 (Fig. 8 and Supplementary data).
Sedimentation rates (SR) for the sampled siltstone intervals show values around 0.2 m kyr^{-1} in the basal part of the section. From these values siltstone SR increase up to 0.35 m kyr^{-1} at about 150 m and drop subsequently again to 0.2 m kyr^{-1} (at ca. 170 m). From these values siltstone SR increase towards the top of the section reaching maximum values of 0.41 m kyr^{-1} (at 635.85 m). The average SR throughout the section is 0.68 m kyr^{-1} and 0.27 m kyr^{-1} on average for the siltstone intervals of the succession. BARs range from 428 to 1020 g m^{-2} yr^{-1} with an average of 680 g m^{-2} yr^{-1} over the entire succession. The upper part from 400 m upward is marked by slightly higher average BARs of 770 g m^{-2} yr^{-1}.
Fluxes for clays, quartz from siltstones (Q-silt), and carbonate were calculated and are shown in Fig. 8. The average flux for the clay fraction is 49 g cm^{-2} kyr^{-1}. The basal 100 m are marked by slightly lower clay fluxes of ~45 g cm^{-2} kyr^{-1} followed by a drop to values of ~40 g cm^{-2} kyr^{-1}, which characterise the interval from ~110 to 170 m. Clay fluxes are rather stable around ~50 g cm^{-2} kyr^{-1} from 200 to 350 m, whereas the upper part of the section is marked by higher variability. The Q-silt flux averages 12.1 g cm^{-2} kyr^{-1} and also shows higher variability from 350 m upward (Fig. 8). Carbonate fluxes show an average of 7.0 g cm^{-2} kyr^{-1} throughout the section but vary considerably. Carbonate fluxes of around 5 g cm^{-2} kyr^{-1} mark the sediments of the Wordie Creek Formation up to ca. 100 m. Between 100 and 200 m carbonate flux shows increased values of ~20 g cm^{-2} kyr^{-1}. Similar to the fluxes of the clay and Q-silt fractions, carbonate fluxes are highly variable in the upper part of the section (Fig. 8). Organic carbon accumulation rates (OCAR) are generally low (1.3 g m^{-2} yr^{-1} on average) with the exception in the interval between 170 and 200 m were peak values of 14.9 g m^{-2} yr^{-1} were reached (Fig. 8 and Supplementary data). Al fluxes scatter around 5.2 g cm^{-2} kyr^{-1}, showing a slight decrease in the interval from ~110 to 170 m corresponding to the decrease in clay flux. High variability of Al fluxes is documented in the upper part of the section (Fig. 8). Excess barium fluxes show values >0 mg cm^{-2} kyr^{-1} only in four distinct intervals around 120, 370, 470, and 550 m of the section. The highest values (185 mg cm^{-2} kyr^{-1}) are reached at 375.35 m (Fig. 8 and Supplementary data).

4.4. Clay mineralogy

The phyllosilicate content (fraction <2 µm) is dominated by smectite, mica, and chlorite in varying degrees, and rather low relative contents of kaolinite and illite/smectite (I/S) mixed layer clay minerals (Fig. 9). Smectite contents are highly variable throughout the section and range from 0 % to peak values of ~75 % at 143.5 m and 361.05 m of the section. Despite the high smectite peak at 143.5 m the lower part of the section (up to 360 m) is characterized by lower smectite percentages of 18.7 % on average. In several intervals in the lower part of the section smectite has not even been detected. In contrast, the upper part (~360 m upsection) is marked by higher smectite contents of 41.3 % on average (Fig. 9).
Mica percentages are 28.7 % on average. The values vary between 4.4 % and 61.6% over the entire succession. High relative contents of mica co-occur i.e., between 250 and 300 m, and around 500 m as shown by the mica/smectite ratio (Supplementary data). Chlorite contents fluctuate between 0 % and 43.7 % but show relative stable average contents of 21.7 % throughout the section, i.e., little variation in the upper part compared to the lower part. Kaolinite accounts for 16.6 % of the phyllosilicate fraction. Its relative contents range between 0 and 44.2 %, being more abundant in the lower part of the section (23.6 % on average) and less abundant (9.6 % on average) in the upper part of the section. Illite/smectite mixed layers represent only a subordinate component of 3.3 % on average, exceeding 10 % only occasionally.
The smectite/kaolinite ratios scatter around an average of 1.34 in the lower part of the section

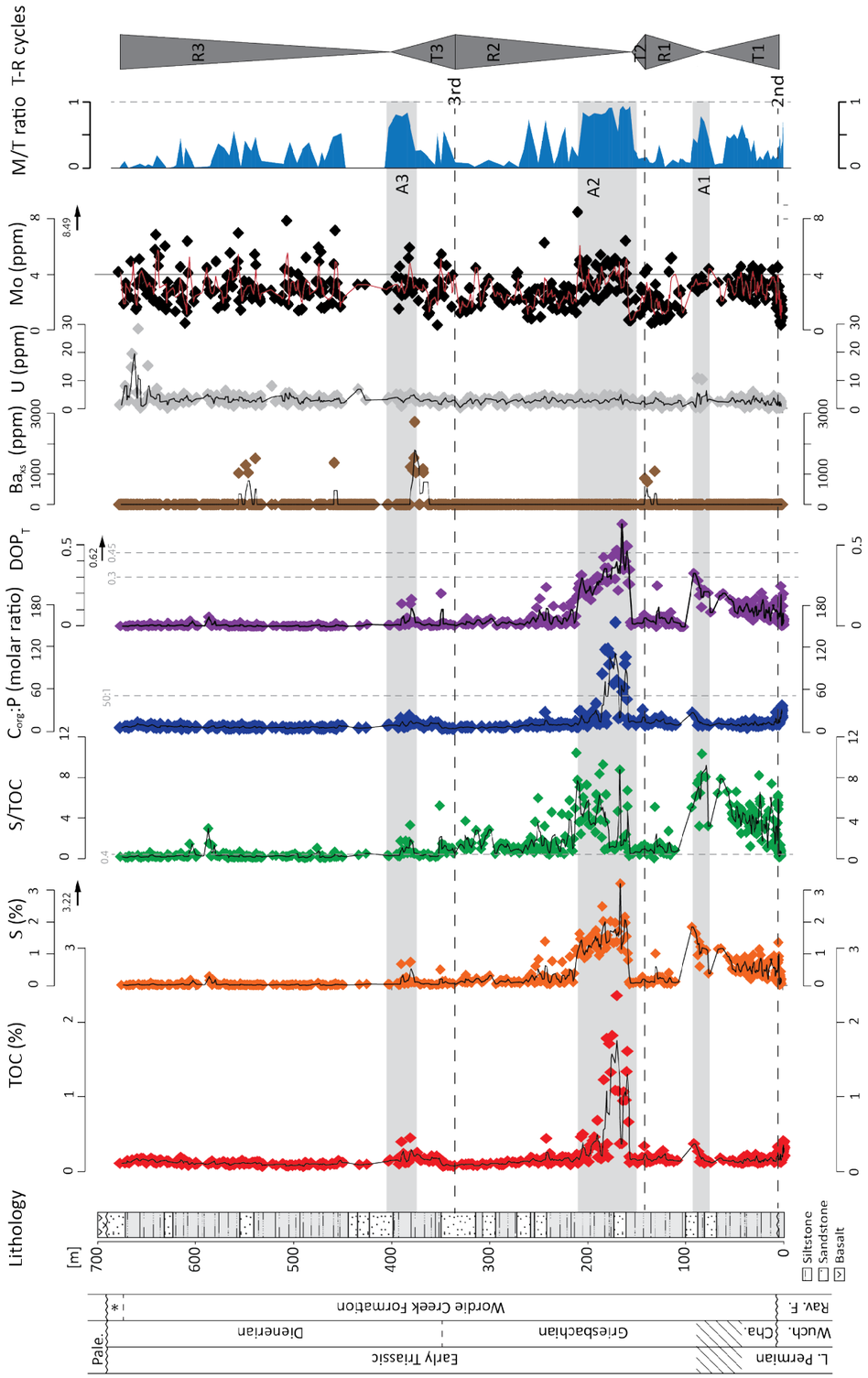

with a minor peak of 8.6 at 143.5 m. The base of the upper part (at 361.05 m) is marked by a distinct peak in smectite/kaolinite ratios of up to 33.5. From ~360 m upsection the smectite/kaolinite ratios are slightly higher compared to the lower part (6.6 on average) (Fig. 9). The smectite/mica+chlorite+kaolinite ratios follow the smectite/kaolinite ratios displaying two distinct peaks at 143.5 and 361.05 m. The average value of smectite/mica+chlorite+kaolinite is 0.74. Clay-mineral compositions may be further modified by diagenetic processes once deposited in the sedimentary environment. Late diagenetic overprint can affect the original sediment composition and the degree of burial diagenesis (e.g., Godet et al. 2008). The presence of smectite (up to 75 %) and the presence of kaolinite imply that diagenetic transformation had a weak impact on the Kap Stosch sedimentary succession.

5. Discussion

5.1. Sea level and tectonic-sedimentary cycles in the Hold-with-Hope basin

Based on sedimentological observations and particulate organic matter data (marine/terrestrial (M/T) ratios) three transgressive-regressive cycles have been documented in the Kap Stosch succession and correlated with sequence stratigraphic interpretations of other Arctic successions (Sanson-Barrera et al. 2015). M/T ratios and transgressive-regressive cycles are plotted together with selected geochemical proxy data on Figure 4. The base of the transgressive episode T1 corresponds to the formational boundary between Ravnefjeld and Wordie Creek formation and has been correlated with the latest Permian second-order sequence boundary of the Arctic (Embry 1997; Mørk et al. 1989; Mørk and Smelror 2001; Seidler et al. 2004; Sanson-Barrera et al. 2015). T1 is followed by the first regressive episode from ca. 90 to 150 m of the section. The following second transgressive-regressive cycle is marked by a very short transgression and a rather extended regression episode from ca. 170 m up to 350 m. There a third-order sequence boundary has been identified close to the Griesbachian–Dienerian boundary which has previously been identified in Spitsbergen and the Barents Sea (Mørk et al. 1990; Worsley and Mørk 1978; Nakrem and Mørk 1991; Sanson-Barrera et al. 2015). This sequence boundary is the base of the third and uppermost transgressive-regressive cycle in the Wordie Creek Formation of Kap Stosch (Sanson-Barrera et al. 2015).

Increased contributions of siliciclastic minerals are associated with increased concentrations of elements such as Al, Mn and Ti (principally residing in quartz, clay minerals and accessory silicates). Therefore these element concentrations as well as the Ti/Al ratios can be used as proxies for sea-level changes. Low concentrations of these elements reflect regressive episodes; increasing concentrations in contrast reflect transgressive episodes. Elemental geochemical proxies in the Kap Stosch section are generally consistent with the sea-level changes inferred from the M/T ratios (Sanson-Barrera et al. 2015). Low Al_2O_3 concentrations in the Ravnefjeld Formation sediments indicate their deposition in a late regressive episode. The sequence boundary at ~150 m also corresponds to a low in Al_2O_3. The third-order sequence boundary is less clearly expressed in the Al_2O_3 data, low values are documented slightly above the sequence boundary (Fig. 4). Similar to aluminum, manganese concentrations usually show low values in low sea-level deposits and high values in high sea-level deposits. The MnO_2 data in Fig. 4 seem to be anomalous to these general trends, showing high values in the Ravnefjeld Formation and around 150 m. However, Mn/Al ratios (Supplementary data) are low during all three sea-level lowstands. This discrepancy might indicate that the high MnO_2 concentrations are due to high clay mineral contents (Jarvis et al. 2001). Maximum flooding surfaces are generally marked by elevated Ti/Al ratios, whereas sequence boundary are characterised by low Ti/Al ratios (Jarvis et al. 2001). At Kap Stosch only the sequence boundary at ~150 m coincides with a clear low in Ti/Al ratios (Fig. 4). A minor decrease in Ti/Al ratios is documented slightly above the third-order sequence boundary. The unconformity at the base of the Wordie Creek Formation is not reflected in the data. The Fe/Al ratios trace the Ti/Al ratios (Fig. 4). Since Al_2O_3 and Ti/Al ratios both display

Figure 5. Redox and paleoproductivity proxies. Anoxic intervals: A1, A2, and A3 following particulate organic matter data of Sanson-Barrera et al. (2015). Marine/terrestrial (M/T) ratios, transgressive-regressive cycles, and lithostratigraphic column from Kap Stosch after Sanson-Barrera et al. (2015).

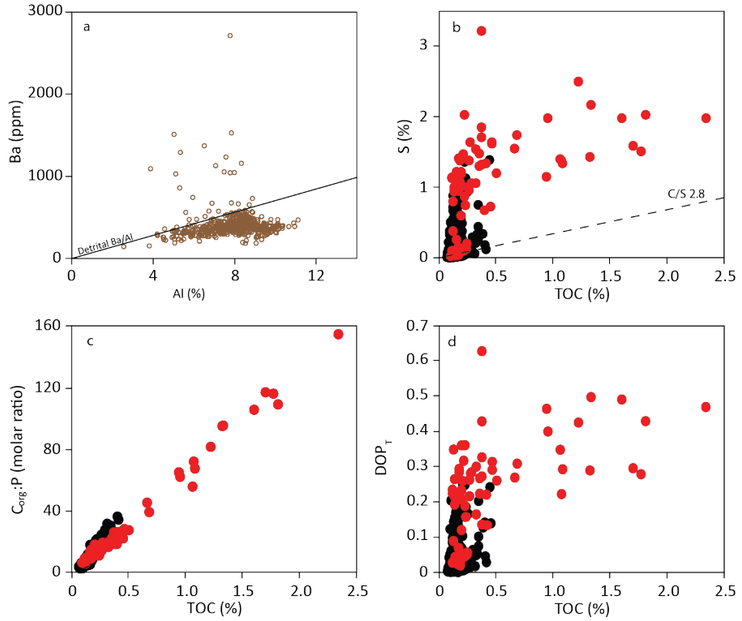

Figure 6. a) Ba/Al crossplot, from which excess Ba (Ba_{xs}) is calculated using Equation 1; b) total sulfur (%)/total organic carbon (%) crossplot, normal marine line C/S = 2.8 (Berner and Raiswell 1983); c) C_{org}:P (molar)/total organic carbon (%) crossplot; d) DOP_T (%)/total organic carbon (%) crossplot. In a, b, and c, samples from the anoxic intervals A1, A2 and A3 are represented by red dots and the remaining samples by black dots.

low values slightly above the third-order sequence boundary, the position of this sequence boundary probably needs to be revised and positioned at ~360 m.

Clay-mineral data are also used to interpret sea-level changes. Clay mineral fluxes indicate slight increases around the sequences boundaries (Fig. 8). The presence of abundant smectite is generally linked to transgressive episodes. Chlorite, kaolinite and mica are deposited close to shorelines, while smectites are transported away from shores (Gibbs 1977; Adatte and Rumley 1989). Increased smectite therefore reflects high sea levels (Chamley et al. 1990), whereas increased kaolinite, chlorite and mica suggest low sea levels. Thus the smectite peaks might indicate transgressive events. The resolution of the three datasets (geochemistry, clay minerals, and particulate organic matter) is quite different, hampering a clear interpretation of these peaks in terms of sea-level changes. The uppermost part of the study section corresponds to a regressive event as interpreted by the marine/terrestrial ratio (Sanson-Barrera et al. 2015) and coincides with higher smectite contents, therefore rather indicating a climatic change as discussed in section 5.3.

5.2. Paleoredox conditions, paleoproductivity, and organic matter preservation

Research on Late Permian and Early Triassic environmental conditions is largely focused on marine sections in the Paleotethys and Neotethys (Algeo et al. 2007, 2008a; Newton et al. 2004; Riccardi et al. 2006; Wignall and Twitchett 1996). The work done along the PTB at Nhi Tao, Vietnam (Algeo et al. 2007, 2008a) suggested that large-scale upwelling of deep waters implies that the Permian–Triassic marine mass extinction was caused by anoxia and/or sulfide toxicity, and that recurrent anoxic episodes during the Early Triassic have been suggested to be the cause for the supposed delayed recovery of marine ecosystems until the start of the Middle Triassic (Chen and Benton, 2012). The description of the recovery in an oxic marine environment setting in Oman during the Griesbachian stated that the fossil assemblage from Wadi Wasit contains one of the most diverse and ecologically complex Griesbachian fauna (Twitchett et al. 2004; Hautmann et al. 2011, 2015). Well-oxygenated shallow-marine conditions

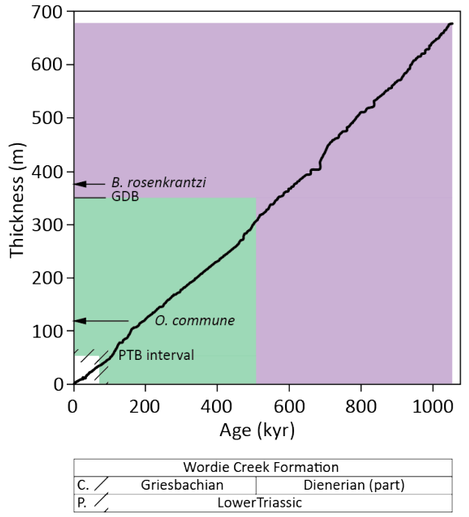

Figure 7. Sedimentation rate crossplot for the Wordie Creek Formation based on the sedimentation rate model defined in Section 3. Ammonoid fossil finds: *Ophiceras commune* and *Bukkenites rosenkrantzi*. C: Changhsingian, P: Permian, PTB: Permian–Triassic boundary, GDB: Griesbachian–Dienerian boundary.

display a level of post-extinction recovery that is not recorded outside the Neotethys region until the Spathian (Twitchett et al. 2004; Hautmann et al. 2011, 2015). The data support the hypothesis that the duration of the marine recovery after the Permian–Triassic extinction event depends on the duration of oceanic anoxic conditions, thus the absence of benthic anoxia promotes a quick recovery (Twitchett et al. 2004; Hautmann et al. 2011, 2015). Boreal realm sections as those from the Sverdrup Basin (Arctic Canada) show well developed anoxic conditions during the Early Triassic with the exception of an oxic interval between the late Dienerian and early Smithian (Grasby et al. 2012). A few sections from the northwestern margin of Pangea recorded densely bioturbated intervals after the Permian–Triassic mass extinction, in contrast to the assumed widespread anoxia at that time. Areas with broad shelves probably sustained benthic life due to the influence of storms that enhanced the development of oxic conditions (Beatty et al. 2008).

For the Kap Stosch section, three suboxic-anoxic intervals (A1-A3) have been inferred from particulate organic matter data characterised by high relative abundances of marine organic matter (Sanson-Barrera et al. 2015). The relationship between the bulk accumulation rates (BAR) and accumulation rates of the organic carbon (OCAR) provide some information about the accumulation of organic matter in sediments. Oxic and suboxic-anoxic facies display different patterns of covariation in modern systems (Tyson 2005). Rapid sedimentation enhances the preservation of organic matter in sediments (Tyson 2005; Dunne et al. 2007). However, TOC values throughout the entire Kap Stosch record are rather low, ca. 0.1%, exceptionally reaching TOC values up to 2.3% in anoxic interval A2 (Fig. 8). In Figure 10, BAR and OCAR data from Kap Stosch is plotted together with the results of other PTB sections, and with data from modern oxic-anoxic environments data (Algeo et al. 2013). Compared with other PTB sections the Kap Stosch section displays the highest sedimentation rates. A strong relationship between OCAR and BAR indicates enhanced preservation of organic carbon at higher sedimentation rates (Algeo et al. 2013; Schoepfer et al. 2015). However, at Kap Stosch the highest OCAR values do not correspond to the highest BAR values (Fig. 10). At this location suboxic-anoxic marine conditions probably enhanced the preservation of organic matter overruling the influence of the sedimentation rate. Rock-Eval and particulate organic matter data show a dominance of terrestrial-derived organic matter for the whole section, with the exception of the suboxic-anoxic intervals A1-A3. These intervals are characterised by the dominance of the amorphous organic matter, which is only preserved under suboxic to anoxic conditions (Tyson 1995; Sanson-Barrera et al. 2015). In general, the organic matter is well preserved as the particulate organic matter data from Kap Stosch proves. Even in the upper part of the section where red sediment colours become more abundant and the particulate organic matter shows higher proportions of opaque woody particles, palynomorphs are still well preserved.

In the study section, redox conditions were evaluated based on a combination of redox-sensitive trace-metal concentrations, such as Mo, U, and V, and S/TOC, C_{org}:P, and DOP_T ratios. These redox proxies did not always yield consistent redox inferences, probably due to factors unique to the study section. Molybdenum (Mo), uranium (U), and vanadium (V) have been widely used as proxies for benthic redox conditions due to their enrichment in organic-rich marine sediments deposited in oxygen-depleted

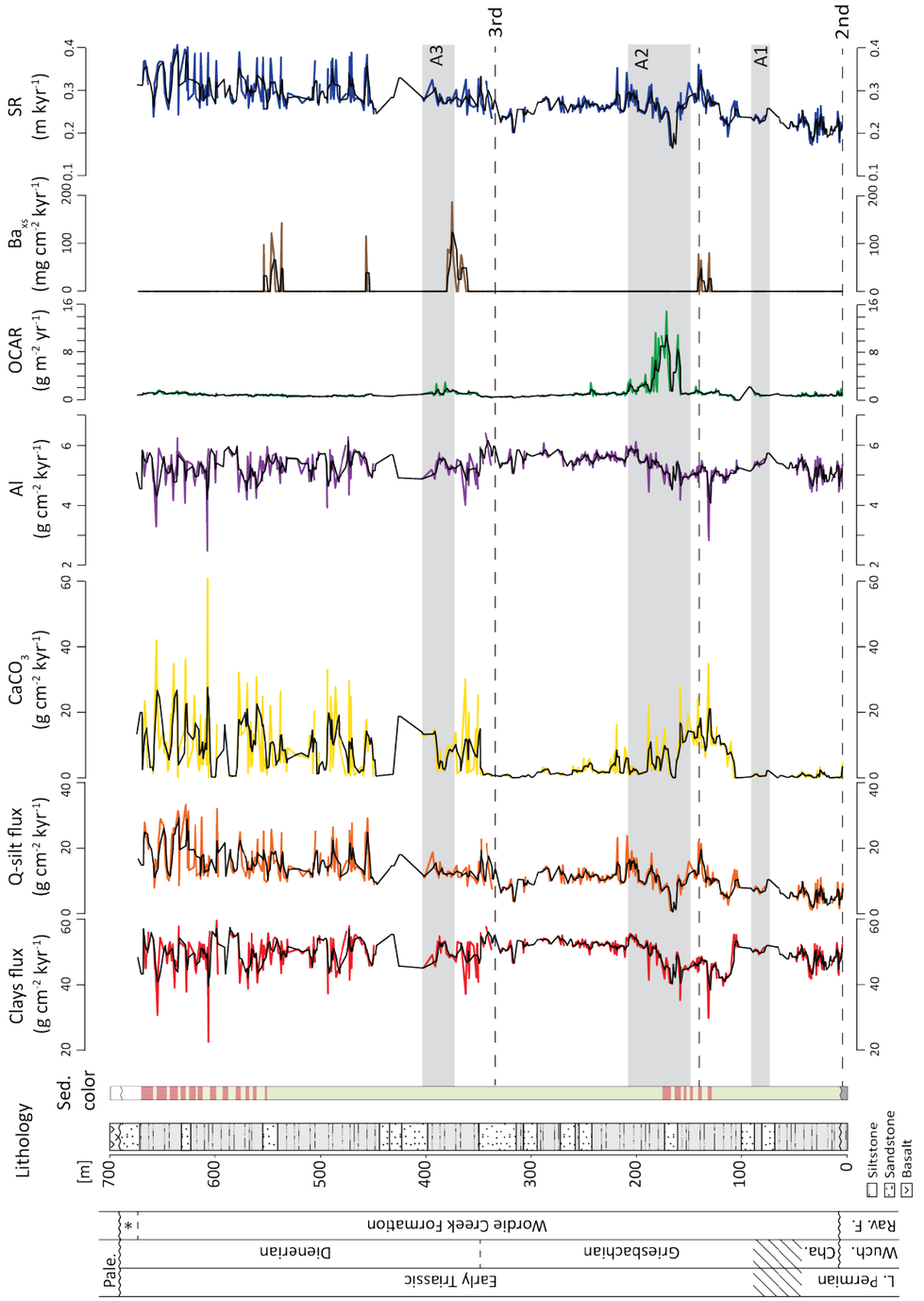

Figure 8. Flux profiles and sedimentation rates (SR). Lithostratigraphy, sediment color (Ravnefjeld Formation: dark grey, Wordie Creek Formation: grey or red).

environments (Algeo and Tribovillard 2009). The majority of trace element concentrations are comparable with average shale concentrations throughout the succession (Table 1). Mo and V show little enrichment above background detrital concentrations through most of the section and no specific enrichment during intervals A1-A3 (Fig. 5 and Table 1).

S/TOC ratios greater than those associated with oxic-suboxic marine sediments (~0.4; Berner and Raiswell 1983) are indicative of sulfur enrichment under euxinic conditions, and this would apply to almost all samples below 400 m (Fig. 5). However, except for interval A2, TOC values are very low (~0.1%) and the S/TOC ratios are therefore regarded as being not reliable for most of the succession. The S/TOC crossplot (Fig. 6) indicates euxinic conditions, which developed most commonly in association with high TOC values, as is the case for interval A2. C_{org}:P ratios of <50:1 are characteristic of oxic environments, whereas values >100 typify anoxic environments (Algeo and Ingall 2007). In the study section C_{org}:P values in the study section are mostly indicative of oxic conditions, except for a short interval of probable anoxia within the Wordie Creek Formation at ~180 m (Fig. 5). The degree of pyritization (DOP) of iron is a measure of the intensity of anoxia, as reflected in the proportion of highly reactive iron (Fe_{HR}) that has been converted to pyrite (Fe_{py}), i.e., Fe_{py} / (Fe_{py} + Fe_{HR}). In oxic conditions, DOP does not exceed 0.45, whereas in anoxic conditions it does not drop below 0.75. The intermediate field characterizes dysoxic or dynamically fluctuating redox settings (Raiswell et al. 1988). In our calculations, total Fe (Fe_T) is used as a proxy for Fe_{HR}, a procedure that enlarges the denominator of the ratio and reduces DOP estimates (which are denoted DOP_T) relative to true DOP. For this reason, our results cannot be strictly interpreted using the redox scale of Raiswell et al. (1988), but stratigraphic variation in DOP_T nonetheless provides an indication of secular patterns of environmental redox variation. In the present record DOP_T values exceed 0.4 in only a few samples located within interval A2 (Fig. 5), which indicates anoxic condition for this interval and oxic conditions for the rest of the succession. Although DOP around 0.3-0.5 would indicate oxic conditions, DOP_T values are commonly lower for the same redox level (Supplementary information in Algeo et al. 2008b). If we interpret DOP_T values between 0.3-0.5 in the Kap Stosch record as probable indication of anoxia, DOP_T values in interval A2 would surely indicate anoxia and one sample in interval A1 would indicate anoxia, data below and above this interval would also reflect oxic conditions.

In the study section, the redox proxies S/TOC, C_{org}:P, and DOP_T thus yield similar interpretations concerning bottom-water redox conditions. The data show clear anoxic conditions for interval A2 and oxic conditions below and above this interval. Suboxic-anoxic conditions in interval A1 and A3 are only indicated by particulate organic matter data and are not expressed in the geochemical proxy data. Therefore, we investigate the geochemical proxy data that are sensitive to paleoproductivity in order to check whether the marine primary productivity was enhanced during intervals A1-A3. Barium is associated with the sinking flux of organic matter, and therefore the Ba_{xs} fluxes potentially show intervals of increased paleoproductivity (Fig. 8). Paleoproductivity assessment is often done in a multiproxy approach, using for example the covariation of fluxes of TOC, C_{org}:P and Ba_{xs}. However, in the Kap Stosch section Ba_{xs} content and fluxes coincide with low TOC values (<0.3 %), and do not correspond to any increased TOC values interval (Figs. 5 and 8). No covariation between TOC, C_{org}:P and Ba_{xs} can be inferred. Reducing conditions tend to diminish the burial fluxes of Ba_{xs} (Tyson 2005). However, oxidizing environments usually facilitate the preservation and retention of biogenic barium in the sediment, whereas the burial efficiency of organic carbon is reduced due to the aerobic conditions (Tyson 2005). In the Kap Stosch section Baxs shows three peaks above 495 ppm at around 130, 375, and 537 m, respectively (Figs. 5 and 8). The peaks at 130 and 537 m appear during intervals with oxic-dominated conditions close to low relative sea-level phases. Only the peak at 375 m falls at least partially within the lower part of interval A3. Additionally, there is a positive correlation between the bulk accumulation rates (BAR) and Baxs; higher BAR values correlate with high Baxs values. Hence, rapid burial induces enhanced preservation of biogenic barium (Dymond et al. 1992). Therefore the increased Baxs peaks in the Kap Stosch section probably reflect periods of increased BAR rather than peaks in primary productivity. Thus, the geochemical

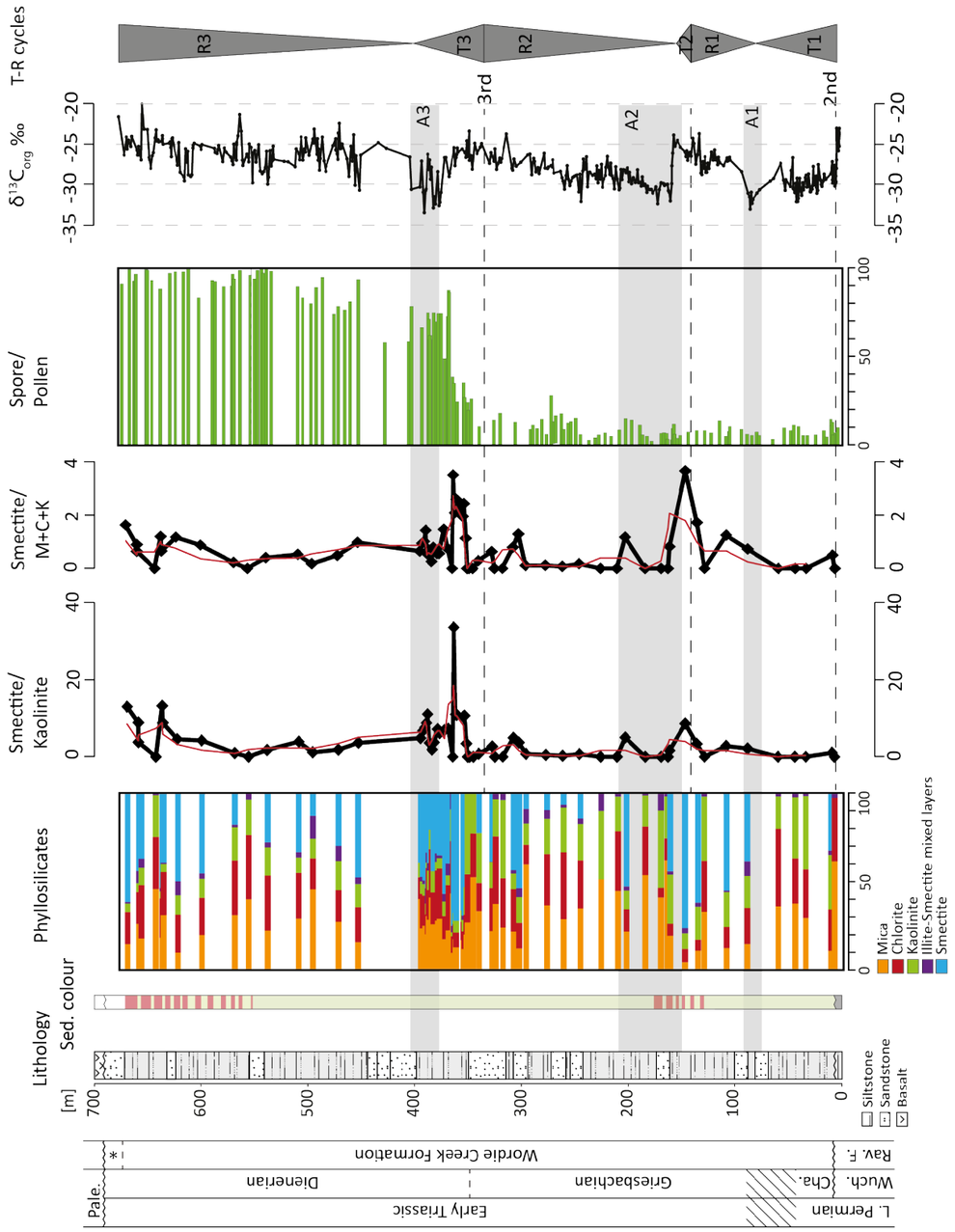

Figure 9. Clay mineralogy data. Lithostratigraphy, sediment color (Ravnefjeld Formation: dark grey, Wordie Creek Formation: grey or red), bulk organic carbon isotopes after Sanson-Barrera et al. (2015). Spore/pollen ratios after Hochuli et al. (2016).

proxy data do not reflect enhanced marine primary productivity for the intervals A1-A3.

At Fiskegrav in Jameson Land (East Greenland), a study integrating sulfur isotope ($\delta^{34}S$) and framboidal pyrite data provided a continuous record of ocean chemistry evolution across the Permian–Triassic transition (Nielsen et al. 2010). This study concluded that in East Greenland there

was no abrupt change in the redox conditions from oxic to anoxic associated the Permian–Triassic transition. Nevertheless, anoxic conditions were established in the Wordie Creek Formation above the extinction horizon (Nielsen et al. 2010). We may conclude that in the top part of the Ravnefjeld Formation (7 m) there is no evidence of strong anoxia, while at least one anoxic episode is present in the Wordie Creek Formation at Kap Stosch.

5.3. Influence of high sedimentation rates

The estimation of sedimentation rates in our record suggests that the 680 m of the Wordie Creek Formation at Hold-with-Hope were probably deposited in about 1 Myr (latest Permian to Dienerian). Our data and observations are in agreement with previous work done by Oftedal et al. (2005) in which they concluded that the combination of opening and deepening of the basin during the Griesbachian allowed a high supply of siliciclastics and the continuous creation of accommodation space to develop the thick Kap Stosch sequence in such a short time.

The high sedimentation rates of the Wordie Creek Formation affect the majority of the presented geochemical proxy data. Geochemical proxies usually indicative for anoxia (Mo, V, and U, DOP_T, C_{org}:P, and S/TOC) or for paleoproductivity (Ba_{xs}, C_{org}:P, TOC) do not reflect suboxic to anoxic episodes documented in the particulate organic matter data (Fig. 5). We suspect that the high sedimentation rates in this section, which are more than 10 times higher than those of average sedimentary successions (Sadler 1981; Anders et al. 1987) led to strong dilution of all authigenic components and TOC, making them unreliable indicators of ambient bottom-water redox conditions.

5.4. Paleoweathering intensity and paleoclimatic signals

Al and Fe concentrations as well as the chemical index of alteration (CIA) are used to evaluate changes in terrestrial weathering. The CIA index is used as proxy to reconstruct paleoweathering intensity (Nesbitt and Young 1989). In the interval between ~8 and 170 m this index shows samples with rather high values indicating increased weathering (between 85 and 90 %, Fig. 4). This interval correlates with the development of more proximal depositional settings and the increasing red over grey color of the siltstone and sandstone beds (Sanson-Barrera et al. 2015) (Figs. 8 and 9). Al and Fe concentrations do not indicate any distinct change in paleoweathering conditions (Fig. 4). Only Al fluxes show higher values between ~110 and 170 m, and from 450 m to the top of the section (Fig. 8). The higher Al flux values upsection can be interpreted as generally increased and highly fluctuating paleoweathering intensity. Both intervals correlate with intervals of alternating grey-red sediment colour (Fig. 8).

Since the CIA is interpreted as a measure of the extent of degradation of feldspars into clay in dependence of the prevailing climatic conditions (Nesbitt and Young 1989; Price and Velbel 2003) the detrital clay mineral assemblages may yield valuable information on the weathering regime and therefore climate condition of the siliciclastics source area during Griesbachian and Dienerian times. Clay minerals can be used as humidity and seasonality proxies. The formation of kaolinites requires perennial warm humid climate (precipitation exceeding evaporation) in combination with extensive leaching. Low pH values (humic acids or elevated CO_2) enhance the kaolinite formation (e.g., Füchtbauer 1988). In contrast, smectites develop in subtropical regions with an annual precipitation of 500-800 mm but with a distinct seasonality of rainfall (Thiry 2000). Therefore, the smectite/kaolinite ratio has been used as a proxy for seasonality, with higher values indicating increased seasonality.

The higher kaolinite content in the lower part of the section might correspond to a higher relative humidity (Fig. 9) compared to the upper part in which the smectite content is slightly increased compared to the kaolinite content under the premise that kaolinite is not reworked from older sediments. In the upper part the smectite/kaolinite ratios slightly higher (Fig. 9 and Supplementary data). This might indicate more humid and decreased seasonality in the Griesbachian part of the section and reduced humidity and increased seasonality in the Dienerian. This climatic change is associated with a negative shift in the organic carbon isotope record (Fig. 9) (Sanson-Barrera et al. 2015). In the upper part of the section not only smectite/kaolinite ratios are increased but the dominant sediment colour also changes from grey to red. Reddish sediments are known to form in climate regimes with seasonal rainfall (Parrish

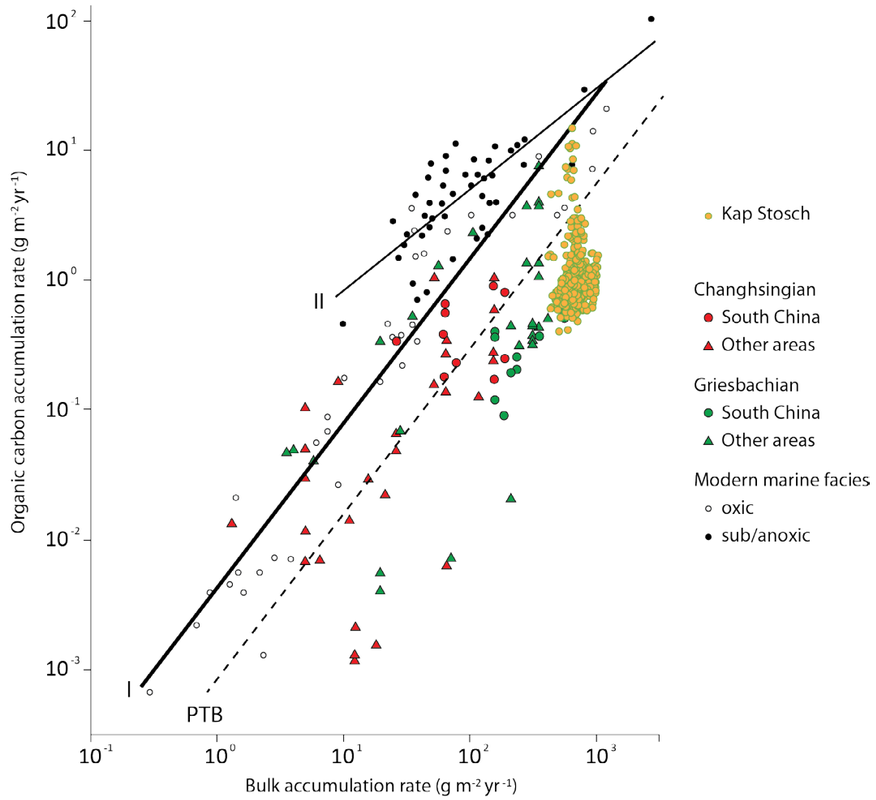

Figure 10. Bulk accumulation rate (BAR)/organic carbon accumulation rate (OCAR) crossplot. Sources: Kap Stosch (this study), other Permian-Triassic sections and modern marine environments (Algeo et al. 2013).

1993, and references therein).

At first glance this seems to be in contradiction with the spore/pollen ratios (Hochuli et al. 2016 and unpublished data). The spore/pollen ratios indicate a marked increase in spores (i.e., hygrophytic plants) in the Dienerian thus indicating more humid conditions in the Dienerian compared to the Griesbachian (Fig. 9). However, palynological data are not able to detect year-round distribution of the precipitation. Therefore, a possible explanation it might be that the humidity increased across the Griesbachian–Dienerian boundary combined with synchronous change to a higher seasonality of the rainfall, i.e., the increased seasonality affected the precipitation regime but not the temperature regime. The Triassic climate is considered to have been dominated by a large monsoon system (Kutzbach and Gallimore 1989; Parrish 1993). With its position at ca. 30°N (Blakey 2012), East Greenland was situated during the Early Triassic in this monsoonal system in a climatically very sensitive position, where three different biomes were close together and the boundary on which precipitation equals evaporation was very close (see Figure 1 in Schneebeli-Hermann et al. 2012). Therefore, slight changes in, for example, the temperature could cause distinct changes in climatic proxies. Sea surface temperatures from 30°S indicate a warming from the Griesbachian to the Dienerian (Romano et al. 2013). However, these data are not directly transferable to East Greenland, but they indicate that at least in the Tethyan realm temperature increased across the Griesbachian–Dienerian boundary.

Additionally, the spacing of clay-mineral data in this study is too broad to resolve climatic changes at a sub-Milankovitch timescale (Thiry 2000). Given a ~1-Myr duration for the study section, the 64 clay-mineral samples offer a resolution of no better than ~30 kyr (versus ~3 kyr for the 605 geochemical samples). Therefore, the change in the smectite/kaolinite ratios at the Griesbachian–Dienerian boundary might be the only true climatic signal documented in the clay-mineral record. The local peaks in the smectite/kaolinite ratios and smectite/mica+chlorite+kaolinite ratios are most probably sedimentological features associated with the sequence boundary at 150 m and the third-order sequence boundary around 330 m (Fig. 9) (Sanson-Barrera et al. 2015).

6. Conclusions

High-resolution geochemical data has been used to describe the latest Permian and earliest Triassic marine and terrestrial environmental variations at Kap Stosch in East Greenland. Major and trace elements, total organic carbon, total sulfur, degree of pyritization and clay mineralogy have been applied as proxies to infer marine redox conditions, marine paleoproductivity, terrestrial paleoweathering and humidity changes on land.

The transgressive-regressive cycles defined according to particulate organic matter (M/T ratios) and field observations (second-order sequence boundary at the Ravnefjeld/Wordie Creek formational boundary, the sequence boundary at ca. 150 m, and the third-order sequence boundary close to the Griesbachian–Dienerian boundary after Sanson-Barrera et al. 2015) are basically reflected in the Al concentrations and Ti/Al ratio. The third-order sequence boundary is indicated to be slightly higher in the chemostratigraphic profiles of Al and Ti/Al compared to the position in the M/T profile (Fig. 4). Calculated sedimentation rates for siltstone intervals with an average of 0.68 cm kyr^{-1} were exceptionally high in the study section that encompasses ~1 Myr.

Only one out of the three suboxic-anoxic intervals (A1-A3) reflected in the particulate organic matter could be identified in the DOP_T, C_{org}:P and S/TOC records. Trace element proxies (Mo, V, and U) usually indicative of these conditions were too diluted due to the extraordinary high sedimentation rates to show any significant variance throughout the profile (Table 1 and Fig. 5).

In the Kap Stosch record, major elements also suggest increased paleoweathering during a brief interval during the Griesbachian and during almost the whole Dienerian. These intervals with increased paleoweathering coincide with the increase in red siltstone and sandstone beds and the predominance of proximal environments. The Dienerian interval with increased weathering intensity and red-siltstone dominance coincides with higher smectite contents in the clay mineral assemblages. The peak in smectite/kaolinite ratios close to the Griesbachian–Dienerian boundary and the higher smectite content during the Dienerian probably indicates a climatic change close to this boundary with increased seasonality of rainfall in the Dienerian, but continued high humidity as indicated by the spore/pollen ratios.

Acknowledgments

ASB, PAH, and HB are thankful for the support of the Swiss SNF project grant 200021-135446. TJA gratefully acknowledges support from the Sedimentary Geology and Paleobiology program of the U.S. National Science Foundation, the NASA Exobiology program, and the State Key Laboratory of Geological Processes and Mineral Resources, China University of Geosciences, Wuhan (program GPMR201301). Elke Schneebeli-Hermann is thanked for her help in improving the manuscript.

References

Adams, J.S., Kraus, M.J., Wing, S.L., 2011. Evaluating the use of weathering indices for determining mean annual precipitation in the ancient stratigraphic record. Palaeogeography, Palaeoclimatology, Palaeoecology 309, 358-366, doi:10.1016/j.palaeo.2011.07.004

Adatte, T., Stinnesbeck, W., Keller, G., 1996. Lithostratigraphic and mineralogic correlations of near K/T boundary clastic sediments in northeastern Mexico: Implications for origin and nature of deposition. In: Ryder, G., Fastovsky, D., Gartner, S. (Eds.), The Cretaceous-Tertiary Event and Other Catastrophes in Earth History: Boulder, Colorado, Geological Society of America Special Paper 307, pp. 211-226.

Adatte, T., Rumley, G., 1989. Sedimentology and mineralogy of Valanginian and Hauterivian in the stratotypic region (Jura mountains, Switzerland). In: Wiedmann, J. (Ed.), Cretaceous of the Western Tethys. Proceedings 3rd International Cretaceous Symposium. Schweizerbart'sche Verlagsbuchhandlung, Stuttgart, pp. 329-351.

Algeo, T.J., Ingall, E., 2007. Sedimentary Corg:P ratios, paleocean ventilation, and Phanerozoic atmospheric pO2. Palaeogeography, Palaeoclimatology, Palaeoecology 256, 130-155.

Algeo, T.J., Tribovillard, N. 2009. Environmental analysis of paleoceanographic systems based on molybdenum-uranium covariation. Chemical Geology 268, 211-225, doi:10.1016/j.chemgeo.2009.09.001

Algeo, T.J., Twitchett, R.J., 2010. Anomalous Early Triassic sediment fluxes due to elevated weathering rates and their biological consequences. Geology 38, 1023-1026, doi: 10.1130/G31203.1

Algeo, T.J., Ellwood, B., Nguyen, T.K.T., Rowe, H., Maynard, J.B., 2007. The Permian–Triassic boundary at Nhi Tao, Vietnam: Evidence for recurrent influx of sulfidic watermasses to a shallow-marine carbonate platform. Palaeogeography, Palaeoclimatology, Palaeoecology 252, 304-327.

Algeo, T.J., Shen, Y., Zhang, T., Lyons, T., Bates, S., Rowe, H., Nguyen, T.K.T., 2008a. Association of 34S-depleted pyrite layers with negative carbonate δ13C excursions at the Permian-Triassic boundary: Evidence for upwelling of sulfidic deep-ocean water masses. Geochemistry, Geophysics, Geosystems 9, doi: 10.1029/2007GC001823.

Algeo, T.J., Rowe, H., Hower, J.C., Schwark, L., Herrmann, A., Heckel, P.H., 2008b. Oceanic denitrification during Late Carboniferous glacial-interglacial cycles. Nature Geoscience 1, 709-714, doi:10.1038/ngeo307.

Algeo, T.J., Hinnov, L., Moser, J., Maynard, J.B., Elswick, E., Kuwahara, K., Sano, H., 2010. Changes in productivity and redox conditions in the Panthalassic Ocean during the latest Permian. Geology 38, 187-190, doi:10.1130/G30483.1

Algeo, T.J., Chen, Z., Fraiser, M.L., Twitchett, R.J., 2011a. Terrestrial-marine teleconnections in the collapse and rebuilding of Early Triassic marine ecosystems. Palaeogeography, Palaeoclimatology, Palaeoecology 308, 1-11.

Algeo, T.J., Kuwahara, K., Sano, H., Bates, S., Lyons, T., Elswick, E., Hinnov, L., Ellwood, B.B., Moser, J., Maynard, J.B., 2011b. Spatial variation in sediment fluxes, redox conditions, and productivity in the Permian-Triassic Panthalassic Ocean. Palaeogeography, Palaeoclimatology, Palaeoecology 308, 65-83, doi:10.1016/j.palaeo.2010.07.007

Algeo, T.J., Henderson, C.M., Tong, J., Feng, Q., Yin, H., Tyson, R.V., 2013. Plankton and productivity during the Permian–Triassic boundary crisis: An analysis of organic carbon fluxes. Global and Planetary Change 105, 52-67, doi:10.1016/j.gloplacha.2012.02.008

Anders, M.H., Krueger, S.W., Sadler, P.M., 1987. A new look at sedimentation rates and the completeness of the stratigraphic record. Journal of Geology 95, 1-14.

Balme, B.E., 1979. Palynology of Permian-Triassic Boundary beds at Kap Stosch, East Greenland. Meddelelser om Grønland 200, 37 pp.

Beatty, T.W., Zonneveld, J-P., Henderson, C.M., 2008. Anomalously diverse Early Triassic ichnofossil assemblages in northwest Pangea: A case for a shallow-marine habitable zone. Geology 36, 771-774, doi: 10.1130/G24952A.1

Berner, R.A., 2002. Examination of hypotheses for the Permo-Triassic boundary extinction by carbon cycle modeling. Proceedings of the National Academy of Sciences (U.S.A.) 99, 4172-4177, doi: 10.1073/pnas.032095199

Berner R.A., Raiswell R., 1983. Burial of organic carbon and pyrite sulfur in sediments over Phanerozoic time: a new theory. Geochimica et Cosmochimica Acta 47, 855-862.

Birkenmajer, K., 1977. Erosional unconformity at the base of marine Lower Triassic at Wegner Ø, Central East Greenland. Bulletin of the Geological Society of Denmark 25, 107-116.

Bjerager, M., Seidler, L., Stemmerik, L., Surlyk, F., 2006. Ammonoid stratigraphy and sedimentary evolution across the Permian-Triassic boundary in East Greenland. Geological Magazine 143, 635-656, doi: 10.1017/S0016756806002020

Blakey, R., 2012. Global Paleogeography. http://www2.nau.edu/rcb7/globaltext2.html (accessed March 2015).

Brayard, A., Bucher, H., Escarguel, G., Fluteau, F., Bourquin, S., Galfetti, T., 2006. The Early Triassic ammonoid recovery: Paleoclimatic significance of diversity gradients. Palaeogeography, Palaeoclimatology, Palaeoecology 239, 374-395, doi: 10.1016/j.palaeo.2006.02.003.

Brayard, A., Escarguel, G., Bucher, H., Monnet, C., Brühwiler, T., Goudemand, N., Galfetti, T., Guex, J., 2009. Good genes and good luck: ammonoid diversity and the end-Permian mass extinction. Science 325, 1118-1121, doi: 10.1126/science.1174638

Brosse, M., Bucher, H., Bagherpour, B., Baud, A., Frisk, A.M., Goudun, K., Goudemand, N., 2015. Conodonts from the Early Triassic microbialite of Guangxi (South China): Implications for the definition of the base of the Triassic system. Palaeontology 58, 563-584, doi: 10.1111/pala.12162

Brosse, M., Bucher, H., Goudemand, N., 2016. Quantitative biochronology of the Permian-Triassic boundary in South China based on conodont Unitary Associations. Earth Science Reviews, in press, doi: 10.1016/j.earscirev.2016.02.003

Bugge, T., Ringas, J.E., Leith, D.A., Mangerud, G., Weiss, H.M., Leith, T.L., 2002. Upper Permian as new play model on the mid-Norwegian continental shelf: investigated by shallow stratigraphic drilling. American Association of Petroleum Geologists Bulletin 86, 107-127.

Burgess, S.D., Bowring, S., Shen, S., 2014. High-precision timeline for Earth's most severe extinction. Proceedings of the National Academy of Sciences (U.S.A.) 111, 3316-3321, doi: 10.1073/pnas.1317692111.

Chamley, H., Deconinck, J.F., Millot, G., 1990. Sur l'abondance des mineraux smectitiques dans les sediments marins communs deposés lors des périodes de haut niveau marin du Jurassique au

Paleogene. Comptes Rendus Academie des Sciences Paris 311 (2), 1529-1536.

Dunne, J.P., Sarmiento, J.L., Gnanadesikan, A., 2007. A synthesis of global particle export from the surface ocean and cycling through the ocean interior and on the seafloor. Global Biogeochemical Cycles 21, 1-16, doi:10.1029/2006GB002907

Dymond, J., Suess, E., Lyle, M., 1992. Barium in deep-sea sediment: A geochemical proxy for paleoproductivity. Paleoceanography 7, 163-181.

Eagle, M., Adina, P., Arrigo, K.R., van Dijken, G., Murray, R.W., 2003. A comparison between excess barium and barite as indicators of carbon export. Paleoceanography 18, 1-13, doi:10.1029/2002PA000793

Embry, A.F., 1997. Global sequence boundaries of the Triassic and their identification in the western Canada sedimentary basin. Bulletin of Canadian Petroleum Geology 45, 415-433.

Erwin, D.H., 2006. Extinction: How Life on Earth Nearly Ended 250 Million Years Ago: Princeton, Princeton University Press, 296 pp.

Feng, Q., Algeo, T.J., 2014. Evolution of oceanic redox conditions during the Permo-Triassic transition: Evidence from deep water radiolarian facies. Earth-Science Reviews 137, 34-51.

Fenton, S., Grice, K., Twitchett, R., Böttcher, M., Looy, C., Nabbefeld, B., 2007. Changes in biomarker abundances and sulfur isotopes of pyrite across the Permian–Triassic (P/Tr) Schuchert Dal section (East Greenland). Earth and Planetary Science Letters 262, 230-239, doi: 10.1016/j.epsl.2007.07.033

Füchtbauer, H., 1988. Sedimente und Sedimentgestein, 4th ed., Schweizerbart'sche, Stuttgart, 1141 pp.

Galfetti, T., Bucher, H., Ovtcharova, M., Schaltegger, U., Brayard, A., Brühwiler, T., Goudemand, N., Weissert, H., Hochuli, P.A., Cordey, F., Guodun, K., 2007. Timing of the Early Triassic carbon cycle perturbations inferred from new U–Pb ages and ammonoid biochronozones. Earth and Planetary Science Letters 258, 593-604, doi: 10.1016/j.epsl.2007.04.023

Gibbs, R.J., 1977. Clay mineral segregation in the marine environment. Journal of Sedimentary Petrology 47, 237-243.

Godet, A., Bodin, S., Adatte, T., Föllmi, K.B., 2008. Platform-induced clay-mineral fractionation along a northern Tethyan basin-platform transect: implications for the interpretation of Early Cretaceous climate change (Late Hauterivian–Early Aptian). Cretaceous Research 29, 830-847.

Grasby, S.E., Beauchamp, B., Embry, A., Sanei, H., 2012. Recurrent Early Triassic ocean anoxia. Geology 41, 175-178.

Hamann, N.E., Whittaker, R.C., Stemmerik, L., 2005. Geological development of the Northeast Greenland Shelf. In: Doré, A.G., Vining, B.A. (Eds.), Petroleum Geology 2, Geological Society of London, Petroleum Geology Conference Series Vol. 6, 887-902, doi: 10.1144/0060887

Hautmann, M., Bucher, H., Brühwiler, T., Goudemand, N., Kaim, A., Nützel, A., 2011. An unusually diverse mollusc fauna from the earliest Triassic of South China and its implications for benthic recovery after the end-Permian biotic crisis. Geobios 44, 71-85, doi:10.1016/j.geobios.2010.07.004

Hautmann, M., Bagherpour, B., Brosse, M., Frisk, A., Hofmann, R., Baud, A., Nützel, A., Goudemand, N., Bucher, H., 2015. Competition in slow motion: the unusual case of benthic marine communities in the wake of the end-Permian mass extinction. Palaeontology 58, 871-901, doi: 10.1111/pala.12186

Hays, L.E., Grice, K., Foster, C.B., Summons, R.E., 2012. Biomarker and isotopic trends in a Permian–Triassic sedimentary section at Kap Stosch, Greenland. Organic Geochemistry 43, 67-82, doi: 10.1016/j.orggeochem.2011.10.010

Hermann, E., Hochuli, P.A., Bucher, H., Brühwiler, T., Hautmann, M., Ware, D., Weissert, H., Roohi, G., Yaseen, A., 2012. Climatic oscillations at the onset of the Mesozoic inferred from palynological records from the North Indian Margin. Journal of the Geological Society of London 169, 227-237, doi: 10.1144/0016-76492010-130

Hochuli, P.A., Sanson-Barrera, A., Schneebeli-Hermann, E., Bucher, H., (in review). Severest crisis overlooked—Worst disruption of terrestrial environments postdates the Permian–Triassic mass extinction. Nature Scientific Reports.

Hofmann, R., Goudemand, N., Wasmer, M., Bucher, H., Hautmann, M., 2011. New trace fossils evidence for an early recovery signal in the aftermath of the end-Permian mass extinction. Palaeogeography, Palaeoclimatology, Palaeoecology 310, 216-226.

Hofmann, R., Hautmann, M., Wasmer, M., Bucher, H., 2013. Palaeoecology of the Spathian Virgin Formation (Utah, USA) and its implications for the Early Triassic recovery. Acta Palaeontologica Polonica 58, 149-173.

Jarvis, I., Murphy, A.M., Gale, A.S., 2001. Geochemistry of pelagic and hemipelagic carbonates: criteria for identifying systems tracts and sea-level change. Journal of the Geological Society of London 158, 685-696.

Klug, H.P., Alexander, L., 1974. X-ray Diffraction Procedures for Polycrystalline and Amorphous Materials, 2nd ed., John Wiley and Sons, New York, 992 pp.

Koch, L., 1931. Carboniferous and Triassic stratigraphy of East Greenland. Meddelelser om Grønland 83, 100 pp.

Kominz, M.A., 1996. Whither cyclostratigraphy? Testing the gamma method on Upper Pleistocene deep-sea sediments, North Atlantic Deep Sea Drilling Project

Site 609. Paleoceanography 11, 481-504.
Kominz, M.A., Bond, G.C., 1990. A new method of testing periodicity in cyclic sediments: application to the Newark Supergroup. Earth and Planetary Science Letters 98, 233-244.
Kominz, M.A., Bond, G.C. 1992. Documenting the reliability and utility of the g method as applied to cyclic sections using forward modeling. Earth and Planetary Science Letters 113, 449-457.
Krystyn, L., Richoz, S., Baud, A., Twitchett, R.J., 2003. A unique Permian–Triassic boundary section from the Neotethyan Hawasina Basin, Central Oman Mountains. Palaeogeography, Palaeoclimatology, Palaeoecology 191, 329-344, doi: 10.1016/S0031-0182(02)00670-3.
Kübler, B., 1983. Cristallinité de l'illite, méthodes normalisées de préparations, méthodes normalisées de mesures. Cahiers Institut Géologie de Neuchâtel, Suisse (série ADX 1), 13 pp.
Kump, L.R., Pavlov, A., Arthur, M.A., 2005. Massive release of hydrogen sulfide to the surface ocean and atmosphere during intervals of oceanic anoxia. Geology 33, 397-400.
Kutzbach, J.E., Gallimore, R.G., 1989. Pangaean climates: megamonsoons of the megacontinent. Journal of Geophysical Research 94, 3341-3358.
Lehrmann, D.J., Ramezani, J., Bowring, S.A., Martin, M.W., Montgomery, P., Enos, P., Payne, J.L., Orchard, M.J., Wang, H., Wei, J., 2006. Timing of recovery from the end-Permian extinction: Geochronologic and biostratigraphic constraints from south China. Geology 34, 1053-1056, doi: 10.1130/G22827A.1
Looy, C.V., Twitchett, R.J., Dilcher, D.L., Van Konijnenburg-Van Cittert, J.H., Visscher, H., 2001. Life in the end-Permian dead zone. Proceedings of the National Academy of Sciences (U.S.A.) 98, 7879-7883, doi: 10.1073/pnas.131218098
Luo, G.M., Kump, L.R., Wang, Y., Tong, J., Arthur, M.A., Yang, H., Huang, J., Yin, H., Xie, S., 2010. Isotopic evidence for an anomalously low oceanic sulfate concentration following end-Permian mass extinction. Earth and Planetary Science Letters 300, 101-111.
McLennan, S. M., 1993. Weathering and global denudation. The Journal of Geology 101, 295-303.
Mørk, A., Smelror, M., 2001. Correlation and non-correlation of high order circum-Arctic Mesozoic sequences. Polarforschung 69, 65-72.
Mørk, A., Embry, A.F., Weitschat W., 1989. Triassic transgressive–regressive cycles in the Sverdrup Basin, Svalbard and the Barents Shelf. In: Collinson, J.D. (Ed.), Correlation in Hydrocarbon Exploration. Norwegian Petroleum Society, Bergen, pp. 113-130.
Mørk, A., Vigran, J.O., Hochuli, P.A., 1990. Geology and palynology of the Triassic succession of Bjørnøya. Polar Research 8, 141-163.
Nakrem, H.A., Mørk, A., 1991. New Early Triassic bryozoa (Trepostomata) from Spitsbergen, with some remarks on the stratigraphy of the investigated horizons. Geological Magazine 128, 129-140.
Nesbitt, H.W., Young, G.M., 1982. Early Proterozoic climates and plate motions inferred from major element chemistry of lutites. Nature 299, 715-717.
Nesbitt, H.W., Young, G.M., 1989. Formation and diagenesis of weathering profiles. Journal of Geology 97, 129-147.
Newton, R., Pevitt, E., Wignall, P.B., Bottrell, S.H., 2004. Large shifts in the isotopic composition of seawater sulphate across the Permo–Triassic boundary in northern Italy. Earth and Planetary Science Letters 218, 331-345, doi: 10.1016/S0012-821X(03)00676-9
Nielsen, E., 1935. The Permian and Eotriassic vertebrate-bearing beds at Gofthaab Gulf (East Greenland). Meddelelser om Grønland 98, 111 pp.
Nielsen, J.K., Shen, Y., 2004. Evidence for sulfidic deep water during the Late Permian in the East Greenland Basin. Geology 32, 1037-1040, doi: 10.1130/G20987.1.
Nielsen, J.K., Shen, Y., Piasecki, S., Stemmerik, L., 2010. No abrupt change in redox condition caused the end-Permian marine ecosystem collapse in the East Greenland Basin. Earth and Planetary Science Letters 291, 32-38, doi: 10.1016/j.epsl.2009.12.043.
Oftedal, B.T., Andresen, A., Müller, R., 2005. Early Triassic syn-rift sedimentation at Hold with Hope, Northeast Greenland. In: Wandas, B., et al. (Eds.), Norwegian Petroleum Society Special Publication 12, Onshore-Offshore Relationships on the North Atlantic Margin. Elsevier, Amsterdam, pp. 191-206.
Ovtcharova, M., Bucher H., Schaltegger, U., Galfetti, T., Brayard, A., Guex J., 2006. New Early to Middle Triassic U–Pb ages from South China: Calibration with ammonoid biochronozones and implications for the timing of the Triassic biotic recovery. Earth and Planetary Science Letters 243, 463-475, doi:10.1016/j.epsl.2006.01.042.
Ovtcharova, M., Goudemand, N., Hammer, Ø., Guodun, K., Cordey, F., Galfetti, T., Schaltegger, U., Bucher, H., 2015. Developing a strategy for accurate definition of a geological boundary through radio-isotopic and biochronological dating: The Early-Middle Triassic boundary (South China). Earth-Science Reviews 146, 65-76, doi:10.1016/j.earscirev.2015.03.006.
Parrish, J.T., 1993. Climate of the supercontinent Pangea. Journal of Geology 101, 215-233.
Payne, J.L., Lehrmann, D.J., Wei, J., Orchard, M.J., Schrag, D.P., Knoll, A.H., 2004. Large perturbations of the carbon cycle during recovery from the end-Permian extinction. Science 305, 506-509, doi: 10.1126/science.1097023.
Perch-Nielsen, K., Birkenmajer, K., Birkelund, T., Aellen, M., 1974. Revision of Triassic stratigraphy of the Scoresby Land and Jameson Land region, East Greenland. Meddelelser om Grønland 193, 86 pp.

Piasecki, S., 1984. Preliminary palynostratigraphy of the Permian-Lower Triassic sediments in Jameson Land and Scoresby Land, East Greenland. Bulletin of the Geological Society of Denmark 32, 139-144.
Piasecki, S., Stemmerik, L., 1991. Late Permian anoxia in central East Greenland. In: Tyson, R.V., Pearson, T.H. (Eds.), Modern and Ancient Continental Shelf Anoxia, Geological Society of London Special Publication 58, pp. 275-290.
Price, J.R., Velbel, M.A., 2003. Chemical weathering indices applied to weathering profiles developed on heterogeneous felsic metamorphic parent rocks. Chemical Geology 202, 397-416.
Raiswell, R., Buckley, F., Berner, R.A., Anderson, T.F., 1988. Degree of pyritization of iron as a paleoenvironmental indicator of bottom-water oxygenation. Journal of Sedimentary Petrology 58, 812-819.
Retallack, G.J., Sheldon, N.D., Carr, P.F., Fanning, M., Thompson, C.A., Williams, M.L., Jones, B.G., Hutton, A., 2011. Multiple Early Triassic greenhouse crises impeded recovery from Late Permian mass extinction. Palaeogeography, Palaeoclimatology, Palaeoecology 308, 233-251.
Riccardi, A.L., Arthur, M.A., Kump, L.R., 2006. Sulfur isotopic evidence for chemocline upward excursions during the end-Permian mass extinction. Geochimica et Cosmochimica Acta 70, 5740-5752, doi: 10.1016/j.gca.2006.08.005.
Romano, C., Goudemand, N., Vennemann, T.W., Ware, D., Schneebeli-Hermann, E., Hochuli, P.A., Brühwiler, T., Brinkmann, W., Bucher, H., 2013. Climatic and biotic upheavals following the end-Permian mass extinction. Nature Geoscience 6, 57-60, doi: 10.1038/ngeo1667.
Sadler, P.M., 1981. Sediment accumulation rates and the completeness of stratigraphic sections. Journal of Geology 89, 569-584.
Sanson-Barrera, A., Hochuli, P.A., Bucher, H., Schneebeli-Hermann, E., Weissert, H., Adatte, T., Bernasconi, S.M., 2015. Late Permian–earliest Triassic high-resolution organic carbon isotope and palynofacies records from Kap Stosch (East Greenland). Global and Planetary Change 133, 149-166, doi: 10.1016/j.gloplacha.2015.08.006.
Schneebeli-Hermann, E., Kürschner, W.M., Hochuli, P.A., Bucher, H., Ware, D., Goudemand, N., Roohi, G., 2012. Palynofacies analysis of the Permian–Triassic transition in the Amb section (Salt Range, Pakistan): Implications for the anoxia on the South Tethyan Margin. Journal of Asian Earth Sciences 60, 225-234.
Schoepfer, S.D., Shen, J., Wei, H., Tyson, R.V., Ingall, E., Algeo, T.J., 2015. Total organic carbon, organic phosphorus, and biogenic barium fluxes as proxies for paleomarine productivity. Earth-Science Reviews 149, 19-48.
Seidler, L., Steel, R., Stemmerik, L., Surlyk, F., 2004. North Atlantic marine rifting in the Early Triassic: new evidence from East Greenland. Journal of the Geological Society of London 161, 583-592, doi: 10.1144/0016-764903-063.
Sheldon, N.D., Retallack, G.J., Tanaka, S., 2002. Geochemical climofunctions from North American soils and application to paleosols across the Eocene-Oligocene boundary in Oregon. The Journal of Geology 110, 687-696.
Shen, S., Crowley, J.L., Wang, Y., Bowring, S.A., Erwin, D.H., Sadler, P.M., Cao, C., Rothman, D.H., Henderson, C.M., Ramezani, J., Zhang, H., Shen, Y., Wang, X., 2011. Calibrating the end-Permian mass extinction. Science 334, 1367-1372.
Song, H., Tong, J., Algeo, T.J., Song, H., Qiu, H., Zhu, Y., Tian, L., Bates, S., Lyons, T.W., Luo, G., Kump, L., 2014. Early Triassic seawater sulfate drawdown. Geochimica et Cosmochimica Acta 128, 95-113.
Spath, L.F., 1935. Additions to the Eotriassic invertebrate faunas of East Greenland. Meddelelser om Grønland 98, 115 pp.
Stemmerik, L., 2000. Late Palaeozoic evolution of the North Atlantic margin of Pangea. Palaeogeography, Palaeoclimatology, Palaeoecology 161, 95-126, doi: 10.1016/S0031-0182(00)00119-X.
Stemmerik, L., Dam, G., Noe-nygaard, N., Piasecki, S., Surlyk, F., 1998. Sequence stratigraphy of source and reservoir rocks in the Upper Permian and Jurassic of Jameson Land, East Greenland. Geology of Greenland Survey Bulletin 180, 43-54.
Stemmerik, L., Bendix-Almgreen, S.E., Piasecki, S., 2001. The Permian-Triassic boundary in central East Greenland: past and present views. Bulletin of the Geological Society of Denmark 48, 159-167.
Sun, Y.D., Joachimski, M.M., Wignall, P.B., Yan, C.B., Chen, Y.L., Jiang, H.S., Wang, L.N., Lai, X.L., 2012. Lethally hot temperatures during the Early Triassic greenhouse. Science 338, 366-370.
Surlyk, F., 1990. Timing, style and sedimentary evolution of Late Palaeozoic-Mesozoic extensional basins of East Greenland. In: Hardman, R.F.P., Brooks, J. (Eds.), Tectonic Events Responsible for Britain's Oil and Gas Reserves, Geological Society of London Special Publication 55, pp. 107-125.
Surlyk, F., Piasecki, S., Rolle, F., Stemmerik, L., Thomsen, E., Wrang, P., 1984. The Permian base of east Greenland. In: Petroleum Geology of the North European Margin, Proceedings of North European Margin Symposium (NEMS'83) Trondheim, Norway, pp. 303-315.
Surlyk, F., Piasecki, S., Rolle, F., Scholle, P.A., Stemmerik, L., Thomsen, E., 1986. The Permian of the western margin of the Greenland Sea—A future exploration target. In: Halbouty, M.T. (Ed.), Future Petroleum Provinces of the World. American Association of Petroleum Geologists Memoir 40, pp. 629-659.

Teichert, C., Kummel, B., 1972. Permian-Triassic boundary in the Kap Stosch area, East Greenland. Bulletin of Canadian Petroleum Geology 20, 659-675.

Thiry, M., 2000. Palaeoclimatic interpretation of clay minerals in marine deposits: an outlook from the continental origin. Earth Science Reviews 49, 201-221.

Tong, J.N., Zuo, J.X., Chen, Z.Q., 2007. Early Triassic carbon isotope excursions from South China: Proxies for devastation and restoration of marine ecosystems following the end-Permian mass extinction. Geological Journal 42, 371-389.

Trümpy, R., 1969. Notes on the Triassic stratigraphic and paleontology of north-eastern Jameson Land (East Greenland). Meddelelser om Grønland 168, 77-116.

Twitchett, R.J., Looy, C. V., Morante, R., Visscher, H., Wignall, P.B., 2001. Rapid and synchronous collapse of marine and terrestrial ecosystems during the end-Permian biotic crisis. Geology 29, 351-354.

Twitchett, R.J., Krystyn, L., Baud, A., Wheeley, J.R., Richoz, S., 2004. Rapid marine recovery after the end-Permian mass-extinction event in the absence of marine anoxia. Geology 32, 805-808, doi: 10.1130/G20585.1.

Tyson, R.V., 1995. Sedimentary Organic Matter—Organic Facies and Palynofacies. Chapman and Hall, 615 pp.

Tyson, R.V., 2005. The "productivity versus preservation" controversy: cause, flaws, and resolution. In: Harris, N.B. (Ed.), The Deposition of Organic-Carbon-Rich Sediments: Models, Mechanisms, and Consequences. Society for Sedimentary Geology Special Publication 82, pp. 17-33.

Wedepohl, K.H., 1971. Environmental influences on the chemical composition of shales and clays. In: Ahrens, L.H., Press, F., Runcorn, S.K., Urey, H.C. (Eds.), Physics and Chemistry of the Earth, vol. 8. Pergamon, Oxford, pp. 305-333.

Wedepohl, K.H., 1991. The composition of the upper earth's crust and the natural cycles of selected metals. Metals in natural raw materials. Natural Resources. In: Merian, E. (Ed.), Metals and Their Compounds in the Environment. VCH, Weinheim, pp. 3-17.

Wei, H.Y., Shen, J., Schoepfer, S.D., Krystyn, L., Richoz, S., Algeo, T.J., 2015. Environmental controls on marine ecosystem recovery following mass extinctions, with an example from the Early Triassic. Earth-Science Reviews 149, 104-131.

Wignall, P.B., Twitchett, R.J., 1996. Oceanic anoxia and the end Permian mass extinction. Science 272, 1155-1158.

Wignall, P.B., Twitchett, R.J., 2002. Permian-Triassic sedimentology of Jameson Land, East Greenland: incised submarine channels in an anoxic basin. Journal of the Geological Society of London 159, 691-703.

Wignall, P.B., Morante, R., Newton, R., 1998. The Permo-Triassic transition in Spitsbergen: δ13Corg chemostratigraphy, Fe and S geochemistry, facies, fauna and trace fossils. Geological Magazine 135, 47-62.

Wignall, P.B., Bond, D.P.G., Sun, Y., Grasby, S.E., Beauchamp, B., Joachimski, M.M., B lomeier, D.P.G., 2015. Ultra-shallow-marine anoxia in an Early Triassic shallow-marine clastic ramp (Spitsbergen) and the suppression of benthic radiation. Geological Magazine, 1-16, doi:10.1017/S0016756815000588

Winguth, C., Winguth, A.M.E., 2012. Simulating Permian-Triassic oceanic anoxia distribution: Implications for species extinction and recovery. Geology 40, 127-130.

Wordie, J.M., 1927. The Cambridge expedition to East Greenland in 1926. Geological Journal 75, 225-265.

Worsley, D., Mørk, A., 1978. The Triassic stratigraphy of southern Spitsbergen. Norsk Polarinstitutt Aarbok 43-60.

Yang, W., Kominz, M.A., 1999. Testing periodicity of depositional cyclicity, Cisco Group (Virgilian and Wolfcampian), Texas. Journal of Sedimentary Research 69, 1209-1231.

Yin, H., Zhang, K., Tong, J., Yang, Z., Wu, S., 2001. The Global Stratotype and Point (GSSP) of the Permian-Triassic Boundary. Episodes 24, 102-114.

Yin, H., Feng, Q., Lai, X., Baud, A., Tong, J., 2007. The protracted Permo-Triassic crisis and multi-episode extinction around the Permian–Triassic boundary. Global and Planetary Change 55, 1-20, doi: 10.1016/j.gloplacha.2006.06.005.

Zhang, Y., Zhang, K.X., Shi, G.R., He, W.H., Yuan, D.X., Yue, M.L., Yang, T.L., 2014. Restudy of conodont biostratigraphy of the Permian–Triassic boundary section in Zhongzhai, southwestern Guizhou Province, South China. Journal of Asian Earth Sciences 80, 75-83.

Supplementary data. Please check the online version of the article after being accepted.

Chapter 4

Severest crisis overlooked — Worst disruption of terrestrial environments postdates the Permian–Triassic mass extinction

Peter A. Hochuli, Anna Sanson-Barrera,
Elke Schneebeli-Hermann, Hugo Bucher

published in Nature Scientific Reports
http://www.nature.com/articles/srep28372

www.nature.com/scientificreports

SCIENTIFIC REPORTS

OPEN

Severest crisis overlooked—Worst disruption of terrestrial environments postdates the Permian–Triassic mass extinction

Received: 11 January 2016
Accepted: 02 June 2016
Published: 24 June 2016

Peter A. Hochuli, Anna Sanson-Barrera, Elke Schneebeli-Hermann & Hugo Bucher

Generally Early Triassic floras are believed to be depauperate, suffering from protracted recovery following the Permian–Triassic extinction event. Here we present palynological data of an expanded East Greenland section documenting recovered floras in the basal Triassic (Griesbachian) and a subsequent fundamental floral turnover, postdating the Permian–Triassic boundary extinction by about 500 kyrs. This event is marked by a swap in dominating floral elements, changing from gymnosperm pollen-dominated associations in the Griesbachian to lycopsid spore-dominated assemblages in the Dienerian. This turnover coincides with an extreme $\delta^{13}C_{org}$ negative shift revealing a severe environmental crisis, probably induced by volcanic outbursts of the Siberian Traps, accompanied by a climatic turnover, changing from cool and dry in the Griesbachian to hot and humid in the Dienerian. Estimates of sedimentation rates suggest that this environmental alteration took place within some 1000 years. Similar, coeval changes documented on the North Indian Margin (Pakistan) and the Bowen Basin (Australia) indicate the global extent of this crisis. Our results evidence the first profound disruption of the recovery of terrestrial environments about 500kyrs after the Permian–Triassic extinction event. It was followed by another crisis, about 1myrs later thus, the Early Triassic can be characterised as a time of successive environmental crises.

Scientists as well as the broad public become more and more aware of modern (manmade) destruction of terrestrial environments caused not only by the obvious effects of air pollution or clearing rain forests but also by the more subtle and long-term climatic change[1,2]. Deforestation is associated with the loss of biodiversity, increased greenhouse gas emissions, disrupted water cycles, increased soil erosion, and disrupted lebensraum[3–7]. These effects are also regularly discussed as consequences of the events leading to the Phanerozoic mass extinctions[8]. In fact there is increasing evidence that we are currently witnessing the sixth–manmade-mass extinction, associated with the destruction of natural environments and climatic change[9]. Thus, the hypothesis published a few years ago that the Permian–Triassic mass extinction (PTME), the biggest extinction event in Earth history (ca. 251myrs ago), was associated with an essentially global deforestation[10,11] was easily accepted by the scientific community. This led to the widely approved concept that the destruction of the gymnosperm forests induced a pioneer vegetation of herbaceous lycopsids that subsequently dominated the terrestrial environments during the entire Early Triassic. Furthermore, the climate of the Early Triassic was interpreted as homogeneously warm and semi-arid[12] or hot and arid[13,14]. These ideas concurred with the commonly hawked hypothesis that Early Triassic biotas reflect a protracted recovery after the PTME. Recent studies, however, show a more complex picture of the development of the biosphere and climate during this time, providing evidence for significant climatic changes[15] as well as for profound faunal and floral turnovers[16–25]. New evidence suggest that not all marine organisms were similarly affected by the PTME. Most linages of conodonts and numerous radiolarians survived this event, but went extinct around the Griesbachian–Dienerian boundary while typical Mesozoic conodont and radiolarian assemblages appeared after this event[17,18]. Other Griesbachian records have reported "incredibly diverse benthic fauna"[19], and "unexpectedly diverse and complex ichnofauna"[20], which reveal at least locally sound living conditions for benthic ecosystems. Hence, these findings suggest that during the Griesbachian environmental conditions were less hostile than generally assumed and that an important extinction event affecting several groups occurred around

Institute and Museum of Palaeontology, University of Zurich, Karl Schmid-Str. 4, CH-8006 Zurich, Switzerland. Correspondence and requests for materials should be addressed to P.A.H. (email: peter.hochuli@pim.uzh.ch)

www.nature.com/scientificreports/

the Griesbachian–Dienerian boundary[17,18,20,23]. Palynological studies of expanded sections with well-preserved pollen and spores have provided insight into the dynamics of the development of plant associations during these critical intervals. New results show that the PTME lead to short term changes in the plant community abundance structure, expressed in the palynological records by a "spore spike"[10,24,26]. Thus, the immediate reaction of the plant communities on the environmental catastrophe of the PTME was similar to those known from the subsequent major cataclysms, such as at the Triassic–Jurassic boundary (TJB) or the Cretaceous-Paleogene events (KPE), which are also characterized by short-lived super-abundance of pteridophyte spores[27–30]. These "spore spikes" systematically concur with negative $\delta^{13}C$ isotope shifts. Thus, they obviously reflect reaction of the vegetation to environmental cataclysms, such as massive volcanic outbursts related to the PTME or the TJB[28,31,32] or to the asteroid impact at the KPB[33]. This shows that different causes of disruption of terrestrial ecosystems lead to a similar reactions of the vegetation, even concerning various groups of pteridophytes–lycopsids at the PTME versus ferns at the TJB and the KPB. In fact in modern disturbed ecosystems ferns and fern allies play an important role in ecosystem restoration due to their tolerance to grow in acidic water-logged conditions or their ability to exploit nutrient-poor substrates–conditions that are associated with volcanic outbursts[29,34,35]. After the clearance of primary forests these opportunistic plants are known to take over and give subsequently way to the succeeding forests[34,36]. High resolution palynological data including the PTME indicate that gymnosperms recovered probably within a few kyrs to become again the dominating floral element[24]. Some typical Permian floral elements (e.g., *Vittatina*) gradually disappeared during this phase of recovery, although without an obvious loss in biodiversity or extinction of major plant groups[24,37]. Instead the detailed records from the Finnmark Platform[24,37] show a distinct diversification of both gymnosperms and pteridophytes, which results in increased diversities after the PTME. New radiometric datings of the Permian–Triassic succession of the Bowen Basin[38] shed a new light on the impact of PTME on plants. According to this new calibration the *Playfordiaspora crenulata*–and the *Protohaploxypinus microcorpus* zones, formerly attributed to the Late Permian, are now dated as Induan. Consequently, the floral turnover between the two zones described by Foster[39] reflects now a mid-Induan event. The palynological assemblages of the *P. crenulata* zone are characterised by high abundance and diversity of taeniate bisaccate pollen changing at the boundary to the *P. microcorpus* zone to a dominance of lycopsid spores. Above all this event is marked by the disappearance of the *Glossopteris* flora[39].

The Griesbachian record from East Greenland and the coeval section in the Trøndelag area of mid-Norway show well diversified spore-pollen assemblages, with clear dominance of gymnosperms[40]. This evidence is in obvious contrast with the previous general conception of depauperate Early Triassic sporomorph assemblages that are assumed to be characterized by overall dominance of lycopsid spores[12]. The present study of the expanded Kap Stosch section (Hold with Hope, East Greenland, 73°60′N/21°12′W–74°04′N/21°43′W) reveals that the profound and sustained floral change leading to the dominance of lycopsids happened ca. 500 kyrs after the PTME[21,41–43] around the Griesbachian–Dienerian boundary (GDB). Here the gymnosperm pollen dominated floral associations of the basal Triassic (Griesbachian) changed to lycopsid spore-dominated assemblages. Evidence from other areas (e.g., Barents Sea, Pakistan, Tibet) shows that lycopsid subsequently dominated the flora up into the middle Smithian, for about 1myrs where other floral changes of global extent led to a renewed and short lived dominance of gymnosperms in the late Smithian[22,23,44]. Late Early Triassic (Spathian) floras are characterised by mixed assemblages showing a general decline of lycopsid spores associated with renewed diversification of terrestrial floras towards the Middle Triassic (e.g., 23, 45, 46).

Results

Here the general bulk palynological record with over 80 samples covering the upper part of the Griesbachian and the Dienerian from Kap Stosch is presented. The studied section is part of the Late Permian–Early Triassic Greenland-Norway rift basin. Deltaic sediments of the Wordie Creek Formation with changing marine influence were deposited during the latest Permian and the Induan (Griesbachian and Dienerian). The Griesbachian part of the formation comprises about 270m of section of which the upper 110 metres are included in the present study (Fig. 1). Age control is provided by a few horizons with ammonoids and bulk organic carbon isotope chemostratigraphy[47,48]. The Griesbachian–Dienerian boundary (GDB) is placed at the onset of a negative $\delta^{13}C_{org}$ shift with the ammonoid *Bukkenites rosenkrantzi* occurring just above this level. Diverging from the interpretation of Bjerager *et al.*[45] *B. rosenkrantzi* is considered here to be of Dienerian age because the worldwide oldest occurrences of proptychitids to which this species belongs are of Dienerian age or younger[21].

For the present study we differentiated seven main floral elements, which are mentioned below together with the essential changes in their distribution (Fig. 1). The first group–***Aratrisporites***-is generally associated with the macrofossils *Annalepis*, a probably herbaceous lycopsid of isoetalean affinity[47]. This group, being very rare in the Griesbachian, becomes a significant element in the upper part of the section. **Cavate trilete spores**, comprising essentially the genera *Densoisporites, Kraeuselisporites,* and *Lundbladispora* can be attributed to lycopsids, probably also to the Isoetales[47]. They show average abundances of 10–20% in the Griesbachian; increasing around the GDB (at ca. 350 m) to about 60%, to become the overwhelmingly dominant group with up to 90% of the assemblages in the uppermost part of the section (from ca. 450 m onward). **Non-cavate spores** comprise a variety of smooth and ornamented spores, which represent various pteridophytes (lycopsids and ferns) but also bryophytes. This group shows no significant abundance change within the record. Pollen grains summarized under ***Cycadopites*** **group** comprise a great variety of possible gymnosperm parent plants (e.g., Bennettiales, Ginkgoales, Cycadales, and Peltaspermales)[47]. They are relatively common in the lower part of the succession and up to 10% in some samples of the GDB interval. They represent essentially the only group of gymnosperms (up to 10%) in the uppermost part of the studied section. **Non-taeniate bisaccate pollen grains** include conifers but also some groups of pteridosperms. This group is rare in the upper part of the Griesbachian and almost disappears in the Dienerian. **Taeniate bisaccate pollen grains,** attributed to pteridosperms, represent the dominant group in the lower part of the record with abundances up to 90%. Around the GDB their abundance decreases gradually over

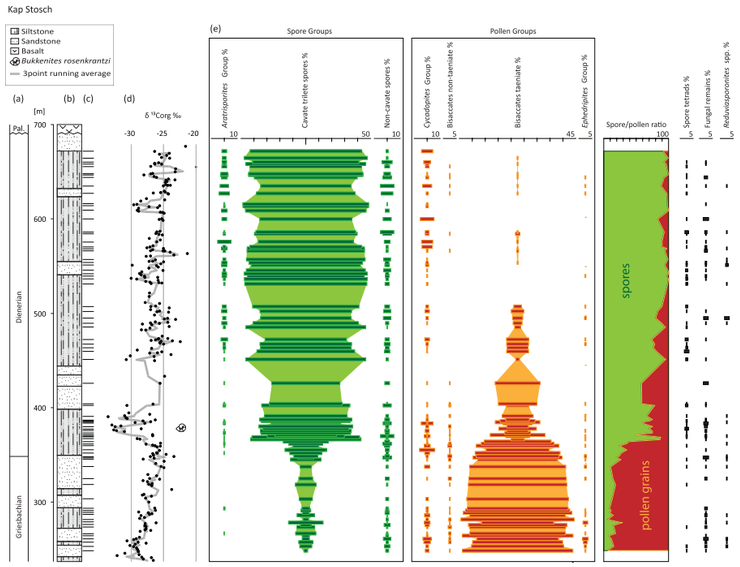

Figure 1. Overview on Griesbachian–Dienerian floras with generalized C-isotope curve. (**a**) Age (**b**) lithology (**c**) sample levels (**d**) bulk organic carbon isotopes[46] (**e**) palynological data including relative abundances of groups of spore and pollen grains, spore/pollen ratios as well as spore tetrads, fungal remains and *Reduviasporonites* spp.

a short interval from around 60% to about 20%, and they become rare (<5%) in the uppermost part of the section. The ***Ephedripites* group**, representing Gnetales[47], is regularly observed in the lowermost part of the record with abundances up to 5% and occurs only sporadically in the upper part of the section. The **spore/pollen ratio** summarizes the essential changes in the plant assemblages. This ratio is regarded as a rough indicator for water availability to the plant communities[24,48] Because they have played a significant role in the interpretation of the environmental disaster of the PTME[11,49] the quantitative distribution of **spore tetrads** (comprising essentially *Densoisporites* spp.), **fungal remains,** and ***Reduviasporonites* spp.** are also included. In the present record their abundances show no significant trend. Generally, the trends in the distribution of all the above mentioned groups are unrelated to changes in the depositional environment[46].

In the Kap Stosch area the Induan (Griesbachian and Dienerian) interval comprises about 600 m of section[46]. Thus, accepting the roughly estimated duration of the Induan of about 1.0 myr[41–43] would result in an average sedimentation rate of ca. 0.6 m/kyr in the studied section. The estimated duration of the Dienerian at 416 kyrs by Ware *et al.*[21] would suggest a sedimentation rate of 0.79 m/kyr for the 328 m of Dienerian section, provided that the entire substage is represented. The described mid-Induan floral turnover takes place over an interval of a ca. 4 metres at the onset of the prominent $\delta^{13}C_{org}$ shift close to the GDB, thus we conclude that the changes occurred over a very short interval in the order of a few kyrs.

Discussion

Compared to the marine fauna relatively little is known about the impacts of the PTME and following events on the terrestrial realm. The record of Early Triassic plant macrofossils is extremely poor and mostly uncalibrated; however, palynological records adequately reflect floral changes during mass extinctions and the subsequent recovery phases[22,23,25]. For the PTME some spectacular scenarios have been inferred from relatively few records, e.g., total extinction[50] totally devastated environments unsuited for plants[12,49,51,52], plant mutagenesis due to ozone layer destruction[10], and collapse of terrestrial ecosystems related to a fungal event[49,52]. Evidence for the latter event is still questionable, mainly because of the ambiguous biological attribution of *Reduviasporonites*, the key witness of this event, assigned by some authors to fungi[53] and by others-with more convincing evidence-to algae[54,55]. However, high abundances of *Reduviasporonites,* as those interpreted as "fungal event", have not been observed in any expanded section. *Reduviasporonites* occurs regularly but not abundantly throughout these records[24,37,39].

Another effect of the PTME has been inferred from high numbers of spore tetrads in sediments comprising this event. It has been proposed that stratospheric ozone layer depletion and subsequent increased UV-B radiation caused genetic damage (mutagenesis) on lycopsids[11]. According to these authors the effect of this event

prevented the spore tetrads of some lycopsids to separate during maturation. In fact peak abundances of tetrads coincide with the above mentioned "spore spike". On the other hand, the tendency to shed the spores in tetrads could also be inherent to the lycopsid groups in question, as it is known for other fossil plants, such as the conifer pollen *Triadispora* or *Classopollis*. Other authors relate the high abundance of tetrads to depositional environments adjacent to the plant's habitat[56]. Thus, the reasons for these occurrences remain ambiguous. In all expanded palynological records (Kap Stosch, Trøndelag and Finnmark platform) spore tetrads are regularly observed throughout the Griesbachian and the Dienerian. In the Kap Stosch record levels with increased numbers seem to be randomly distributed and are certainly unrelated to the GDB event (Fig. 1).

Due to the lack of adequate sections, preservational bias, or lack of stratigraphic calibration basal Early Triassic terrestrial successions are relatively poorly known. Numerous palynological studies of the Late Permian contain relatively rich assemblages whereas the overlying Triassic sections appear impoverished or consist of a few samples only[12,55,57–60] and therefore emphasise the impression of an impoverished Early Triassic flora. A few well calibrated quantitative palynological records exist for the basal Triassic of the Barents Sea area as well as for the classical Early Triassic sections in the Salt Range and the Surghar Range in Pakistan, and based on recent radiometric age datings, for the Bowen Basin (eastern Australia)[23–25,37,39,40]. Calibration of the so far poorly constrained Australian Permian–Triassic palynostratigraphic succession shows that the most important floral turnover, associated with the extinction of the glossopterids, happened not at the Permian–Triassic boundary but within the Induan. Similar to the changes observed in E-Greenland this turnover is expressed by a strong reduction of the abundance and diversity of the pteridosperms (taeniate bisaccate pollen) and by a corresponding increase in lycopsids[38,39].

The present record from East Greenland together with other high resolution terrestrial datasets challenges some of the running hypothesis associated with the PTME and its consequences for the Early Triassic flora. In contrast to the above mentioned spectacular extinction scenarios, the data from expanded latest Permian–earliest Triassic interval from the Southern Barents Sea (Finnmark platform) shows a distinct "spore spike" in reaction to the PTME[37], i.e. reflecting not an extinction event, but a shift in the vegetation's abundance structure. This event is also documented in a coeval section in East Greenland[10,26]. The data from the Finnmark platform[24] and from E-Greenland[10] suggest that this spore spike was of short duration–in the order of 10 kyrs. The succession following this "spore spike", well documented in the Finnmark section, suggests a return to conditions similar to pre-event status, although with a gradual loss of some typical Late Permian elements during the Griesbachian[24,37,40]. The detailed study of this section shows the disappearance of several species–namely of the *Vittatina* group-near the PTB associated with numerous taxa appearing near this level[7,61]. The Griesbachian assemblages from Kap Stosch illustrate a rich and diverse flora subsequent to the PTME, similar to coeval records previously documented from the Finnmark and the Trøndelag platforms[40]. For eastern Australia Foster[39] described the difference between the palynozone "Upper Stage 5", now attributed to the Late Permian, and the basal Induan *P. crenulata* zone as gradual, marked only by the first occurrence of a few marker species. Thus the evidence for a sudden plant extinction related to the PTME becomes more and more scanty.

The presented floral record provides a so far unique insight on environmental changes during the aftermath of the PTME. Pronounced dominance of pteridosperms can be inferred from the lower part of the Induan records from the Northern hemisphere (Kap Stosch area, Finnmark and Trøndelag platforms) as well as from eastern Australia[39]. In the Kap Stosch section we can document a take-over of lycopsid spores of isoetalean affinity around the calibrated GDB. This turn-over is followed by a further decline of the gymnosperms during the Dienerian, ending in the top part of the section with an overall dominance of the lycopsids. The first decisive floral change coincides with the onset of a marked negative $\delta^{13}C_{org}$ isotopic shift[46]. A subsequent change to the total dominance of spores in the middle part of the Dienerian concurs with the onset of another, although minor, negative $\delta^{13}C_{org}$ shift (Fig. 1).

Comparable quantitative palynological records of Griesbachian and especially of Dienerian age from other areas are extremely rare. However, Schneebeli-Hermann *et al.*[25] documented a coeval succession from the Salt Range (Pakistan). Although this section is strongly condensed (4m of section), it shows for the Griesbachian a strong dominance of gymnosperms-including pollen grains of glossopteridalean affinity, traditionally considered Permian markers, together with Triassic floral elements (e.g., Corystospermales, *Dicroidium* spp.)-followed by a gradual change to spore dominance in the Dienerian. In the Bowen Basin the significant decrease in the diversity and abundance of gymnosperms and the corresponding increase of lycopsids, coinciding with the disappearance of glossopterids, falls within the Induan, without further precision[38,39]. Detailed faunal data from the Salt Range sections reveals a low diversity ammonoid fauna at the base of the Dienerian, followed by a further diversity decrease in the middle Dienerian, and by a slight increase in the late Dienerian and finally by a significant diversification in the early Smithian[21]. Supposing that these ammonoid faunas reflect the general environmental quality, the middle Dienerian faunal assemblages would suggest most hostile conditions. The almost total demise of the gymnosperms in the Kap Stosch section might coincide with this faunal crisis and confirm a severe and prolonged global environmental crisis during the Dienerian.

Generally climatic changes are the primary trigger for changes in vegetation patterns. Fast reactions of the plant communities-within time spans of 100 yrs-are reliably recorded in changes in pollen assemblages (e.g., Early Holocene afforestation in the Alps[62]). In order to understand terrestrial environmental changes in the Early Triassic indicated by pronounced negative $\delta^{13}C_{org}$ shifts and the coeval floral turnovers we try to infer the corresponding climatic conditions. Proliferation of spores is generally associated with more humid conditions, based on the fact that pteridophytes need liquid water at least during part of their life cycle. Thus spore dominated assemblages are considered to reflect relatively humid conditions. Temperature values are much more delicate to infer from plant records. Recent data of $\delta^{18}O$ measurements of pristine biogenic apatite of conodonts reveal considerable changes in temperatures near the PTME and during the Early Triassic[15]. These authors inferred relatively cool temperatures for the Griesbachian and a temperature increase for the Dienerian. The $\delta^{18}O$ record

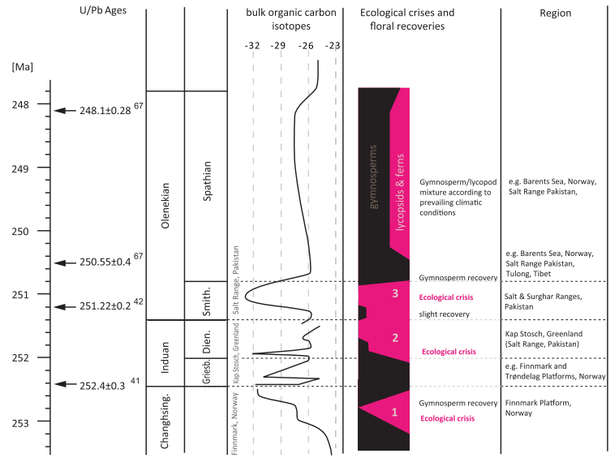

Figure 2. Summary of Early Triassic floral events. Radiometric ages[41,42,67] together with a simplified bulk organic carbon isotope curve[24,48,50] are shown in relation to floral events documented in the Boreal Realm[22,24,26,45] and on the North Indian margin[23,25,44].

of the Early Triassic follows the trends in the carbon cycle reflected in the $\delta^{13}C$ curve. The marked shifts in these records, reflecting severe environmental disturbances, are accompanied by major changes in plant assemblages (Fig. 2). For the Salt Range sections the increased spore ratios near the GDB and in the middle Smithian can be directly linked to negative shifts of $\delta^{13}C_{org}$ and to lower $\delta^{18}O$[15,23]. These trends are interpreted to correspond to higher pCO_2 and to higher temperatures that apparently induced at least seasonally increased humidity[15]. In contrast, the gymnosperms dominated assemblages of the late Smithian/early Spathian are associated with relatively positive $\delta^{13}C_{org}$ values and $\delta^{18}O$ values reflecting relatively cool temperatures[15]. Applying this relationship to the Induan succession of Kap Stosch, we suggest that the gymnosperm pollen dominated Griesbachian assemblages reflect relatively cool and dry conditions, which rapidly changed to hot and humid at the GDB.

Similar to the GDB event the onset of the $\delta^{13}C$ negative shift leading to the minimum near the PTB, coincides with a sudden increase of spores[24]. Similar relationships have been observed in the middle Smithian[23]; near the TJB[28,32,63] and near the KPB[64] where spore maxima are also associated with negative $\delta^{13}C$ shifts. These changes reflect severe environmental and climatic changes, which in the case of the Early Triassic are probably associated with effects of successive volcanic outbursts related to the Siberian Large Igneous Province. Within the studied interval the dominance of lycopsids got stepwise accentuated, with increasing percentages of herbaceous forms, which become regular elements of the vegetation during the Dienerian. In contrast to the PTME, where the vegetation is interpreted to have recovered within a short time, the dominance of the lycopsids, appearing at the GDB, lasted–with a slight recovery in the early Smithian-for several 100 kyrs, up to the late Smithian[23]. Similar changes documented for the mid Induan of the North Indian Margin and eastern Australia suggest a global extent of this event. Thus, the GDB event, reflected in the floral turn-over associated with the extinction of the glossopterids, the pronounced negative $\delta^{13}C_{org}$ shift, and the extinction in some marine groups (conodonts and radiolarians) is interpreted to represent another severe environmental disruption in a series of events such as at the PTB-, the mid-Smithian-, the TJB or the KPB. Recent progress in the technique of radiometric dating enables us to calibrate changes in continental sections and to put these deep-time environmental cataclysms within precise temporal frameworks and make them comparable to rapid changes that happened during the last 100kyrs. The floral turnovers related to the PTME and to the GDB event are thought to have happened within a few kyrs; thus, they become realistic models for future changes.

Methods

Sampling for palynology essentially focussed on fine grained, dark siltstones and mudstones; gaps in the record correspond to coarse clastic intervals. For the studied section 94 samples have been prepared following standard palynological preparation technique[23] 80 samples contain well preserved sporomorphs. For each sample a minimum of 250 sporomorphs has been counted. The detailed description of the section, palynofacies analysis, isotope measurements and palaeoenvironmental interpretations has been previously published by Sanson-Barrera *et al.*[48].

References

1. Cramer, W. *et al.* Global response of terrestrial ecosystem structure and function to CO_2 and climate change: results from six dynamic global vegetation models. *Global Change Biology* **7,** 357–373 (2001).
2. Vitousek, P. M. Beyond global warming: Ecology and global change. *Ecology* **75,** 1861–1876 (1994).
3. Harper, G. J., Steininger, M. K., Tucker, C. J., Juhn, D. & Hawkins, F. Fifty years of deforestation and forest fragmentation in Madagascar. *Environmental Conservation* **34,** 325–333 (2007).
4. Fearnside, P. M. Deforestation in Brazilian Amazonia: History, Rates, and Consequences. *Conservation Biology* **19,** 680–688 (2005).
5. Werth, D. & Avissar, R. The local and global effects of Amazon deforestation. *Journal of Geophysical Research* **107,** 8087, doi: 10.1029/2001JD000717 (2002).
6. Skole, D. & Tucker, C. Tropical deforestation and habitat fragmentation in the Amazon: Satelite Data from 1978 to 1988. *Science* **260,** 1905–1910 (1993).
7. Zheng, F. L. Effect of vegetation change on soil erosion on the Loess Plateau. *Pedosphere* **16,** 420–427 (2006).
8. Erwin, D. H., Bowring, S. A. & Jin, Y. End-Permian mass extinctions: A review. *Geological Society of America Special Paper 356*, 363–383 (2002).
9. Barnosky, A. D. *et al.* Has the Earth's sixth mass extinction already arrived? *Nature* **471,** 51–57 (2011).
10. Looy, C. V., Twitchett, R. J., Dilcher, D. L., van Konijnenburg-van Cittert, J. H. A. & Visscher, H. Life in the end-Permian dead zone. *Proceedings of the National Academy of Sciences of the United States of America* **98,** 7879–7883 (2001).
11. Visscher, H. *et al.* Environmental mutagenesis during the end-Permian ecological crisis, *Proceedings of the National Academy of Sciences of the United States of America* **101,** 12952–12956 (2004).
12. Looy, C. V., Brugman, W. A., Dilcher, D. L. & Visscher, H. The delayed resurgence of equatorial forests after the Permian-Triassic ecologic crisis. *Proceedings of the National Academy of Sciences of the United States of America* **96,** 13857–13862 (1999).
13. Chumakov, N. M. & Zharkov, M. A. Climate during the Permian-Triassic biosphere reorganization. Article 2. Climate of the Late Permian and Early Triassic: General inferences. *Stratigraphy and Geological Correlation* **11,** 361–375 (2003).
14. Preto, N., Kustatscher, E. & Wignall, P. B. Triassic climate—State of the art and perspectives. *Palaeogeography, Palaeoclimatology, Palaeoecology* **290,** 1–10 (2010).
15. Romano, C. *et al.* Climatic and biotic upheavals following the end-Permian mass extinction. *Nature Geoscience* **6,** 57–60 (2013).
16. Brühwiler, T., Bucher, H., Brayard, A. & Goudemand, N. High-resolution biochronology and diversity dynamics of the Early Triassic ammonoid recovery: The Smithian faunas of the Northern Indian Margin. *Palaeogeography, Palaeoclimatology, Palaeoecology* **297,** 491–501 (2010).
17. Orchard, M. J. Conodont diversity and evolution through the latest Permian and Early Triassic upheavals. *Palaeogeography, Palaeoclimatology, Palaeoecology* **252,** 93–117 (2007).
18. O'Daugherty, L., Carter, E. S., Gorican, S. & Dumitrica, P. Triassic readiolarian biostratigraphy. Geological Society, London Special Publications 334, 163–200 (2010).
19. Twitchett, R. J., Krystyn, L., Baud, A., Wheeley, J. R. & Richoz, S. Rapid marinerecovery after the end-Permian mass-extinction event in the absence of marineanoxia. *Geology* **32,** 805–808 (2004).
20. Hofmann, R., Goudemand, N., Wasmer, M., Bucher, H. & Hautmann, M. New trace fossil evidence for an early recovery signal in the aftermath of the end-Permian mass extinction. *-Palaeogeography, Palaeoclimatology, Palaeoecology* **310,** 216–226 (2011).
21. Ware, D., Bucher, H. Brayard, A. Schneebeli-Hermann, E. & Brühwiler, T. High-resolution biochronology and diversity dynamics of the Early Triassic ammonoid recovery: The Dienerian faunas of the Northern Indian Margin. *Palaeogeography, Palaeoclimatology, Palaeoecology* **440,** 363–373 (2015).
22. Galfetti, T. *et al.* Smithian–Spathian boundary event: Evidence for global climatic change in the wake of the end-Permian biotic crisis. *Geology* **35,** 291–294 (2007).
23. Hermann, E. *et al.* Terrestrial ecosystems on North Gondwana following the end-Permian mass extinction. *Gondwana Research* **20,** 630–637 (2011).
24. Hochuli, P. A., Hermann, E., Vigran, J. O., Bucher, H. & Weissert, H. Rapid demise and recovery of plant ecosystems across the end-Permian extinction event. *Global and Planetary Change* **74,** 144–155 (2010).
25. Schneebeli-Hermann, E. *et al.* Vegetation history across the Permian–Triassic boundary in Pakistan (Amb section, Salt Range). *Gondwana Research* **24,** 911–924 (2015).
26. Stemmerik, L., Bendix-Almgreen, S. E. & Piasecki, S. The Permian-Triassic boundary in central East Greenland: past and present views. *Bulletin of the Geological Society of Denmark* **48,** 159–167 (2001).
27. Tschudy, R. H., Pillmore, C. L., Orth, C. J., Gilmore, J. S. & Knight, J. D. Disruption of the terrestrial Plant ecosystem at the Cretaceous-Tertiary boundary, Western Interior. *Science* **225,** 1030–1032 (1984).
28. van de Schootbrugge, B. *et al.* Floral changes across the Triassic/Jurassic boundary linked to flood basalt volcanism. *Nature Geoscience* **2,** 589–594 (2009).
29. Vajda, V., Raine, J. I. & Hollis, C. J. Indication of global deforestation at the Cretaceous-Tertiary boundary by New Zealand fern spike. *Science* **294,** 1700–1702 (2001).
30. Maruoka, T., Koeberl, C. & Bohor, B. F. Carbon isotopic compositions of organic matter across continental Cretaceous–Tertiary (K–T) boundary sections: Implications for paleoenvironment after the K–T impact event. *Earth and Planetary Science Letters* **253,** 226–238 (2007).
31. Hesselbo, S. P., Robinson, S. A., Surlyk, F. & Piasecki, S. Terrestrial and marine extinction at the Triassic-Jurassic boundary synchronized with major carbon-cycle perturbation: A link to initiation of massive volcanism? *Geology* **30,** 251–254 (2002).
32. Bonis, N. R., Ruhl, M. & Kürscher W. M. Milankovitch-scale palynological turnover across the Triassic–Jurassic transition in St. Audrie's Bay, SW UK. *Journal of the Geological Society, London* **167,** 877–888 (2010).
33. Alvarez. L. W., Alvarez, W., Asaro, F. & Michel, H. V. Extraterrestrial cause for the Cretaceous–Tertiary extinction. *Science* **208,** 1095–1108 (1980).
34. Walker L. R. & Sharpe, J. M. Ferns, disturbance and succession in *Fern ecology* (eds Mehltreter, K. Walker, L. R. & Sharpe, J. M.) 177–219 (Cambridge University Press, 2010).
35. Page, C. N. 2004. Adaptive ancientness of vascular plants to exploitation of low-nutrient substrates–a neobotanical overview in *The evolution of plant Physiology* (eds Hemsley, R. A. & Poole, I.) 446–466 (Elsevier Academic Press, 2004).
36. Whittaker, R. J., Bush, M. B. & Richards, K. Plant recolonization and vegetation succession on the Krakatau Islands, Indonesia. *Ecological Monographs* **59,** 59–123 (1989).
37. Mangerud, G. Palynostratigraphy of the Permian and lowermost Triassic succession, Finnmark Platform, Barents Sea. *Review of Palaeobotany and Palynology* **82,** 317–349 (1994).
38. Nicoll, R. *et al.* CA-ICTIMS dating of tuffs, calibration of palynostratigraphy and stratigraphy of the Bowen and Galilee basins. Bowen Basin Symposium 2015. 211–218 (2015).
39. Foster, C. B. Spore-pollen assemblages of the Bowen Basin, Queensland (Australia): Their relationship to the Permian/Triassic boundary, *Review of Palaeobotany and Palynology* **36,** 165–183 (1982).
40. Hochuli, P. A., Vigran, J. O., Hermann, E. & Bucher, H. Multiple climatic changes around the Permian–Triassic boundary event revealed by an expanded palynological record from mid-Norway. *Geol. Soc. Am. Bull.* **122,** 884–896 (2010).
41. Mundil, R., Ludwig, K. R., Metcalfe, I. & Renne, P. R. Age and timing of the Permian mass extinction: U/Pb dating of closed-system zircon. *Science* **305,** 1760–1763 (2004).

42. Galfetti, T. *et al.* Timing of the Early Triassic carbon cycle perturbations inferred from new U/Pb ages and ammonoid biochronozones. *Earth and Planetary Science Letters* **258,** 593–604 (2007).
43. Gradstein, F. M., Ogg, J. G., Schmitz, M. D. & Ogg, G. M. *The geological time scale* (Elsevier, 2012).
44. Schneebeli-Hermann, E. *et al.* Palynology of the Lower Triassic succession of Tulong, South Tibet—Evidence for early recovery of gymnosperms. *Palaeogeography, Palaeoclimatology, Palaeoecology* **339–341,** 12–24 (2012).
45. Hochuli, P. A. & Vigran, J. O. Climate variations in the Boreal Triassic-inferred from palynological records from the Barents Sea. *Palaeogeography, Palaeoclimatology, Palaeoecology* **290,** 20–42 (2010).
46. Orłowska-Zwolińska, T. Palynostratigraphy of the Buntsandstein in section of Western Poland. *Acta Palaeontologica Polonica* **29,** 161–226 (1984).
47. Bjerager, M., Seidler, L., Stemmerik, L. & Surlyk, F. Ammonoid stratigraphy and sedimentary evolution across the Permian–Triassic boundary in East Greenland. *Geological Magazine* **143,** 635–656 (2006).
48. Sanson-Barrera, A. *et al.* Late Permian-earliest Triassic high-resolution organic carbon isotope and palynofacies records from Kap Stosch (East Greenland). *Global and Planetary Change* **133,** 149–166 (2015).
49. Balme, B. E. Fossil *in situ* spores and pollen grains: an annotated catalogue. *Review of Palaeobotany and Palynology* **87,** 81–323 (1995).
50. Hermann, E. *et al.* Climatic oscillations at the onset of the Mesozoic inferred from palynological records from the North Indian Margin. *Journal of the Geological Society, London* **169,** 227–237 (2012).
51. Visscher, H. *et al.* The terminal Paleozoic fungal event: Evidence of terrestrial ecosystem destabilization and collapse. *Proceedings of the National Academy of Sciences of the United States of America* **93,** 2155–2158 (1996).
52. Utting, J., Spina, A., Jansonius, J., McGregor, D. C. & Marshall, C. E. A. Reworked miospores in the upper Palaezoic and Lower Triassic of the northern circum-polar area and selected localities. *Palynology* **28,** 75–119 (2004).
53. Peng, Y. *et al.* High-resolution terrestrial Permian–Triassic eventostratigraphic boundary in western Guizhou and eastern Yunnan, southwestern China. *Palaeogeography, Palaeoclimatology, Palaeoecology* **215,** 285–295 (2005).
54. Eshet, Y., Rampino, M. R. & Visscher, H. Fungal event and palynological record of ecological crisis and recovery across the Permian-Triassic boundary. *Geology* **23,** 967–970 (1995).
55. Visscher, H., Sephton, M. A. & Looy, C. V. Fungal virulence at the time of the end-Permian biosphere crisis? *Geology* **39,** 883–886 (2011).
56. Foster, C. B., Stephenson, M. H., Marshall, C., Logan, G. A. & Greenwood, P. F. A revision of Reduviasporonites Wilson 1962: description, illustration, comparison and biological affinities. *Palynology* **36,** 35–58 (2002).
57. Spina, A., Cirilli, S., Utting, J. & Jansonius, J. Palynology of the Permian and Triassic of the Tesero and Bulla sections (Western Dolomites, Italy) and consideration about the enigmatic species Reduviasporonites chalastus. *Review of Palaeobotany and Palynology* **218,** 3–14 (2015).
58. Krassilov, V. A. & Karasev, E. Paleofloristic evidence of climate change near and beyond the Permian–Triassic boundary. *Palaeogeography, Palaeoclimatology, Palaeoecology* **284,** 326–336 (2009).
59. Tewari *et al.* The Permian-Triassic palynological transition in the Guryul Ravine section, Kashmir, India: implications for Tethyan-Gondwana correlations. Earth Science Reviews 149, 53–66 (2015).
60. Peng, Y. & Shi, G. R. Life crises on land across the Permian-Triassic boundary in South China. *Global and Planetary Change* **65,** 155–165 (2009).
61. Ouyang, S. & Utting, J. Palynology of Upper Permian and Lower Triassic rocks, Meishan, Changxing County, Zhejiang Province, China. *Review of Palaeobotany and Palynology* **66,** 65–103 (1990).
62. Ouyang, S. & Norris, G. Earliest Triassic (Induan) spores and pollen from the Junggar Basin, Xinjiang, northwestern China. *Review of Palaeobotany and Palynology* **106,** 1–56 (1999).
63. Vigran, J. O., Mangerud, G., Mørk, A., Worsley, D. & Hochuli, P. A. Palynology and geology of the Triassic succession of Svalbard and the Barents Sea. Geological Survey of Norway, *Spec. Pub.* **14,** 1–270 (2014).
64. Gobet, E., Tinner, W., Bigler, C., Hochuli, P. A. & Ammann, B. Early Holocene afforestation processes in the lower subalpine belt of the Central Swiss Alps as inferred from macrofossil and pollen records. *Holocene,* **15,** 5, 672–686 (2005).
65. Lindström, S., van de Schootbrugge, B., Pedersen, G. K., Fiebig, J., Nielsen, L. H. & Richoz, S. No causal link between terrestrial ecosystem change and methane release during the end-Triassic mass extinction. *Geology* **40,** 531–534 (2012).
66. Vajda, V. & Bercovici, A. The global vegetation pattern across the Cretaceous–Paleogene extinction interval: a template for other extinction event. *Global and Planetary Change* **122,** 29–49 (2015).
67. Ovtcharova, M. *et al.* New Early to Middle Triassic U–Pb ages from South China: calibration with ammonoid biochronozones and implications for the timing of the Triassic biotic recovery. *Earth and Planetary Science Letters* **243,** 463–475 (2006).

Acknowledgements

Maximiliano Meier is thanked for his assistance during field work. The project was supported by the Swiss NSF project 20021-135446/1 to HB. We acknowledge comments from two anonymous reviewers.

Author Contributions

H.B. and P.A.H. designed the project; fieldwork has been carried out by H.B., P.A.H. and A.S.-B. Palynology analysis has been done by P.A.H., A.S.-B. and E.S.-H. and the write-up by P.A.H., E.S.-H., A.S.-B. and H.B.

Additional Information

Competing financial interests: The authors declare no competing financial interests.

How to cite this article: Hochuli, P. A. *et al.* Severest crisis overlooked—Worst disruption of terrestrial environments postdates the Permian–Triassic mass extinction. *Sci. Rep.* **6**, 28372; doi: 10.1038/srep28372 (2016).

Conclusions

The present thesis addresses the interrelation between climate, environmental disturbances, and land plant ecosystems during the earliest Triassic in East Greenland. The two main aims was to study the influence of environmental and carbon cycle disturbances on terrestrial ecosystems, and to distinguish between local and global signals. This thesis is based on a multidisciplinary approach including high-resolution organic carbon isotope, palynofacies, bulk-rock geochemistry, clay mineralogy, and palynological data. This multidisciplinary approach allowed to i) produce a chemostratigraphic framework of the latest Permian–earliest Triassic, ii) to describe the depositional environments of East Greenland sub-basins during this interval, and iii) to link climatic and land plants ecosystem changes during the earliest Triassic.

The most important findings of this study are summarized below:

- High-resolution bulk organic carbon isotope and palynofacies data have been used to build a chemostratigraphic framework for the latest Permian–earliest Triassic of the sedimentary succession at Kap Stosch (East Greenland). Correlation with other, globally distributed Permian–Triassic sections, allowed for the identification of two globally recognisable carbon isotope negative shifts, one in the latest Permian, and the second at the Griesbachian–Dienerian boundary (Chapter 1, Fig. 4).

- The chemostratigraphic pattern from Kap Stosch record closely resembles the record from the Trøndelag Platform. It shows similarities in the burial of organic carbon at both margins of the Greenland–Norway Basin. The two records represent the most expanded earliest Triassic records of the Boreal realm and probably worldwide.

- A relative sea-level curve based on the particulate organic matter content (marine/terrestrial ratio) permitted the identification of three transgressive-regressive cycles and two sequence boundaries. The latest Permian sedimentary gap at Kap Stosch corresponds to the second-order sequence boundary identified in the northern margin of Pangea and in other globally distributed sections, representing the global latest Permian regression. A third-order sequence boundary has been identified close to the Griesbachian–Dienerian boundary at Kap Stosch, and in southern Spitsbergen and the Barents Sea (Chapter 1, Figs. 6 and 7).

- Bulk organic carbon isotope, ammonoid and palynofacies data provided the basis for an interbasinal correlation between two areas of East Greenland, the Scoresby Land sub-basin (represented by the Aggersborg and Triaselv sections), and the Hold-with-Hope sub-basin (Kap Stosch section). The latest Permian negative carbon isotope shift proves to be a reliable tool for correlating Permian–Triassic sections, overcoming the diachronous clastic fill of the sub-basins in East Greenland (Chapter 2, Fig. 5).

- Average sedimentation rates of the Kap Stosch section, spanning ca. 1 million years, have been calculated at 0.27 m ka-1 thus representing the so far the highest sedimentation rates for the latest Permian–earliest Triassic interval.

- Using the common redox proxies, as the degree of pyritization, organic carbon/phosphorous ratio and total sulfur/total organic carbon ratio, only one out of the three suboxic-anoxic intervals reflected

in the particulate organic matter could be identified. Due to the extraordinary high sedimentation rates trace element proxies (Mo, V, and U), usually indicative of redox conditions are too strongly diluted to show significant variance throughout the record (Chapter 3, Fig. 5).

- In the Kap Stosch section major element data suggests increased paleoweathering during a brief interval within the Griesbachian and during almost the whole Dienerian, showing higher amplitude in the data. These increased weathering intervals coincide with the development of more proximal depositional environments associated with increased occurrence of red siltstone and sandstone beds. Increased weathering and red colour dominance coincide also with higher smectite contents and smectite/kaolinite ratios in the clay mineral assemblages (Chapter 3, Fig. 9).

- Across the Griesbachian–Dienerian boundary clay mineralogy data show increased seasonality, whereas spore/pollen ratios indicate increased humidity. Therefore, this combined increase in humidity and increase in seasonality suggest that the precipitation regime was primarily affected, and the temperature regime was affected only to a lesser degree.

- Palynological data show a profound floral turnover, coinciding with the Griesbachian–Dienerian boundary. The pollen-dominated floral associations of the Griesbachian are substituted by spore-dominated floral associations in the Dienerian (Chapter 4, Fig. 1). A concomitant negative shift of organic carbon isotopes shows a close link between carbon cycle disturbance and changes land plant ecosystems. Correlation with coeval data from the North Indian Margin (Pakistan) indicates that this floral turnover is of global extent.

Appendix

List of conference abstracts

Geophysical Research Abstracts
Vol. 15, EGU2013-7107, 2013
EGU General Assembly 2013

High-resolution stable carbon isotope record of the Permian to earliest Triassic from East Greenland

Anna Sanson Barrera (1), Peter A. Hochuli (1,2), Hugo Bucher (1,2), Maximiliano Meier (1), Elke Schneebeli Hermann (1), Helmut Weissert (2), and Stefano M. Bernasconi (2)

(1) Paleontological Institute and Museum, University of Zurich, Karl Schmid-Strasse 4, 8006 Zurich, Switzerland (anna.sanson@pim.uzh.ch, Peter.Hochuli@erdw.ethz.ch, hugo.fr.bucher@pim.uzh.ch, maximiliano.meier@uzh.ch, ElkeSchneebeli@gmx.net), (2) Department of Earth Sciences, ETH Zurich, Sonneggstrasse 5, 8092 Zurich, Switzerland (Peter.Hochuli@erdw.ethz.ch, hugo.fr.bucher@pim.uzh.ch, helmut.weissert@erdw.ethz.ch, stefano.bernasconi@erdw.ethz.ch)

The Late Permian and Early Triassic organic carbon isotope records show global major excursions probably triggered by episodic volcanic degasing of the Siberian Large Igneous Province. Important and rapid fluctuations of the global carbon cycle are also reflected in the biosphere. The geological record seems to comprise several major floral and marine faunal turnovers indicating short-lived biotic recoveries. In northwest Pangea, the active Early Triassic Greenland – Norway rifting system led to the accommodation of thick sedimentary sequences. This basin has a great potential for detailed studies of regional and global biotic and climatic changes with high temporal resolution during this critical interval in Earth's history. The western part of this basin is exposed in north-eastern Greenland and is represented by a succession of deltaic sediments organized in a general regressive trend ranging throughout the Griesbachian and the onset of the Dienerian. On the eastern side of the basin the succession has been drilled off the Norwegian coast. On Hold with Hope (East Greenland, 74°N) up to ca. 800m thick sections of the ammonoid-bearing Early Triassic Wordie Creek Formation have been logged and sampled. Here we present a high-resolution organic carbon isotope record and preliminary palynofacies data of a 500m thick composite section ranging from the Permian into the earliest Triassic. The organic carbon isotope record is closely comparable to the coeval section from the Trøndelag platform in Mid-Norway. The two records show a first major negative shift (ca. -6‰ representing the unconformity between the Ravnefjeld and the Wordie Creek formations, regionally known as the lithological Permian-Triassic boundary. Higher up, a second negative shift of ca. -4‰ correlates with the carbon shift associated with the GSSP Permian-Triassic boundary as defined at Meishan (China), represented by carbon isotope values around -30‰This negative shift is followed by a steady positive trend, which is interrupted by two striking events, (a) a positive shift reaching values of ca. -22‰ comparable to the values of the Permian Ravnefjeld Formation, and (b) another negative shift of ca. -7‰ bringing the carbon record back to values around -31‰Our data from north-eastern Greenland indicate multiple and major events recorded by the carbon cycle within less than a million years at the onset of the Triassic.

4.13

Latest Permian to Early Triassic high-resolution stable carbon isotope record from North-east Greenland

Sanson-Barrera, A.[1]; Hochuli, P. A.[1]; Bucher, H.[1]; Meier, M.[1]; Schneebeli-Hermann, E.[1]; Weissert, H.[2] and Bernasconi, S. M.[2]

[1] *Paleontological Institute and Museum, University of Zurich, Karl Schmid-Strasse 4, 8006 Zurich, Switzerland (anna.sanson@pim.uzh.ch)*
[2] *Department of Earth Sciences, ETH Zurich, Sonneggstrasse 5, 8092 Zurich, Switzerland*

Large and rapid fluctuations of the global carbon cycle during the Late Permian and Early Triassic left a global imprint in the organic carbon isotope record observed in numerous Permian–Triassic sections (Payne et al., 2004; Galfetti et al., 2007). Expanded and well preserved successions, i.e. Norway and NE Greenland covering the lower part of the Lower Triassic (Griesbachian/Dienerian), are crucial for assessing the evolution of the carbon cycle in detail. Sections of this interval are rare, and often incomplete or condensed. Expanded sections also allow the construction of a reliable biostratigraphic zonation, and therefore a better assessment of the temporal patterns of recovery after the end Permian mass extinction events, in both marine and terrestrial ecosystems.

At the north-western margin of Pangea, the rifting system between Greenland and Norway led to the accommodation of thick sedimentary sequences of earliest Triassic age. In East Greenland this interval is represented by a succession of deltaic sediments reflecting a general regressive trend. They are an excellent archive to study the evolution of terrestrial and marine ecosystems during this time. At Hold with Hope (East Greenland, 74°N) a 700m a thick fossiliferous succession of the Wordie Creek Formation has been logged and sampled.

Here we present a high resolution lithostratigraphic and organic carbon isotope record of a composite section, covering the uppermost Permian and the lower part of the Lower Triassic (Dienerian). Palynofacies data are used to assess the composition of the organic matter.

Measurements of about 580 samples show several distinct trends and major shifts in the organic carbon isotope record. The following major excursions can be recognised (from 1 to 8): 1. a first negative shift of ca. -6‰ corresponds to the unconformity between the Late Permian Ravnefjeld Fm. and earliest Triassic Wordie Creek Fm., regionally known as the lithological Permian–Triassic boundary; 2. after a short interval with stable carbon isotope values around -28‰ a second negative shift of -4‰ (to values of ca. -32‰) follows. This correlates with the negative carbon isotope shift recorded in numerous globally distributed Permian–Triassic successions. 3. This shift is followed by a steady trend to more positive carbon isotope values. 4. This trend culminates in a distinct positive shift reaching values of ca. -22‰, comparable to the values of the Ravnefjeld Fm.; 5. Another negative shift of ca. 7‰ leads again to negative values of around -31‰; 6. This interval of low carbon isotope values is followed by a steady positive trend reaching values around -26‰. 7. At around 350m a step-like negative shift follows with a minimum at around -32‰, its most negative values are observed close to the *Bukkenites rosenkrantzi*-bearing layers, possibly corresponding to the Griesbachian–Dienerian boundary (Bjerager et al., 2006). 8. The last part of the curve shows fluctuating but progressively more positive values, reaching ca. -23‰ at the top of the section. Palynofacies data reflect alternating marine and terrestrial conditions in the lower part of the section changing to predominant terrestrial conditions near the top.

At basinal scale our isotope data are closely comparable with the coeval section from the Trøndelag platform in Mid-Norway (Hermann et al., 2010). At global scale similar trends can be observed in organic carbon isotope records from Pakistan (Hermann et al., 2012). In NE Greenland the distinct negative shift (7) tentatively interpreted to be close to the Griesbachian–Dienerian boundary can be compared and correlated to the shifts in the carbonate carbon isotope records from the Arabic Peninsula (Clarkson et al., 2013) and from China (Galfetti et al., 2007; Korte & Kozur, 2010). Thus our data from NE Greenland reflect multiple and major changes in the global carbon cycle, which occurred at the onset of the Triassic within less than one million years.

REFERENCES

Bjerager, M., Seidler, L., Stemmerik, L., & Surlyk, F. (2006). Ammonoid stratigraphy and sedimentary evolution across the Permian – Triassic boundary in East Greenland, 143, 635–656. doi:10.1017/S0016756806002020

Clarkson, M. O., Richoz, S., Wood, R. A., Maurer, F., Krystyn, L., Mcgurty, D. J., & Astratti, D. (2013). A new high-resolution $\delta^{13}C$ record for the Early Triassic : Insights from the Arabian Platform. Gondwana Research, 24(1), 233–242. doi:10.1016/j.gr.2012.10.002

Galfetti, T., Bucher, H., Brayard, A., Hochuli, P. A., Weissert, H., Guodun, K., Atudorei, V., et al. (2007). Late Early Triassic climate change : Insights from carbonate carbon isotopes , sedimentary evolution and ammonoid paleobiogeography,

243, 394–411. doi:10.1016/j.palaeo.2006.08.014

Galfetti, T., Bucher, H., Ovtcharova, M., Schaltegger, U., Brayard, A., Brühwiler, T., Goudemand, N., et al. (2007). Timing of the Early Triassic carbon cycle perturbations inferred from new U – Pb ages and ammonoid biochronozones. Earth and Planetary Science Letters, 258, 593–604. doi:10.1016/j.epsl.2007.04.023

Hermann, E., Hochuli, P. A., Bucher, H., Vigran, J. O., Weissert, H., & Bernasconi, S. M. (2010). A close-up view of the Permian – Triassic boundary based on expanded organic carbon isotope records from Norway (Trøndelag and Finnmark Platform). Global and Planetary Change, 74, 156–167. doi:10.1016/j.gloplacha.2010.10.007

Hermann, E., Hochuli, P. A., Bucher, H., Ware, D., Weissert, H., Roohi, G., & Yaseen, A. (2012). Climatic oscillations at the onset of the Mesozoic inferred from palynological records from the North Indian Margin. Journal of the Geological Society, 169, 227–237.

Korte, C., & Kozur, H. W. (2010). Carbon-isotope stratigraphy across the Permian – Triassic boundary : A review. Journal of Asian Earth Sciences, 39(4), 215–235. doi:10.1016/j.jseaes.2010.01.005

Payne, J. L., Lehrmann, D. J., Wei, J., Orchard, M. J., Schrag, D. P., & Knoll, A. H. (2004). Large Perturbations of the Carbon Cycle During Recovery from the End-Permian Extinction. Science, 305(July), 506–509.

Geophysical Research Abstracts
Vol. 17, EGU2015-14477, 2015
EGU General Assembly 2015

Interbasinal correlation between Jameson Land and Hold-with-Hope (Northeast Greenland) organic carbon isotope records during the latest Permian–earliest Triassic

Anna Sanson Barrera (1), Maximiliano Meier (1), Peter A. Hochuli (1), Hugo Bucher (1), Helmut Weissert (2), and Stefano M. Bernasconi (2)

(1) Paleontological Institute - University of Zurich, Zurich, Switzerland (anna.sanson@pim.uzh.ch), (2) Department of Earth Sciences - ETH Zurich, Zurich, Switzerland

Latest Permian–earliest Triassic sequences in Northeast Greenland were deposited during the main rift phase between the two margins of the Greenland–Norway Basin, and were influenced by several relative sea-level fluctuations. The associated crustal extension created several sub-basins that led to marked lateral thicknesses between the latest Permian and earliest Triassic formations. These formations outcrop along the Northeast Greenland coast and can be followed from Jameson Land around 71°N up to Wollaston Forland around 74.5°N. Due to a latest Permian relative sea-level fall, northern sub-basins show a sedimentary gap close to the Permian–Triassic boundary, while southern sub-basins show continuous sedimentation across the Permian–Triassic transition. Earlier studies focused just on the Permian–Triassic boundary from continuous sections from Jameson Land. This study presents the correlation between two new sections from Jameson Land, and one section of a northern sub-basin (Hold-with-Hope) merging terrestrial and marine geochemical and paleontological data. The combination of organic carbon isotopes, palynofacies and palynology analyses, few ammonoids belonging to the Ophiceratidae family found in the sections, and sedimentological observations provides a robust correlation between both sub-basins, and the first interbasinal organic carbon isotope correlation for Northeast Greenland during the latest Permian–earliest Triassic.

GSA 2014
19-22 October | Vancouver, BC, Canada
THE GEOLOGICAL SOCIETY OF AMERICA®

Start | View Uploaded Presentations | Author Index | Meeting Information

2014 GSA Annual Meeting in Vancouver, British Columbia (19–22 October 2014)

Paper No. 166-4
Presentation Time: 1:45 PM

UNIQUE LATE PERMIAN–EARLIEST TRIASSIC HIGH-RESOLUTION ORGANIC CARBON ISOTOPE AND PALYNOFACIES RECORDS FROM EAST GREENLAND

SANSON-BARRERA, Anna[1], HOCHULI, Peter A.[1], BUCHER, Hugo[1], SCHNEEBELI-HERMANN, Elke[1], MEIER, Maximiliano[1], WEISSERT, Helmut[2] and BERNASCONI, Stefano M.[2], (1)Paleontological Institute and Museum, University of Zurich, Karl Schmid-Strasse 4, Zürich, 8006, Switzerland, (2)Institute of Geology, Dpt. of Earth Sciences, Swiss Federal Institute of Technology, Universitätstrasse 16, Zurich, 8092, Switzerland, anna.sanson@pim.uzh.ch

The deltaic marine record from Kap Stosch in East Greenland represents one of the thickest siliciclastic sequence of Late Permian–earliest Triassic age. About 700 meters of section have been sampled at high-resolution to produce records of bulk organic carbon isotope ($\delta^{13}C_{org}$) and palynofacies spanning the Late Permian to early-mid Dienerian interval. This study is focused on the identification of regional and global signals within the Kap Stosch record. The combination of bulk organic carbon isotope and palynofacies data shows the influence of the origin of organic matter and the depositional environment on $\delta^{13}C_{org}$ values. Based on palynofacies and sedimentological evidence three transgressive-regressive cycles can be identified, which can be correlated to sequence stratigraphy of Arctic Canada and the Barents Shelf. Correlation of the Kap Stosch record with other carbon isotope records (East Greenland, Norway, Arctic Canada, China, and Arabic Peninsula) allows the identification of two major global shifts. First, the negative carbon isotope shift recorded on a global scale prior to the Permian–Triassic boundary, and second, the negative shift at the Griesbachian–Dienerian boundary. The correlation with the Trøndelag Platform, offshore Norway, shows regional carbon isotope signals that are probably linked to increased tectonic activity of the basin during the Griesbachian.

Session No. 166

T195. Extreme Environmental Conditions and Biotic Responses during the Permian-Triassic Boundary Crisis and Early Triassic Recovery I
Monday, 20 October 2014: 1:00 PM-5:00 PM

215/216 (Vancouver Convention Centre-West)

Geological Society of America *Abstracts with Programs.* Vol. 46, No. 6, p.418

See more of: Extreme Environmental Conditions and Biotic Responses during the Permian-Triassic Boundary Crisis and Early Triassic Recovery I
See more of: Topical Sessions

<< Previous Abstract | Next Abstract >>

Acknowledgements

I am very thankful to my supervisors Prof Peter A. Hochuli and Prof Hugo Bucher (both Paleontological Institute and Museum, University of Zurich, PIMUZ) for their guidance during my thesis. Dr Elke Schneebeli-Hermann (PIMUZ) is thanked for her support and expertise. I am thankful to our collaborators during the thesis: Prof Helmut Weissert and Prof Stefano Bernasconi (both Institute of Earth Sciences, ETH Zurich), Dr Thierry Adatte (Institute of Earth Sciences, University of Lausanne) and Prof Thomas J. Algeo (Department of Geology, University of Cincinnati). I am in debt with Prof Winand Brinkmann (PIMUZ)for teaching me how to shoot a revolver and a rifle. Prof Peter Linder (Institute of Systematic Botany, University of Zurich), Dr Sofie Lindström (Stratigraphy Department, Geological Survey of Denmark and Greenland), and Dr Ulrich Heimhofer (Institute of Geology, University of Hannover) are thanked for being part of my PhD committee.

My two (very special) office mates deserve a special mention, Dr Madeleine Geiger and Alexandra Wegmann, thank you girls for such a wonderful time (and the booze) together! I fondly thank my former and present PIMUZ colleagues and friends for the scientific discussions, friendship and shared leisure activities (a.k.a. aperos and parties).

I thank my ETH Earth Sciences colleagues, the Stable Isotope Lab technicians, and the HF Lab technicians. From my short stay in Cincinnati, I want to thank my lab mates (Alex Reis, Allison Young, Zach Altman, and Kayla McKinley), and Dr Juana Serrano and Prof Yurena Yanes, who always kept my spirits high and taught me a lot about post-doc life.

I warmly thank my friends from the Autonomous University of Barcelona, who always cheer me up and believe in me, and to my friend and conferences mate, Prof Carme Huguet, for her inspiration, support, and motivation during my master and PhD.

I deeply thank my closest friends in Barcelona, who have been always by my side despite the distance, especially Maria Turró, and my friends in Zurich, Marina Escala and Rebekka Wolfensberger, who have followed my personal and PhD evolution since the beginning.

A heartfelt thanks to my partner Siniša Bratulić, for his love and companionship.

And last but not least, I thank and dedicate this thesis to my parents, Francesca and Albert, and to my brother Quim. I began to discover and love nature during my early life thanks to my family.

Curriculum Vitae

SANSON BARRERA, Anna

Date of birth: 13.12.1981
Place of birth: Barcelona (Spain)
Nationality: Spanish

EDUCATION

1999-2006 *Bachelor in Geology*, University of Barcelona, Spain
Bachelor thesis: Seismic activity monitoring of the Campi Flegrei and Mt Vesuvio, Napoli (Italy) during 2004-2005.

Supervisor: Dr Juan José Ledo.

2009-2010 *MSc in Environmental Sciences*, Institute of Environmental Sciences and Technology, Autonomous University of Barcelona, Spain
Master thesis: Sea surface temperature and primary productivity records of the Benguela upwelling system during the Plio-Pleistocene.

Supervisor: Dr Antoni Rosell Melé.

2011-2015 PhD student at the Paleontological Institute and Museum, University of Zurich, Switzerland
Dissertation: Climatic and floral evolution of the earliest Triassic in East Greenland.

Supervisors: Prof Dr Peter A. Hochuli and Prof Dr Hugo Bucher.